



THE UNIVERSITY OF AUCKLAND
NEW ZEALAND

Department of
Civil and
Environmental
Engineering

**SHEAR STRENGTH OF CONCRETE
MASONRY WALLS**

by

Kok Choon Voon

Dr. Jason M. Ingham

October 2003

School of Engineering
Report No. 611



CIVIL AND ENVIRONMENTAL ENGINEERING
Whakapukahatanga Taiao

The School of Engineering

Whakapukahatanga Taiao

New Zealand Maori for

Strengthening the environment – built and natural

For further information contact:

Department of Civil and Environmental Engineering, School of Engineering

The University of Auckland, Private Bag 92019, Auckland, New Zealand

Telephone 64-9-3737599 ext. 88166 or ext. 85715 Facsimile 64-9-3737462

Web www.cee.auckland.ac.nz Email cee-enquiries@auckland.ac.nz

Shear Strength of Concrete Masonry Walls

by

Kok Choon Voon

Dr. Jason M. Ingham

School of Engineering Report No. 611

Department of Civil and Environmental Engineering

The University of Auckland

New Zealand.

October 2003

Abstract

There is general consensus that the New Zealand masonry design standard, NZS 4230:1990, is overly conservative in its treatment of masonry shear strength, therefore restricting cost-effective masonry design. This report presents an experimental study that investigated the shear strength of reinforced concrete masonry walls. Also included in this report is a study that compares the accuracy of shear equations in predicting masonry shear strength.

Valuable information about masonry shear strength was captured during the testing of full scale masonry walls. It was concluded that horizontal reinforcement and axial compression load provided additional shear resistance to masonry walls. Therefore the nominal shear strength of reinforced masonry walls could be evaluated as a sum of contributions from masonry, shear reinforcement and applied axial stress. In addition, it was concluded that masonry shear strength decreases inversely in relation to an increase in H/L ratio.

Seven shear equations were selected to examine their accuracy in predicting masonry shear strength. Of the seven predictive equations, there were four equations currently prescribed by codes and the remaining three were proposed formulations which used different functional forms for the effect of various parameters on masonry shear strength. It was found that the NEHPR shear expression provides the closest shear prediction for both the fully and partially grouted masonry walls. However, the NEHPR shear expression does not address masonry shear strength within potential plastic hinge zone. Also, the use of $0.5\rho_h f_{yh}$ in its v_s term is contrary to well established split beam theory. Consequently, a new shear equation was developed in this study.

It was shown that the newly developed shear equation provided significant improved masonry shear prediction than the NZS 4230:1990 shear expression. It was also shown that shear prediction using the newly developed shear equation produced results with similar accuracy to that of NEHPR. Consequently, it is recommended that this shear equation to be implemented into the New Zealand masonry design standard.

Disclaimer

This report was prepared for the Department of Civil and Environmental Engineering at the University of Auckland, New Zealand. The opinions and conclusions presented herein are those of the authors, and do not necessarily reflect those of the University of Auckland or any of the sponsoring parties to this project.

Acknowledgements

The authors greatly appreciate the financial support provided by the Earthquake Commission (EQC). Thanks also go to Firth Industries Ltd., W. Stevenson and Sons Ltd., and Ready Mix Concrete Ltd. for donating the necessary masonry block units, grout and man power in the construction of masonry walls. Their contributions are gratefully appreciated. The authors also like to thank the contribution by Pacific Steel in providing the necessary reinforcing steel for this project. Thanks also go to Hank Moor and Tony Daligan for providing assistance in setting up the test specimens. Finally, thanks go to Associate Professor Guido Magenes of the University of Pavia, for his advises in developing the new masonry shear equation.

Table of Contents

Summary	i
Disclaimer	ii
Acknowledgements	iii
Table of Contents	iv
List of Figures	xi
List of Tables	xvii
List of Symbols	xviii

Chapter 1 General Introduction

1.1 Introduction	1-1
1.2 Advantage of Structural Masonry	1-2
1.2.1 Cost	1-3
1.2.2 Durability	1-3
1.2.3 Sound Insulation.....	1-3
1.2.4 Ease of Combination with other Materials.....	1-4
1.2.5 Thermal Insulation	1-4
1.2.6 Speed of Erection	1-4
1.2.7 Aesthetics	1-5
1.3 Common New Zealand Masonry Construction.....	1-5
1.4 Scope of Study.....	1-6

Chapter 2 Literature Review

2.1 Introduction	2-1
2.2 Failure of Shear Walls	2-2
2.2.1 Flexural Failure	2-2
2.2.2 Sliding Failure	2-3
2.2.3 Shear Failure	2-4
2.3 Flexural Resistance.....	2-4

2.4	Shear Resistance.....	2-6
2.4.1	Unreinforced Masonry Walls.....	2-7
2.4.2	Reinforced Masonry Walls	2-8
2.5	Initiation of Diagonal Cracking.....	2-11
2.6	Compilation of Past Research	2-12
2.6.1	Past Research in New Zealand.....	2-12
2.6.2	Past Research Overseas.....	2-18
2.7	Conclusions	2-33
2.8	Code Recommendation	2-34
	Uniform Building Code.....	2-34
	NEHPR.....	2-35
	Australian Masonry Design Standard	2-36
	New Zealand Masonry Design Standard.....	2-37

Chapter 3 Test Programme

3.1	Introduction	3-1
3.2	Test Set-up	3-2
3.3	Construction Materials	3-5
3.3.1	Concrete Masonry Block.....	3-5
3.3.2	Mortar and Grout.....	3-6
3.3.3	Reinforcing Steel.....	3-6
3.4	Unit Reinforcing Details	3-6
3.5	Instrumentations	3-9
3.5.1	Installation of Instrumentation	3-10
3.6	Material Properties	3-10
3.6.1	Reinforcing Steel.....	3-11
3.6.2	Mortar and Grout.....	3-11
3.6.3	Prisms.....	3-12
3.7	Prediction of Wall Strength.....	3-13
3.8	Testing Procedure.....	3-14
3.8.1	Miscellaneous.....	3-15
3.9	Data Reduction	3-16

Chapter 4 Experimental Results

4.1	Wall 1	4-1
4.2	Wall 2	4-4
4.3	Wall 3	4-6
4.4	Wall 4	4-8
4.5	Wall 5	4-10
4.6	Wall 6	4-12
4.7	Wall 7	4-14
4.8	Wall 8	4-16
4.9	Wall 9	4-18
4.10	Wall 10	4-20

Chapter 5 Comparison of Tested Wall Behaviour

5.1	Introduction	5-1
5.2	Force-displacement Envelope	5-3
5.2.1	Effect of Horizontal Reinforcement	5-3
5.2.2	Effect of Axial Compression Stresses	5-5
5.2.3	Partial Grouting	5-6
5.2.4	Effect of Wall H/L Ratio	5-7
5.2.5	Masonry Compressive Strength	5-9
5.3	Stiffness Degradation	5-9
5.3.1	Effect of Horizontal Reinforcement	5-10
5.3.2	Effect of Axial Compression Stresses	5-10
5.3.3	Partial Grouting	5-11
5.3.4	Effect of Wall H/L Ratio	5-11

Chapter 6 Comparison of Available Test Results

6.1	Introduction	6-1
6.2	Correlation of Predictive Equations	6-1
6.3	Fully Grouted Walls	6-4
6.3.1	Experimental Data Sets	6-4
6.3.2	Correlation between Predicted and Measured Response	6-6
6.3.3	Analysis of Data	6-18

6.4	Partially Grouted Walls	6-20
6.4.1	Experimental Data Sets	6-20
6.4.2	Correlation between Predicted and Measured Response	6-21
6.4.3	Analysis of Data	6-30

Chapter 7 Shear Equation Improvement

7.1	New Shear Equation	7-1
7.1.1	Modification of V_m	7-1
7.1.2	Modification of V_s	7-3
7.1.3	Modification of V_p	7-4
7.2	Correlation between Predicted and Measured Strength	7-5
7.2.1	Fully Grouted Walls	7-6
7.2.2	Partially Grouted Walls	7-8

Chapter 8 Conclusion

8.1	Summary of Findings	8-1
8.1.1	Experimental Results	8-1
8.1.2	Masonry Shear Equation	8-2
8.2	Recommendation for Future Research	8-3

Chapter 9 References

Appendix A – Experimental Results: Series A

A.1	Test Set-up	A-1
A.2	Testing Procedure	A-2
A.3	Material Properties	A-3
A.4	Experimental Results	A-3
A.4.1	Wall A1	A-3
A.4.2	Wall A2	A-5
A.5	Conclusion	A-7

Appendix B - Experimental Results: Series B

B.1	Wall 1	B-1
	B.1.1	Pre-test.....	B-2
	B.1.2	Testing.....	B-2
	B.1.3	Summary Behaviour.....	B-8
	B.1.4	Force-displacement Envelope	B-9
	B.1.5	Panel Displacement Components.....	B-10
	B.1.6	Stiffness Degradation.....	B-11
B.2	Wall 2	B-13
	B.2.1	Pre-test.....	B-13
	B.2.2	Testing.....	B-14
	B.2.3	Summary Behaviour.....	B-19
	B.2.4	Force-displacement Envelope	B-20
	B.2.5	Panel Displacement Components.....	B-20
	B.2.6	Stiffness Degradation.....	B-21
B.3	Wall 3	B-23
	B.3.1	Pre-test.....	B-23
	B.3.2	Testing.....	B-24
	B.3.3	Summary Behaviour.....	B-30
	B.3.4	Force-displacement Envelope	B-31
	B.3.5	Panel Displacement Components.....	B-31
	B.3.6	Stiffness Degradation.....	B-32
B.4	Wall 4	B-34
	B.4.1	Pre-test.....	B-35
	B.4.2	Testing.....	B-35
	B.4.3	Summary Behaviour.....	B-41
	B.4.4	Force-displacement Envelope	B-42
	B.4.5	Panel Displacement Components.....	B-43
	B.4.6	Stiffness Degradation.....	B-43
B.5	Wall 5	B-45
	B.5.1	Pre-test.....	B-46
	B.5.2	Testing.....	B-46
	B.5.3	Summary Behaviour.....	B-52

B.5.4	Force-displacement Envelope	B-53
B.5.5	Panel Displacement Components.....	B-53
B.5.6	Stiffness Degradation	B-54
B.6	Wall 6	B-56
B.6.1	Pre-test.....	B-57
B.6.2	Testing.....	B-57
B.6.3	Summary Behaviour.....	B-63
B.6.4	Force-displacement Envelope	B-64
B.6.5	Panel Displacement Components.....	B-65
B.6.6	Stiffness Degradation	B-66
B.7	Wall 7	B-68
B.7.1	Pre-test.....	B-69
B.7.2	Testing.....	B-69
B.7.3	Summary Behaviour.....	B-77
B.7.4	Force-displacement Envelope	B-78
B.7.5	Panel Displacement Components.....	B-78
B.7.6	Stiffness Degradation	B-79
B.7.7	Axial Compression Force.....	B-80
B.8	Wall 8	B-82
B.8.1	Pre-test.....	B-83
B.8.2	Testing.....	B-83
B.8.3	Summary Behaviour.....	B-87
B.8.4	Force-displacement Envelope	B-88
B.8.5	Panel Displacement Components.....	B-89
B.8.6	Stiffness Degradation	B-90
B.8.7	Axial Compression Force.....	B-91

Appendix C - Additional Experimental Testing: Series C

C.1	Wall 9	C-1
C.1.1	Pre-test and Testing Procedure.....	C-3
C.1.2	Testing.....	C-3
C.1.3	Summary Behaviour.....	C-10
C.1.4	Force-displacement Envelope	C-11

C.1.5	Panel Displacement Components.....	C-12
C.1.6	Stiffness Degradation.....	C-13
C.1.7	Axial Compression Force.....	C-14
C.2	Wall 10	C-16
C.2.1	Pre-test.....	C-18
C.2.2	Testing.....	C-18
C.2.3	Summary Behaviour.....	C-23
C.2.4	Force-displacement Envelope	C-24
C.2.5	Panel Displacement Components.....	C-25
C.2.6	Stiffness Degradation.....	C-26
C.2.7	Axial Compression Force.....	C-27

Appendix D - Shear Displacement ComponentD-1

Appendix E - Properties of Available Wall Tests

Fully Grouted Walls	E-1
Partially Grouted Walls	E-3

Appendix F – Material Properties..... F-1

Appendix G - Photos..... G-1

List of Figures

Figure 1.1 Common forms of masonry construction in New Zealand .	1-5
Figure 2.1 Typical perforated shear wall and crack patterns after earthquake loading.	2-2
Figure 2.2 Reinforced masonry shear wall failure modes.	2-3
Figure 2.3 Idealised flexural strain and stress.	2-5
Figure 2.4 Modes of shear failure.	2-7
Figure 2.5 Failure criteria for unreinforced masonry shear walls	2-8
Figure 2.6 Role of reinforcement in resisting masonry shear failure.	2-9
Figure 2.7 Shear carries by dowel action	2-10
Figure 2.8 Aggregate interlocking across through crack	2-11
Figure 2.9 Principal stresses acting on masonry.	2-11
Figure 2.10 Reinforcement details of nominally reinforced masonry wall.	2-14
Figure 2.11 Crack develops at low axial compressive stress.	2-15
Figure 2.12 Cracks develop in the bricks during diagonal tension failure.	2-16
Figure 2.13 Reinforcing details for concrete masonry wall.	2-17
Figure 2.14 Sliding shear failure.	2-21
Figure 2.15 Typical tests set-up.	2-31
Figure 2.16 Test set-up to determine the shear strength of bed joint.	2-31
Figure 2.17 Loading and support arrangement.	2-32
Figure 2.18 Effective area for shear	2-38
Figure 3.1 Typical test set-up	3-3
Figure 3.2 Details of concrete footing.	3-4
Figure 3.3 15-Series concrete masonry units.	3-5
Figure 3.4 Hooked horizontal reinforcement around the vertical reinforcement.	3-6
Figure 3.5 Series B, wall reinforcing details.	3-8
Figure 3.6 Series C, wall reinforcing details.	3-9
Figure 3.7 Portal displacement transducer.	3-10
Figure 3.8 Instrumentation for test wall.	3-11
Figure 3.9 Stress-strain curve for D20 reinforcing bars.	3-12
Figure 3.10 Imposed displacement history.	3-14
Figure 3.11 Nominal yield displacement.	3-15
Figure 3.12 Rocking displacement	3-17

Figure 3.13 Flexural displacement.....	3-17
Figure 4.1 Force-displacement history for Wall 1.....	4-3
Figure 4.2 Wall 1 cracking pattern at end of testing.....	4-3
Figure 4.3 Force-displacement history for Wall 2.....	4-5
Figure 4.4 Wall 2 cracking pattern at end of testing.....	4-5
Figure 4.5 Force-displacement history for Wall 3.....	4-7
Figure 4.6 Wall 3 cracking pattern at end of testing.....	4-7
Figure 4.7 Force-displacement history for Wall 4.....	4-9
Figure 4.8 Wall 4 cracking pattern at end of testing.....	4-9
Figure 4.9 Force-displacement history for Wall 5 ($F_n = 229$ kN).....	4-11
Figure 4.10 Wall 5 cracking pattern at end of testing.....	4-11
Figure 4.11 Force-displacement history for Wall 6 ($F_n = 142$ kN).....	4-13
Figure 4.12 Wall 6 cracking pattern at end of testing.....	4-13
Figure 4.13 Force-displacement history for Wall 7.....	4-15
Figure 4.14 Wall 7 cracking pattern at end of testing.....	4-15
Figure 4.15 Force-displacement history for Wall 8.....	4-17
Figure 4.16 Wall 8 cracking pattern at end of testing.....	4-17
Figure 4.17 Force-displacement history for Wall 9.....	4-19
Figure 4.18 Wall 9 cracking pattern at end of testing.....	4-19
Figure 4.19 Force-displacement history for Wall 10.....	4-21
Figure 4.20 Wall 10 cracking pattern at end of testing.....	4-21
Figure 5.1 Effect of horizontal reinforcement on masonry shear strength.	5-3
Figure 5.2 Force-displacement envelopes normalised with V_{max}	5-4
Figure 5.3 Effect of axial compression stress on masonry shear strength.	5-5
Figure 5.4 Effect of grouting on masonry shear strength.	5-6
Figure 5.5 Effect of grouting on force-displacement envelope.	5-7
Figure 5.6 Effect of H/L on masonry shear strength.	5-8
Figure 5.7 The relationship of $v_n / \sqrt{f'_m}$ vs H/L ratio.....	5-9
Figure 5.8 Effect of horizontal reinforcement on stiffness degradation.	5-10
Figure 5.9 Effect of axial compression stress on stiffness degradation.....	5-11
Figure 5.10 Effect of grouting on stiffness degradation.	5-11
Figure 5.11 Effect of H/L on stiffness degradation.	5-12
Figure 6.1 Comparison of shear formulae.	6-3

Figure 6.2 Comparison of shear formulae.	6-3
Figure 6.3 Comparison of shear formulae.	6-4
Figure 6.4 Experimental results versus prediction by NZS4230:1990.	6-12
Figure 6.5 Experimental results versus prediction by AS3700.	6-13
Figure 6.6 Experimental results versus prediction by NEHPR.	6-14
Figure 6.7 Experimental results versus prediction by UBC.	6-15
Figure 6.8 Experimental results versus prediction by Matsumura.	6-15
Figure 6.9 Experimental results versus prediction by Shing et al.	6-16
Figure 6.10 Experimental results versus prediction by Anderson and Priestley.	6-17
Figure 6.11 Experimental results versus prediction by NZS4230:1990.	6-25
Figure 6.12 Experimental results versus prediction by AS3700.	6-26
Figure 6.13 Experimental results versus prediction by NEHPR.	6-27
Figure 6.14 Experimental results versus prediction by UBC.	6-28
Figure 6.15 Experimental results versus prediction by Matsumura.	6-28
Figure 6.16 Experimental results versus prediction by Shing et al.	6-29
Figure 6.17 Experimental results versus prediction by Anderson and Priestley.	6-30
Figure 7.1 Relationship between ductility and masonry shear resisting mechanism.	7-2
Figure 7.2 Contribution of axial force to masonry shear strength.	7-5
Figure 7.3 Experimental results versus prediction by Equation 7-4.	7-8
Figure 7.4 Experimental results of partially grouted walls vs prediction by Equation 7-4. ...	7-9
Figure A.1 Series A, test set-up.	A-1
Figure A.2 Reinforcement details of masonry walls in Series A.	A-1
Figure A.3 Test procedure.	A-2
Figure A.4 Force-displacement behaviour for Wall A1.	A-4
Figure A.5 Structural damage at the bond beam accompanied by diagonal cracks after ductility 1 displacement.	A-5
Figure A.6 Force-displacement behaviour for Wall A2.	A-6
Figure A.7 Structural damage at bond beam causing significant steel channel-masonry wall slippage.	A-6
Figure B.1.1 Wall 1 reinforcement details.	B-2
Figure B.1.2 Force-displacement behaviour for Wall 1.	B-9
Figure B.1.3 Force-displacement envelope of Wall 1.	B-10
Figure B.1.4 Components of displacement.	B-11

Figure B.1.5 Stiffness vs lateral force.....	B-12
Figure B.1.6 Stiffness vs lateral displacement.....	B-12
Figure B.2.1 Wall 2 reinforcement details.....	B-13
Figure B.2.2 Force-displacement history of Wall 2.....	B-19
Figure B.2.3 Force-displacement envelope for Wall 2.....	B-20
Figure B.2.4 Components of displacement.....	B-21
Figure B.2.5 Stiffness vs lateral force.....	B-22
Figure B.2.6 Stiffness vs lateral displacement.....	B-22
Figure B.3.1 Wall 3 reinforcement details.....	B-23
Figure B.3.2 Force-displacement behaviour for Wall 3.	B-30
Figure B.3.3 Force-displacement envelope of Wall 3.	B-31
Figure B.3.4 Components of displacement.....	B-32
Figure B.3.5 Stiffness vs lateral force.....	B-33
Figure B.3.6 Stiffness vs lateral displacement.....	B-33
Figure B.4.1 Wall 4 reinforcement details.....	B-34
Figure B.4.2 Force-displacement history of Wall 4.....	B-41
Figure B.4.3 Force-displacement envelope of Wall 4.	B-42
Figure B.4.4 Components of displacement.....	B-43
Figure B.4.5 Stiffness vs lateral force.....	B-44
Figure B.4.6 Stiffness vs lateral displacement.....	B-44
Figure B.5.1 Wall 5 construction details.	B-45
Figure B.5.2 Force-displacement behaviour of Wall 5.....	B-52
Figure B.5.3 Force-displacement envelope of Wall 5.	B-53
Figure B.5.4 Components of displacement.....	B-54
Figure B.5.5 Stiffness vs lateral force.....	B-55
Figure B.5.6 Stiffness vs lateral displacement.....	B-55
Figure B.6.1 Wall 6 construction details.	B-56
Figure B.6.2 Force-displacement behaviour of Wall 6.....	B-64
Figure B.6.3 Force-displacement envelope of Wall 6.	B-65
Figure B.6.4 Components of displacement.....	B-66
Figure B.6.5 Stiffness vs lateral force.....	B-67
Figure B.6.6 Stiffness vs lateral displacement.....	B-67
Figure B.7.1 Wall 7 construction details.	B-69

Figure B.7.2 Test set-up for Wall 7. B-70

Figure B.7.3 Force-displacement behaviour of Wall 7..... B-77

Figure B.7.4 Force-displacement envelope of Wall 7. B-78

Figure B.7.5 Components of displacement..... B-79

Figure B.7.6 Stiffness vs lateral force..... B-80

Figure B.7.7 Stiffness vs lateral displacement..... B-80

Figure B.7.8 Axial compression force history..... B-81

Figure B.8.1 Wall 8 reinforcement details..... B-82

Figure B.8.2 Force-displacement behaviour for Wall 8. B-88

Figure B.8.3 Force-displacement envelope of Wall 8. B-89

Figure B.8.4 Components of displacement..... B-90

Figure B.8.5 Stiffness vs lateral force..... B-91

Figure B.8.6 Stiffness vs lateral displacement..... B-91

Figure B.8.7 Axial compression force history..... B-92

Figure C.1.1 Wall 9 construction details. C-2

Figure C.1.2 Imposed displacement history. C-3

Figure C.1.2 Force-displacement behaviour for Wall 9. C-11

Figure C.1.3 Force-displacement envelope of Wall 9. C-12

Figure C.1.4 Components of displacement..... C-13

Figure C.1.5 Stiffness vs lateral force..... C-14

Figure C.1.6 Stiffness vs lateral displacement..... C-14

Figure C.1.7 Axial compression force history..... C-15

Figure C.2.1 Wall 10 construction details. C-16

Figure C.2.2 Test set-up for Wall 10 C-16

Figure C.2.3 Force-displacement behaviour for Wall 10. C-24

Figure C.2.4 Force-displacement envelope of Wall 10. C-25

Figure C.2.5 Components of displacement..... C-26

Figure C.2.6 Stiffness vs lateral force..... C-27

Figure C.2.7 Stiffness vs lateral displacement..... C-27

Figure C.2.8 Axial compression force history..... C-28

Figure D.1 Wall panel section. D-1

Figure D.2 Nodal displacement of a panel section. D-2

Figure D.3 Components of panel deformation. D-3

Figure F.1 Stress-strain curve for the threaded and unthreaded D20 reinforcing bars..... F-2
Figure G.1 Wall 10 cracking pattern..G-2

List of Tables

Table 3.1 Masonry wall reinforcement details	3-7
Table 3.2 Prediction of wall strengths, based upon measured material properties.....	3-13
Table 5.1 Summary of test results	5-2
Table 6.1 Masonry shear strength expressions	6-2
Table 6.2 Measured and predicted strength of fully grouted masonry walls.....	6-7
Table 6.3 Mean (x_m), standard deviation (s_d) for v_{max}/v_n	6-18
Table 6.4 Measured and predicted strength of partially grouted masonry walls	6-22
Table 6.5 Mean (x_m), standard deviation (s_d) for v_{max}/v_n	6-31
Table 7.1 Shear prediction of fully grouted masonry walls using Equation 7-4	7-7
Table 7.2 Shear prediction of partially grouted masonry walls using Equation 7-4	7-9
Table A.1 Wall A1, strength prediction.....	A-3
Table A.2 Wall A2, strength prediction.....	A-5
Table B.1.1 Wall strength predictions	B-2
Table B.2.1 Wall strength predictions	B-13
Table B.3.1 Wall strength predictions	B-23
Table B.4.1 Combinations of shear reinforcement	B-34
Table B.4.2 Wall strength predictions	B-35
Table B.5.1 Wall strength predictions	B-45
Table B.6.1 Wall strength predictions	B-57
Table B.7.1 Wall strength predictions	B-69
Table B.8.1 Wall strength predictions	B-83
Table C.1.1 Wall strength predictions	C-2
Table C.2.1 Wall strength predictions	C-18
Table E.1 Properties of specimens, fully grouted.....	E-1
Table E.2 Properties of specimens, partially grouted	E-3
Table F.1 Series B and C, mortar and grout strength	F-1
Table F.2 Yield strength of reinforcing steel.....	F-1

List of Symbols

a	=	depth of compression
A_h	=	area of single horizontal reinforcing steel
A_n	=	net cross-sectional area
A_s	=	area of vertical reinforcing steel
b	=	width of compressive stress block
b_f	=	maximum width of ungrouted flue
C	=	compression force
C_d	=	nominal shear strength coefficient
D_{eff}	=	effective depth of section
d	=	distance from end of wall to the extreme wall vertical reinforcement
d'	=	distance between wall edge and outermost wall vertical reinforcing steel
d_b	=	diameter of reinforcing steel
F_n	=	nominal flexural strength
f'_{cb}	=	compressive strength of masonry unit
f'_g	=	compressive strength of grout
f'_j	=	compressive strength of mortar
f'_m	=	masonry compressive strength
f_{vr}	=	masonry shear stress
f_{yh}	=	yield strength of horizontal reinforcing steel
f_{yv}	=	yield strength of vertical reinforcing steel
H	=	wall height
h_e	=	effective height
jd	=	level arm
k	=	ductility reduction factor
k_p	=	coefficient of the effect of flexural reinforcement
k_u	=	reduction factor
L_{dh}	=	development length of shear reinforcement
M_n	=	nominal bending moment
M/V_d	=	shear span ratio

N	=	axial compressive load
s_h	=	Spacing of horizontal reinforcement
T	=	Tension force in reinforcing steel
t	=	thickness of masonry wall
U_b	=	flexure displacement
U_r	=	Rocking displacement
U_s	=	shear displacement
V_m	=	shear strength provided by masonry
V_{max}	=	maximum lateral strength recorded during testing in positive direction
V_{min}	=	maximum lateral strength recorded during testing in negative direction
V_n	=	nominal shear strength
V_p	=	shear strength provided by axial compressive load
V_s	=	shear strength provided by shear reinforcement
W_t	=	wall self weight
x	=	depth of masonry block unit
y	=	width of masonry block unit
Δ_y	=	nominal yield displacement
α	=	parameter for compressive stress block
β	=	parameter for compressive stress block
δ	=	factor concerning loading method
ϵ_s	=	reinforcing steel strain
φ	=	wall section curvature
ϕ	=	strength reduction factor
ℓ_w	=	wall length
μ	=	ductility level
μ_f	=	coefficient of internal friction
μ^*	=	Reduced coefficient of friction
ρ_h	=	horizontal reinforcement ratio
ρ_v	=	Vertical reinforcement ratio
σ_n	=	axial compressive stress
τ_m	=	shear stress
τ_o	=	shear bond strength

- τ_o^* = Reduced cohesion
- τ'_{tb} = masonry tensile strength
- θ = wall section rotation

Chapter 1

General Introduction

1.1 Introduction

For many decades, masonry has been used as a common structural material in a large proportion of all New Zealand building projects. While some traditional materials, such as stone, are rarely used today, masonry block now provides a rapid and economical method of producing structures of a few stories high. However, since 1931 several generations of New Zealand engineers have been brought up on the ‘lesson’ of the 1931 Napier earthquake (Scott, 1999) which, like many others throughout the world before and since, highlighted the extreme vulnerability of unreinforced masonry systems to seismic attack. Consequently, New Zealand was amongst the first countries to develop reinforced masonry seismic design procedures based on the principle of capacity design (Priestley, 1980), which requires the dependable shear strength to exceed the maximum lateral loading necessary to develop the wall flexural overstrength. It is therefore necessary to accurately account for the shear strength provided by masonry in order to satisfy the capacity design philosophy and provide a cost effective design solution.

There is general consensus within New Zealand that the existing masonry design standard, NZS4230:1990, is overly conservative in its treatment of masonry shear strength, restricting cost-effective masonry design. The commentary to the current New Zealand Standard for the Design of Masonry structures (NZS4230:Part2:1990) notes in clause C7.3.1.6 that “tests on masonry walls of both brick reinforced cavity masonry and concrete reinforced hollow unit masonry have indicated that properly designed and detailed masonry shear walls can sustain average shear stresses well in excess of 2.0 MPa, while exhibiting a ductile flexural failure mode. It is now considered that the limits placed on the total shear stress in NZS4230P:1985 were unduly conservative”. Similar comments regarding uncertainty of the shear strength

provided by masonry due to the lack of data are made in clause C7.3.2.1 related to shear and axial compression, C7.3.2.2 related to shear and axial tension, C7.3.3 related to shear strength of prestressed masonry, and C7.5.2 related to masonry shear strength in potential plastic hinge zones. At the time NZS4230:1990 was released there was a scarcity of relevant data on the shear strength of masonry. The data sources used in the preparation of the standard were published in 1980 or earlier, such that no data obtained during the last two decades has been used in the preparation of the standard.

The masonry design standard is currently being revised to accommodate changes since made to the New Zealand Loadings Standard and the New Zealand Building Code. During this revision there is an opportunity to update masonry shear strength criteria based on experimental and analytical research conducted over the last two decades. Also, there was an opportunity to conduct supplementary experimental testing at the University of Auckland to gain a greater insight into the behaviour of concrete masonry walls when subjected to shear failure under in-plane cyclic loading. In addition, this study compares results derived when using different equations to predict the maximum shear strength of reinforced concrete masonry walls under different conditions, such as different shear reinforcement ratios, shear span ratios, axial compression stresses and masonry strengths. The objective of this study was to establish criteria most suitable for inclusion in the revised New Zealand masonry design standard.

1.2 Advantage of Structural Masonry

In reinforced masonry, steel reinforcing bars are placed in the hollow cores of masonry, so that the steel can be used to resist tensile forces and flexural bending. Reinforcing steel also imparts ductility to masonry structures, where ductility can dissipates energy generated by earthquake actions. This section of the chapter describes some of the advantages of using masonry as a construction material.

1.2.1 Cost

1. In steel and concrete frame structures, masonry is usually used to form the partitions, staircase and corridor walls. In many instances, if these partitions or other walls are designed as load bearing masonry they can be made to carry the loads, dispensing with the need for columns and beams (Beck et al., 1988).
2. Masonry buildings tend to be faster to build, which could result in lower site overhead costs. In particular, masonry does not require formwork.
3. The maintenance costs of masonry are minimal.
4. A high degree of thermal and sound insulation is automatically provided for within the structural requirements of masonry buildings, therefore economical saving are made by eliminating the extra cost for installing additional insulation (Christie and Isaac, 1976).
5. The general contractor can usually construct a masonry structure by themselves, unlike the situation for some steel structures which normally require specialists or sub-contractors for the more delicate or sophisticated work. Experience shows that generally the less amount of work put out to sub-contractors, the lower the construction cost - provided the contractor is capable of constructing the masonry structures themselves (Beck et al., 1988).

1.2.2 Durability

The excellent durability of masonry gives it a great advantage. Many historical buildings and engineered structures are proof of the durability of masonry. Provided that masonry structures are properly designed and are built with competence, they should last much longer than their required life.

1.2.3 Sound Insulation

Vibrating bodies create sound. Sound is carried from the source to the receiver--the ears, by a push-pull compression and decompression wave effect. The majority of noise intrusion is by airborne sound and the best defence against this is mass--the heavier the partition, the less the noise transmitted through the medium. Masonry provides the mass required to effectively reduce the noise transmitted to a relatively low value.

1.2.4 Ease of Combination with other Materials

The main structural quality of masonry is its ability to resist compression forces. However, this does not prevent it from being used in areas where bending and tension conditions have to be resisted. In most situations, sufficient reinforcing can be provided within the masonry to overcome the problem of high tensile stresses.

1.2.5 Thermal Insulation

The good thermal property of masonry walls has long been recognised. The thermal property of masonry has become more and more critical in the attempt for conservation of energy. Masonry construction combines good thermal insulation with the ability to support heavy loads. Generally, materials with good thermal insulation properties are incapable of supporting heavy loads. Conversely, most good load supporting materials are poor insulators. Masonry is a notable exception to these general rules (Christie and Isaac, 1976)

1.2.6 Speed of Erection

This, as mentioned previously, is one of the main advantages of masonry construction. A masonry wall can be easily constructed in one day, and support a floor or beam load soon after. This can be compared with a concrete column or beam where time has to be taken to fix reinforcement, build formwork, cast concrete, cure, and finally remove the formwork. This process of constructing a reinforced concrete structure will normally consume time of more than a week.

It is commonly assumed that because the prefabricated frame of a building can be erected to a high level in a very short time, this must then result in an early completion of the whole project. Unfortunately though, a steel frame which rises rapidly to the roof level is frequently left standing and rusting while waiting for the follow-on trades to work their way through the building. Ignoring the fabrication time, it is true that a steel frame has a short site erection time. On the other hand, it should be appreciated that no other construction work can take place during the erection period. This is not the case for masonry construction, where other

trades can quickly follow on, thus achieving a faster overall construction time for the whole project (Beck et al., 1988).

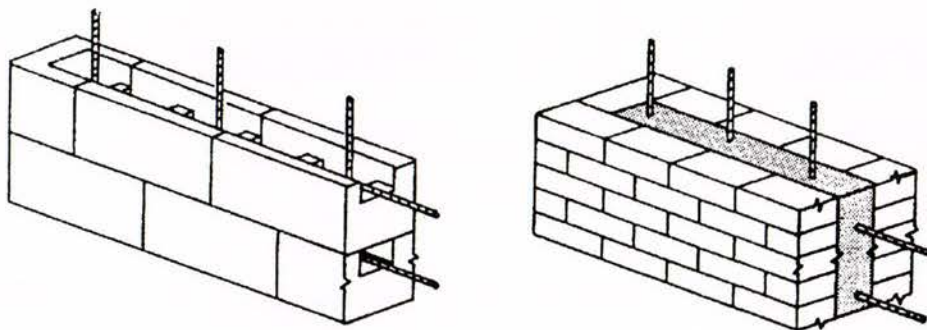
1.2.7 Aesthetics

Masonry is available in a vast range of colours and textures, and due to the small module size of masonry bricks and blocks, is extremely flexible in application where masonry can be used to form a great variety of shapes and sizes of walls, piers, arches, chimneys, etc. Masonry structures tend to wear well with time (Christie and Isaac, 1976).

1.3 Common New Zealand Masonry Construction

The two common forms of masonry construction within New Zealand are shown in Figure 1.1:

1. Hollow-block masonry consisting of vertical flues to allow vertical reinforcement and grout to be placed. Figure 1.1(a) shows masonry wall construction using bond beam units with depressed webs to facilitate placement of horizontal reinforcement and to provide a passage for grout to flow horizontally.
2. Two skins of solid masonry units (e.g. brick) are separated by a gap which is typically 50-100 mm wide. Vertical and horizontal reinforcement are then placed within the gap and subsequently grouted, see Figure 1.1(b).



(a) Reinforced hollow unit masonry.

(b) Reinforced cavity masonry.

Figure 1.1 Common forms of masonry construction in New Zealand (Paulay and Priestley, 1992).

1.4 Scope of Study

Chapter 2 of this report reviews previous studies that have attempted to establish the shear resistance of masonry walls. Chapter 3 describes the construction and loading procedure used in the testing of ten reinforced concrete masonry walls constructed of varying shear reinforcement ratios, axial compression stress levels, extent of grout filling and different H/L ratios. Chapter 4 presents experimental results and Chapter 5 investigates the effect of design parameters on these experimental results. Chapter 6 of this report compares results derived when using different equations to predict the maximum shear strength of reinforced masonry walls under different conditions, such as different shear reinforcement ratios, shear span ratios, axial compression stresses and masonry compressive strength. Experimental data currently available from both New Zealand and abroad related to the total shear strength of reinforced masonry walls were compared with these predictions. The principal objective of this study was to establish the most suitable shear strength criteria for inclusion in the revised New Zealand masonry design standard.

Chapter 2

Literature Review

2.1 Introduction

A shear wall carries in-plane horizontal loads, generated by wind or earthquake, which are distributed to the wall primarily via diaphragms such as floors or the roof. Hence, buildings in earthquake-prone regions require adequate seismic shear strength and ductility to complement their vertical load carrying capacity. With the discovery made during the 1950s that the provision of reinforcement provided some ductility to normally brittle masonry, reinforced masonry became a popular and relatively inexpensive means to resist seismic loads in New Zealand.

Observations from multi-storey buildings damaged in past earthquakes revealed that piers are the most vulnerable elements of buildings that use perforated shear walls as the load carrying system, see Figure 2.1 (Sucuoglu and McNiven, 1991). Section 2.2 of this report summaries the possible modes of failure a wall can suffer when being loaded laterally, and section 2.3 considers the resistance mechanisms of a masonry shear wall. A comprehensive literature review has indicated that many investigations have been carried out on masonry shear wall behaviour. A large number of these were of full or model scale tests on wall panels (e.g. Priestley, 1976; Sveinsson et al., 1985, Shing et al., 1988, Matsumura, 1988; Larbi and Harris, 1990; Brammer, 1995; Brunner and Shing, 1996). Section 2.6 reviews past analytical and experimental studies that have attempted to investigate the performance of masonry shear walls subjected to lateral loads.

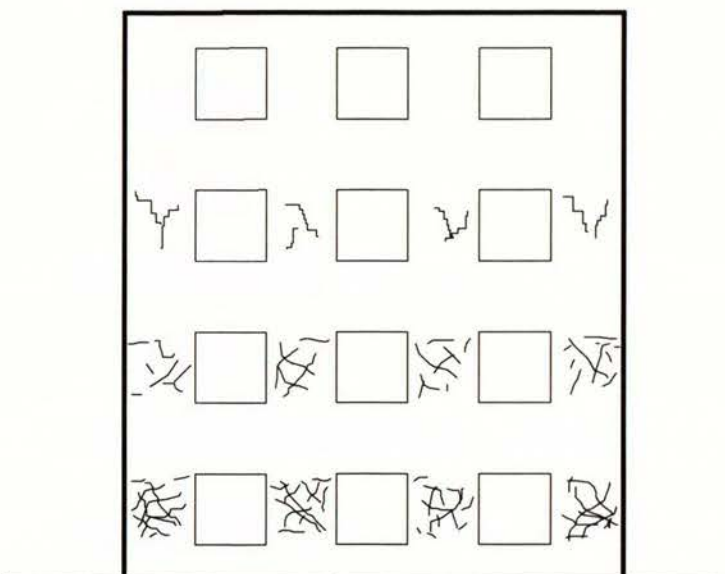


Figure 2.1 Typical perforated shear wall and crack patterns after earthquake loading.

2.2 Failure of Shear Walls

Shear walls are required to resist horizontal loads, often termed as ‘racking loads’. Excluding premature lap-splice or bond failure of reinforcement, a shear wall subject to horizontal loads may fail in one of three ways: by sliding horizontally, in flexure, or in shear (Park, 1986). The mode of failure will be influenced by many factors such as wall aspect ratios, axial compression stress levels, wall boundary conditions and the strength properties of the materials used in wall construction. These types of failure are shown diagrammatically in Figure 2.2. Therefore the name ‘shear wall’ may not be particularly representative since the dominant mode of failure of a shear wall may be other than shear.

2.2.1 Flexural Failure

This type of failure occurs due to yielding of the vertical reinforcement near the wall heel or crushing of the masonry at the wall toe when the wall behaves as a vertical cantilever. Generally this is the preferred mode, as failure is ductile and effectively dissipates energy in conjunction with reinforcement yielding.

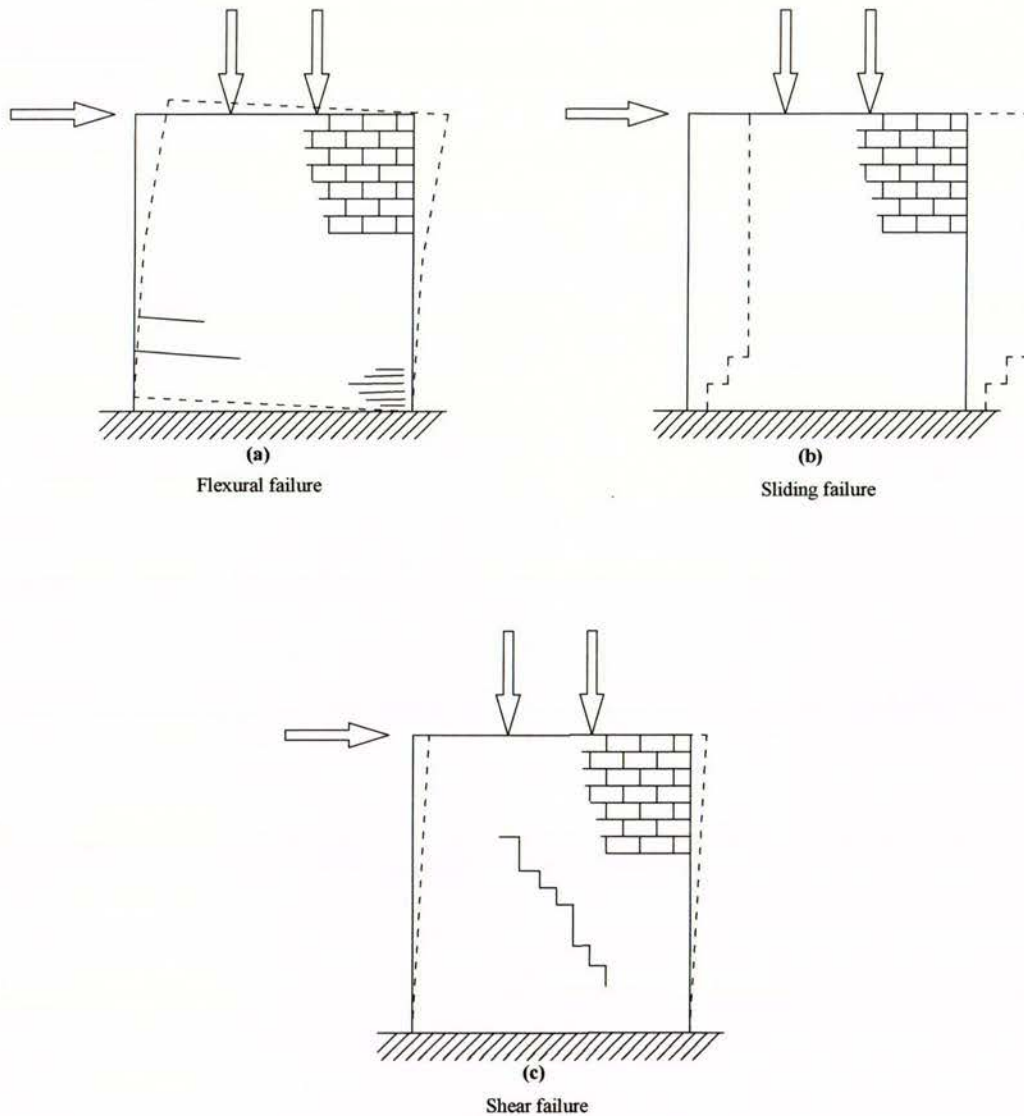


Figure 2.2 Reinforced masonry shear wall failure modes.

2.2.2 Sliding Failure

Sliding shear is the movement of entire parts of the wall on the base or other mortar bed, and is resisted by dowel action of the vertical reinforcement anchored in the base and by friction on the mortar bed (Priestley, 1976). This type of failure may become significant in any situation where there is a low friction coefficient, such as when using a friction breaker or water proof membrane, or when the wall is positioned on a smooth finished slab. This failure mode may create a problem particular in unreinforced masonry walls.

2.2.3 Shear Failure

This type of failure is characterised by the initiation of visible diagonal cracking along the shear wall when the principal tensile stresses exceed the tensile strength of the masonry under increasing imposed lateral displacements. Depending on the amount and anchorage of horizontal reinforcement, two types of shear failure are possible: a “ductile shear failure” and a “brittle shear failure” (Sveinsson et al., 1985).

Whenever there is adequate horizontal reinforcement with proper anchorage, redistribution of the stresses across the shear wall will be achieved after the initiation of diagonal cracking. Therefore the initial diagonal cracks do not open under increasing horizontal loads, but instead new sets of diagonal cracks form and gradually spread throughout the masonry wall, accompanied by high energy dissipation which results in a ductile behaviour. Failure occurs gradually in this case as the strength of masonry wall deteriorates under cyclic lateral loading. Partial crushing of the masonry at severely cracked portions of the wall diagonals finally leads to complete loss of strength. This type of failure is described as “ductile shear failure”.

When the amount and/or anchorage of the horizontal reinforcement is not adequate to transfer the tensile stresses across the diagonal cracks, these cracks open extensively and results in a major X-shaped diagonal crack pair, leading to a relatively sudden and destructive failure. This type of failure is described as “sudden shear failure”.

Although a flexural mode of failure is sought after, and sliding failure may at least partly occur in well-designed masonry shear walls, the primarily objective of this study was to consider the shear failure of masonry shear walls.

2.3 Flexural Resistance

The flexural strength of a vertically reinforced masonry shear wall is usually calculated by means of simple flexural theory, based on the assumption that plane sections remain plane after bending. The nominal flexural strength of a masonry wall can be approximately ascertained using a rectangular compression stress block with a stress level of $0.85f'_m$, and with a depth of “a”. The maximum strain, ϵ_u , allowed by the New Zealand masonry design

standard (NZS4230:1990) at the extreme compression fibre of an unconfined section is 0.0025. These assumptions are shown in Figure 2.3.

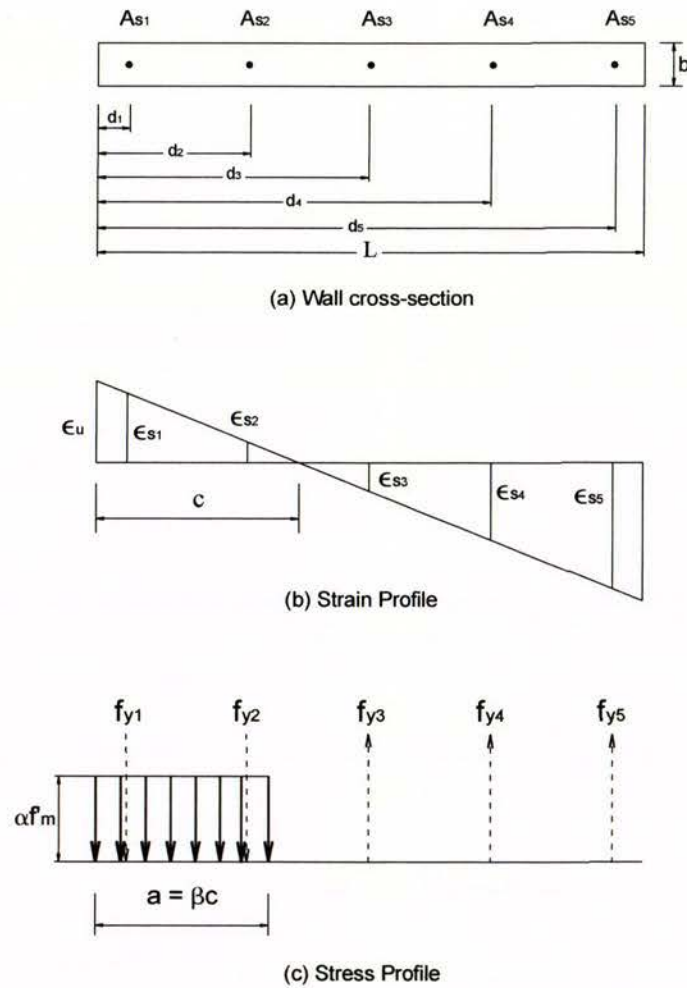


Figure 2.3 Idealised flexural strain and stress.

Based on these assumptions, the nominal moment capacity of a wall section with distributed vertical reinforcement can be evaluated by:

$$M_n = \frac{1}{2} W_t (L - a) + \sum_i^n T_i j d_i \quad (2-1)$$

$\sum_i^n T_i$ is the nominal tensile strength of the vertical reinforcement, found from:

$$\sum_i^n T_i = \sum_i^n A_{s_i} f_{y_i} \quad (2-2)$$

The compression force, C within the masonry is found by:

$$C = W_t + \sum_i^n A_{si} f_{yi} \quad (2-3)$$

and the compressive block depth is found by solving the following:

$$a = \frac{C}{0.85f'_m b} \quad (2-4)$$

Hence, substituting Equations 2-2, 2-3 and 2-4 into Equation 2-1 gives the following:

$$M_n = \frac{W_t}{2} \left(L - \frac{W_t + \sum_i^n A_{si} f_{yi}}{0.85f'_m b} \right) + \sum_i^n A_{si} f_{yi} j d_i \quad (2-5)$$

Therefore the nominal strength, F_n of a shear wall with an effective height of H_e can be expressed as:

$$F_n = \frac{\frac{W_t}{2} \left(L - \frac{W_t + \sum_i^n A_{si} f_{yi}}{0.85f'_m b} \right) + \sum_i^n A_{si} f_{yi} j d_i}{H_e} \quad (2-6)$$

2.4 Shear Resistance

During a shear failure, unreinforced masonry walls behave as brittle structural elements with limited energy dissipation capacity, especially when subjected to high compression stresses (Page., 1989, Shing et al., 1989; Sucuoglu and McNiven, 1991; Tomažević, 1999). Therefore masonry walls are frequently provided with steel reinforcement, both horizontally and vertically, in order to improve lateral resistance and ductility.

If a masonry wall is reinforced horizontally, the horizontal reinforcement prevents separation of the wall's cracked parts at shear failure, therefore improving the resistance and energy dissipation capacity of the wall when subjected to cyclic loading. In the case of unreinforced

masonry walls, a single diagonal crack causes severe deterioration in strength and subsequent brittle collapse, see Figure 2.4(a). However, if the wall is adequately reinforced horizontally, many smaller cracks will be evenly distributed over the entire surface of the wall, see Figure 2.4(b).

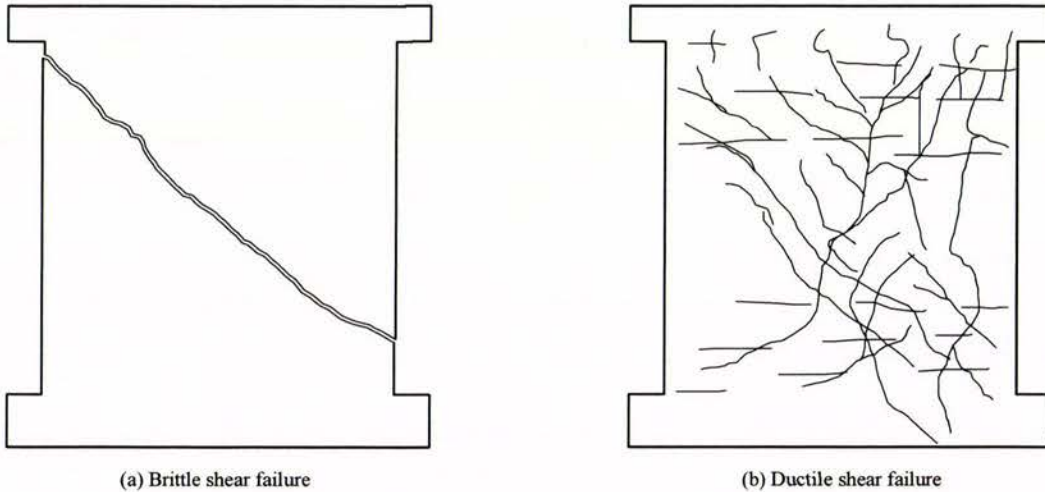


Figure 2.4 Modes of shear failure.

2.4.1 Unreinforced Masonry Walls

Researchers (e.g. Yokel and Fattal, 1976; Mann and Muller, 1982; Page, 1989) during the past decade have identified two different forms of behaviour for unreinforced masonry shear walls. For low axial compression stresses, the basic form of shear strength expression is based on the Mohr Coulomb shear friction expression, as demonstrated in Equation 2-7 below:

$$\tau_m = \tau_o + \mu_f \sigma_n \quad (2-7)$$

where τ_m and σ_n are the average shear and normal stresses, τ_o is the shear bond strength and μ_f is the coefficient of internal friction. In parametric form, Equation 2-7 can be expressed as:

$$V_n = fn(f'_m, N) \quad (2-8)$$

where V_n represents the nominal shear strength of the masonry wall and N is the axial compression force. As demonstrated from experimental studies, values for the constants τ_o

and μ_f vary considerably and are influenced by test method and type of masonry. Paulay and Priestley (1992) recommended a typical range of values of $0.1 \leq \tau_o \leq 1.5$ MPa and $0.3 \leq \mu \leq 1.2$.

When the axial compression force approaches a sufficiently large stress, the wall reaches peak strength and its behaviour changes, with failure mode including combination of shear and crushing of masonry. For even larger compression stresses, shear strength decreases as compression failure of masonry dominates response to loads. Therefore, Equation 2-7 does not apply in these cases. This compression failure corresponds to the second part of the curve shown in Figure 2.5.

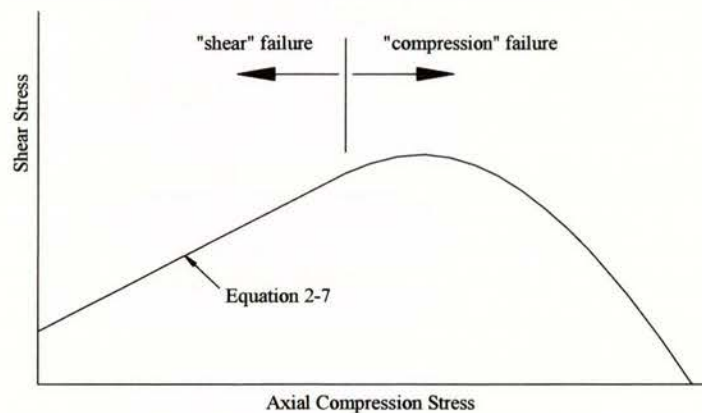


Figure 2.5 Failure criteria for unreinforced masonry shear walls (Page, 1989).

2.4.2 Reinforced Masonry Walls

For the case when masonry walls are reinforced with distributed vertical and horizontal reinforcement, the basic mechanisms of reinforcement action at shear failure are shown in Figure 2.6 (a) and (b). Past researchers (e.g. Brunner and Shing, 1996; Shing et al., 1988; Tomažević, 1999) have concluded that the shear resistance of reinforced masonry walls comes from several mechanisms, such as tension of horizontal reinforcement, dowel action of vertical reinforcement, as well as aggregate interlocking between the parts of the walls separated by diagonal cracks.

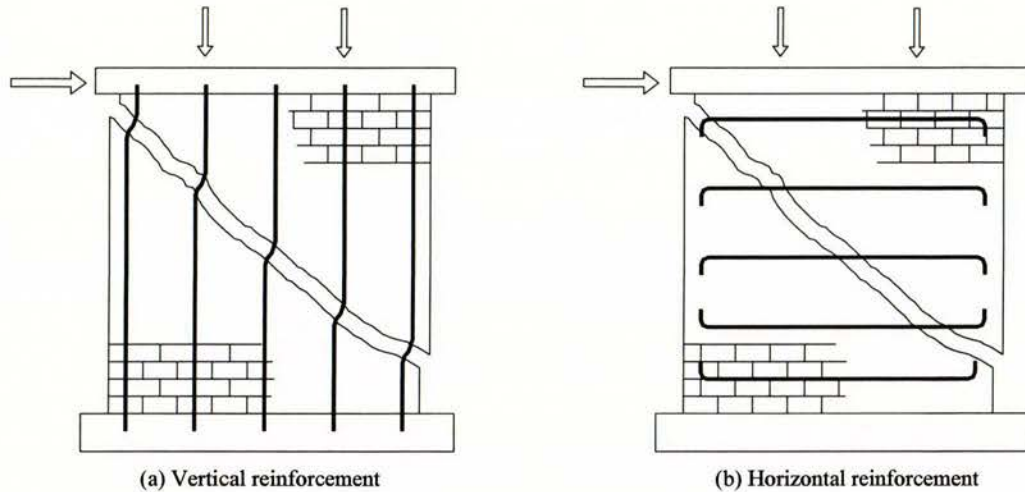


Figure 2.6 Role of reinforcement in resisting masonry shear failure.

Due to the complexity of these mechanisms, no effective theoretical models have yet been proposed to predict the shear strength of a masonry wall panel. Therefore, in practical calculation the nominal shear strength, V_n , of reinforced masonry walls is evaluated as the sum of contributions from masonry, reinforcement and applied axial compression load. The three shear resistance mechanisms are incorporated into an equation of the following form:

$$V_n = V_m + V_s + V_p \quad (2-9)$$

Where:

V_m is the contribution of masonry to shear strength;

V_s is the contribution of shear reinforcement to shear strength;

V_p is the contribution of applied axial compressive load to shear strength.

As indicated by experimental results (Shing et al., 1988; Sveinsson et al., 1985, Matsumura, 1987), masonry shear strength, V_n is strongly dependent on the masonry compressive strength, f'_m , since there is strong evidence that V_m increases with an increase in f'_m . However, the relationship is not linear, with the increase in V_m diminishing as f'_m increases. Consequently, it is acceptable that V_m increases approximately in proportion to $\sqrt{f'_m}$. Also, in the case where masonry walls are provided with vertical reinforcement, part of the shear resistance capacity can be attributed to dowel action of the vertical reinforcement. Shear forces can be transferred along a well-defined plane (e.g. a diagonal crack) by the shear,

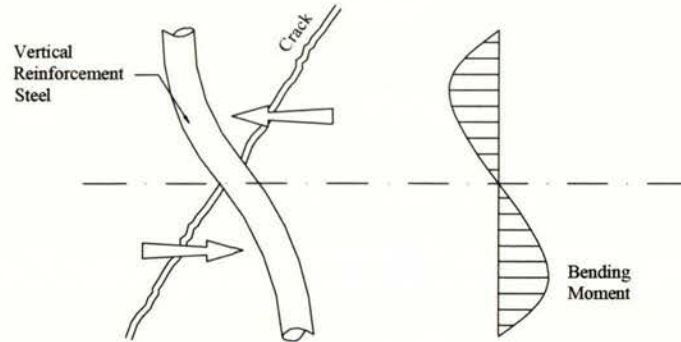


Figure 2.7 Shear carries by dowel action (Tomažević, 1999).

flexural and kinking actions which are activated locally in reinforcing bars due to their relative displacement along a crack, see Figures 2.6(a) and 2.7.

Shear reinforcement, generally in the form of horizontal steel bars, is placed at right angle to the axis of a masonry wall member (see Figure 2.6(b)) in order to provide V_s . Before diagonal cracking occurs, the horizontal reinforcement carries little force. However once diagonal cracks occur, the shear resistance is redistributed among the horizontal steel bars. When adequate shear reinforcement is provided, diagonal cracks do not open excessively but distribute evenly across the wall as shown in Figure 2.4(b).

Axial compressive load suppresses the formation of cracking in a masonry wall since the tensile stresses induced by the lateral load must first overcome the compressive field created by the axial compressive load, before diagonal cracks can initiate, see Figure 2.9 in section 2.5. In addition, axial compressive load contributes to masonry shear strength by enhancing the aggregate interlocking mechanism. When a crack is developed in a concrete mass, the surfaces of the crack are usually rough and irregular (see Figure 2.8). The majority of the coarse aggregate particles remain embedded in one of the two crack faces. When this crack forms along a continuous plane, a parallel displacement in this plane is possible and projecting particles from one face of the crack come into contact with the matrix of the other face. Further movement is then restricted by bearing and friction of the aggregate particles on the crack surface. Provided that restraint is available to prevent large increases in the crack width, substantial shear forces can be transmitted across the crack interface (Paulay and Loeber, 1974; Hendry, 1991).

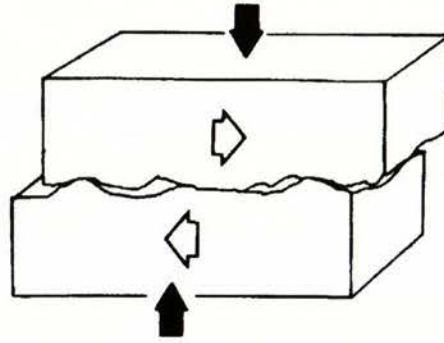


Figure 2.8 Aggregate interlocking across through crack (Hendry, 1991).

2.5 Initiation of Diagonal Cracking

The tensile strength of masonry is an important parameter in the behaviour of structural masonry elements such as shear walls, where horizontal forces will produce tension or shear stresses, or both. Initiation of diagonal cracks occur when the principal tensile stresses, p_t , exceed the tensile strength of masonry. The Mohr diagram, shown in Figure 2.9(b), is employed to evaluate the p_t and p_c (principal compression stress) under the given external loading shown in Figure 2.9(a). The principal tensile stress, p_t , can be evaluated according to Equation 2-10:

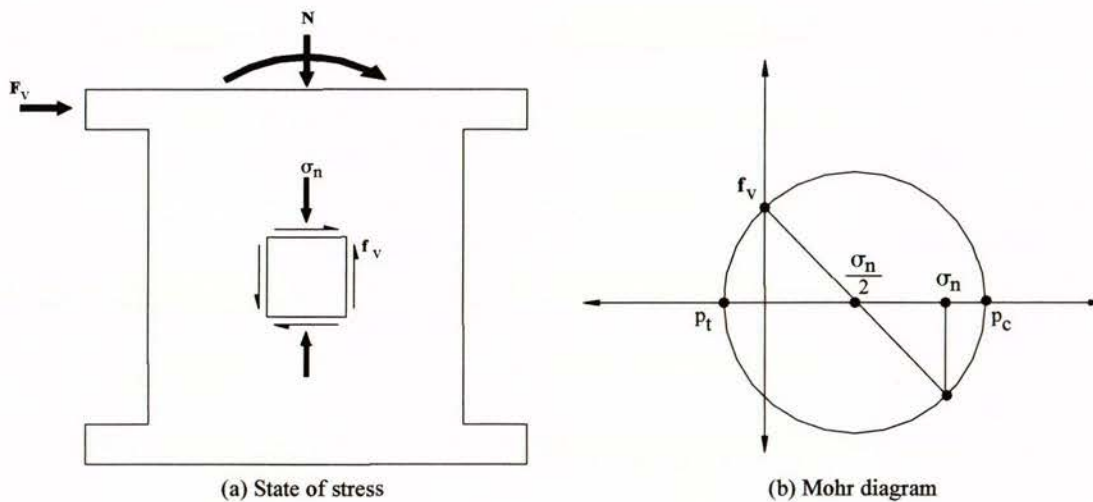


Figure 2.9 Principal stresses acting on masonry.

$$p_t = \frac{\sigma_n}{2} - \sqrt{(f_v)^2 + \left(\frac{\sigma_n}{2}\right)^2} \quad (2-10)$$

2.6 Compilation of Past Research

The data sources used in the preparation of the New Zealand masonry design standard, NZS4230:1990, were published in 1980 or earlier. However, significant research relating to masonry shear strength has been conducted in both North America and Japan since 1980. Therefore a considerable amount of additional information is now available. This section of the report reviews past experimental and analytical studies now available in the field of masonry shear strength. Research conducted within New Zealand and overseas, along with related design recommendations in the current national and international codes of practice, are discussed. Exploration is divided into three categories:

- Research conducted within New Zealand.
- Research conducted Overseas.
- Code recommendations.

Reviews are sorted by the date of publication in each category. They cover a brief description of tests performed and the main conclusions from each reference.

2.6.1 Past Research in New Zealand

Priestley (1976, 1977) conducted a comprehensive study on the cyclic behaviour of reinforced concrete masonry shear walls and established that the maximum shear stresses allowed in the former New Zealand masonry design standard, DZ4210 were unrealistically low.

A total of six heavily reinforced concrete masonry walls were subjected to cyclic shear. Aspects investigated included the influence of vertical and horizontal reinforcement ratios (0.66% and 0.45% vertical steel, 0.66% and 0.34% horizontal steel) and the magnitude of axial compression stress levels on masonry shear strength. Confinement at potential crushing areas by mortar bed confining plates was included to examine their effectiveness in enhancing the performance of masonry shear walls at high ductility levels. Two walls were subjected to axial stress levels of 0.69 MPa (100 psi) and the other four walls were not

subjected to axial stresses. Three walls had thin stainless steel confining plates installed in the bottom three mortar courses.

The maximum experimental loads were compared with theoretical and design loads. Priestley analysed the influence of base course slip and compared experimental displacement ductility with code required ductility. The author concluded the following:

1. The maximum allowance for shear stress in the former New Zealand masonry design standard, DZ4210 was unreasonably low. None of the six walls suffered diagonal shear failure, despite the experimentally obtained shear stresses being in excess of the maximum code allowable value of 0.62 MPa.
2. The test results indicated that the former (i.e. 1977) New Zealand design practice overestimated the cracked stiffness of walls by a factor of more than 2.
3. Mortar-bed confining plates did not significantly reduce stiffness degradation of the walls in this study, but substantially reduced damage to the walls at high ductility levels.

Priestley and Elder (1982) tested three slender concrete block masonry walls under cyclic reversals of in-plane displacements to examine the ductility and strength degradation of such walls. The nominal 200 mm block walls were 6100 mm high and 2440 mm long. Reinforced concrete floor slabs, approximately 1220 mm wide, were cast at the first and second floor levels and a reinforced concrete bond beam was placed at the top to distribute the lateral force and anchor the vertical reinforcement. Steel reinforcement of 16 mm diameter was placed in the vertical cells with a centre to centre spacing of 400 mm. The vertical reinforcement ratio was 0.72% for all walls. The main vertical steel was lapped to starter bars that were anchored in the foundation beam. Two of the walls were subjected to an axial stress of 1.95 MPa and one wall was subjected to an axial stress of 0.74 MPa. Confining plates were placed in the mortar beds in the compression zones of the potential plastic hinge area for one wall. The lap length of vertical reinforcing was 975 mm for two of the walls and 1310 mm for the third wall.

Results from the wall tests indicated that problems must be expected when lapping reinforcement within plastic hinge regions and that testing is needed to better define ductility of walls without lapping of vertical reinforcement in the plastic hinge region zone.

Brammer (1995) performed quasi-static in-plane cyclic load tests on twelve nominally reinforced cantilever concrete masonry walls. The main objective of this study was to compare the attained test behaviour with that assumed and predicted by the New Zealand masonry design standard, NZS4230:1990, and to investigate the response of nominally reinforced masonry when subjected to cyclic loading. Attention was given to maximum strengths, stiffness, ductility, modes of failure, force-displacement characteristics, base course slip, and also the shear and flexural components of displacement.

Nine of these walls were partially grout-filled while the remaining three were solid grout-filled. All walls were constructed to a height of 2400 mm with horizontal reinforcement placed in a bond beam within the top two block courses (see Figure 2.10), but varied in length and width (15 series and 10 series concrete masonry block). None of the twelve walls had applied axial compression load.

Due to the lack of horizontal shear reinforcement, most walls failed in diagonal tension with failure characterized by the development of early flexural cracking which was later exaggerated by diagonal cracking that extended throughout the whole masonry wall. Despite significant stiffness degradation, none of the walls suffered sudden strength loss and strengths were maintained at high ductility levels. This desirable behaviour in the nominally reinforced partially and solid grout-filled masonry walls was created by the solid filled bond beam at the top of the walls, which caused a frame-type action at the latter stage of testing.

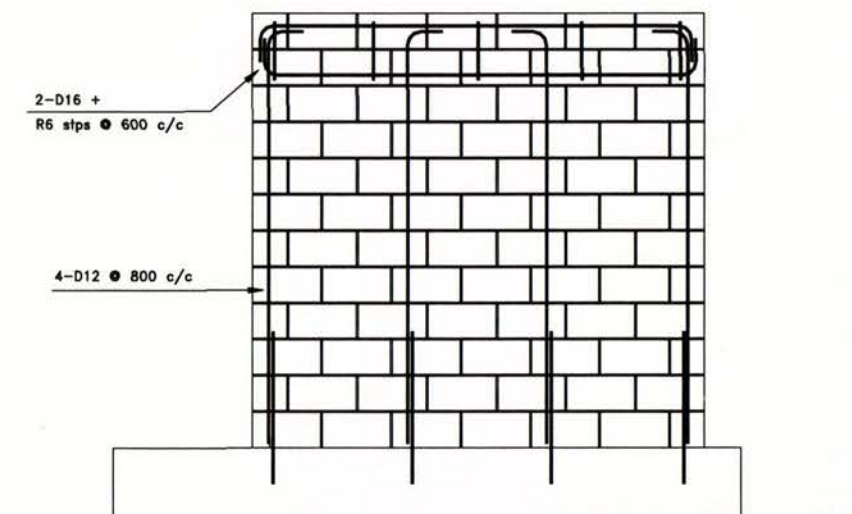


Figure 2.10 Reinforcement details of nominally reinforced masonry wall.

An important finding concluded from this study was that ductile diagonal tension mode developed even in the case when the dependable shear strength predicted by the New Zealand masonry design standard, NZS4230:1990, was less than the wall's evaluated nominal strength using Equation 2-6. This indicated that the predicted shear strength using NZS4230:1990 is of limited relevance for concrete masonry structures having a reinforcement distribution as indicated in Figure 2.10 and supporting little axial compressive load. It was concluded that this was partially because shear strength is not well predicted by the New Zealand masonry design standard, NZS4230:1990, but more importantly due to the frame action generated by the use of the bond beam shown in Figure 2.10 and the shear friction generated between blocks during lateral deformation. The information collected from this study was used to develop the bracing capacity tables presented in NZS4229:1999.

Crisafulli et al. (1995) conducted finite element analysis to determine the shear strength of unreinforced brick masonry panels. The researchers concluded that the shear strength of a masonry panel could be evaluated according to the properties of the masonry and its constitutive materials: the tensile strength of the brick, the shear strength of the mortar joints and the compressive strength of masonry. It was also concluded that three modes of failure may occur in masonry panels depending on the magnitude of axial compressive stress levels.

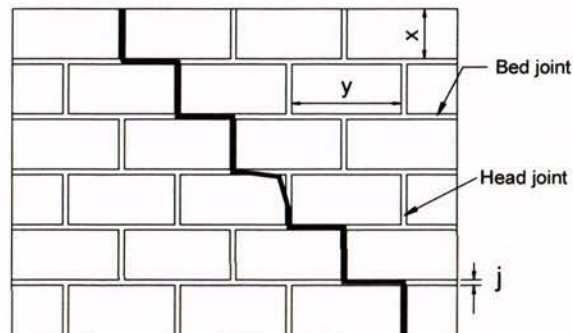


Figure 2.11 Crack develops at low axial compressive stress.

The first type of failure is caused by debonding of the mortar bed at low axial compressive stress. Cracks develop in stepped form as shown in Figure 2.11. For low axial compressive stress, the shear strength is resulted from the combination of bond strength and friction resistance between the mortar joint and bricks. Hence, shear strength is a function of normal stress at the bed joint σ_n and has the form of a Coulomb type equation:

$$\tau_m = \tau_o^* + \mu^* \sigma_n \quad (2-11)$$

$$\tau_o^* = \frac{\tau_o}{1 + 2\mu \frac{x}{y}} \quad \mu^* = \frac{\mu}{1 + 2\mu \frac{x}{y}} \quad (2-12)$$

where x and y are the height and length respectively of the brick as shown in Figure 2.11 and the stresses τ_o and σ_n are considered in absolute value.

Crisafulli et al. concluded that for medium to high axial compressive stress, a diagonal tension failure of the bricks occurs, as shown in Figure 2.12. The shear strength of the bricks increases due to the effect of compressive normal stress and cracks develop in the bricks instead of the bed joint. It is therefore assumed that failure occurs when the principal tensile stress (caused by the combined effect of compressive and shear stresses) in the brick is equal to its tensile strength, τ'_{tb} and Equation 2-13 has been proposed:

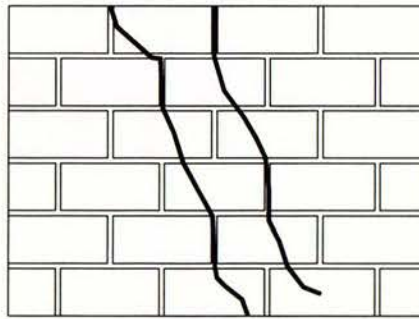


Figure 2.12 Cracks develop in the bricks during diagonal tension failure.

$$\tau_m = \frac{\tau'_{tb}}{C_s} \sqrt{1 + \frac{\sigma_n}{\tau'_{tb}}} \quad (2-13)$$

where

$$C_s = \frac{\frac{x}{j} + 1}{\frac{x}{2j} + 1} \quad (2-14)$$

Davidson (1996) extended Brammer's research to investigate the behaviour of walls with openings and an applied axial compression load of 24 kN (equivalent to an axial compressive stress of 51 kPa, based on net masonry cross-sectional area). Two nominally reinforced

concrete masonry walls (4200 mm long x 2400 mm high x 190 mm wide) were constructed using 15 series concrete masonry block so that they had an identical arrangement of a 2000 mm x 600 mm 'doorway' and a 1200 mm x 600 mm 'window' (see Figure 2.13), with the only difference being the magnitude of the applied axial compressive load. The 'doorway' and 'window' were arranged in a way to enable the vertical reinforcement to be placed at 800 mm centres.

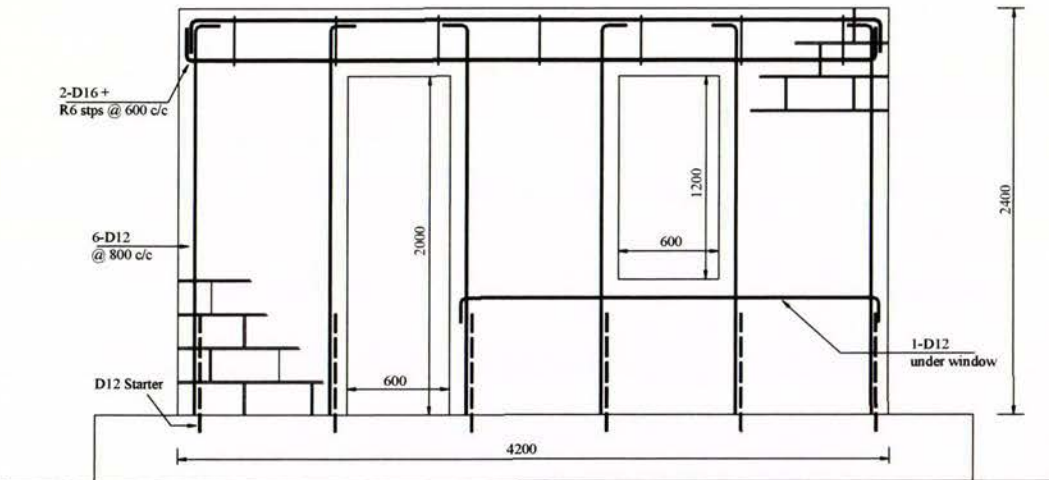


Figure 2.13 Reinforcing details for concrete masonry wall.

A comparison of test results with those obtained by Brammer illustrated that the capacities of the two walls with openings, tested by Davidson, were approximately half that of the complete wall, and that the compression stress slightly increased the lateral strength of the test wall. It was concluded from this study that openings have a detrimental effect on the lateral strength of masonry walls while axial compression stress is beneficial.

In addition to the experimental studies conducted by Brammer and Davidson at the University of Auckland, two research projects were conducted at the University of Canterbury as part of the development of NZS4229:1999. The first of these was conducted by Singh et al. (1999). The study established that ductile response could be achieved for long walls loaded out-of-plane. This study was further extended (Zhang, 1998) to investigate the performance of two walls that had door and window openings at structurally inappropriate locations. The information gathered at the University of Canterbury was used in the development of the bond beam criteria in NZS4229:1999.

Laursen and Ingham (2000a and 2000b) conducted a series of eight laboratory tests to explore the in-plane wall response of post-tensioned concrete masonry. The main variables considered in this experimental study included the wall dimensions, prestressing steel content, prestress force and types of grouting: full grouting, partial grouting and ungrouted wall.

Laursen and Ingham concluded that fully grouted unbonded post-tensioned concrete masonry is a competent material combination for ductile structural wall systems. Despite the absence of shear reinforcement, the prestressed masonry walls exhibited a near non-linear response dominated by rocking behaviour. Limited damage of the lower wall corners were observed at large displacement capacities beyond drifts of 1.4%.

It was also concluded from this study that the prestressed partially and ungrouted concrete masonry walls are vulnerable to shear dominated behaviour, which ultimately led to diagonal shear cracking failure mode. However, the tests indicated that the partially and ungrouted prestressed concrete masonry walls are capable of developing significant strength, exceeding the predicted wall flexural strength. Hence, it was concluded that the prestressed partially and ungrouted concrete masonry walls may be suitable for use in non-ductile strength design.

2.6.2 Past Research Overseas

Yokel and Fattal (1975) compared failure hypotheses with the results of 32 plain single wythe clay brick masonry walls tested in diagonal compression. Three types of masonry units designated by A, B and S were combined with two types of mortar- conventional and high strength, designated by C and H, to build four types of masonry walls, i.e. AC, AH, BH and SH (eight walls of each type).

The authors concluded the following:

1. Shear failure under diagonal compression and axial load could occur by debonding along mortar joints or splitting of the masonry units.
2. For a given type of wall, failure could occur by joint debonding under low axial load and change to unit splitting under higher axial load. Debonding strength was

characterised by a linear relationship and had the function of a Coulomb type relationship:

3. Splitting failure originated at the centre of the walls at a splitting strength governed by a critical relationship between the principal biaxial stresses.

Mayes et al. (1976a and 1976b) tested seventeen concrete block masonry double pier systems coupled with heavily reinforced top and bottom spandrels under cyclic lateral loading at the University of California at Berkeley. The pier system was allowed to rotate at the top under lateral load applied to the top spandrel.

The variables investigated in this study included:

1. The rates of loading, i.e. specimens were tested in identical pairs using a slow and fast rate of loading (0.02 Hz and 3 Hz).
2. Four types of reinforcement arrangement:
 - a) None.
 - b) Vertical end bars with two reinforcement ratios.
 - c) Vertical end bars and horizontal bars with different reinforcement ratios.
 - d) Vertical end bars, horizontal bars and toe reinforcement in the form of perforated steel plates in bed joints.
3. Three types of grouting: none, partially and fully grouted.

The authors concluded the followings at the end of the test programme:

1. Sufficient amounts of horizontal reinforcement enhance the ductility of shear mode response significantly.
2. Use of perforated steel plates in the toe area improved flexural mode response.
3. Partial grouting improves the elasto-plastic shear mode response compared with no grouting.
4. Dynamic loading increased ultimate strength for the case of shear mode failures and decreased ultimate strength for the case of flexural mode failure compared with strengths obtained from a slow rate of loading.

Hidalgo et al. (1978, 1979), Chen et al. (1978) and Sveinsson et al. (1985) conducted experiments to evaluate the seismic behaviour of window piers typical of high-rise masonry construction. Principal test parameters considered in the test programme were:

1. The type of masonry construction.
2. The height-to-width ratio.
3. The amount of horizontal reinforcement.
4. The distribution of vertical steel.
5. The effect of different types of anchorage of horizontal reinforcement (90° bend, 180° bend and end plate).
6. The level of axial stress.

Three types of masonry material were used throughout the test programme, namely hollow concrete masonry block, hollow clay brick and double wythe grouted core clay brick piers. Out of the ninety-three fixed end piers, twenty-nine of them were constructed of hollow concrete masonry blocks and subjected to cyclic in-plane loads at the Earthquake Research Centre of the University of California. The test-programme included fully and partially grouted single piers with three aspect ratios (h/ℓ_w) of 0.5, 1 and 2.

The studies concluded that the strength associated with shear mode of failure was a function of the compressive strength (f'_m) of the masonry material, the magnitude of gravity stress and of the aspect ratio of the pier. The distribution of vertical reinforcement did not significantly influence the behaviour of piers that failed in shear, and anchorage of horizontal reinforcement with 180° bends was proven to be more effective than any of the other two types of anchorage. It was also observed that the maximum shear strength was approximately the same for fully and partially grouted piers as long as the stress was based on the net area of the cross section of the wall. Among the parameters studied in the test programme, the amount of horizontal reinforcement was found to be the most influential on masonry shear strength, as discussed below.

Horizontal reinforcement was effective in inhibiting the opening of diagonal cracks, but gave diminishing returns as the amount of reinforcing steel was increased. After a certain ratio, increasing the reinforcement content had an adverse effect on the post-cracking deformation

capacity. The researchers concluded that when a specified minimum amount of horizontal reinforcement was provided and allowed to yield, a ductile shear failure could be achieved in which diagonal cracks did not open excessively but distributed evenly throughout the panel as shown in Figure 2.4(b). Higher amounts of horizontal reinforcement, on the other hand, restrained the post-cracking deformation capacity since the reinforcing steel remained in the elastic range and did not contribute much to the overall lateral deformation. The masonry wall finally reached its maximum lateral deformation capacity due to crushing of masonry at the toes, which were already damaged by the extensions of diagonal cracks. The masonry wall failed when the web slides with respect to the bottom of the spandrel as shown in Figure 2.14.

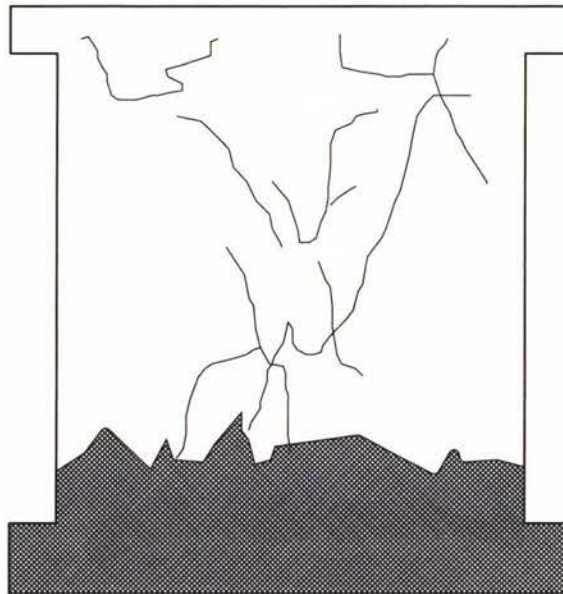


Figure 2.14 Sliding shear failure.

The findings from this test programme allowed Sucuoglu and McNiven (1991) to propose Equation 2-15 to predict the minimum required horizontal reinforcement ratio for a masonry wall that fails in the shear mode in order to exhibit a ductile post-cracking performance:

$$\rho_h = 1.41 \frac{f'_m}{f_y} \left[-\frac{1}{2} \left(\frac{\sigma_n}{f'_m} \right) + \sqrt{0.0016 + 0.0128 \left(\frac{\sigma_n}{f'_m} \right) + 0.2756 \left(\left(\frac{\sigma_n}{f'_m} \right)^2 \right)} \right] \quad (2-15)$$

where

$$\rho_h = \frac{A_h}{t.s_h} \quad (2-16)$$

Matsumura (1987, 1988 and 1990) presented an empirical formula to predict the shear strength of reinforced masonry walls subjected to in-plane lateral and axial loads, on the basis of the results of testing fifty-seven concrete masonry walls and twenty-three brick masonry walls. Specimens tested were under different conditions such as various shear reinforcement ratios, shear-span ratios, axial stresses, and strength of materials, as well as two kinds of grouting, namely, partial grouting and full grouting. About 2/3 of the experimental specimens were partially grouted, with the remainder being fully grouted.

Nominal 200 mm hollow concrete or 150 mm clay brick units were used to construct reinforced, partially grout-filled or fully grout-filled walls of varying sizes. Full size walls ranged in height from 1600 mm to 1800 mm while the lengths ranged from 790 mm (i.e. 31 in) to 2000 mm. There was a set of smaller size walls with dimensions of 610 mm to 1220 mm in height, 400 mm to 500 mm long and 100 mm and 150 mm thick. Two test set-ups were used:

1. Fifty-five full size walls were subjected to horizontal shear loads with a fixed base and the top free to move horizontally (cantilever).
2. Twenty-five of the smaller size walls were laid horizontally and subjected to vertical shear loads like the loading of a restrained deep beam.

From the test results of eighty masonry walls, Matsumura was able to conclude the following:

1. Shear strength of masonry increases nonlinearly with masonry compressive strength, f'_m . The increase in rate of masonry shear strength becomes gradually lower as f'_m increases. Consequently, it may be acceptable that masonry shear strength increases approximately in proportion to $\sqrt{f'_m}$.
2. Masonry shear strength increases in relation to the increase of horizontal shear reinforcement, while it decreases inversely in relation to the shear span ratio $\frac{M}{V.d}$.
3. Axial compressive stress is found to have a beneficial effect on masonry shear strength.

Based upon these conclusions, Matsumura developed Equation 2-17 to predict the maximum shear strength of reinforced masonry shear walls:

$$V_n = \left[k_u k_p \left(\frac{0.76}{(h/d) + 0.7} + 0.012 \right) \sqrt{f'_m} + 0.18 \gamma \delta \sqrt{\rho_h f_{yh} f'_m} + 0.2 \sigma_n \right] (0.875 t d) \quad (2-17)$$

where:

- k_u = 1.0 for fully grouted concrete masonry
0.64 for partially grouted concrete masonry
- k_p = coefficient of the effect of flexural reinforcement ratio
= $1.16 \rho_{ve}^{0.3}$
- γ = 1.0 for fully grouted concrete masonry
= 0.6 for partially grouted concrete masonry
- δ = 1.0 for loading which yields inflection point at the mid-height of wall (double bending)
= 0.6 for loading of cantilever type (single bending)

Hirashi (1985) tested nine walls to investigate the flexural behaviour of reinforced masonry walls. Of the nine walls, six were constructed using concrete block and two were constructed of hollow brick units, with the final wall being constructed of reinforced concrete. The horizontal reinforcement used was 0.29% and 1.16%. However, the nine walls had the following common identities:

1. Same geometry (i.e. $h/\ell_w = \text{constant}$),
2. Fully grouted core,
3. Constant flexural reinforcement in the end cores with confinement at critical compression zones,
4. Constant axial load, and
5. Rotational fixity of top and bottom surfaces.

From the test results, the author was able to conclude the followings:

1. Increasing the amount of horizontal reinforcement (four-fold) had no significant effect on the cracking and maximum shear strengths.
2. Increasing the amount of horizontal reinforcement increased the maximum shear-to-maximum flexural strength ratio and significantly improved deformation capacity: the ability to simultaneously develop large deformations without substantial strength degradation.

3. The ability of a shear wall to develop a large deformation capacity under cyclic load is largely attributed to the presence of confinement at critical compression zones.
4. The ratio of maximum strength-to-cracking shear strength was in the range of 1.3 to 1.8, indicating that substantial post-cracking strength gain is possible in shear mode failures, depending primarily on the effective use, rather than the amount of horizontal reinforcement.

Woodward and Rankin (1985a and 1985b) conducted two studies on masonry shear walls. The first study was to examine the effect of block and mortar strength on the in-plane shear resistance of concrete masonry walls, while the second study was to examine the influence of aspect ratio on the relationship between lateral in-plane load resistance and vertical in-plane compressive stress.

The first study involved the testing of seventeen 1630 mm high concrete masonry walls with the following variables:

1. Two types of concrete block units with gross area unit strengths of 9.0 MPa and 12.4 MPa.
2. The mortar used in the study was of Type S and Type N.
3. The axial compressive stress varied from 0.69 MPa to 2.76 MPa (based on net cross-sectional area).
4. Of the seventeen walls, thirteen were 1630 mm long, two were 1220 mm long and the remaining two were 2440 mm long.

The conclusions obtained from the first study were as follows:

1. For the lower levels of applied vertical compressive stress, the influence of block and mortar strengths on the maximum shear resistance was negligible. The influence of the component strengths became more significant as the vertical load increased.
2. The interaction effect of block and mortar strength on wall shear strength was greater than the effect of either component's strength taken alone.
3. In general, the linear relationship between maximum shear resistance and applied vertical compressive stress was unaffected by block or mortar strength.

4. The diagonal tensile strain threshold at which diagonal cracking occurred was unaffected by the variation in block and mortar strength. The range of threshold strain was between 110 and 165 microstrain.

The second study involved the testing of seven 1630 mm high, ungrouted and unreinforced concrete masonry walls with fixed-fixed boundary conditions. The aspect ratio was varied by using three different lengths of wall: 1220 mm, 2030 mm and 2440 mm. The axial stress levels for the two 1220 mm long walls were 1.1 MPa and 3.0 MPa. The stress levels for the two 2030 mm long walls were 1.58 MPa and 2.69 MPa respectively, and the remaining three 2440 mm long walls had stress levels of 1.52 MPa, 2.14 MPa and 2.82 MPa.

At completion of the study, the authors concluded the following:

1. There was a relatively weak effect of aspect ratio on the diagonal cracking strength for aspect ratios less than or equal to 1.
2. There was a nearly linear relationship between axial compressive stress and maximum lateral resistance.
3. The maximum lateral load resistance was affected by aspect ratio for higher levels of axial compressive stress.

Okamoto et al. (1987) tested eighteen shear walls constructed from hollow concrete block masonry, hollow clay brick masonry and reinforced concrete. The walls were fully grouted and tested under controlled axial load combined with programmed cyclic lateral loading applied in a manner to keep the top and bottom surfaces rotationally fixed. The parameters investigated in this study included:

1. Aspect ratio: 0.9, 1.6 and 2.3.
2. Axial stress: 2% to 26% of f'_m .
3. Horizontal reinforcement ratio: 0.17% to 0.67% (noted that the vertical reinforcement ratio was kept constant).

The authors concluded the following from this study:

1. Shear cracking load and maximum shear strength increased at decreasing rates with increasing axial load. Gain in shear strength was in the 60% to 66% range with axial load increasing from 2% to 26% of f'_m .
2. Shear strength increased 20% to 30% respectively as the aspect ratio decreased from 2.3 to 1.6 and from 1.6 to 0.9.
3. Specimens that failed in the shear mode had 50% of the deformation capacity of those that failed in a flexure mode.

Kaminosono et al. (1988) tested twenty-two walls under double curvature deformation to represent the stress condition due to earthquake motions. Of the twenty-two walls, fourteen were concrete masonry walls, five were clay brick masonry walls and the remaining three were reinforced concrete walls. Eighteen of these walls were “I” shaped, three were “T” shaped wall and one was “+” shaped. The principal objective of this study was to evaluate the effect of axial stress (0.5 MPa – 6 MPa), shear span ratio (0.452 – 1.139), and amount of shear reinforcement (0.175% - 0.699%) on the wall.

From the test results, the authors concluded the following:

1. For masonry walls that failed in shear, the maximum shear strength increased and the deformation capacity decreased with increase in axial stress, and also with decrease of shear span ratio.
2. Masonry walls with shear span ratio less than 0.8 reached the maximum strength at 0.002 radian, followed by rapid strength deterioration.
3. For walls that failed in flexure, the deformation capacity increased with increase in the amount of shear reinforcement and with increase in the confinement of the compression toe by spiral reinforcement.

Tomažević et al. (1986, 1987 and 1988) tested two series of sixty concrete block reinforced masonry walls with different geometry (series C with $h/\ell_w = 1.25$ and series D with $h/\ell_w = 2.30$) at the Institute for Testing and Research in Materials and Structures (ZRMK) in Ljubljana, Yugoslavia. The walls were constructed in 1:2 scale reduced size with specially manufactured concrete blocks in cement mortar which consisted of 0-2 mm sand and

Portland cement in the proportion of 1:3:5. Deformed steel (grade 400) 10 mm diameter bars ($\rho_v = 0.26\%$ in series C and $\rho_v = 0.52\%$ in series D) were used as vertical reinforcement, whereas smooth steel (grade 200) 6 mm diameter bars (0.14%) or burned wire, 4.2 mm diameter (0.28%) and 3.1 mm in diameter (0.14%), in the shape of closed stirrups were used as horizontal reinforcement. Stirrups were placed around the vertical bars in each horizontal mortar joint. All walls were tested as simple cantilevers with a constant vertical load of 60 kN and were subjected to cyclic lateral loading.

The study concluded that by reinforcing the masonry walls with vertical and horizontal reinforcement, improved seismic behaviour could be expected. In this respect, the horizontal reinforcement in the bed joint improved the shear and ductility capacity of the walls by causing yielding of the vertical reinforcement and the development of full flexural capacity of the wall's section.

Tomažević et al. (1996) conducted 32 more tests on identically reinforced masonry walls to further investigate the influence of different testing procedure: monotonic loading, two different loading histories, and a simulated displacement seismic response.

Tomažević et al. noted that higher resistance and larger ultimate displacement were measured in the case of monotonic loading than in the case of cyclic loading of any type. Tomažević et al. noted that strength and stiffness degradation took place when the walls were subjected to repeated cyclic lateral load reversals. Consequently, a significantly higher resisting force was measured when monotonic loading was applied than for the corresponding displacement when testing using cyclic loading. It was also observed from the experimental study that the maximum lateral resistance attained by monotonic loading was much higher than corresponding values attained in the case of cyclic loading. It was therefore concluded that at the same amplitude of lateral displacement, less severe stiffness degradation could be obtained in the case of monotonic loading than in the case of cyclic loading.

Shing et al. (1988, 1989, 1990a, 1990b, 1991, 1993) conducted comprehensive experimental testing on sixteen squat concrete masonry walls at the University of Colorado in order to examine the flexural and shear strength of reinforced masonry shear walls. The main variables considered in the experimental study included the amount of vertical and horizontal

reinforcement, and the magnitude of applied axial stress. All test specimens were 1.8 m high and 1.8 m long, and 140 mm wide. All specimens were fully grouted, with uniformly distributed vertical and horizontal reinforcement.

The study found that simple flexure theory based on the plane-section assumption could be applied to square wall panels with good accuracy. However, the actual flexural strength of a shear wall subjected to seismic loads could be slightly higher than that predicted by flexure theory due to strain hardening under cyclic loads. In addition, the flexural strength of the shear wall increased with the magnitude of the applied axial load. Nevertheless, it was also found that the axial compressive load had the detrimental effect in reducing the ductility capacity of the shear walls since high axial compressive stress could lead to more severe toe crushing. However, proper toe confinement was found to substantially improve the flexural ductility of shear walls.

Shing et al. concluded from experimental results that specimens that failed in shear tended to exhibit a more brittle behaviour than those failing in flexure. The shear strength of reinforced masonry depends on the tensile strength of masonry as well as on several other mechanisms, such as aggregate interlocking, the dowel action of vertical steel, and the action of horizontal shear reinforcement. It was found that the occurrence of the first major diagonal crack depends primarily on the tensile strength of masonry and the applied load condition, but not on the amount of reinforcement present. However, the post-cracked shear resistance depends on the amount of vertical and horizontal reinforcement.

Due to the complexity in predicting the shear strength of reinforced masonry, a semi-empirical design formula based on the mechanisms mentioned has been proposed by Shing et al. for square and slender walls:

$$V_m = (0.0217\rho_v f_{yv} + 0.166)A_n \sqrt{f'_m} \quad (2-18)$$

$$V_s = \left(\frac{\ell_w - 2d'}{s_h} - 1 \right) A_h f_{yh} \quad (2-19)$$

$$V_p = (0.0217N) \sqrt{f'_m} \quad (2-20)$$

in which the term V_m represents the contribution to shear strength provided by the masonry and vertical steel, V_s represents the contribution of the horizontal steel and V_p represents the contribution of the axial load.

Equation (2-19) has been proposed in order to take into account that not all the horizontal reinforcement will be activated to develop the tensile strength to resist masonry shear stress. For example, only the interior reinforcement can be activated by a 45° diagonal crack, while the top and bottom reinforcing bars do not have adequate development length to develop tensile resistance.

Larbi and Harris (1990) conducted a series of ten 1/3rd scale model low rise masonry shear wall tests to determine the effect of the amount of vertical and horizontal reinforcement on shear and flexural strength. However, the main objective of the study was to assess the effectiveness of the modelling technique used to duplicate the component materials at 1/3rd scale.

In order to demonstrate the effectiveness of the 1/3rd scale model, the results obtained from this study were presented along with the corresponding results attained by Shing et al. at the University of Colorado at Boulder, on similar full scale masonry wall panels. Based on the overall correlation obtained, it was concluded that the modelling technique was efficient and that it represented a good alternative to full scale testing.

Anderson and Priestley (1992) proposed an equation to predict the maximum in-plane shear and sliding strength of concrete/clay brick masonry walls. The predictive equation is as follow:

$$V_n = C_{ap} \sqrt{f'_m} A_n + 0.5 A_h f_{yh} \frac{d}{s} + 0.25N \quad (2-21)$$

where:

$$C_{ap} = \begin{array}{l} 0.24 \text{ for concrete masonry} \\ 0.12 \text{ for clay brick masonry} \end{array}$$

Equation 2-21 gives zero correlation between the shear strength and vertical steel, A_v . However, it was thought that as the vertical reinforcement helped to control diagonal cracks, the friction along these cracks would be enhanced, and therefore there would be an increase in shear strength due to the presence of vertical steel. The 0.50 factor for the horizontal reinforcement component was only half that normally used in reinforced concrete since not all the shear reinforcement is effective in providing the shear resistance.

Brunner and Shing (1996) undertook an experiment in which walls of low aspect ratio were tested in order to investigate the influence of aspect ratio on the strength and failure mechanism of a reinforced masonry shear wall. Therefore, a series of three fully grout-filled masonry wall panels was built with aspect ratios (h/ℓ_w) of 0.929, 0.722 and 0.591. A high vertical steel ratio was chosen for all three walls to increase the flexural strength and force the walls to fail in shear.

All walls exhibited shear failure in this study. It was found that wall panels with lower aspect ratios had higher stiffness and reached their maximum resistance at smaller displacement.

Schultz (1996) explored the potential benefits and advantages of partially-grouted masonry shear walls. A total of six partially-grouted masonry shear walls were constructed according to Figure 2.15. Only the outermost vertical cells and a single course bond beam at the mid-height of the wall were reinforced and grouted. All walls were constructed to a height of 1422 mm, but varied in length. Two horizontal reinforcement schemes were used for the bond beams to define reinforcement ratios of 0.05% and 0.12%, based on gross dimensions.

The test observations suggested that partially grouted masonry is a viable lateral load resisting system for regions of moderate and low seismic risk. Decrease in the height-to-length (h/ℓ_w) ratio was observed to have a beneficial effect on the ultimate shear stress, but a detrimental effect on the strength deterioration, deformation capacity and energy dissipation capacity. Increasing the horizontal steel ratio had a modest effect on the maximum shear stress. Finally, it was concluded that the resisting mechanism of partially grouted masonry walls is vastly differently from that of reinforced masonry walls. Vertical cracks arising from stress concentrations between ungrouted and grouted masonry appear to dominate wall

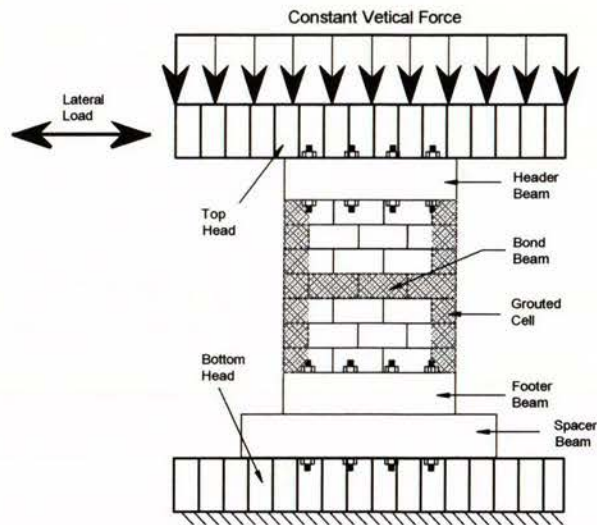


Figure 2.15 Typical tests set-up.

behaviour, and sliding friction between masonry panels and concrete surfaces contributes to the resistance mechanisms.

Hansen et al. (1998) used the test set-up shown in Figure 2.16 to conduct twenty-six deformation controlled shear tests to determine the shear strength and shear stiffness as well as the post peak behaviour of bed joints, including mode II fracture energy (which is the fracture energy related to shear failure and joint dilatancy). The tests were carried out with three types of mortar and four types of bricks: Danish clay solid and perforated, Finnish calcium silicate solid and clay perforated, and three levels of precompression of 0.1 MPa, 0.2 MPa and 0.5 MPa.

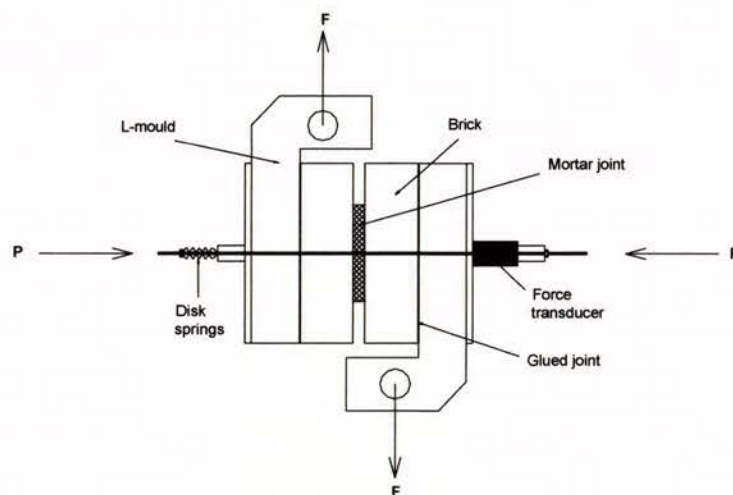


Figure 2.16 Test set-up to determine the shear strength of bed joint.

Based on the test observations, the researchers noted the following points:

- ◆ The use of strong mortars does not generally improve the shear properties of bed joints. However, the consequence of using strong mortars is a decrease in the mode II fracture energy of the bed joints that leads to a more brittle masonry with many cracks in the bricks in the ultimate limit state.
- ◆ With respect to the mode II fracture energy for bed joints, perforated bricks produce significantly higher values than solid bricks, especially when relatively weak mortars were used.

Cavalheiro and Pedroso (2000) tested triplet specimens to investigate the bond shear strength of masonry with and without precompression forces perpendicular to the bed joints. The loading and support arrangement for the triplet test is shown in Figure 2.17.

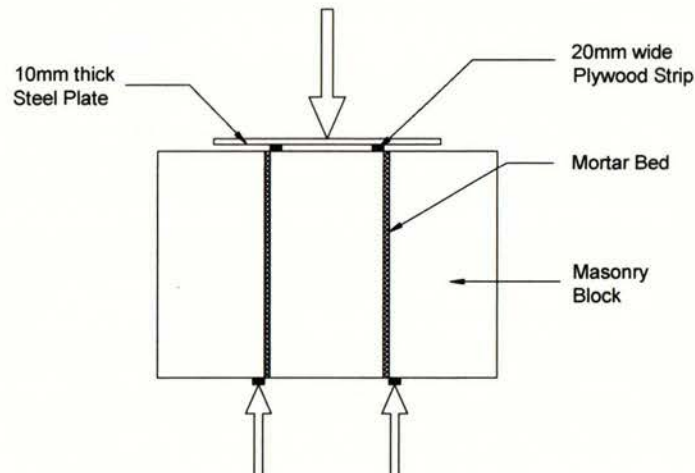


Figure 2.17 Loading and support arrangement.

The experiments were carried out on two types of masonry, namely hollow clay and concrete masonry, and two types of mortar mixes at the ages of seven, twenty-eight and ninety days. Precompression forces of 0.57 MPa and 1.14 MPa were taken to represent the vertical loads induced by four and eight storey building.

Cavalheiro and Pedroso observed that the shear strength of masonry in general increased with age, but the increase in shear strength was more significant in specimens without precompression. The results showed strong effect of the precompression in increasing the bond shear strength. However, this bond shear strength was strongly dependent on the

vertical forces up to a certain precompression level, Cavalheiro and Pedroso predicted this level to be about 0.6 MPa based on the materials tested in their study.

2.7 Conclusions

The brief conclusions below can be drawn from the literature presented:

1. The shear resistance of reinforced masonry walls results from complex mechanisms, such as tension of horizontal reinforcement, dowel action of vertical reinforcement, as well as aggregate interlocking between the parts of the walls separated by diagonal cracks. However, due to the complexity of these mechanisms, no effective theoretical models have yet been proposed to predict the shear strength of a masonry wall panel. Hence, the nominal shear strength (V_n) of reinforced masonry walls is evaluated as a sum of contributions from masonry, reinforcement and applied axial compression load during practical calculation, i.e. $V_n = V_m + V_s + V_p$.
2. Past research has concluded that masonry shear resistance is closely related to the compressive strength of masonry, f'_m , and that there is strong evidence that masonry shear strength increases with f'_m . However, the rate of increase is not linear in all ranges of f'_m , but the rate becomes gradually lower as f'_m increases. Consequently, it is acceptable that masonry shear strength increases approximately in proportion to $\sqrt{f'_m}$.
3. Horizontal reinforcing steel is effective in providing additional shear resistance to masonry shear walls and an adequate amount of horizontal reinforcement can ensure a ductile shear failure. The increase in masonry shear strength is further enhanced by using 180° bend rather than 90° bend horizontal reinforcement anchorage and by evenly distributing the horizontal reinforcement up the height of masonry walls. However, past research has noted that increased horizontal reinforcement ratios above a certain level does not result in a corresponding increase in shear strength.
4. Axial load has a strong influence on the in-plane shear performance of masonry shear walls, mainly because it suppresses the tensile field in a material inherently weak in tension. Axial load in the range of 0 to 18 percent of prism compressive strength has a significant positive effect on cracking strength as well as maximum shear strength

under lateral loading. However, post-cracking deformation capacity is reduced with increasing bearing stress since the failure type becomes more brittle due to earlier diagonal crushing at the web.

2.8 Code Recommendation

Uniform Building Code

The 1997 UBC contains an empirical formula, shown in Equation 2-22, for calculating the shear strength of reinforced masonry walls. The nominal shear strength is obtained by adding two terms: the first term is for strength provided by the masonry and the second term accounts for the strength provided by the shear reinforcement. The UBC presents several design assumptions that are essential when using the formula to calculate the nominal shear strength:

1. The nominal shear strength of an individually reinforced masonry wall cross-section is based on applicable conditions of equilibrium and strain compatibility;
2. Strains in the reinforcement and masonry are assumed to be directly proportional to the distance from the neutral axis;
3. Maximum usable strain at the extreme masonry compression fibre is assumed to be equal to 0.003;
4. Stress in the reinforcement below the specified yield strength, f_y , is taken as the elastic modulus, E_s , times the steel strain;
5. For strains greater than the yield strain the stress in the reinforcement is equal to yield stress, f_y .

The UBC formulae for predicting the shear strength of masonry are as follows:

$$V_n = V_m + V_s \leq 0.33A_n\sqrt{f'_m} \quad (2-22)$$

$$V_m = 0.083C_dA_n\sqrt{f'_m} \quad (2-23)$$

$$V_s = A_n\rho_h f_{yh} \quad (2-24)$$

where:

$$\begin{aligned} C_d &= \text{nominal shear strength coefficient} \\ &= 2.4 \text{ when } \frac{M}{Vd} \leq 0.25, \text{ or} \\ &= 1.2 \text{ when } \frac{M}{Vd} \geq 1.0 \end{aligned}$$

Interpolation can be by straight line for $\frac{M}{Vd}$ values between 0.25 and 1.00.

NEHPR

The Technical Coordinating Committee for Masonry Research was formed in February 1984. It comprised of researchers from academic and industrial organisations who have strong backgrounds in research into the properties and characteristics of reinforced masonry materials, structural components and systems, analytical techniques, structural dynamics, building codes, and earthquake engineering. The primary program objectives of TCCMaR were:

1. Make recommendations for limit state design of reinforced masonry buildings and components.
2. Development of a consistent experimental database on the behaviour of masonry materials, components and systems.
3. Development of analytical non-linear models for research and design office use for detailed analysis, system analysis, and dynamic loads determination.
4. Improved material and subassemblage experimental procedures for obtaining masonry properties.
5. Improve masonry fabrication procedures and standard.
6. Developing an increased awareness among engineers, architects, code bodies and the public of the capabilities of reinforced masonry in all seismic zones.
7. Interfacing with standards development groups to support development of a consensus limit state standard for masonry.

TCCMaR (BSSC, 1998) chose to adopt the Anderson and Priestley equation to predict masonry shear strength. However, a $\frac{h_e}{\ell_w}$ ratio was incorporated as part of the masonry equation rather than just a straight function of $0.24\sqrt{f'_m}$ as in the original Anderson and Priestley equation. Consequently, the final form of the TCCMaR equation is as follows:

$$V_n = V_m + V_s + V_p \leq 0.33A_n\sqrt{f'_m}$$

where

$$V_m = 0.083 \left[4.0 - 1.75 \left(\frac{h_e}{\ell_w} \right) \right] A_n \sqrt{f'_m} \quad \text{where } \frac{h_e}{\ell_w} \text{ need not greater than 1}$$

$$V_s = 0.5\rho_n f_{yh} A_n \quad (2-25)$$

$$V_p = 0.25N$$

Australian Masonry Design Standard

The Australian standard (AS3700-1998) provides an empirical formula, as shown below, for calculating the in-plane shear strength of reinforced masonry walls:

$$V_n = f_{vr} A_n + 0.8f_{yh} A_s \quad (2-26)$$

where:

$$f_{vr} = \left(1.50 - 0.5 \frac{H}{L} \right) \text{ MPa}$$

A_s = the cross-sectional area of reinforcement, as follows:

$$(i) \text{ If } \frac{H}{L} > 1.0$$

A_s = area of horizontal reinforcement.

$$(ii) \text{ If } \frac{H}{L} \leq 1.0$$

A_s = the total cross-sectional area of horizontal reinforcement, or total cross-sectional area of vertical reinforcement, whichever is less.

The Australian masonry design standard states that the following requirements are essential when using the above formula to calculate the masonry shear strength:

1. The reinforcement shall be located symmetrically in the cross-section.
2. Vertical reinforcement shall be spaced at centres not exceeding $0.75H$ and in any case not greater than 200 mm horizontally. Horizontally reinforcement shall be spaced at centres not exceeding $0.75L$ and in any case not greater than 3000 mm vertically.
3. The vertical reinforcement shall be such that $A_s \geq 0.0013A_n$ and the horizontal reinforcement be such that $A_s \geq 0.0013A_n$. If the reinforcement does not meet these requirements then the wall shall be designed as an unreinforced masonry wall.

New Zealand Masonry Design Standard

The New Zealand masonry design standard (NZS4230:1990) states that the nominal shear strength of the wall, V_n , is comprised of two parts which is similar to Equation 2-22. Hence;

$$V_n = V_m + V_s$$

$$\text{and } \frac{V_n}{A_n} \leq 2.4 \text{ MPa}$$

The shear strength provided by the masonry is as follows:

$$V_m = v_m b_w d \quad (2-27)$$

where:

$$v_m = 0.30 \text{ MPa or}$$

$$0.03f'_m + 0.3 \frac{P}{A_n} \leq 0.72 \text{ MPa}$$

$$d = 0.8\ell_w$$

and;

$b_w = t$ for fully grouted wall (see Figure 2.18(a)).

$b_w = t - b_f$ for partially grouted wall (see Figure 2.18(b)).

The shear strength provided by the horizontal reinforcement is given by:

$$V_s = A_h f_{yh} \frac{d}{s_h} \quad (2-28)$$

Figure 2.18 Effective area for shear (from NZS4230: 1990: Part 2).

Chapter 3

Test Programme

3.1 Introduction

Three series (A, B and C) of reinforced concrete masonry walls were tested in the Civil Engineering Test Hall at the University of Auckland, consisting of a total of twelve reinforced concrete masonry walls. The primary objective of this experimental programme was to investigate the shear strength of masonry walls constructed of materials locally available in New Zealand and to supplement worldwide experimental data currently available.

The two specimens tested in Series A were served as a trial run to determine the adequacy of the test set-up and loading procedure described in Appendix A. However, due to premature failure during the testing of both specimens, it was concluded that the test set-up and loading procedure adopted in Series A were inadequate. It was therefore decided that amendments to the test set-up and loading procedure described in Appendix A were necessary in order to successfully test the ten specimens in Series B and C, so that the primary objective described in section 1.4 could be achieved.

The test set-up and method of loading adopted in this experimental programme were designed to simulate the response that a masonry shear wall would experience during seismic loading. It is emphasised that the test set-up and loading procedure described in this chapter were intended for the eight specimens considered in Series B. The test set-up and loading procedure used in the Series C tests (two specimens) were slightly modified from those described here. For detailed description of test set-up, loading procedure and other relevant information regarding the four specimens in Series A and C, please refer to Appendices A

and C. Reinforcing details, material properties and other relevant information are summarised in the tables and figures contained within this chapter.

The main variables being considered in Series B were as follows:

1. The amount of horizontal reinforcement,
2. Distribution of horizontal reinforcement,
3. The level of axial compression stress,
4. The type of grouting,

and Series C was designed to investigate the influence of H/L ratios on masonry shear strength.

3.2 Test Set-up

The testing of specimens in Series B reported herein was conducted according to the set-up shown in Figure 3.1. The test specimens were designed based upon the limiting capacity of the hydraulic actuators at the University of Auckland, from which it was established that a maximum test design force, when using a single hydraulic jack, of 275 kN and 370 kN in the respective pulling and pushing directions would be appropriate.

Figure 3.1 shows the dimensions adopted, resulting in an aspect ratio of 1.0 and a width of 140 mm. The dimensions of the walls were such that the block size was sufficiently small compared to the panel size. The test set-up essentially consisted of a 2.5 m high strong reaction frame and reinforced concrete base, and a horizontally mounted hydraulic actuator providing a horizontal shear force to the top of the wall through a 150 x 75 steel channel section (loading beam). Two parallel horizontal struts were hinged to the two ends of the loading beam to prevent out-of-plane wall deformations. It is recognised that this type of horizontal force transfer is of a cantilevered wall type and therefore may not be representative of all structures.

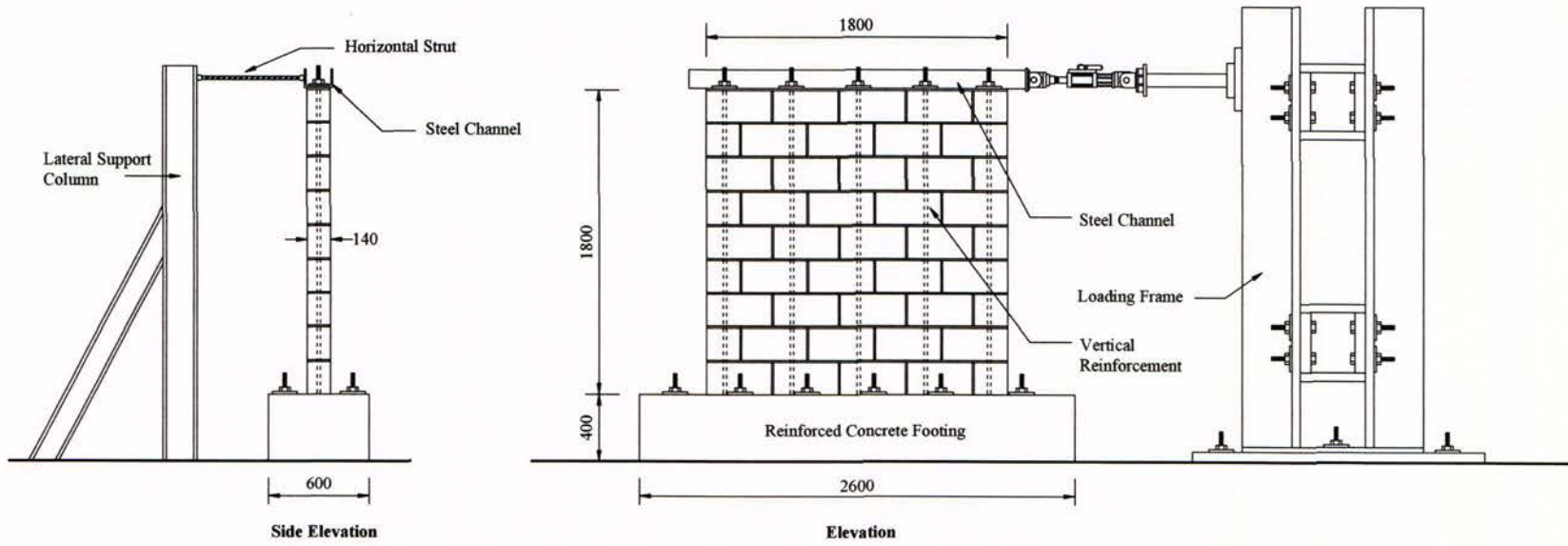


Figure 3.1 Typical test set-up.

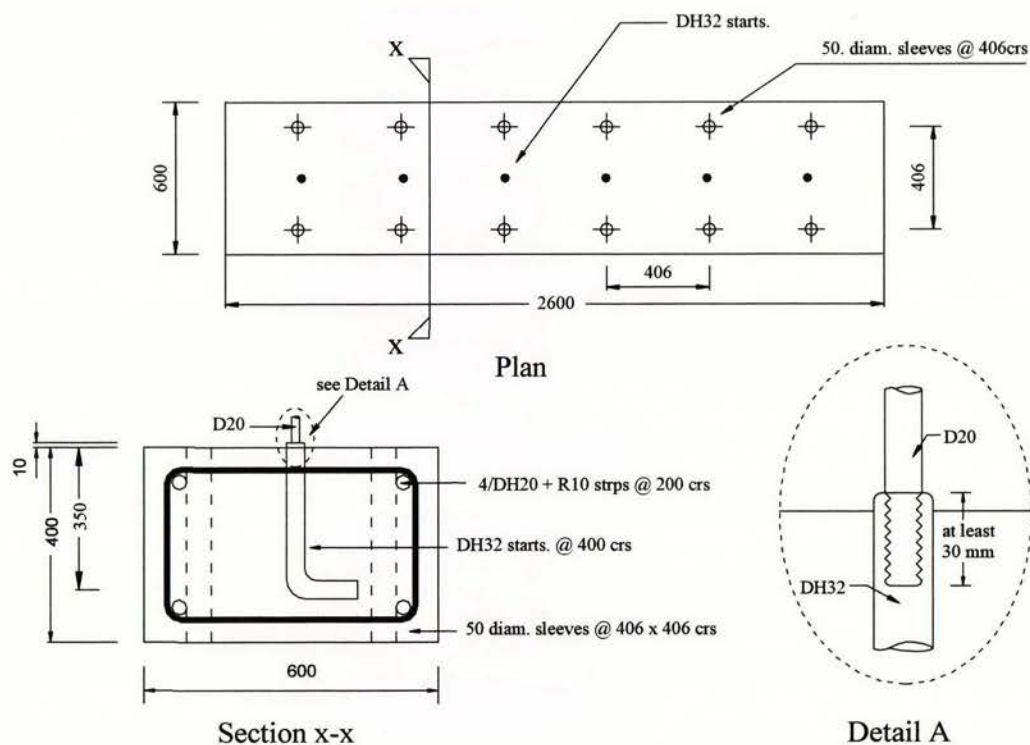


Figure 3.2 Details of concrete footing.

All walls were constructed on two identical re-usable reinforced concrete footings so that two walls were built during each construction cycle. The concrete footing shown in Figure 3.2 and Photo 1 (all photos are presented in Appendix G) had DH32 starter bars spaced at 400 mm centres that were drilled and tapped to accommodate D20 vertical reinforcement. The concrete footing was stressed down to the laboratory floor with 12 high strength steel rods, each loaded to approximately 300 kN so that sufficient shear friction was provided to eliminate any slip between the footing and the floor. Each of the wall vertical reinforcement bars was first tapped at both ends, then threaded into the DH32 starters that protruded from the reinforced concrete base. Once the loading beam was placed on top of the concrete masonry wall using a pack of trade mortar for best possible shear force transfer between the wall and the loading beam, the vertical reinforcement was tightened. It was verified through bar testing that threading on the D20 reinforcing bars had negligible effect on the yield strength for this type of reinforcing bar (please refer to Figure F.1 in Appendix F). If the test set-up for any particular wall in Series B differed from that described above, the difference is detailed in Appendix B for the relevant wall.

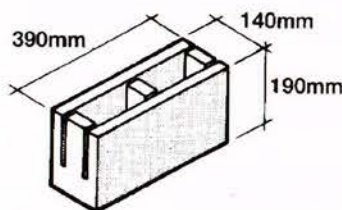
The test set-up for the four concrete masonry walls in Series A and C differed from that described above, with detailed description of the irrespective test set-ups presented in Appendices A and C respectively.

3.3 Construction Materials

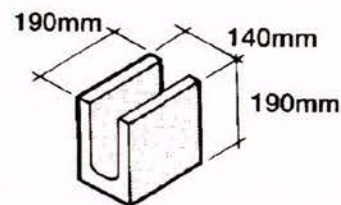
The walls were constructed by experienced blocklayers under supervision, and consisted of a running bond pattern of standard grey precast concrete masonry block units using DRICON™ trade mortar. Prior to wall construction, the vertical reinforcing bars were first tapped at both ends and then threaded into the starters, reaching an approximate height of 1.9 m above the base as depicted in Photo 2.

3.3.1 Concrete Masonry Block

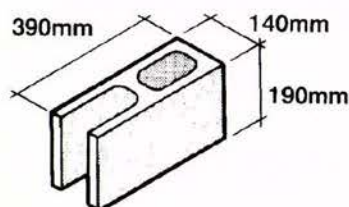
The masonry blocks used in this study were standard production 15 series concrete masonry precast units (CMUs). Open-end bond beam CMUs were used throughout the wall height allow horizontal reinforcing steel to be positioned at all levels, and also provided the passage of grout through the flues within the test walls. Half end-closer blocks were also used at the edge.



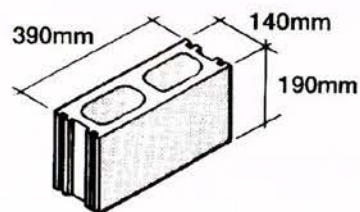
Knock-in bond beam



Lintel & half end closer



Open end



Standard whole

Figure 3.3 15-Series concrete masonry units.

3.3.2 Mortar and Grout

DRICON™ mortarmix – a mortar that is commonly used in masonry construction throughout New Zealand, was used as mortar for construction of the test walls. High slump ready-mix grout using small aggregate was employed to ensure full dispersion through the cavities within the test walls. An expansive chemical additive (SIKA Cavex) was also added to the grout to avoid formation of voids caused by high shrinkage of the grout. Photo 3 shows wall construction and Photo 4 shows the grouting process.

3.3.3 Reinforcing Steel

All reinforcing steels used was grade 300 MPa (except Wall 9 in Series C), consisting of D20 for the vertical reinforcement, and R6 or D10 for the horizontal reinforcement. The vertical reinforcement was erected as discussed in section 3.2, while the horizontal shear reinforcement was hooked around the extreme vertical reinforcement as shown in Figure 3.4. Wall 9 was the only specimens that was constructed on a purpose-built reinforced concrete footing with cast-in DH25 vertical reinforcement spaced at 400 mm centres.

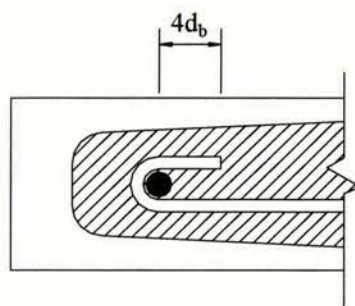


Figure 3.4 Hooked horizontal reinforcement around the vertical reinforcement (plan view).

3.4 Unit Reinforcing Details

Table 3.1 summarises the reinforcement details of all test walls in Series B and C. All walls, with the exception of Walls 5 and 6, were fully grout-filled and had the same amount of vertical reinforcing steel (see Figure 3.5), i.e. 5-D20 spaced at 400 mm c/c, but varied in horizontal reinforcement. Walls 5 and 6 were partially grout-filled with no horizontal reinforcement and their D20 vertical reinforcement spaced at 400 mm and 800 mm respectively. For the two partially grout-filled walls, only cells containing reinforcing steel bars were filled with grout.

Table 3.1 Masonry wall reinforcement details

	Wall specimen	Height (mm)	Length (mm)	Vertical reinforcement	Horizontal reinforcement	Grouting	Axial stress (MPa)
Series B	1	1800	1800	5 x D20	5 x R6	Full	---
	2	1800	1800	5 x D20	1 x R6	Full	---
	3	1800	1800	5 x D20	5 x D10	Full	---
	4	1800	1800	5 x D20	2 x D10	Full	---
	5	1800	1800	5 x D20	---	Partial	---
	6	1800	1800	3 x D20	---	Partial	---
	7	1800	1800	5 x D20	5 x R6	Full	0.5
	8	1800	1800	5 x D20	5 x R6	Full	0.25
Series C	9	3600	1800	5 x DH25	9 x R6	Full	0.25
	10	1800	3000	8 x D20	5 x R6	Full	0.25

Walls 1 to 6 were tested without externally applied vertical axial compression load. Walls 7 and 8 were the duplicates of Wall 1, but with externally applied axial compressive stress of 0.5 MPa and 0.25 MPa, providing an average compressive load of 126 kN and 63 kN respectively to the two walls.

The two walls in Series C were fully grout-filled and constructed to the dimensions of 3600 mm x 1800 mm and 3000 mm x 1800 mm respectively, see Figure 3.6, giving H/L ratios of 2.0 and 0.6. As shown in Figure 3.6, the vertical reinforcement was spaced at 400 mm c/c to consist of DH25 and D20 respectively for Walls 9 and 10, while the horizontal reinforcing steel was R6, also spaced at 400 mm c/c. Both Walls 9 and 10 were subjected to axial compression stress of 0.25 MPa, providing an average compressive load of 63 kN and 105 kN in each wall.

The walls tested at the University of Auckland supplemented existing experimental data by providing new data for masonry walls with low shear reinforcement ratios ($\rho_h \leq 0.0625\%$) and low axial compression stress levels ($0 \leq \sigma_n \leq 0.5$ MPa). Experimental studies reported in Chapter 2 investigated shear strength of masonry walls with higher shear reinforcement ratios ($0 \leq \rho_h \leq 0.668\%$) and higher axial compression stress levels ($0 \leq \sigma_n \leq 5.87$ MPa).

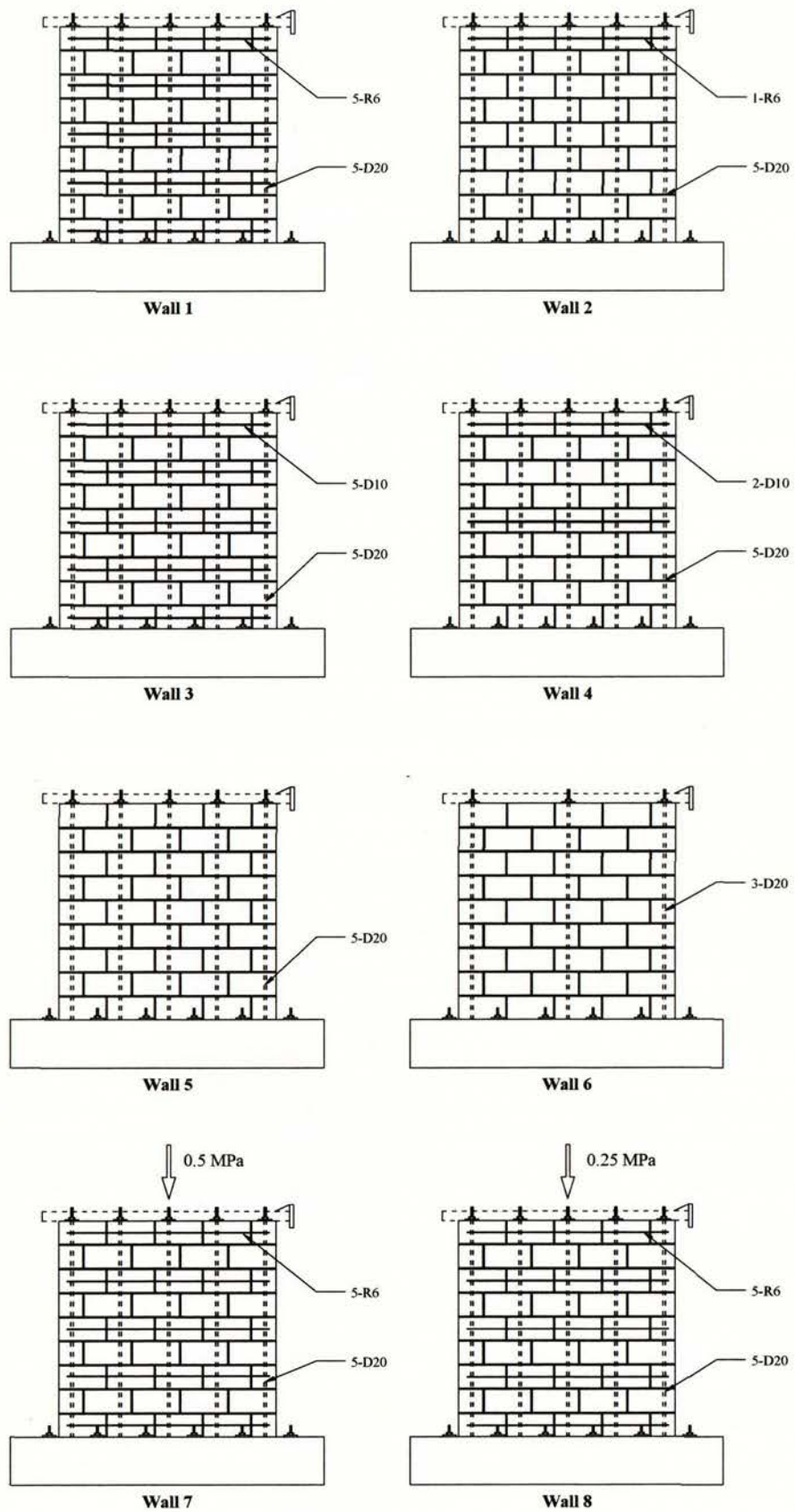


Figure 3.5 Series B, wall reinforcing details.

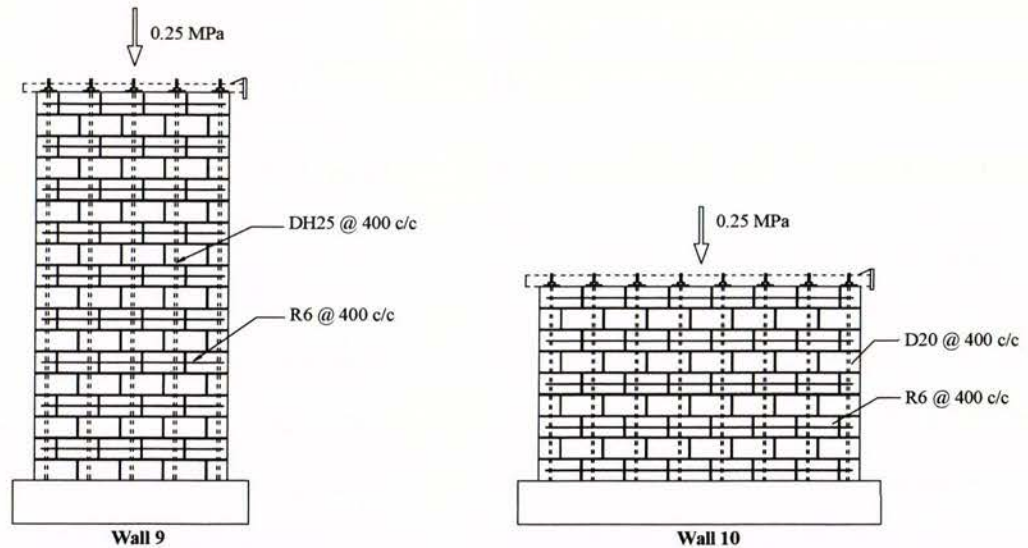


Figure 3.6 Series C, wall reinforcing details.

3.5 Instrumentation

The wall instrumentation included two types of instruments: load cell and portal displacement transducer. Both types of devices were calibrated on a regular basis. At various stages of testing, all displacement transducers and the load cell were scanned by a data logger and the measured displacement from the transducer and force magnitudes from the load cell were recorded by a computer.

Portal displacement transducer

The portal displacement transducer consisted of a strain gauge attached to a spring steel strip between two rigid portal legs as shown in Figure 3.7. This type of instrument is capable of measuring relative movement between the legs. Any axial movement causes the steel strip to be subjected to flexure, and the transducer is calibrated so that the resulting strain in the strain gauge correlates to the axial displacement. This type of device is capable of measuring displacement of about ± 50 mm with acceptable accuracy.

Load cell

This device measures the magnitude of applied force from the hydraulic actuator. It consists of a steel cylinder with strain gauge attached to the outer surface. Any deformation of the cylinder due to applied force causes a change in voltage output in the strain gauge.

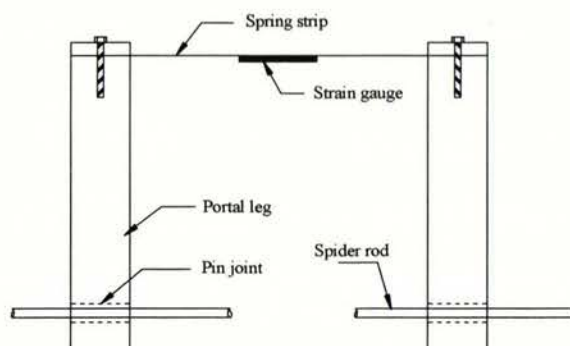


Figure 3.7 Portal displacement transducer.

3.5.1 Installation of Instrumentation

The arrangement for the measuring instrumentation is shown in Figure 3.8 and Photo 5. A load cell to measure the magnitude of the lateral force was placed between the actuator and the steel channel, denoted as [0] in the figure. Portal displacement transducers, denoted as [1] and [2], measured lateral displacement at the top of the wall. Portal displacement transducers [42] – [45] were used to measure sliding of the wall relative to the concrete footing, and transducers [46] and [47] measured the uplift. Any slip in the steel channel and the concrete footing were measured by transducers [6] and [50] respectively. Further transducers were placed according to the configuration shown in Figure 3.7 to attain the shear and flexural components of deformation. All transducers except [48] and [49] were attached on the same side of the wall, while [48] and [49] were placed on the other side of the wall to measure any out-of-plane deformation.

Measuring points were formed by drilling into the masonry and epoxy grouting 10 mm diameter mild steel studs that were threaded to accept aluminium rosettes. Steel rods of 4 mm diameter were fixed to the rosettes in a formation of ‘spider webs’ that triangulated the wall between the measuring points, as shown Figure 3.8.

3.6 Material Properties

Material testing was carried out to evaluate the key material properties: concrete masonry crushing strength (f'_m), compressive strength of mortar (f'_j) and grout (f'_g) used in wall

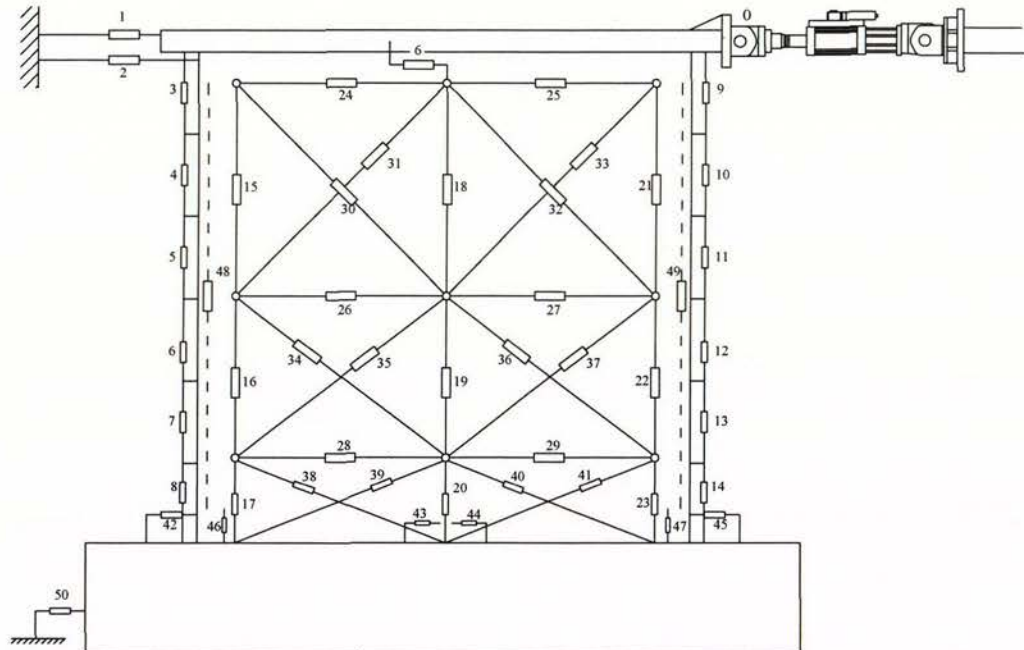


Figure 3.8 Instrumentation for test wall.

construction, and the yield strength of the reinforcing steel. Facilities for the compressive and tensile tests were both available at the University of Auckland.

3.6.1 Reinforcing Steel

Samples were taken from steel reinforcement used as flexural and shear reinforcement in the wall panels. The samples were subjected to tensile testing using the Avery Universal Testing Machine at the University, see Photo 6. Each type of reinforcing steel used in the walls was from the same batch, therefore only the average strength of each type of reinforcing steel is reported in Appendix F. An illustration of the tensile test results is presented in Figure 3.9.

3.6.2 Mortar and Grout

Standard test cylinders (100 mm diameter x 200 mm high) were taken from each batch of mortar and grout mixes. The average strength of the mortar and grout for each wall is reported in Appendix F.

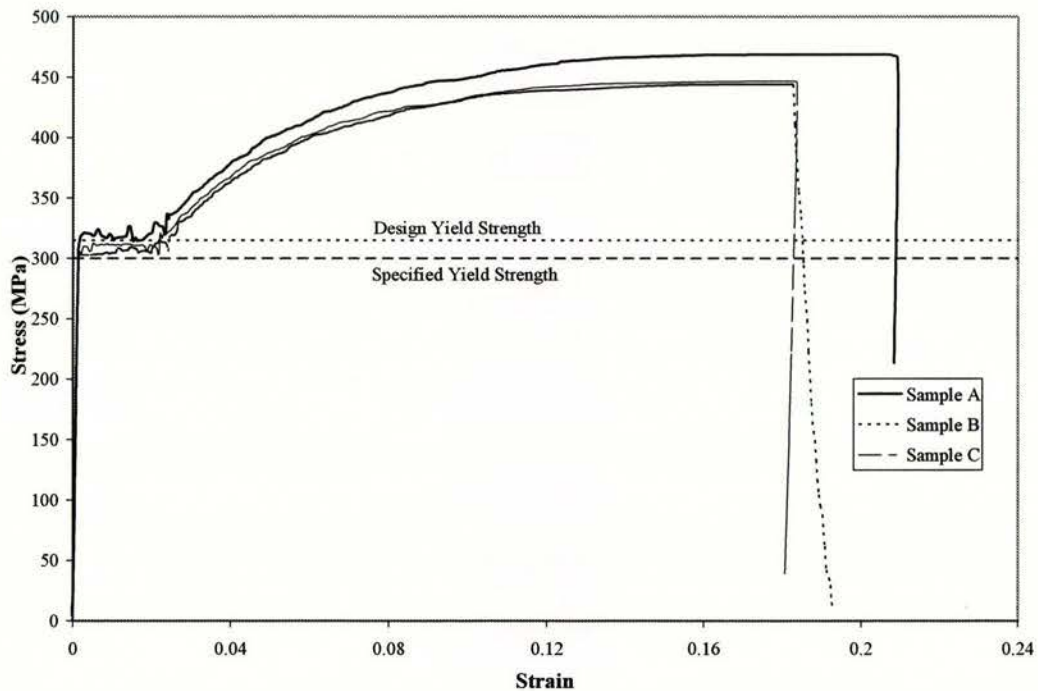


Figure 3.9 Stress-strain curve for D20 reinforcing bars.

3.6.3 Prisms

Masonry prisms were built at the completion of laying each wall (see Photo 7), using the same mortar and CMUs used in the wall. These prisms were built of three CMUs stacked on top of each other using the same construction technique as was used for the wall. The prisms were then filled at the same time as the walls, using the same grout. The prisms were tested using an Avery Testing Machine as shown in Photo 8. This type of test specimen provided the most accurate estimate of masonry wall compressive strength, f'_m . It is noted that f'_m for concrete masonry walls constructed of regular materials, found by prism testing at the University of Auckland, has consistently been around 17 MPa, which is about twice the value given in NZS4230:1990.

In the absence of machine testing, NZS 4230:1990 presents the below equation to estimate a lower bound to f'_m :

$$f'_m = 0.45\alpha f'_{cb} + 0.675(1 - \alpha)f'_g \quad (3-1)$$

where α represents the fraction of the gross cross-sectional area occupied by the masonry unit, and f'_{cb} and f'_g represent the compressive strength of CMUs and grout respectively.

3.7 Prediction of Wall Strength

The nominal flexural and shear strength of the tested walls was calculated before experimental testing was conducted. The wall nominal flexural strength was calculated using the procedure outlined in section 2, while a preliminary study presented by Voon and Ingham (2001) suggested that the shear strength of fully grout-filled masonry walls was satisfactorily estimated by the NEHPR (1998) provisions using Equation 2-25. Hence, it was decided to use Equation 2-25 to determine the predicted shear strength of masonry walls tested at the University of Auckland. Table 3.2 presents the estimated flexural and shear strength for each masonry wall according to the material properties presented in Tables F.1 and F.2 (see Appendix F). Shear strength predicted by NZS 4230:1990 was included in Table 3.2 for comparison purpose as discussed at a later stage of this report.

All walls, except Walls 1 and 3, were designed to have a dominant shear type of failure. Wall 3 was designed to have a predominantly flexural type of failure. Although Wall 1 had $F_n/V_n > 1.0$, it was expected this wall to fail in a flexure/shear mode due to the arrangement of shear reinforcement and the absence of axial stress.

Table 3.2 Prediction of wall strengths, based upon measured material properties

	Wall	f'_m (MPa)	F_n (kN)	V_n (kN)		Expected Failure Mode
				NEHPR	NZS 4230	
Series B	1	17.6	229	219	142	Flexure/Shear
	2	17.6	229	195	105	Shear
	3	17.0	228	250	191	Flexure
	4	17.0	228	219	152	Shear
	5	18.5	229	91	50	Shear
	6	18.5	142	91	50	Shear
	7	18.8	282	256	176	Shear
	8	18.8	256	240	161	Shear
Series C	9	24.3	272	268	178	Shear
	10	24.3	702	558	297	Shear

Note: no strength reduction factor applied to F_n and V_n .

3.8 Testing Procedure

The masonry walls were tested after a curing time of at least 14 days. Material testing was carried out on the day of testing to determine f'_m . The cyclic loading sequence adopted for all tests was that shown in Figure 3.10, and consisted of a series of displacement-controlled components. Each stage of loading consisted of two cycles to the selected tip displacement. In each case, wall testing was terminated when sufficient strength degradation was evident. This usually coincided with a marked change in the slope of the force-displacement curve. This report defines failure as the point on the loading curve at which the wall strength has reduced to 80% of the maximum strength recorded in whichever direction this occurs first, see Figure 3.10. The displacement capacity, d_u , is the point at which failure occurs, see Figure 3.11.

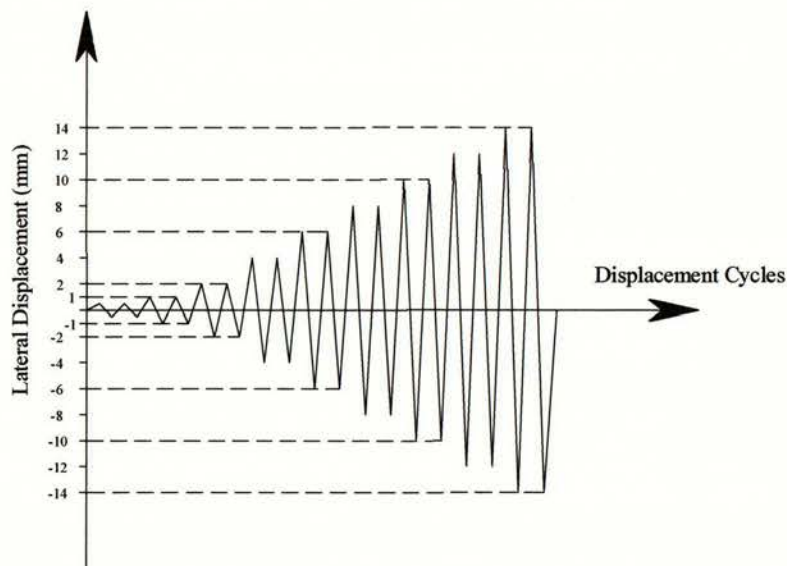


Figure 3.10 Imposed displacement history.

There were two reasons for applying this testing procedure: (1) Avoiding a high level of dependency on instrument readings during the process of testing, in this case only the readings of overall wall displacement were used in the load excursion. Hence, the test proceeded without knowledge of the actual strength or maximum displacement capacity of the test specimen. (2) The non-ductile nature (shear type of failure) of the test specimens mean small displacement increments are necessary to avoid the specimen being loaded to failure at an early stage of testing.

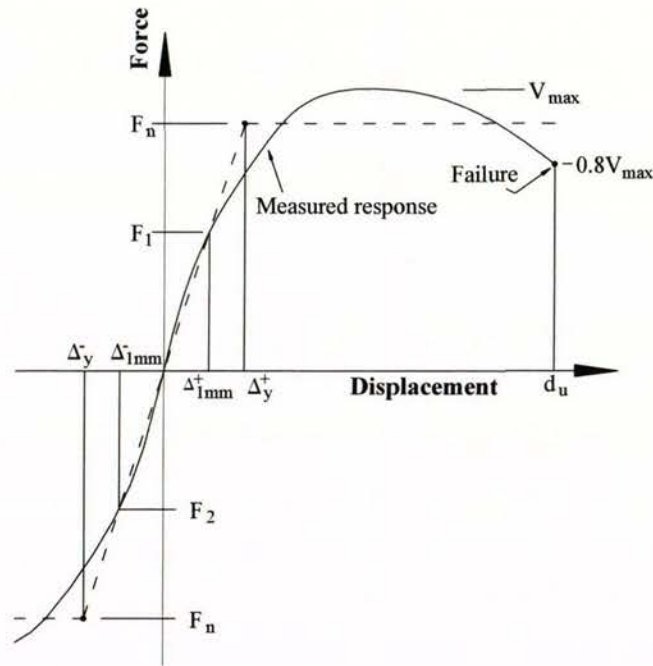


Figure 3.11 Nominal yield displacement.

The procedure for calculating the nominal yield displacement Δ_y is illustrated in Figure 3.11. This procedure involves the measurement of lateral forces F_1 and F_2 when the wall is being loaded to the first cycle of ± 1 mm displacement (Δ_{1mm}), and Δ_y (in mm units) is calculated according to Equation 3-2:

$$\Delta_y = \Delta_{1mm} \left(\frac{F_n}{\frac{1}{2}(F_1 - F_2)} \right) \quad (3-2)$$

3.8.1 Miscellaneous

Precondition

Prior to initiation of the loading procedure, the specimens were inspected for any pre-test cracking or damage, to avoid confusion with any damage attributed to the applied loading.

Crack marking

During testing, visual observations were carefully noted along with key force and displacement readings at the extreme of each load excursion. Cracks due to applied loading in the push directions were marked in red and cracks due to pull excursions were marked in black. Also, photos were taken of any significant structural event during testing. These photos

are presented in Appendix G. In reporting, the term “compression toe” was used to describe the end of the wall by the base in compression due to flexural action, and the term “heel” described the opposite end of the wall that was experiencing decompression/uplift. The position of “compression toe” and “heel” depended on loading direction, the two reversed in position when the loading direction was reversed.

3.9 Data Reduction

It was determined that the displacement of the wall consisted of four components: rocking and sliding deformation, flexural deformation, and shear deformation. As described earlier in this chapter, instrumentation was attached to the wall as shown in Figure 3.8 to allow the deformation components to be isolated.

Rocking deformation:

The rocking (uplift) deformation was recorded by the two portal displacement transducers placed at the two ends of the wall-foundation base interface. At a given wall state, the rocking displacement component was calculated by extrapolating the rotation measured between the wall ends. This is demonstrated in Figure 3.12. Hence, the rotation, θ_r of the wall due to rocking on its base was:

$$\theta_r = \frac{d_{r1} - d_{r2}}{\ell_w + 2\ell_s} \quad (3-3)$$

where d_{r1} and d_{r2} are the deformations measured by the portal displacement transducer, noting that elongation is represented by positive displacement, and ℓ_s is the distance between the wall end and the transducer. Therefore, the resulting rocking displacement recorded was evaluated as:

$$U_r = \theta_r h_e \quad (3-4)$$

Flexural deformation

Instrumentation mounted on both ends of the wall allowed the calculation of flexural deformation. Assuming that plane sections remain plane, the wall rotation, θ_i at height (x_i) above the base could be evaluated by Equation 3-5.

$$\theta_i = \frac{d_{b1} - d_{b2}}{\ell_w + 2\ell_s} \quad (3-5)$$

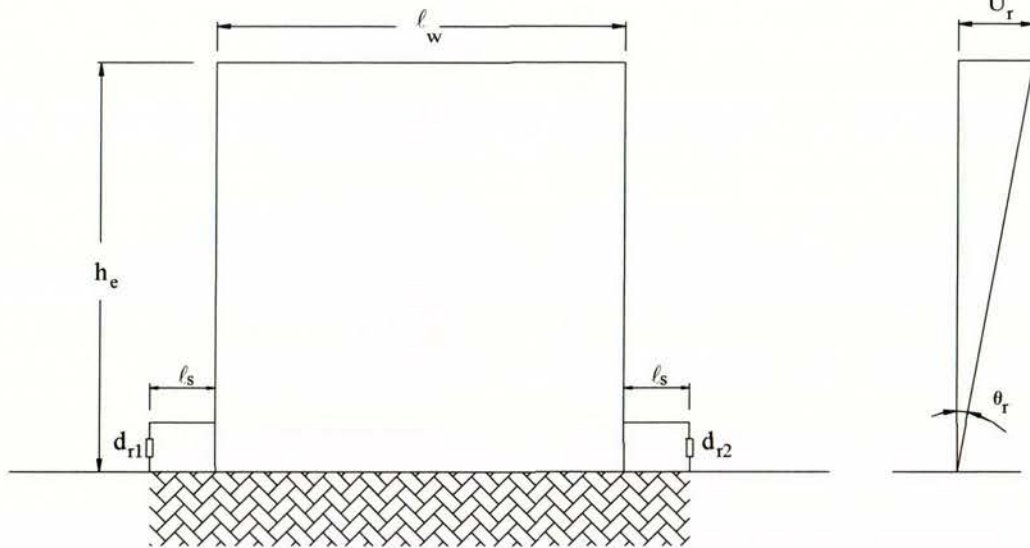


Figure 3.12 Rocking displacement

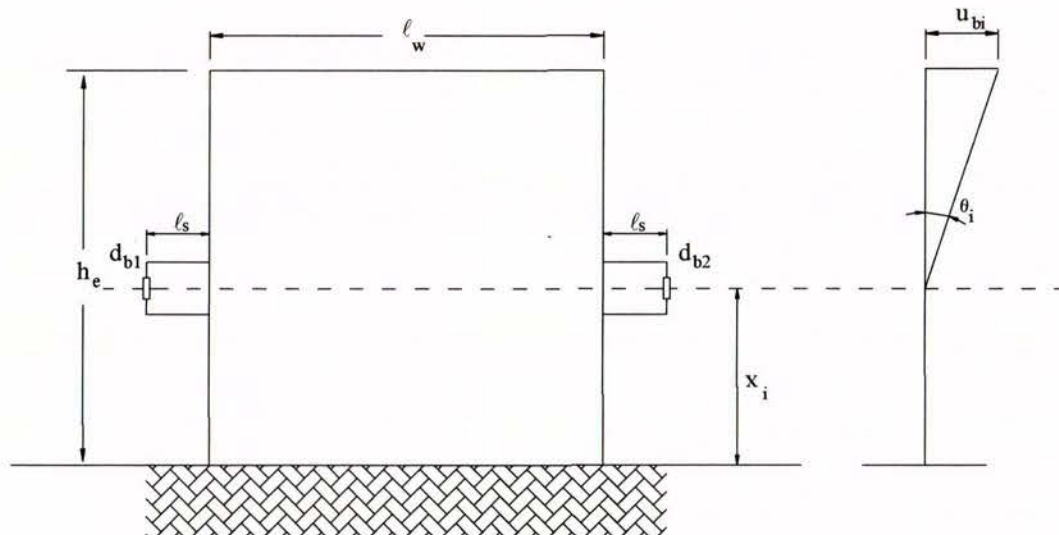


Figure 3.13 Flexural displacement.

where d_{b1} and d_{b2} were the displacement measured by the pair of instruments shown in Figure 3.13. The resulting displacement u_{bi} at the top of the wall due to θ_i could be evaluated as:

$$u_{bi} = \theta_i (h_e - x_i) \text{ and } U_b = \sum_i u_b \quad (3-6)$$

Shear deformation

The method used in this report for calculating the shear deformation component was based on Hiraishi (1984) and Brammer (1995), with more detailed description provided in Appendix D. The mentioned method utilised the measured relative displacements between points on the

wall face (transducers mounted diagonally on the wall, as shown in Figure 3.8) to evaluate the shear component of deformation.

All walls tested at the University of Auckland had at least six panel sections attached to the wall face in a 3x2 pattern. The dimensions of each panel section were defined by the length, ℓ , the height, h , and the diagonal length, d . The following formula was used to calculate the shear deformation component (u_s) for each panel:

$$u_s = \frac{d(\delta_1 - \delta_2)}{2\ell} - \frac{h^2}{6(2d_u + h)}(\delta_{v1} - \delta_{v2}) \quad (3-7)$$

$$\text{and } U_s = \sum u_s$$

where δ 's were the measured relative deformation within each panel section, and d_u was the distance between the two upper points of each panel section and the top of the wall. The sum of u_s from one side of the panel section was necessary to evaluate U_s , if two sides of a panel section were considered, then the results of the two may be averaged.

Sliding deformation

This component was used to measure the slip between the wall and the base. Sliding may become significant when there is a low friction coefficient, such as when using a friction breaker or water proof membrane, or when the wall is positioned on a smooth finished slab. All walls reported here were built on a purposely roughened concrete surface in order to reduce the magnitude of sliding.

Chapter 4

Experimental Results

This chapter summarises the behaviour of the ten walls tested in Series B and C. For detailed descriptions of the experimental results, please refer to Appendices B and C. This chapter evaluates the overall force-displacement response of the ten tests, the maximum strength developed in each test specimen, and the type of failure mechanism. The nominal strengths, F_n and V_n , drawn in the force-displacement (F-D) curve are without a strength reduction factor (i.e. $\phi=1.0$). This report defines loading in the push direction as positive and loading in the pull direction as negative. Note that the experimental results for the two masonry walls tested in Series A are not included in this chapter, but are instead available in Appendix A.

4.1 Wall 1

The measured force-displacement curve for Wall 1 is presented in Figure 4.1, depicting the lateral displacement at the top of the wall as a function of the applied lateral shear force.

The maximum push direction strength of 215 kN was measured during the first cycle to +10 mm displacement, and the maximum pull direction strength of -205 kN was measured at the first cycle to -6 mm displacement. The wall cracking pattern was characterised by the initiation of horizontal flexural cracking of the mortar joints at low displacement (less than ± 2 mm displacement, or drift of 0.11%). As the wall was being pushed/pulled to further lateral displacement, initiation of diagonal cracks occurred when the principal tensile stresses exceeded the tensile strength of masonry under increasing lateral displacement (see section 2.5). This type of failure was expected for this wall since the predicted wall shear strength was slightly lower than its flexural strength.

Figure 4.1 shows the wall did not exhibit sudden loss of strength. It was therefore possible to classify Wall 1 as having a flexure/shear failure. This type of failure was made possible due to the adoption of closely distributed horizontal shear reinforcement using small size bars (R6). Accordingly, the initial diagonal cracks did not widen significantly under increasing horizontal load, but instead new sets of diagonal cracks formed and gradually spread over the wall diagonals, accompanied by high energy dissipation and ductile behaviour. Failure occurred gradually in this case as the strength of the wall deteriorated under cyclic horizontal loading. Finally, partial crushing at the compression toe and at severely cracked portions of the wall diagonals took place at larger imposed lateral displacement. Due to the significant diagonal shear cracking and the absence of abrupt strength degradation, this wall may also be classified as suffering a “ductile shear failure”. The cracking pattern for this wall is depicted in Figure 4.2.

It is shown in Figure 4.1 that the maximum strength developed by the wall was less than the calculated flexural strength. It is also shown that the shear strength predicted by the current New Zealand masonry standard, NZS 4230:1990 was significantly lower than the actual wall shear strength. The shear strength predicted by NEHPR more closely matched the experimentally measured wall shear strength.

The yield displacement for Wall 1 was evaluated to be 3.0 mm. The wall was defined as failing during the second cycle to 12 mm displacement.

An initial wall stiffness of 108 kN/mm was calculated from the peak strength measured during the cycle to ± 0.5 mm displacement. The wall stiffness dropped significantly to 22 kN/mm when maximum push direction strength developed at +10 mm displacement.

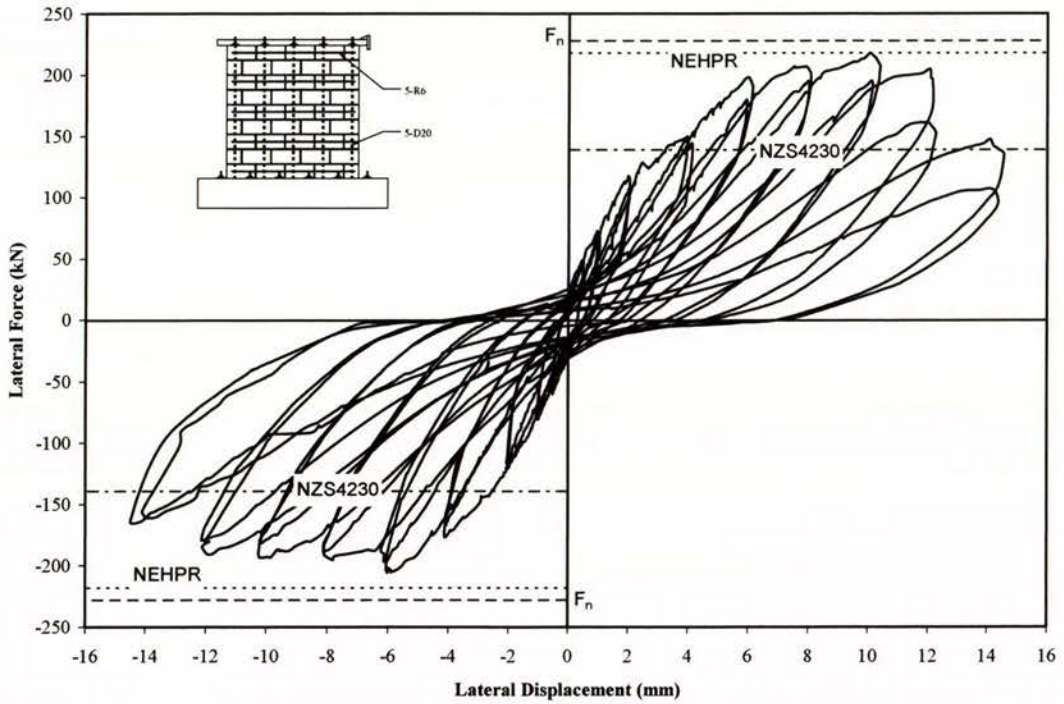


Figure 4.1 Force-displacement history for Wall 1.

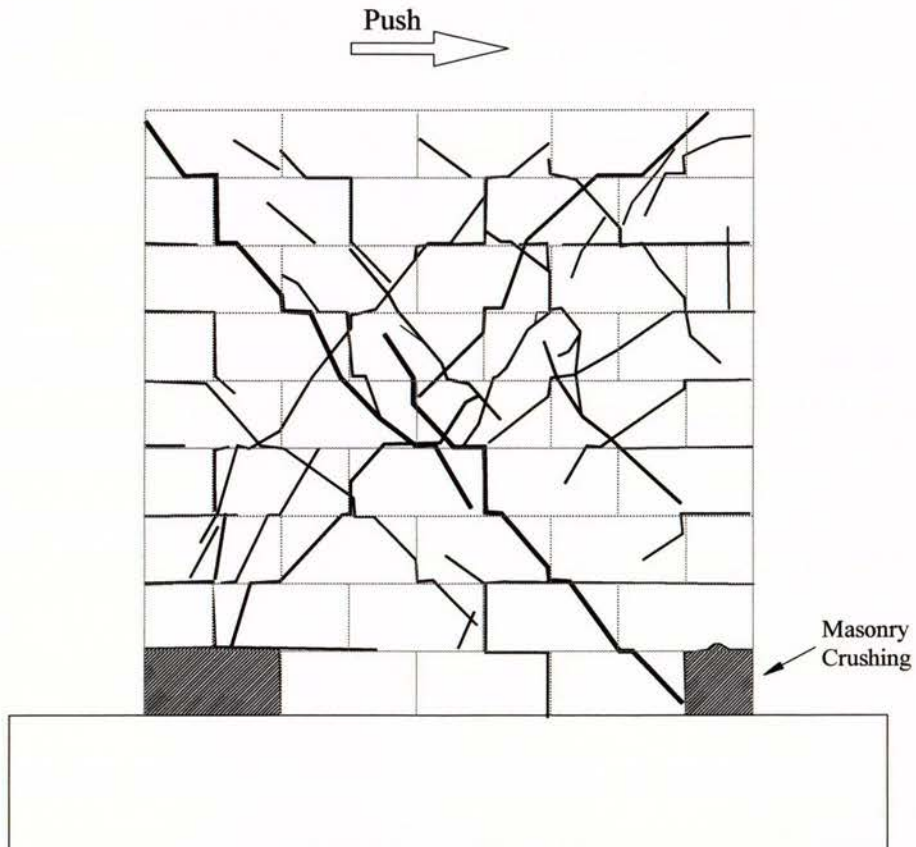


Figure 4.2 Wall 1 cracking pattern at end of testing.

4.2 Wall 2

The measured force-displacement curve for Wall 2 is presented in Figure 4.3, depicting the lateral displacement at the top of the wall as a function of the applied lateral shear force.

The maximum push and pull direction strengths of +177 kN and -195 kN were measured during the first cycle to ± 6 mm of displacement. Significant strength degradation took place in both directions after the wall developed its maximum strength. The wall exhibited a shear type failure, characterised by the initiation of horizontal cracks at low displacement levels (less than ± 2 mm), and the formation of diagonal cracks at larger displacement levels. This type of failure was expected for this wall since the predicted wall shear strength was less than its flexural strength.

Figure 4.3 shows that rapid strength degradation took place immediately after the maximum strength was reached. It was therefore possible to classify Wall 2 as having a “brittle shear failure”. This type of failure was due to the lack of shear reinforcement to provide proper shear transfer across the diagonal cracks, therefore the initial diagonal cracks opened extensively with poor energy dissipation capacity. Finally, the formation of a major diagonal crack pair caused rapid strength degradation at larger imposed lateral displacements. The cracking pattern for this wall is depicted in Figure 4.4.

It is shown in Figure 4.3 that the maximum strength developed by the wall was significantly less than the calculated flexural strength, indicating that the wall failed in shear. It is shown that the wall shear strength was about 77% more than that predicted by NZS4230:1990, and that the shear strength predicted by NEHPR more closely matched the experimentally measured wall strength. The yield displacement for Wall 2 was evaluated to be 2.3 mm. The wall was defined as failing during the second cycle to 8 mm displacement.

An initial wall stiffness of 144 kN/mm was calculated from the peak strength measured during the cycle to ± 0.5 mm displacement. The wall stiffness dropped to 30 kN/mm when maximum wall strength developed during the first cycle to ± 6 mm displacement.

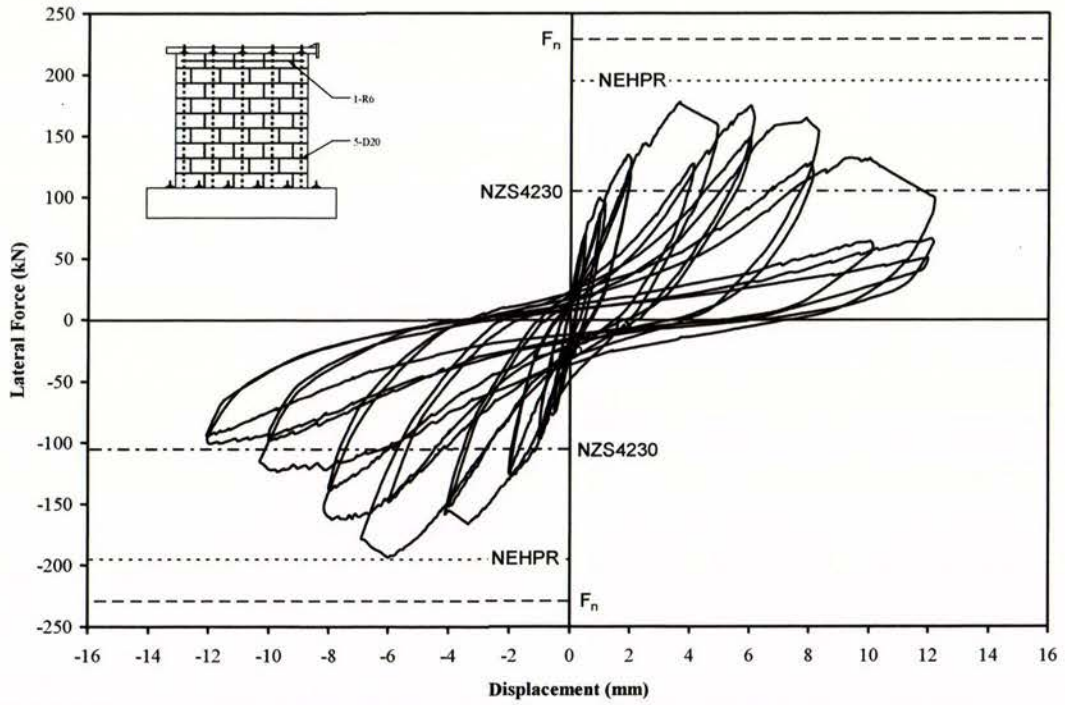


Figure 4.3 Force-displacement history for Wall 2.

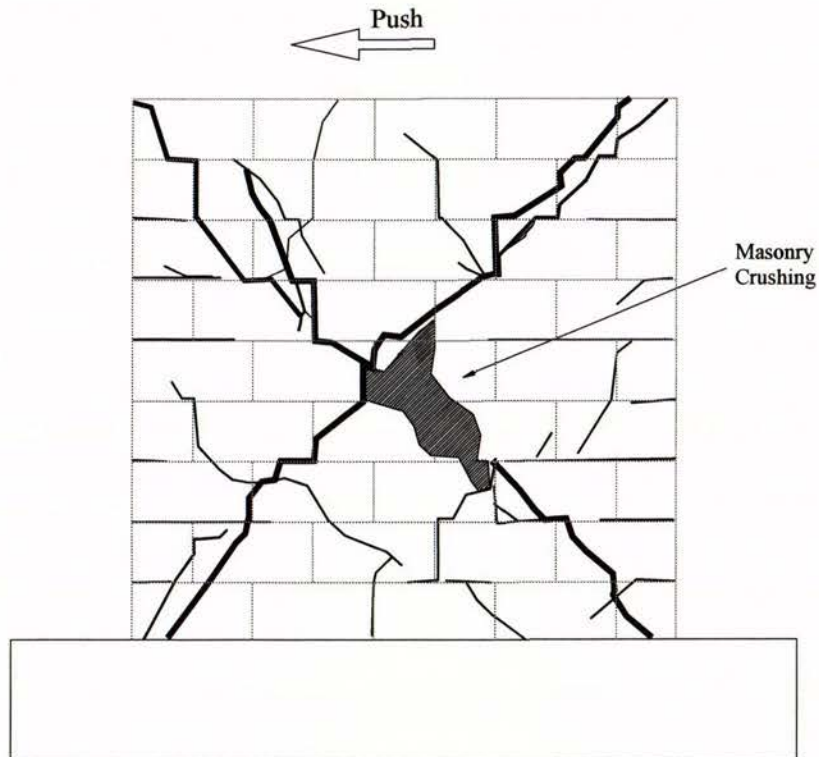


Figure 4.4 Wall 2 cracking pattern at end of testing.

4.3 Wall 3

The force-displacement curve for Wall 3 is presented in Figure 4.5, showing the relationship between the wall lateral displacement and the lateral force as the wall was cycled back and forth.

The wall developed a maximum push direction strength of 215 kN during the first cycle to +8 mm displacement, and a maximum pull direction strength of -203 kN during the first cycle to -6 mm displacement. As shown in Figure 4.5, it is noted that the maximum strength developed was about 94% of the calculated flexural strength of 229 kN. It was observed that a continuous crack at the wall base caused significant sliding to take place along the wall-foundation base interface (sliding contributed about 20% of the wall lateral displacement). Due to the sliding displacement that occurred during displacement reversal, a significant portion of the shear force was transferred by dowel action of the vertical reinforcement. This, in turn, led to a reduction in wall strength, and consequently led to the failure of the wall to develop its predicted flexural strength.

As shown in Figure 4.5, the wall did not exhibit sudden loss of strength after maximum strength was developed. Although horizontal and diagonal shear cracks were prominent on the wall face, the ultimate failure mode was characterised by face shell spalling and significant sliding at wall-foundation base interface. It is therefore possible to classify Wall 3 as having a sliding-flexure type of failure.

The yield displacement for Wall 3 was evaluated to be 2.46 mm. The wall was defined as failing during the second cycle to 10 mm displacement.

An initial wall stiffness of 114 kN/mm was calculated from the peak strength measured during the cycle to ± 0.5 mm displacement. The wall stiffness dropped significantly to 34 kN/mm when the maximum strength developed at -6 mm displacement.

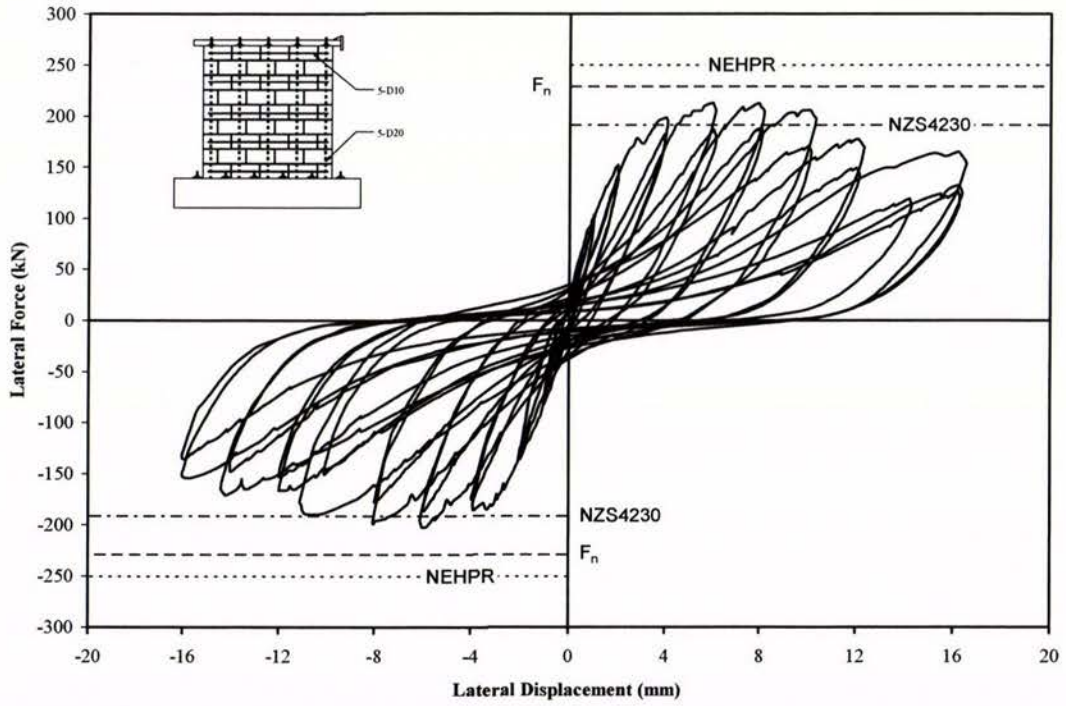


Figure 4.5 Force-displacement history for Wall 3.

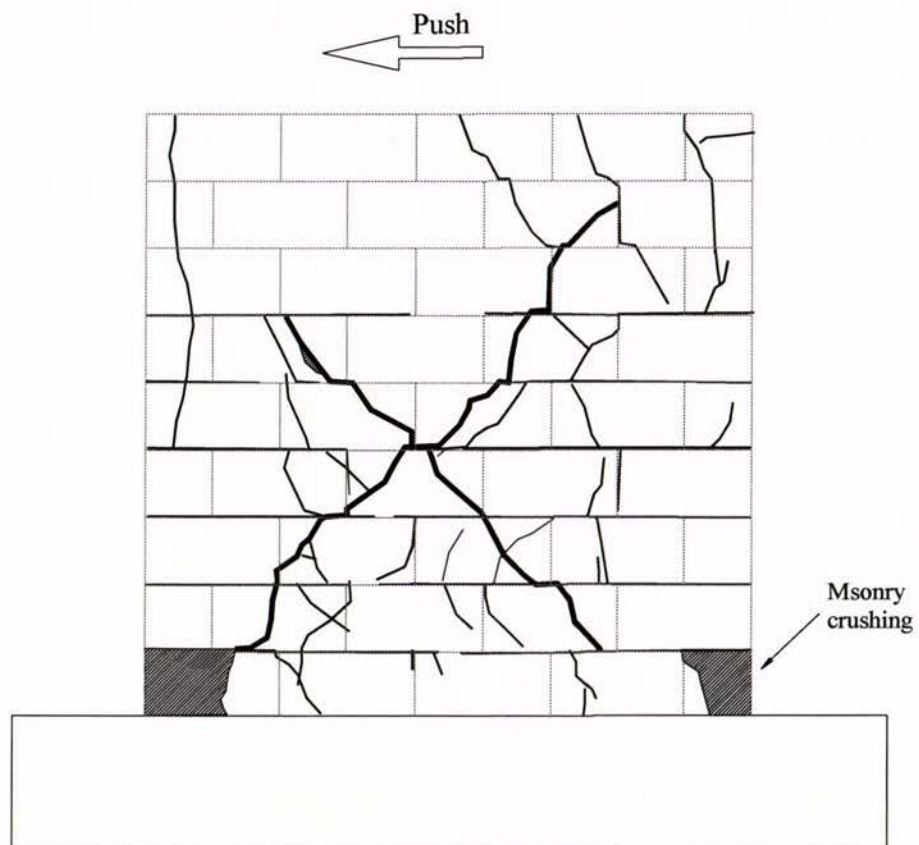


Figure 4.6 Wall 3 cracking pattern at end of testing.

4.4 Wall 4

The measured force-displacement curve for Wall 4 is presented in Figure 4.7, showing the lateral displacement at the top of the wall as a function of the applied lateral force.

The maximum push direction strength of +223 kN was measured during the first cycle to +8 mm displacement, and the maximum pull direction strength of -201 kN was measured during the first cycle to -6 mm displacement. The wall exhibited a shear type of failure, characterised by the initiation of horizontal cracks at low displacement levels. As the wall was pushed/pulled to further displacement, initiation of diagonal cracking occurred when the principal stresses due to applied lateral force exceeded the masonry tensile strength (see section 2.5). This type of failure was expected for this wall since the predicted wall shear strength was less than its flexural strength.

As shown in Figure 4.7, rapid strength degradation took place after the maximum strength was reached. It was therefore possible to classify Wall 4 as having a “brittle shear failure”. This type of shear failure was expected since the wall was constructed without closely distributed shear reinforcement. Therefore the tensile stress due to applied shear load could not be adequately transferred across the diagonal cracks. Hence the cracks opened extensively, resulting in a major x-shaped diagonal crack pair, which led to a relatively sudden and destructive failure. The cracking pattern for this wall is depicted in Figure 4.8.

It is shown in Figure 4.7 that the maximum strength developed by the wall was less than the calculated flexural strength, indicating that the wall failed in shear. It is shown that the wall shear strength was about 40% more than that allowed by NZS4230:1990, and that the shear strength predicted by NEHPR more closely matched the measured wall strength.

The yield displacement of Wall 4 was evaluated to be 2.74 mm. The wall was defined as failing during the first cycle to -10 mm displacement.

An initial wall stiffness of 111 kN/mm was calculated from the peak strength measured during the first cycle to ± 0.5 mm displacement. The wall stiffness dropped to 34 kN/mm when maximum strength developed during the cycle to -6 mm displacement.

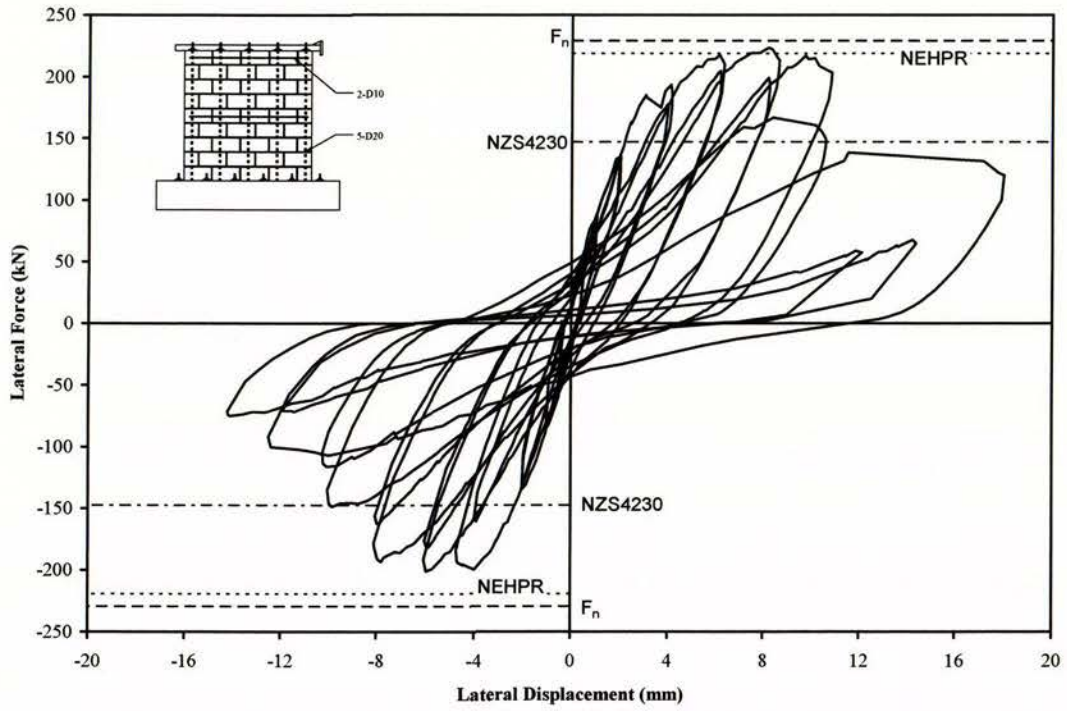


Figure 4.7 Force-displacement history for Wall 4.

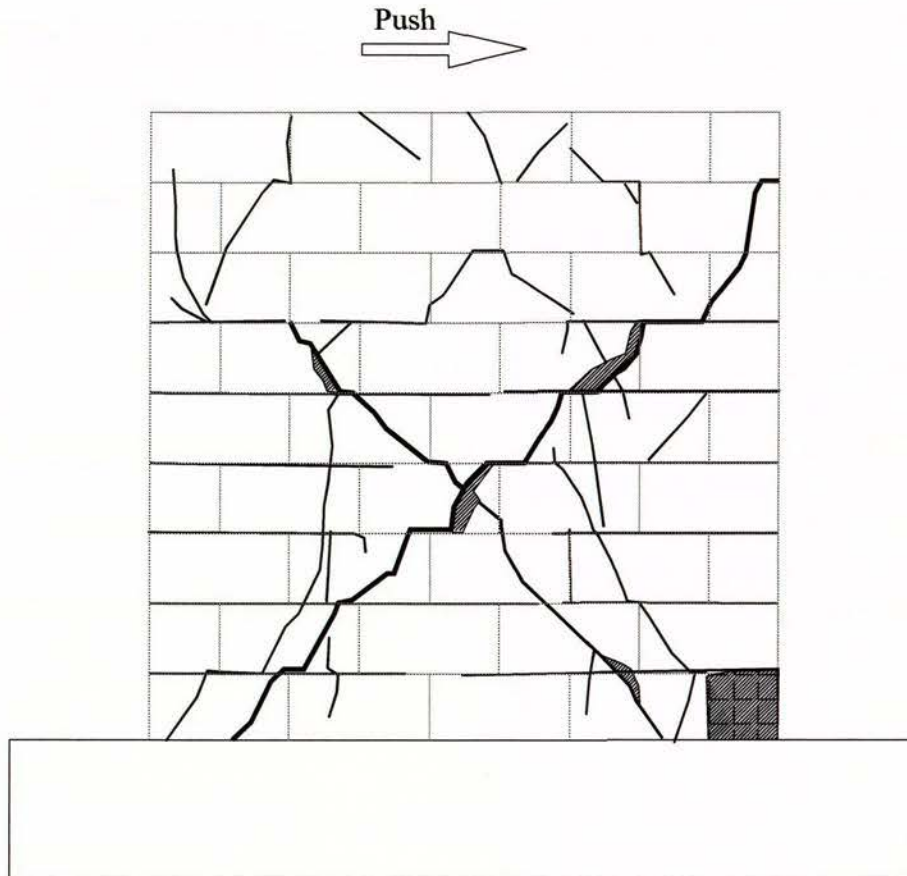


Figure 4.8 Wall 4 cracking pattern at end of testing.

4.5 Wall 5

Inspection of wall 5 prior to testing revealed significant structural damage on the wall side closest to the actuator, therefore affecting the wall strength in the pull direction. This damage was caused by an object falling onto the wall during the period between erection and testing. It was decided that the wall would be loaded according to the loading sequence described in section 3.8, but that measured strength in the pull direction was considered to be non-representative of the actual wall strength.

The wall exhibited shear response, signified by the opening of large diagonal shear cracks across the wall face. This diagonal crack was initiated by tension splitting of masonry in the compression strut that formed in the wall. Horizontal cracking was observed at low displacement levels before the onset of shear cracking. The wall was expected to exhibit a shear type of failure based on relatively low masonry shear strength due to partial grouting and because no horizontal shear reinforcement was employed.

Diagonal cracking initiated at the displacement level of ± 2 mm. The initiation of diagonal cracking did not cause immediate strength loss. The wall strength continued to develop until a maximum push direction strength of +143 kN and maximum pull direction strength of -134 kN were measured during the first cycle to ± 8 mm displacement. The measured force-displacement curve for Wall 5 is presented in Figure 4.9, depicting the lateral displacement at the top of the wall as a function of the applied lateral shear force. The figure shows that rapid strength degradation took place after the wall developed its maximum strength. This phenomenon is particularly obvious in the pull direction. Figure 4.9 shows that neither of the two shear equations could properly capture the actual shear strength of this partially grouted masonry wall.

The yield displacement for this partially grouted wall was evaluated to be 4.68 mm. The wall was defined as failing during the second push cycle to 10 mm displacement. A wall stiffness of 74 kN/mm was calculated during the first cycle to +0.5 mm displacement. The stiffness dropped significantly to 17 kN/mm when the wall developed its maximum strength during the first push cycle to +8 mm displacement.

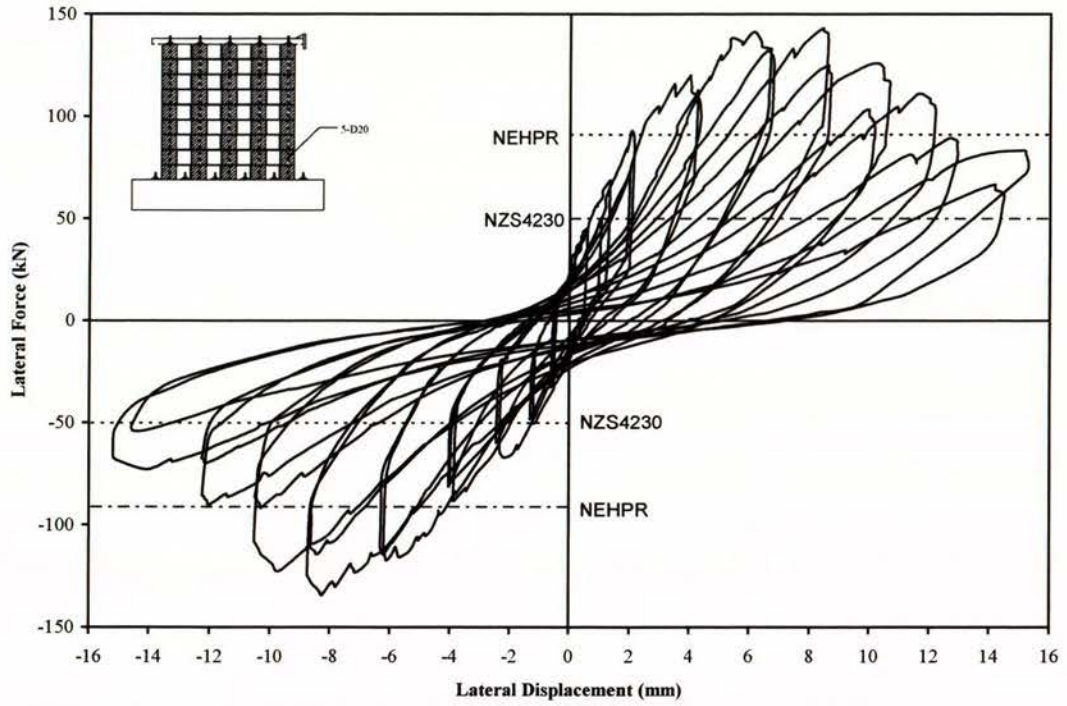


Figure 4.9 Force-displacement history for Wall 5 ($F_n = 229$ kN).

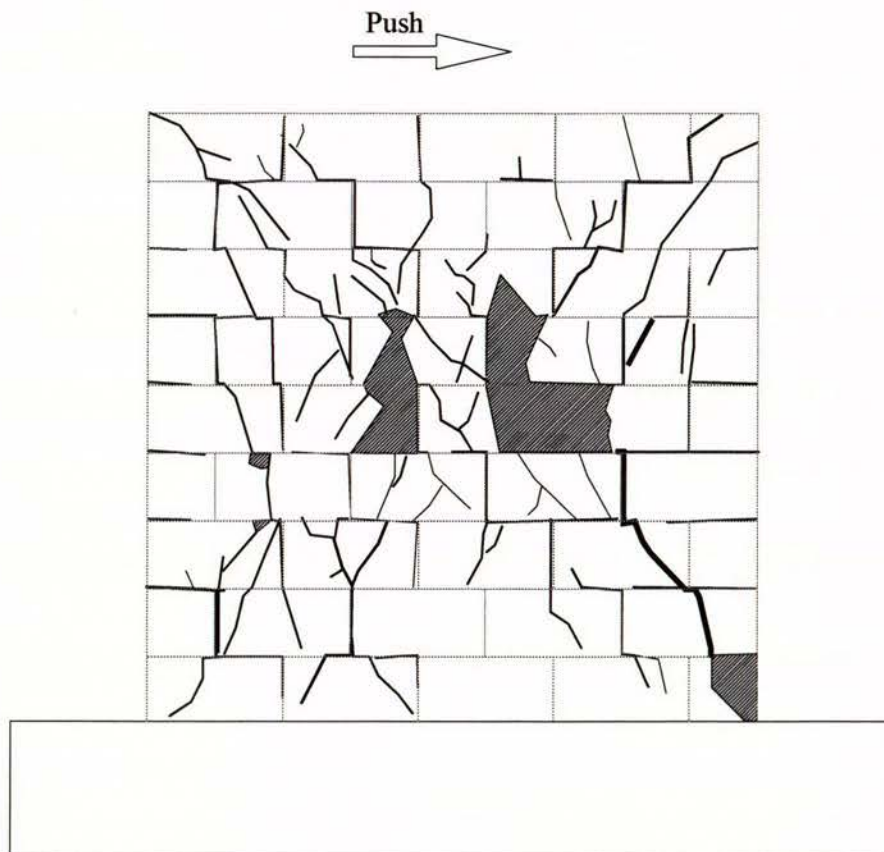


Figure 4.10 Wall 5 cracking pattern at end of testing.

4.6 Wall 6

The measured force-displacement curve for Wall 6 is presented in Figure 4.11, showing the relationship between the lateral displacement at the top of the wall and the applied lateral shear force.

The wall exhibited shear response, signified by the opening of large diagonal cracks across the wall face. These diagonal cracks were initiated when the principal tensile stresses exceeded the tensile strength of masonry under increasing imposed horizontal displacements. This wall was expected to exhibit shear dominated behaviour based on the relatively low masonry shear strength due to partial grouting and because no horizontal shear reinforcement was employed. The cracking pattern for this wall is depicted in Figure 4.12.

Diagonal cracking initiated during the first displacement cycle to -1 mm. The initiation of diagonal cracking did not cause immediate strength loss. The wall strength continued to develop until maximum strengths of +93 kN and -93 kN were measured in the first cycle to +8 mm and -10 mm displacement.

It is shown in Figure 4.11 that the maximum shear strength developed by the wall was about 86% more than that calculated using NZS4230:1990, and that the shear strength predicted by NEHPR matched the experimental result.

The yield displacement of Wall 6 was evaluated to be 5.09 mm. The wall was defined as failing during the second cycle to -14 mm displacement.

A wall stiffness of 35 kN/mm was calculated during the first cycle to ± 0.5 mm displacement. However, the stiffness dropped to 11 kN/mm when the wall developed its maximum strength in the first push cycle to +8 mm displacement.

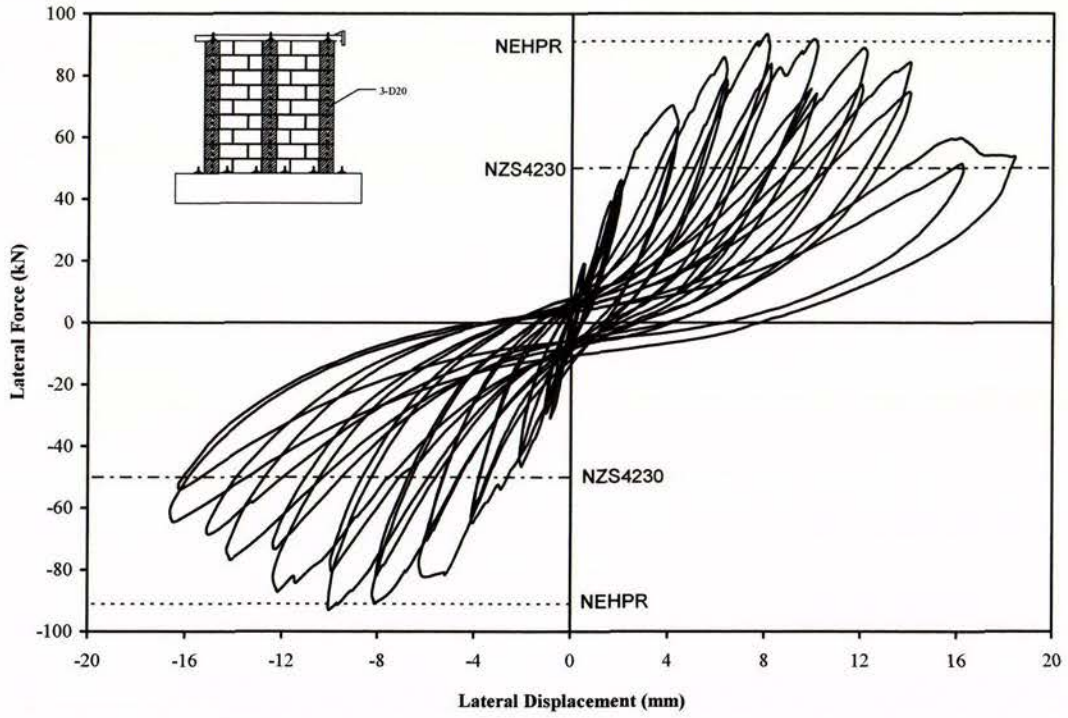


Figure 4.11 Force-displacement history for Wall 6 ($F_n = 142$ kN).

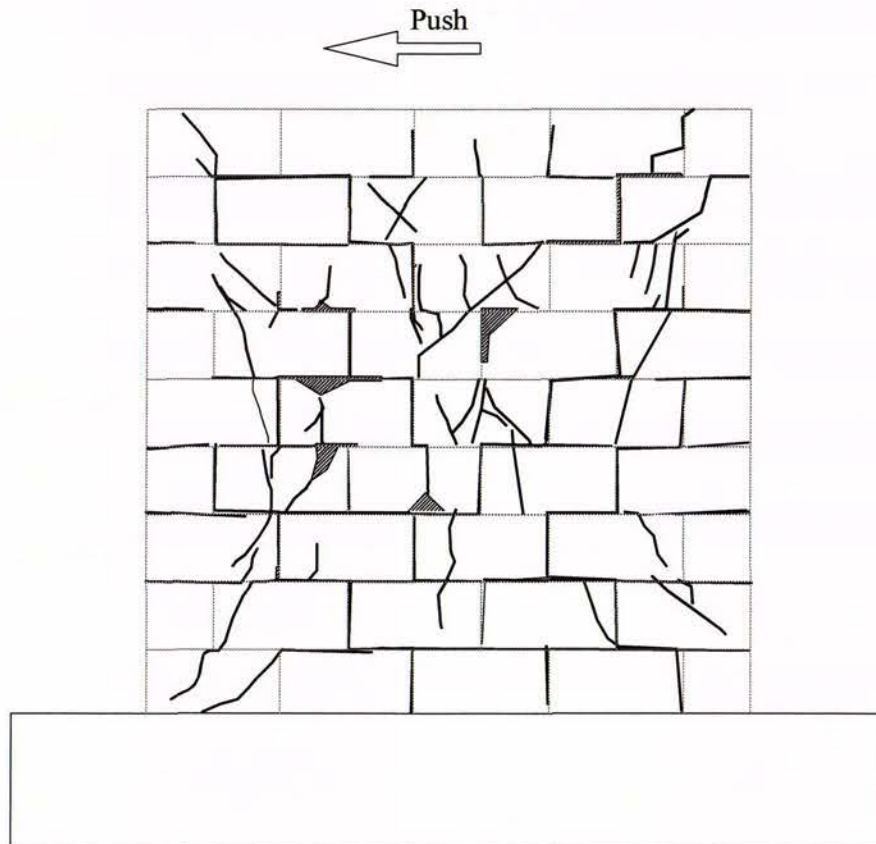


Figure 4.12 Wall 6 cracking pattern at end of testing.

4.7 Wall 7

The measured force-displacement curve for Wall 7 is presented in Figure 4.13, depicting the lateral displacement at the top of the wall as a function of the applied lateral shear force.

The wall exhibited flexure response for low displacement levels of up to ± 1 mm, signified by the opening of horizontal cracks on mortar joints. The first diagonal crack initiated when the wall was loaded towards -2 mm. As shown in Figure 4.13, the wall exhibited near symmetrical response throughout the test.

The wall resistance built up to a maximum of about +263 kN/-261 kN during the first cycle to ± 6 mm displacement. Rapid strength degradation took place in both loading directions after the maximum strengths were reached. The rapid loss of strength coincided with the significant widening of the x-shaped diagonal crack pair. See Figure 4.14 for the wall's cracking pattern.

The failure mode was characterised by diagonal shear cracking forming on the wall and crushing of wall toes. The observed failure could therefore be categorised as a shear type of failure. This type of failure was expected since the predicted wall shear strength was lower than the predicted wall flexural strength.

As shown in Figure 4.13, the maximum shear strength achieved by the wall was about 50% more than that allowed by NZS4230:1990, suggesting that the current New Zealand masonry standard is excessively conservative in its shear strength provisions. The shear strength predicted by NEHPR is shown to closely match the experimental result.

The yield displacement of Wall 7 was evaluated to be 2.20 mm. The wall was defined as failing during the second cycle to +8 mm displacement. A wall stiffness of 147 kN/mm was calculated at the first cycle to ± 0.5 mm displacement. The stiffness dropped to 43 kN/mm when maximum strength developed in the first cycle to ± 6 mm displacement.

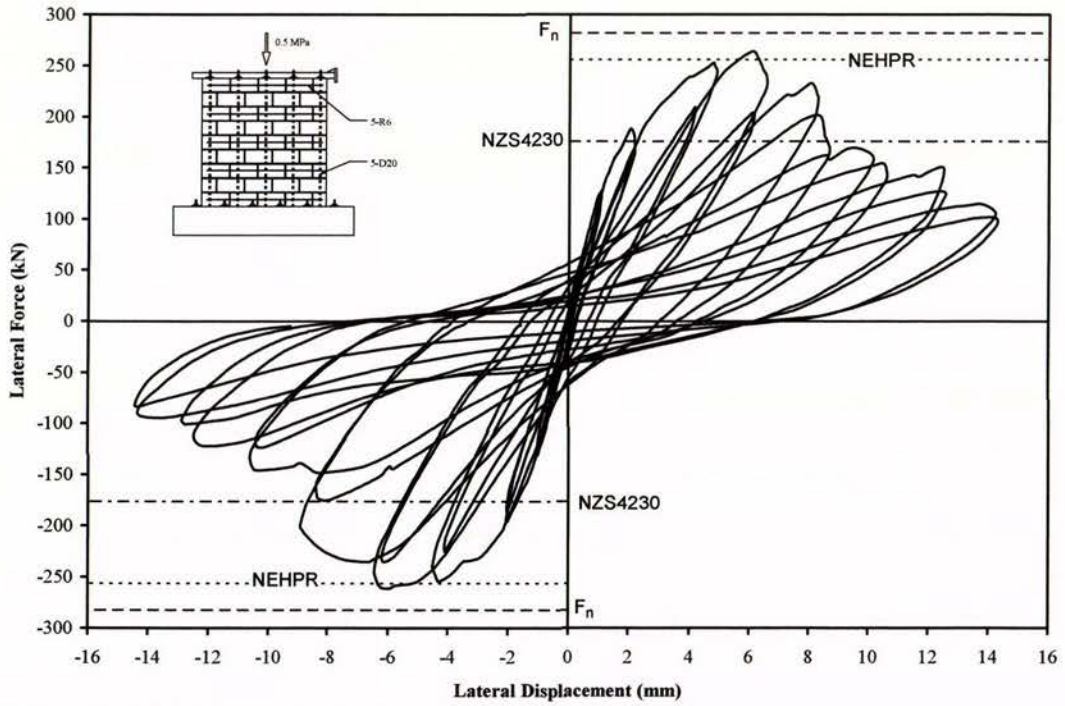


Figure 4.13 Force-displacement history for Wall 7.

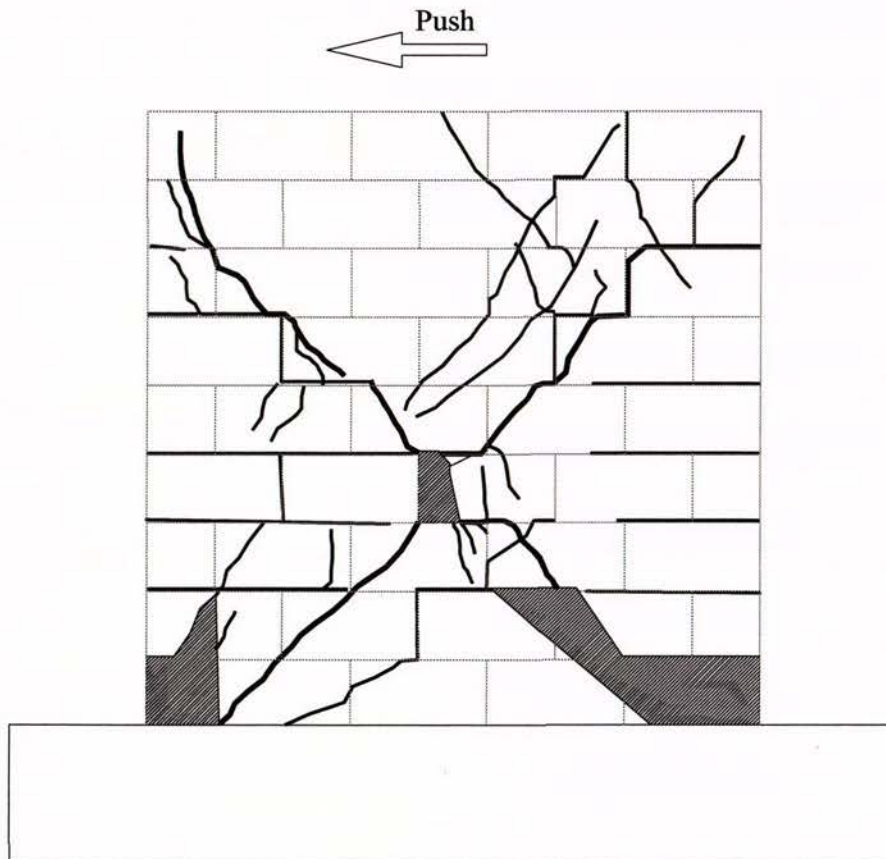


Figure 4.14 Wall 7 cracking pattern at end of testing.

4.8 Wall 8

The measured force-displacement curve for Wall 8 is presented in Figure 4.15, depicting the lateral displacement at the top of the wall as a function of the applied shear force.

The wall exhibited shear response, signified by the opening of large diagonal shear cracks across the wall face. Flexural response was observed at lower displacement levels before the onset of diagonal shear cracking.

The wall resistance built up to a maximum of about +244 kN/-250 kN at the displacement level of ± 6 mm. Significant diagonal crack widening occurred when the wall was pulled to -6 mm displacement, causing significant strength degradation in the subsequent push and pull directions. See Figure 4.16 for the wall cracking pattern.

The failure mode was characterised by diagonal shear cracking initiated by tension splitting in the diagonal compression strut forming on the wall when laterally loaded. The wall was expected to exhibit a shear mode of failure since the predicted shear strength was lower than the calculated flexural strength.

Figure 4.15 shows that the maximum shear strength achieved by the wall was about 53% more than that calculated using NZS4230:1990, suggesting that the current New Zealand masonry standard is excessively conservative in its shear strength provisions. Conversely, the shear strength predicted by NEHPR closely matched the experimental result.

The yield displacement of Wall 8 was evaluated to be 2.20 mm. The wall was defined as failing during the second cycle to 6 mm displacement.

A wall stiffness of 138 kN/mm was calculated during the first cycle to ± 0.5 mm displacement. The stiffness dropped to 40 kN/mm when maximum strength developed during the first cycle to ± 6 mm displacement.

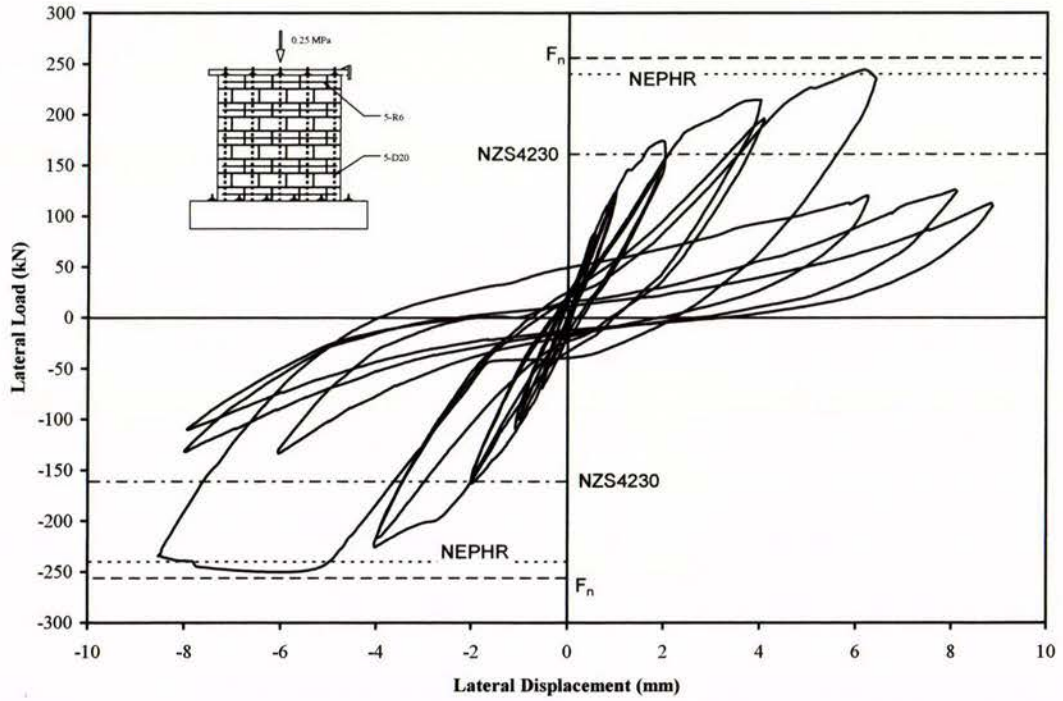


Figure 4.15 Force-displacement history for Wall 8.

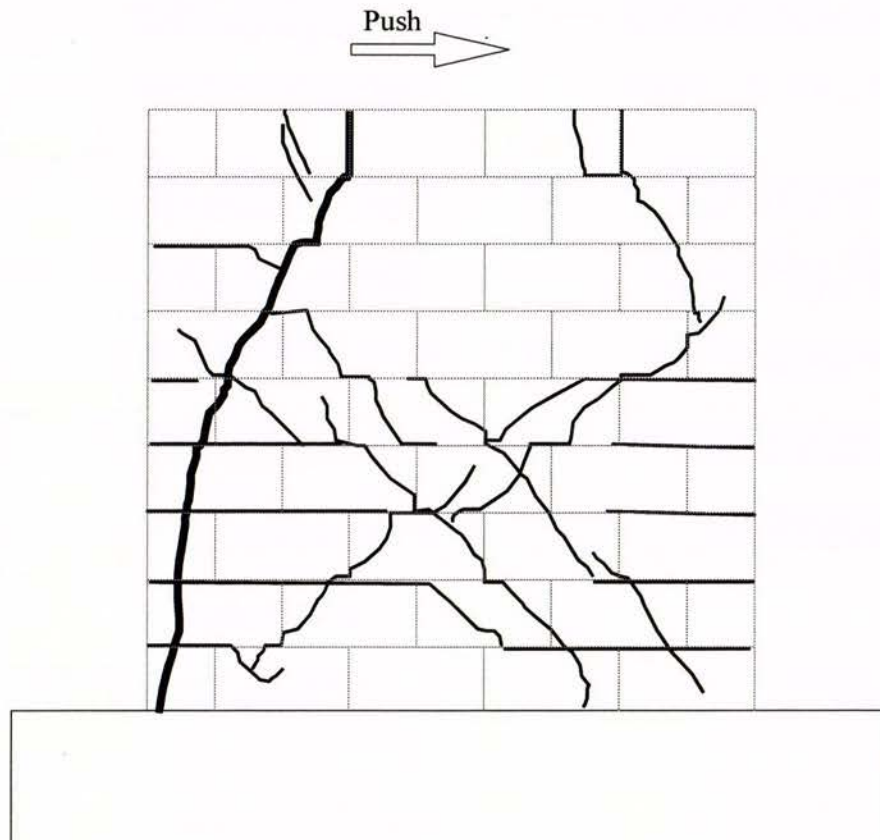


Figure 4.16 Wall 8 cracking pattern at end of testing.

4.9 Wall 9

The measured force-displacement curve for Wall 9 is presented in Figure 4.17, depicting the lateral displacement at the top of the wall as a function of the applied lateral shear force. The wall exhibited flexure response for displacements of up to ± 4 mm, signified by the formation of horizontal cracks on mortar joints. The first diagonal crack initiated when the wall was pushed to +8 mm displacement. As shown in Figure 4.17, Wall 9 exhibited near symmetrical response throughout the test.

The wall strength built up to a maximum of +204 kN/-207 kN during the first cycle to ± 20 mm displacement. Wall 9 displayed a shear type of failure. This was characterised by early flexural horizontal cracks on mortar joints at low displacement level which were later augmented with diagonal cracks that extended across the wall. Shear failure took place after the wall developed its maximum strength, which was followed by rapid strength degradation (see Figure 4.17), characterised by the opening of diagonal cracks and crushing of the compression toe. See Figure 4.18 for the wall's cracking pattern.

It is clearly illustrated in Figure 4.17 that the maximum strength developed by Wall 9 was significantly less than the calculated flexural strength, therefore strongly indicated the wall failed in shear. It is also shown in Figure 4.17 that the shear strength predicted by NZS4230:1990 was only slightly less than the actual shear strength achieved by the masonry wall. The NEHPR expression had however over-predicted the actual shear strength of this slender masonry wall by about 23%. Consequently, the test result of this 3.6 m tall masonry wall indicated the possible likelihood of NEHPR to unsafely over-estimate the shear strength of masonry walls that have h_e/ℓ_w ratios of more than 1.

The yield displacement for Wall 9 was evaluated to be 7.0 mm. The wall was defined as failing during the first cycle to -24 mm displacement. A wall stiffness of 43 kN/mm was calculated during the first cycle to ± 1.0 mm displacement. The wall stiffness dropped to 10 kN/mm when maximum wall strength developed at ± 20 mm displacement.

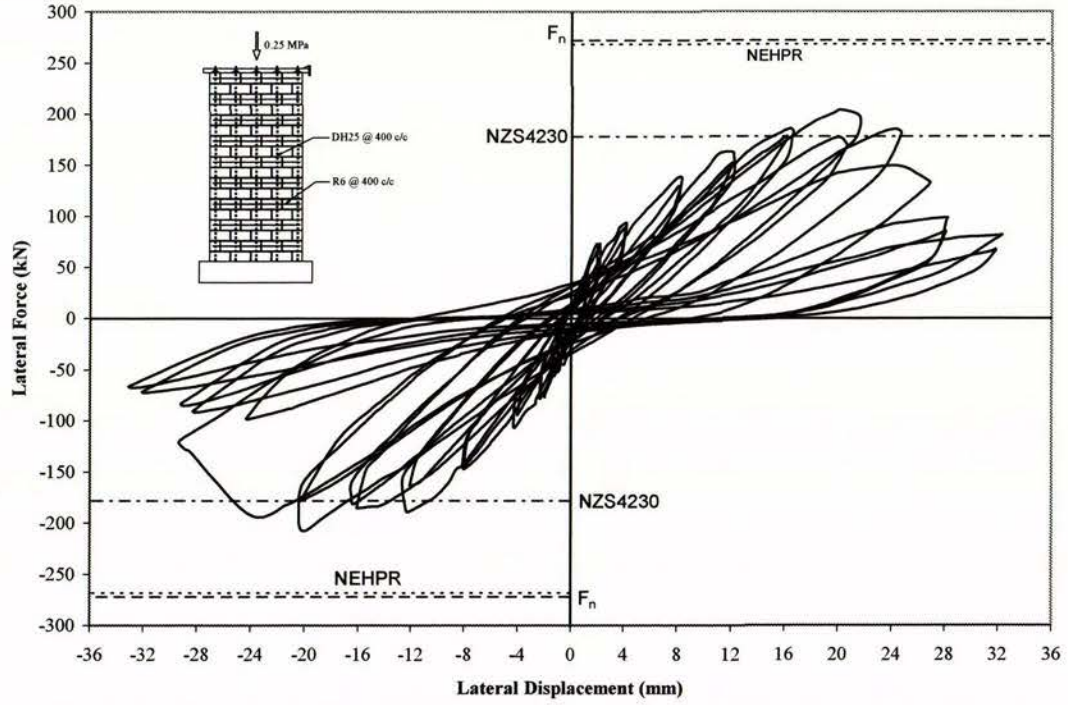


Figure 4.17 Force-displacement history for Wall 9.

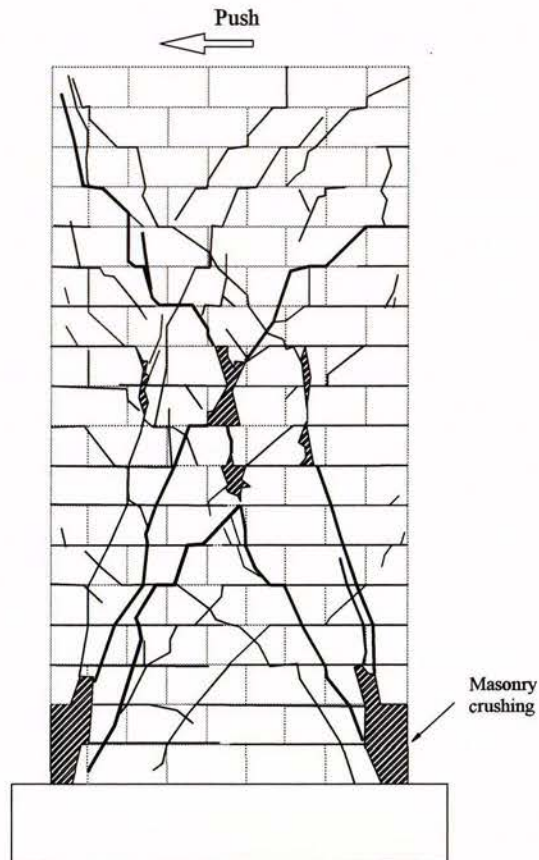


Figure 4.18 Wall 9 cracking pattern at end of testing.

4.10 Wall 10

The measured force-displacement curve for Wall 10 is presented in Figure 4.19, depicting the lateral displacement at the top of the wall as a function of the applied shear force. The wall exhibited shear response, characterised by significant diagonal shear cracking. Similar to other tested walls, flexural cracking was observed at a low displacement level (up to ± 0.5 mm) before the onset of shear cracking.

The maximum push and pull direction strengths of +572kN and -598kN were measured during the first cycle to ± 4 mm displacement. Rapid strength degradation took place immediately after a wide diagonal crack grew abruptly near the wall edge when the wall was pulled to -4 mm. See Figure 4.20 for the wall cracking pattern.

The failure mode was characterised by significant diagonal shear cracking forming on the wall. These cracks were initiated by tension splitting of masonry in the compression strut that formed on the wall. The observed failure could therefore be categorised as a shear type of failure. This type of failure was expected because the predicted shear strength was lower than the predicted flexural strength.

Figure 4.19 shows that the maximum strength developed by Wall 10 was significantly less than the calculated flexural strength, therefore confirming that the wall failed in shear. As shown in Figure 4.19, the maximum shear strength achieved by the wall was about double that allowed by the NZS4230:1990, therefore confirming the conservative shear strength provisions of NZS4230:1990. This was mostly due to the low v_m that is allowed by NZS4230:1990 (since NZS4230:1990 allows $v_m \leq 0.72$ MPa) despite of high f'_m value. Conversely, the shear strength predicted by NEHPR closely matched the actual wall strength recorded during testing.

The yield displacement of Wall 10 was evaluated to be 3.0 mm. The wall was defined as failing during the second push cycle to +4 mm displacement. A wall stiffness of 283 kN/mm was calculated when the wall was loaded to ± 0.5 mm displacement. The wall stiffness dropped to 142 kN/mm when maximum strength developed during the first cycle to ± 4 mm displacement

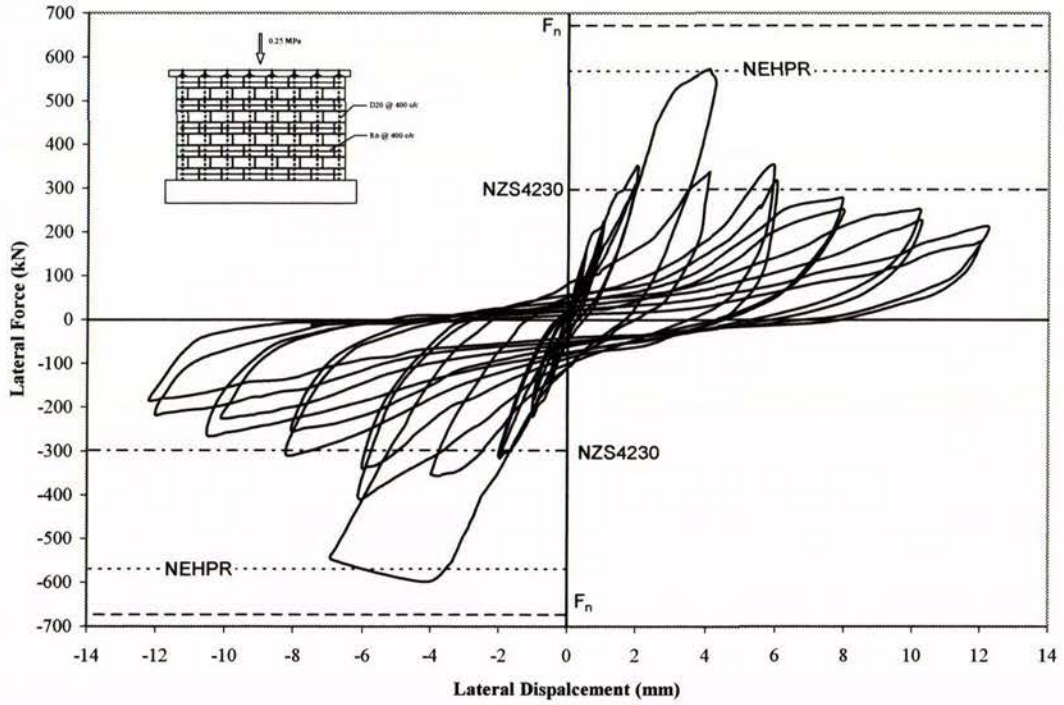


Figure 4.19 Force-displacement history for Wall 10.

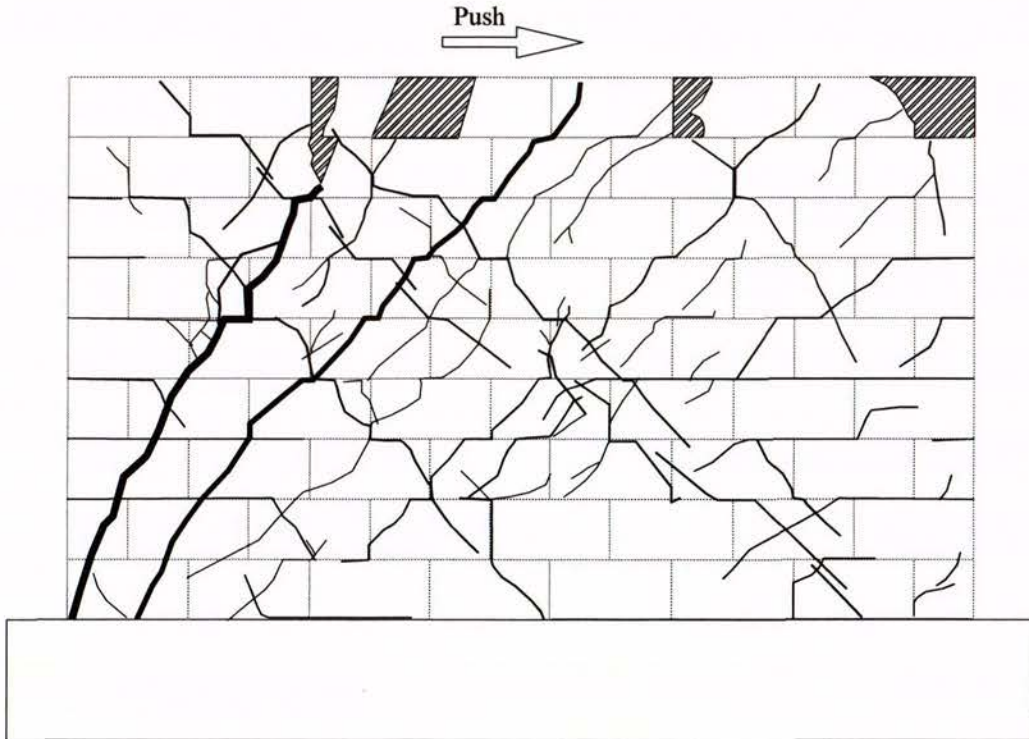


Figure 4.20 Wall 10 cracking pattern at end of testing.

Chapter 5

Comparison of Tested Wall Behaviour

5.1 Introduction

The test matrix shown in Table 3.1 was conceived to facilitate comparison of wall behaviour between two or more walls with respect to variation of a given design parameter. The test results are discussed in this section with reference to parameters that were varied during these ten wall tests (Series B and C). These parameters were defined in section 1.4 as:

1. Amount of horizontal reinforcement,
2. The distribution of horizontal reinforcement,
3. The type of grouting, i.e. full grouting vs partial grouting,
4. The level of axial compression stress,
5. Different H/L ratio.

The figures in this section are limited to force-displacement (F-D) envelopes and stiffness degradation curves, arranged in groups to show the effect of a particular parameter. A full set of curves for each test is presented in Appendices B and C.

The main method of displaying the test results is by means of F-D envelopes. These are curves that relate the peak strength recorded in the first cycle for each displacement level. In addition, curves are developed to show stiffness degradation of walls as the lateral displacement/force increases. The stiffness is obtained by dividing the extreme positive and negative lateral forces by the corresponding displacement in each displacement cycle. The stiffness values obtained from the first cycle of loading were averaged and plotted against the corresponding lateral displacement or force. The stiffness degradation curve is truncated when maximum strength is attained.

Table 5.1 shows key test results for the individual wall. The results are given for both directions of loading. V_{max} corresponds to the maximum wall strength measured in the test, and Δ_y is the evaluated yield displacement of tested walls. d_{vmax} is defined as the displacement at which the maximum strength was measured, while d_u is the displacement at which wall strength dropped below $0.8 V_{max}$. $K_{0.5}$ is defined as the wall stiffness when loaded to ± 0.5 mm displacement.

Table 5.1 Summary of test results

Wall specimen	Prediction			Test result									
	F_n	V_n^*	$\frac{F_n}{V_n}$	Δ_y	d_{vmax}	V_{max}	$\frac{V_{max}}{V_n}$	$\frac{V_{max}}{F_n}$	d_u	μ_{vmax}^{**}	$K_{0.5}$	Failure mode	
Series B	1	229	219	1.05	3.0	10 -6	215 -205	0.96	0.92	12 -14	2.67	108	Flexure/ Shear
	2	229	195	1.17	2.3	6 -6	177 -195	0.95	0.81	8 -8	2.61	144	Shear
	3	229	250	0.92	2.5	8 -6	215 -203	0.84	0.91	10 -10	2.80	114	Sliding/ Flexure
	4	229	219	1.05	2.7	8 -6	223 -201	0.97	0.93	10 -10	2.59	111	Shear
	5	229	91	2.52	4.7	8 -8	143 -134	1.57	0.62	10 -10	1.70	74	Shear
	6	142	91	1.56	5.1	8 -10	93 -93	1.02	0.65	14 -14	1.76	35	Shear
	7	282	256	1.10	2.2	6 -6	263 -261	1.02	0.93	8 -8	2.73	147	Shear
	8	256	240	1.07	2.2	6 -6	244 -250	1.03	0.96	6 -6	2.73	138	Shear
Series C	9	272	268	1.01	7.0	20 -20	204 -207	0.77	0.76	24 -24	2.86	43 ^{***}	Shear
	10	672	568	1.18	3.0	4 -4	572 -598	1.03	0.87	4 -4	1.33	283	Shear
Units	kN	kN	--	mm	Mm	kN	--			mm		kN/mm	--

* V_n is the calculated masonry shear strength, based on net cross-sectional area using NEHPR (1998) recommendations; no strength reduction factor (ϕ) applied.

** $\mu_{vmax} = \frac{d_{vmax}}{\Delta_y}$

*** Stiffness of this wall when loaded to ± 1.0 mm displacement.

5.2 Force-displacement Envelope

The force-displacement (F-D) envelopes derived from the tests provide considerable information about the behaviour of the specimens and how that behaviour was affected by various parameters under investigation. The maximum shear strength and the shape of the F-D envelope are all dependent to a varying degree upon these parameters. These are discussed in the following subsections.

5.2.1 Effect of Horizontal Reinforcement

In this study both the amount and distribution of horizontal reinforcing bars was varied throughout the height of the wall. The general comment that can be made is that a change in the amount of horizontal reinforcement resulted in relatively little change in the maximum shear strength of the wall. This is illustrated in Figure 5.1, which shows the force-displacement envelopes for all fully grouted walls that had the same dimension and vertical reinforcement, but with varying horizontal reinforcement and no applied axial compression stress. The maximum shear strength increased from about 186 kN (average for push and pull) for Wall 2 to 210 kN for Wall 1 when the horizontal reinforcement increased from 1-R6 to 5-R6, resulted in a strength increase of about 12%. However, this increase in the maximum

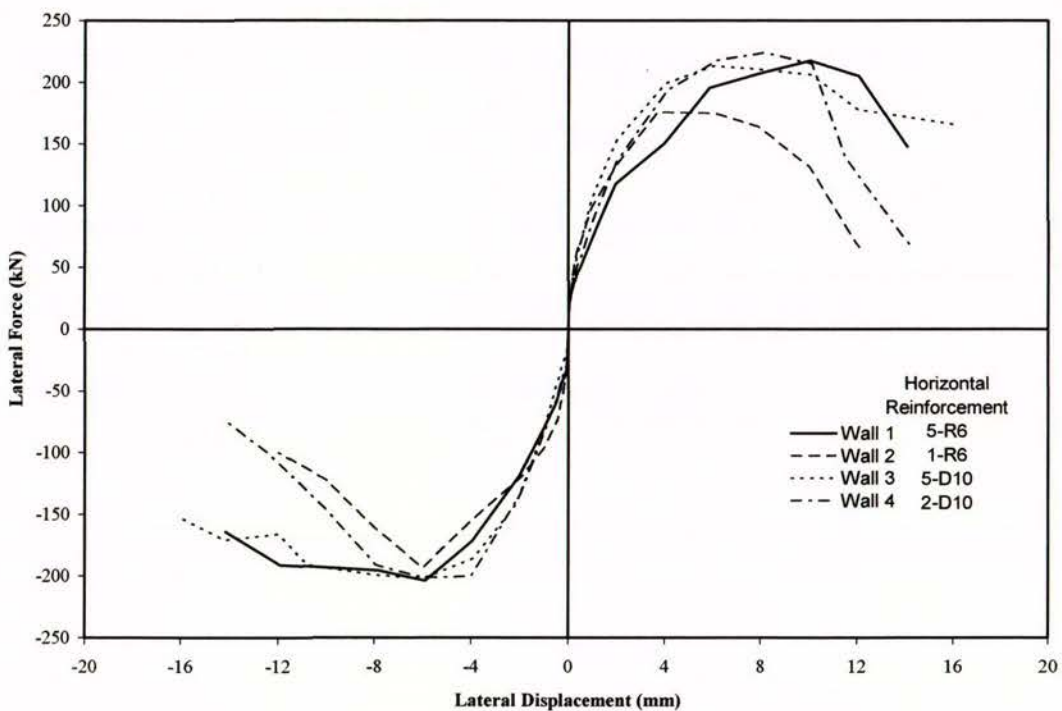


Figure 5.1 Effect of horizontal reinforcement on masonry shear strength.

shear strength with increasing amounts of horizontal reinforcement was not observed in Wall 3. In this case, the average maximum shear strength attained by Wall 3 was about the same as those recorded for Walls 1 and 4 although the horizontal reinforcement employed in Wall 3 was about 2.5 times the reinforcement area used in the other two walls.

Figure 5.2 shows the effectiveness of horizontal reinforcement in enhancing the post cracking performance of the walls. It can be seen that the form of the F-D envelopes improved when the amount of horizontal reinforcement increased from 1-R6 to 5-R6 reinforcing bars for the case of Walls 2 and 1, and when the horizontal reinforcement increased from 2-D10 to 5-D10 reinforcing bars for the case of Walls 4 and 3. However, the advantage of distributing horizontal reinforcement (using a larger number of reinforcing bars of smaller diameter) throughout the height of the wall can be undoubtedly observed from the F-D envelopes of Walls 1 and 4. The two walls contained approximately the same total cross-sectional area of shear reinforcement, but the shear reinforcement was distributed differently according to Figure 3.5. As shown in Figure 5.2, Wall 4 exhibited abrupt strength degradation after the peak wall strength was attained, whereas Wall 1 exhibited much more gradual strength degradation. This type of failure was made possible for Wall 1 due to the adoption of 400 mm

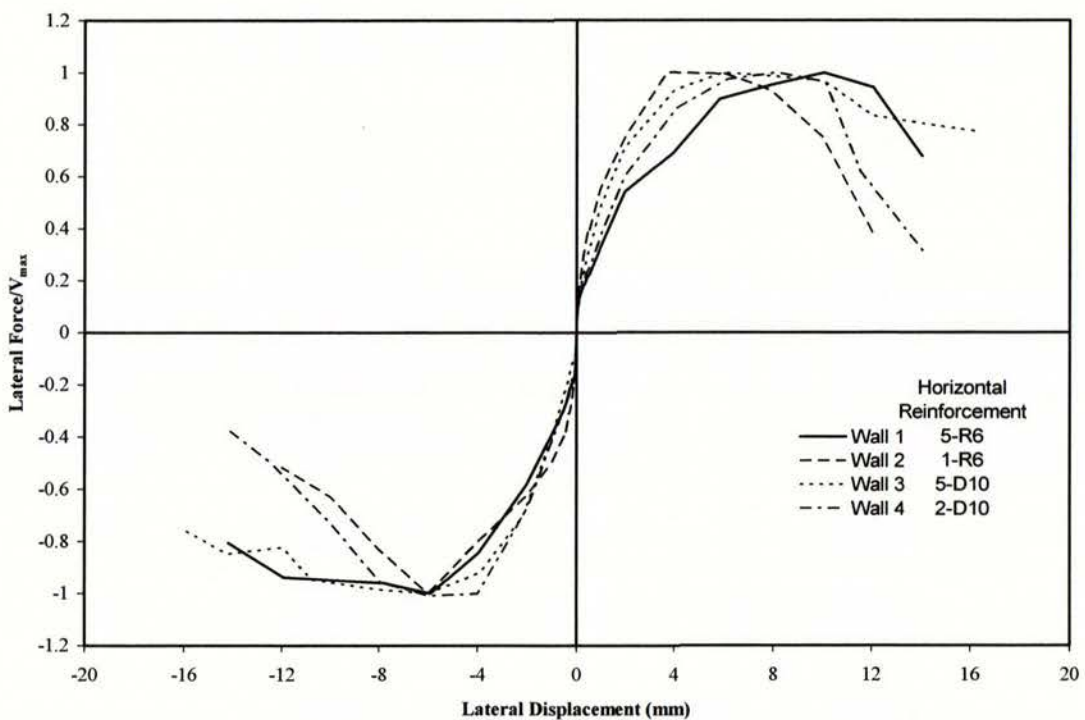


Figure 5.2 Force-displacement envelopes normalised with V_{max} .

spaced R6 horizontal reinforcement. The closely spaced horizontal reinforcement enabled the distribution of stresses throughout the wall diagonals after the initiation of shear cracking. Accordingly, the initial diagonal cracks did not widen significantly under increasing lateral displacements, but instead new sets of diagonal cracks formed and gradually spread over the wall diagonals, accompanied by higher energy dissipation and more ductile behaviour.

5.2.2 Effect of Axial Compression Stresses

The influence of axial compression stress on masonry shear strength is discussed in this subsection. It is clearly illustrated in Chapter 4 that the axial compression load affects the wall ultimate strength considerably. Figure 5.3 shows the force-displacement envelopes for Walls 1, 7 and 8, which had the same dimensions and reinforcement details, but were subjected to varying levels of axial compression stress. The maximum shear strength increased from about 210 kN (average of push and pull) for Wall 1 to 247 kN (Wall 8) and 263 kN (Wall 7) when the axial compression stress was increased from zero to 0.25 MPa and 0.50 MPa, resulted in an increase of about 18% and 25% respectively.

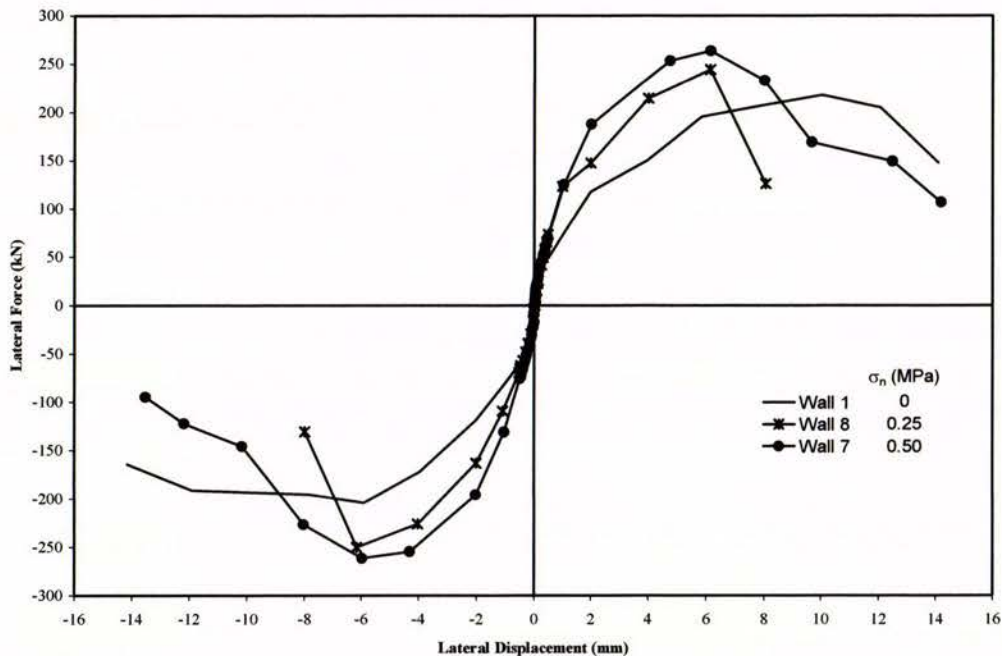


Figure 5.3 Effect of axial compression stress on masonry shear strength.

It was noted from observations made during the experimental process that an increase in axial compression stress delayed the initiation of cracking until larger lateral force was applied.

This can be explained from principal stresses (please refer to section 2.5): a larger lateral force is required to exceed the compressive field resulting from the larger axial load. This compressive field must first be overcome for the introduction of tension stresses before cracking can initiate.

As can be seen in Figure 5.3, the two walls that were subjected to axial compression loads exhibited rapid strength degradation immediately after the ultimate strength had been reached. In addition, these two axially loaded walls had smaller values of Δ_y and d_u as compared to Wall 1 (see Table 5.1).

5.2.3 Partial Grouting

Figure 5.4 shows the force-displacement envelopes of the two partially grouted walls. It is illustrated that Wall 5, which consisted of 5 grouted flues had about 50% more strength than the corresponding Wall 6, which had only three grouted flues. However, this increase in strength could have been easily attributed to the increased number of D20 vertical reinforcing bars used in Wall 5. Although the effect of grouting is significant as far as maximum shear strength is concerned, it is shown in Figure 5.4 that the force-displacement curve for the wall with fewer grouted flues exhibited a much more desirable shape.

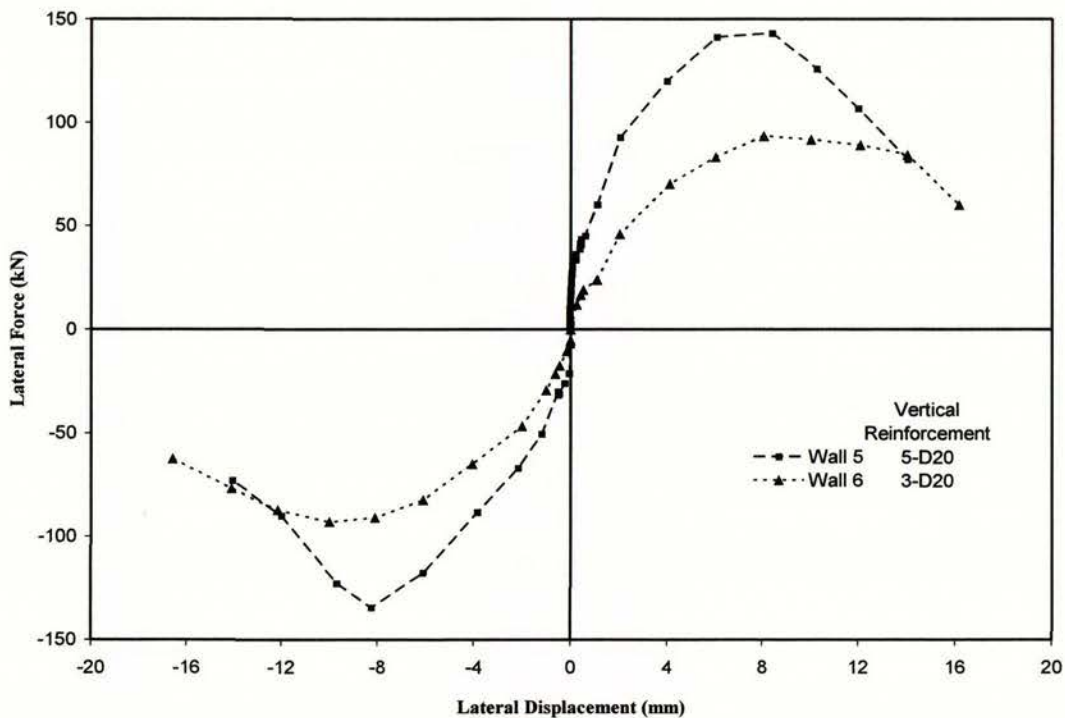


Figure 5.4 Effect of grouting on masonry shear strength.

Figure 5.5 shows the comparison of force-displacement envelopes of fully (without axial load) and partially grouted walls (Walls 5 and 6) using net shear stresses (note that for partially grouted walls, $A_n = (t - b_f) \times l_w$). It can be seen that the partially grouted walls had about the same maximum shear strength, if not more than those of the fully grouted walls when the net shear stress is considered.

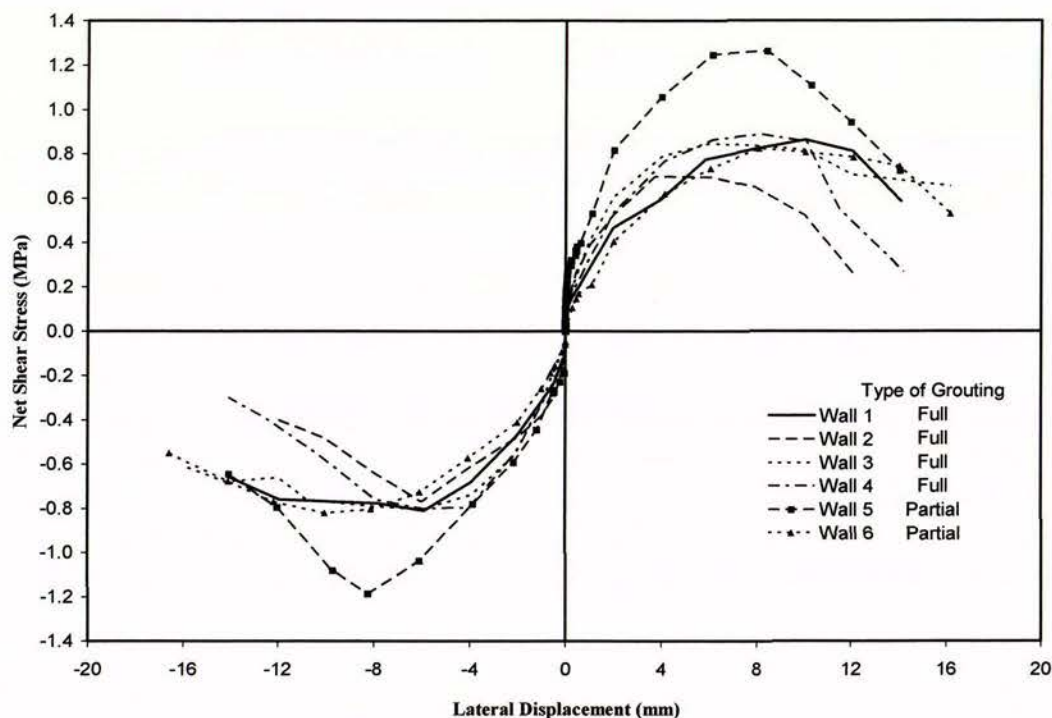


Figure 5.5 Effect of grouting on force-displacement envelope.

5.2.4 Effect of Wall H/L Ratio

The influence of wall H/L ratio on masonry shear strength was included in this study and the results are discussed in this subsection. It is illustrated in Chapter 4 that the wall H/L ratio affects the wall ultimate strength considerably. Figure 5.6 shows the force-displacement envelopes for Walls 8, 9 and 10. These three walls had the same axial compression stress and similar reinforcement details (although Wall 9 had a higher vertical steel ratio than others), but were built to varying H/L ratios. A higher longitudinal reinforcement ratio of $\rho_v f_{yv} = 4.82$ MPa was necessary in Wall 9 to increase the flexural strength in order to generate shear failure.

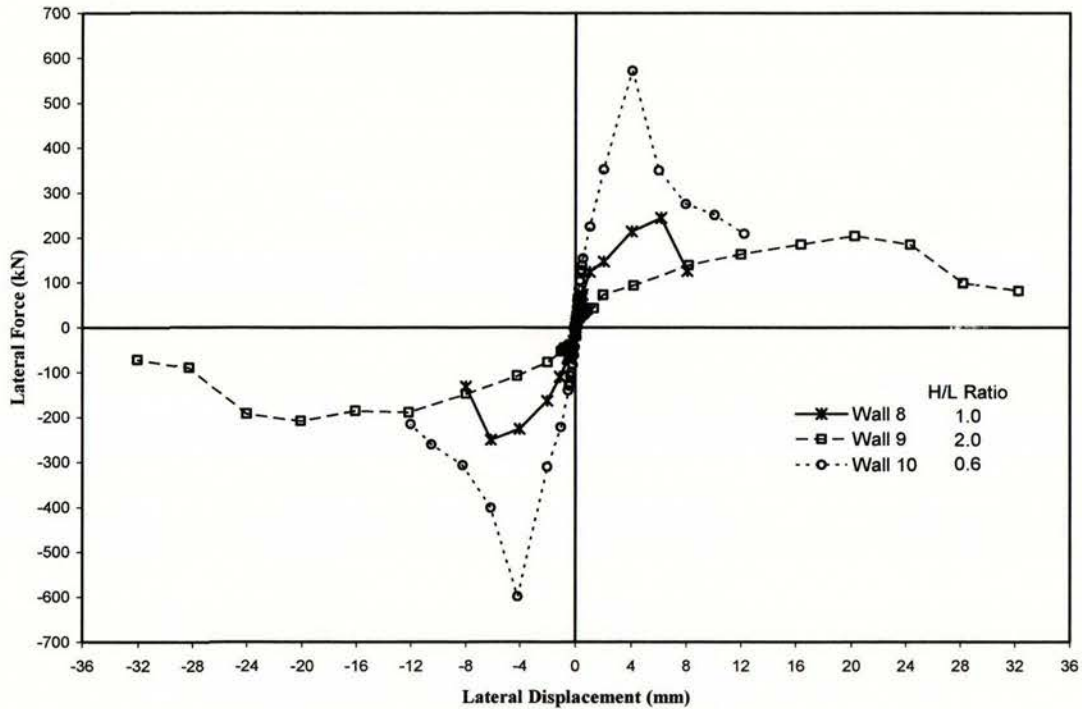


Figure 5.6 Effect of H/L on masonry shear strength.

It is illustrated in Figure 5.6 that the maximum shear strength decreased from an average of about 247 kN for Wall 8 (H/L = 1.0) to 206 kN when the H/L ratio was increased to 2.0 in the case of Wall 9, resulting in a decrease of 17%. Figure 5.6 also shows that the shear strength of Wall 10 was 585 kN for an H/L ratio of 0.60, therefore resulting in a strength increase of 137%. Hence, a conclusion to be extracted from Figure 5.6 was that masonry shear strength increases when H/L ratio decreases, while it decreases inversely in relation to an increase in H/L ratio. In addition, Figure 5.6 illustrates that wall panels with lower aspect ratios would have higher stiffness and reached their maximum resistance at smaller displacements, but abrupt strength degradations take place immediately after peak strengths are reached.

It is however realised that the different shear strength in Walls 8, 9 and 10 could have been due to the variations in A_n and f'_m . In order to meaningfully observe the relation between masonry shear strength and H/L ratio, the influence of A_n and f'_m must be excluded from the test results. Consequently, a plot of $v_n/\sqrt{f'_m}$ is presented in Figure 5.7. As anticipated, Figure 5.7 produced results similar to those presented in Figure 5.6, but the strength difference between Walls 8 and 10 was significantly reduced. Tendency similar to that

observed in Figure 5.6 is evident. Consequently, it is concluded that H/L has an inverse effect on $v_n/\sqrt{f'_m}$ since the figure shows that $v_n/\sqrt{f'_m}$ decreases when the H/L ratio is increased.

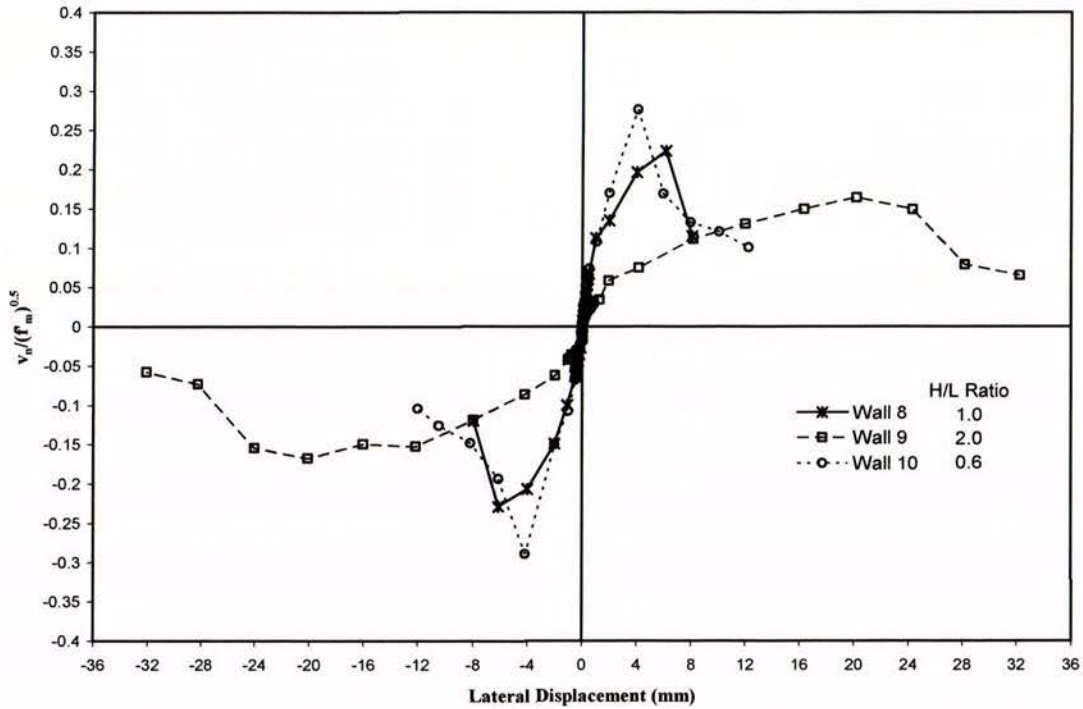


Figure 5.7 The relationship of $v_n/\sqrt{f'_m}$ vs H/L ratio.

5.2.5 Masonry Compressive Strength

All tests conducted in this study used standard material, and resulted in only minor variations in masonry compression strength (f'_m) between various test, as shown in Table F.1, and therefore the effect of f'_m is not considered in this study. However, it is expected that masonry shear strength will increase with masonry crushing strength, as suggested by the various shear equations described in Chapter 2. In addition, the wall masonry shear strength is dependent on wall dimensions, in particular the wall cross-sectional area defined by the wall length ℓ_w , and wall thickness, t . Therefore, an increase in both ℓ_w and t results in an increase of shear strength.

5.3 Stiffness Degradation

All walls suffered substantial stiffness degradation when subjected to increasing lateral displacements. The stiffness degradation properties of each wall are presented in Appendices

B and C as stiffness vs lateral force, and stiffness vs lateral displacement curves. These relationships indicate the sensitivity of the stiffness of masonry walls with respect to the level of horizontal force, or the lateral displacement.

The stiffness during a loading cycle is obtained by dividing the extreme positive and negative lateral forces by the corresponding displacement in each loading cycle. The stiffness values obtained from the first cycle of loading were averaged and plotted against the average of the corresponding lateral displacement, or the corresponding lateral force (both displacement and force are in absolute value). The stiffness degradation curve was truncated at the stage when maximum wall strength was attained.

5.3.1 Effect of Horizontal Reinforcement

Stiffness degradation curves of the four fully grouted, square masonry walls without axial compression stress are compared in Figure 5.8 for different amounts of horizontal reinforcement. It can be seen from the figure that all walls, except Wall 2, had similar stiffness and stiffness degradation rate. It is therefore possible to conclude that no relationship exists between the amount of horizontal reinforcement and the rate at which the stiffness degrades.

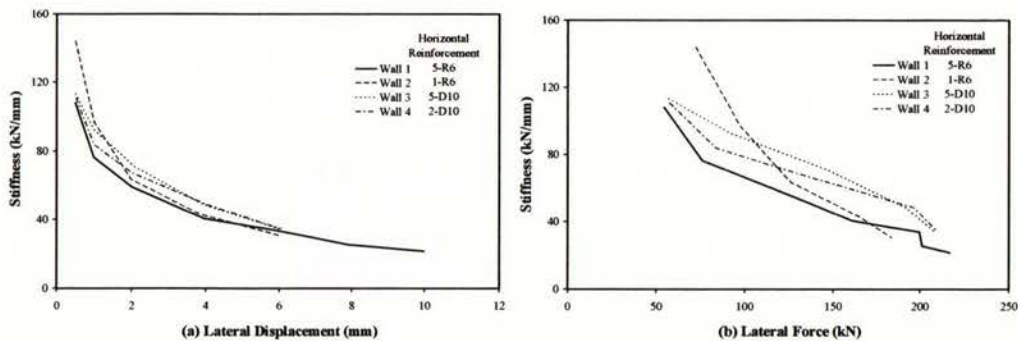


Figure 5.8 Effect of horizontal reinforcement on stiffness degradation.

5.3.2 Effect of Axial Compression Stresses

Figure 5.9 compares the stiffness degradation curves for three square fully grouted walls subjected to different levels of axial compression stress. The dependence of wall stiffness on axial compression stress level is illustrated, i.e. wall stiffness increases when the axial

compression stress increases. However, the rate of stiffness degradation appears to be independent of the axial compression stress levels.

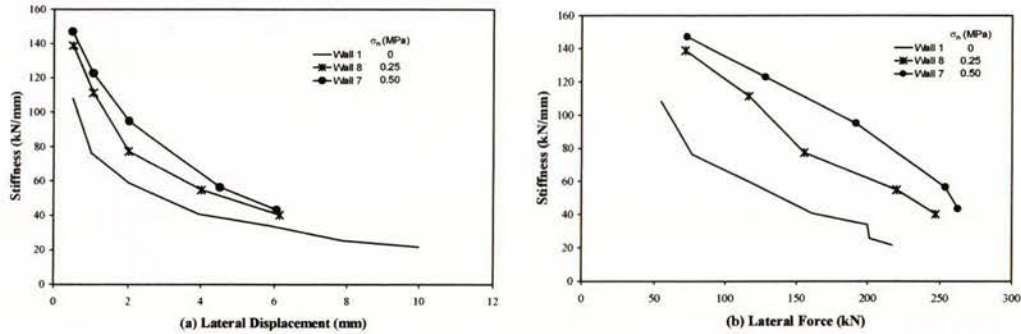


Figure 5.9 Effect of axial compression stress on stiffness degradation.

5.3.3 Partial Grouting

Figure 5.10 compares the stiffness degradation curves for the fully and partially grouted masonry walls. The figure shows that grouting increases wall stiffness, but the rate at which stiffness degraded appears to be independent of the type of grouting.

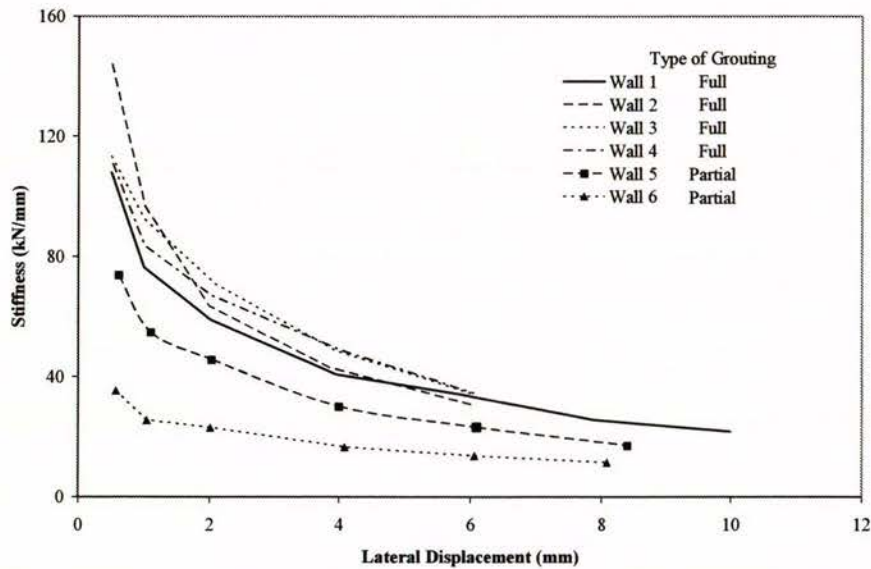


Figure 5.10 Effect of grouting on stiffness degradation.

5.3.4 Effect of Wall H/L Ratio

Figure 5.11 shows the stiffness degradation curves for walls built to different H/L ratios. The figure shows that wall panels with lower H/L ratios possess higher stiffness. However, the

test results are insufficient to provide conclusive evidence to indicate any correlation between stiffness degradation and wall's H/L ratio.

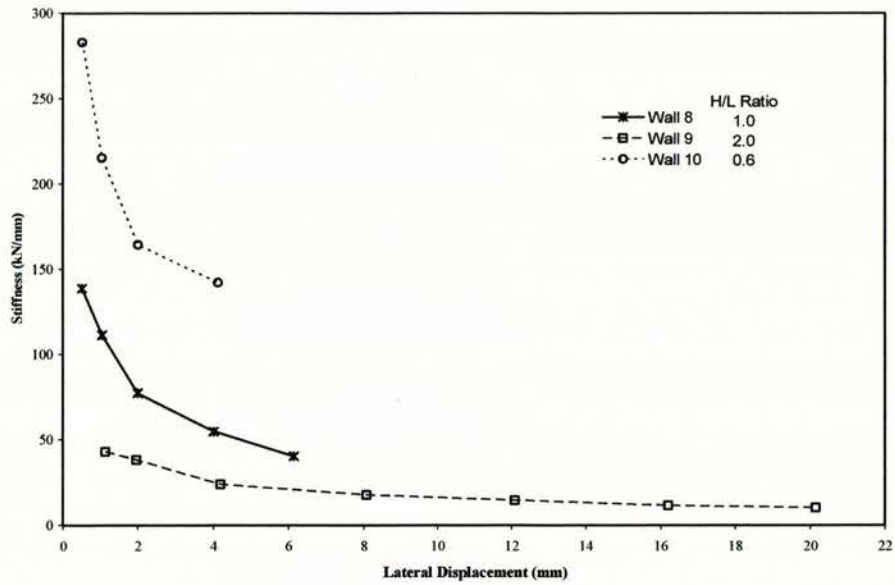


Figure 5.11 Effect of H/L on stiffness degradation.

Chapter 6

Comparison of Available Test Results

6.1 Introduction

This chapter compares results derived when using different equations presented in Chapter 2 to predict the maximum in-plane shear strength of reinforced masonry walls under different conditions, such as different reinforcement ratios, shear span ratios, axial compression stresses, masonry compressive strength and different types of grouting. These expressions are correlated with a comprehensive data base of test results to establish their suitability. Wall characteristics from various test specimens were used as input to the predictive equations, and the predicted shear strengths are then compared to the actual measured strength of the test results.

Table 6.1 presents a selection of masonry shear strength expressions currently available. Of the available equations shown, the first four are currently prescribed by codes and the remaining three are proposed formulations which use different functional forms for the effect of various parameters on masonry shear strength. The original formats of some of the presented equations were modified to introduce a common notation and consistent units. All equations shown in Table 6.1 are in SI units. The definitions of symbols used in the equations are given in Chapter 2. The accuracy of the equations in predicting the shear strength of fully and of partially grouted reinforced masonry walls is discussed in sections 6.3 and 6.4 respectively.

6.2 Correlation of Predictive Equations

This section examines the correlation between seven predictive equations (see Table 6.1) under different conditions, with the results presented in Figures 6.1-6.3. The parameters selected are based on a 140 mm thick square masonry wall reinforced longitudinally with

Table 6.1 Masonry shear strength expressions

Source	Equations	
NZS4230:1990	$0.8v_m A_n + 0.8\rho_h A_n f_{yh}$	2-28
AS3700-1998	$f_{vr} A_n + 0.8\rho_h A_n f_{yh}$	2-26
NEHPR (1998)	$0.083 \left[4 - 1.75 \left(\frac{h_e}{\ell_w} \right) \right] A_n \sqrt{f'_m} + 0.5\rho_h A_n f_{yh} + 0.25N$	2-25
Uniform Building Code (1997)	$0.083C_d A_n \sqrt{f'_m} + \rho_h A_n f_{yh}$	2-22
Matsumura (1987)	$\left[k_u k_p \left(\frac{0.76}{(h/d) + 0.7} + 0.012 \right) \sqrt{f'_m} + 0.18\gamma\delta \sqrt{f'_m \rho_h f_{yh}} + 0.2\sigma_n \right] (0.875b_{eff}d)$	2-17
Shing et al. (1991)	$(0.0217\rho_v f_{yv} + 0.166) A_n \sqrt{f'_m} + \left(\frac{\ell_w - 2d'}{s_h} - 1 \right) \frac{s_h}{\ell_w} \rho_h A_n f_{yh} + (0.0217N) \sqrt{f'_m}$	2-18
Anderson and Priestley (1992)	$C_{ap} A_n \sqrt{f'_m} + 0.5\rho_h A_n f_{yh} \frac{d}{\ell_w} + 0.25N$	2-21

20 mm diameter bar spaced at 400 mm centres. In each figure, only a single parameter is varied with other conditions unchanged. Hence, Figure 6.1 investigates the influence of f'_m , and Figures 6.2 and 6.3 examine the influence of $\rho_h f_{yh}$ and σ_n respectively. It is considered that $f'_m = 30$ MPa, $\rho_h f_{yh} = 3.0$ MPa and $\sigma_n = 4.0$ MPa are deemed to be realistic upper limits to the magnitude of these parameters.

Figure 6.1 illustrates that the shear strength predicted by the Australian masonry standard is independent of f'_m , as indicated by Equation 2-26. The figure also shows that the New Zealand masonry standard (NZS4230:1990) and the Uniform Building Code (UBC) conservatively predicted masonry shear strength at high values of f'_m . It is realised that the low shear prediction by these two standards could have been partly caused by neglecting the beneficial effect of axial compression towards masonry shear strength.

Figure 6.2 shows the effect of horizontal reinforcement on masonry shear strength. It demonstrates that all formulae, except those predicted by Matsumura, UBC and NEHPR, result in linear increase with $\rho_h f_{yh}$. NEHPR and UBC provide the lowest shear prediction at high $\rho_h f_{yh}$, due to the maximum shear stress allowed by these codes being limited to $v_n \leq 0.33\sqrt{f'_m}$. Matsumura considers the rate of increase in shear resistance to be associated with

f'_m . Consequently, he proposed the effect of shear reinforcement to be approximately proportional to $\sqrt{f'_m \rho_h f_{yh}}$.

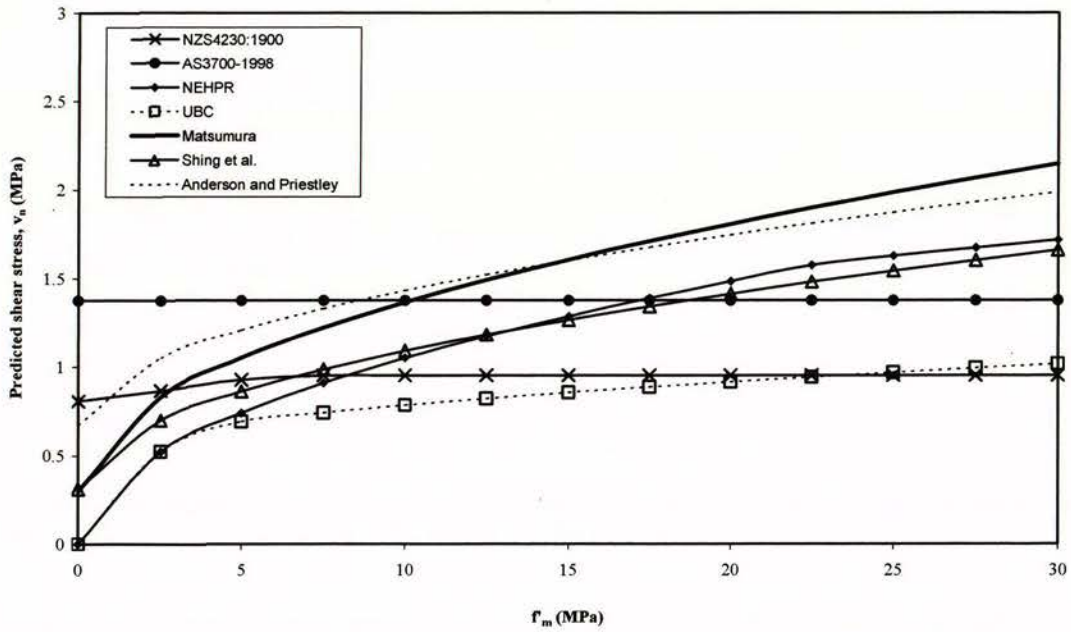


Figure 6.1 Comparison of shear formulae.

$(h/\ell_w = 1.0, \sigma_n = 1.8 \text{ MPa}, \rho_h f_{yh} = 0.47 \text{ MPa}, \rho_v f_{yv} = 1.9 \text{ MPa})$

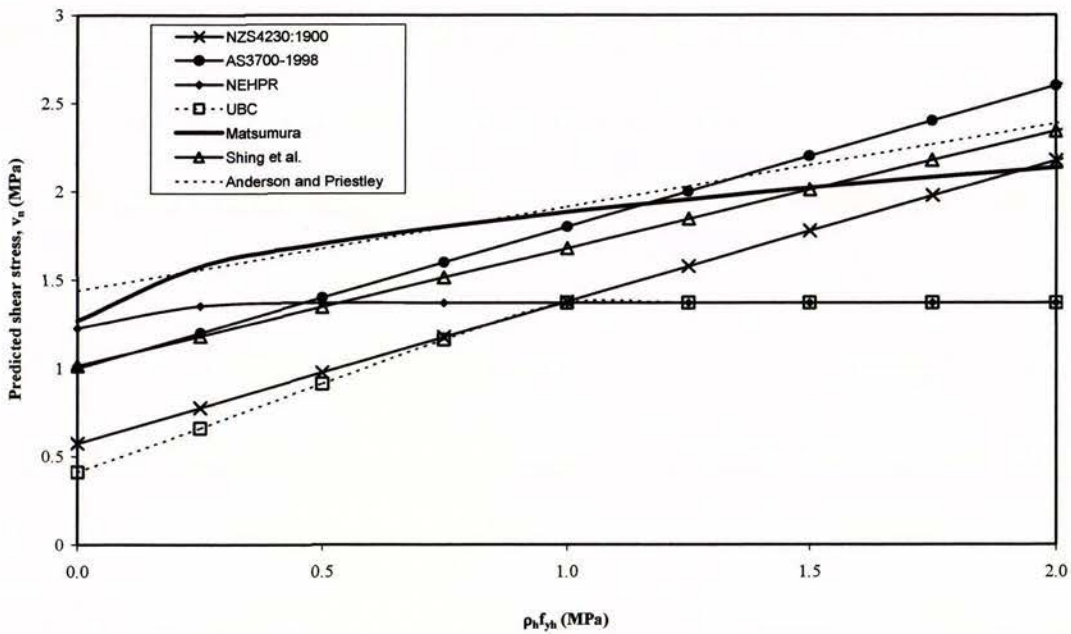


Figure 6.2 Comparison of shear formulae.

$(h/\ell_w = 1.0, f'_m = 17 \text{ MPa}, \sigma_n = 1.8 \text{ MPa}, \rho_v f_{yv} = 1.9 \text{ MPa})$

Figure 6.3 illustrates the disadvantage of the New Zealand and Australian masonry standards, and the UBC when the beneficial effect of axial compression was not properly considered when calculating masonry shear strength. The other four predictive shear equations show good correlation when σ_n increases, despite a noticeable margin separating the four.

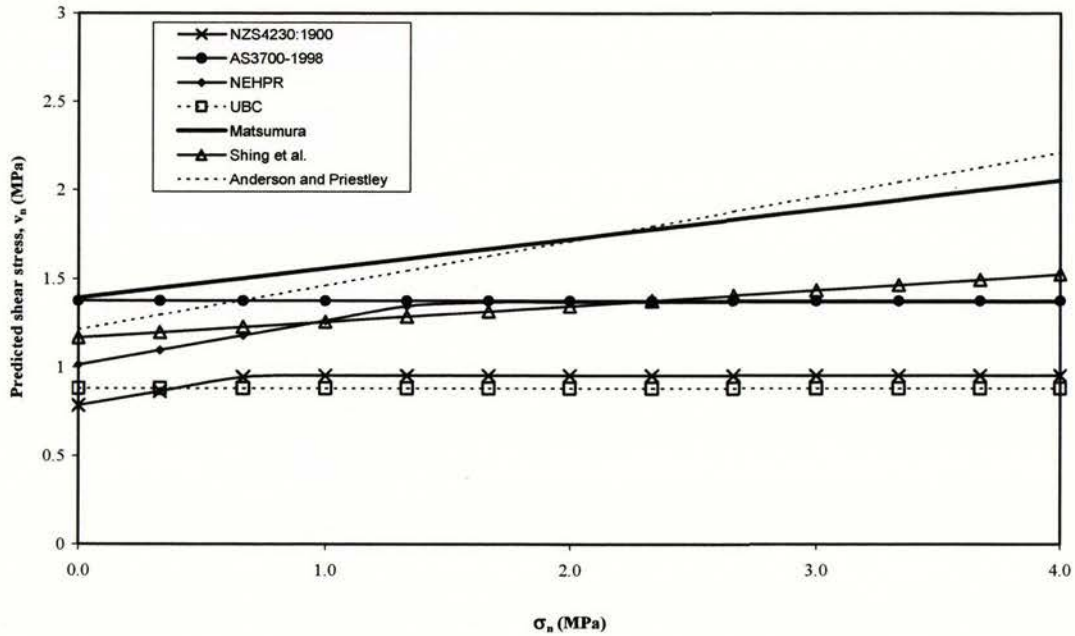


Figure 6.3 Comparison of shear formulae.

$$\left(\frac{h}{\ell_w} = 1.0, f'_m = 17 \text{ MPa}, \rho_h f_{yh} = 0.47 \text{ MPa}, \rho_v f_{yv} = 1.9 \text{ MPa} \right)$$

6.3 Fully Grouted Walls

This section compares the suitability of the predictive equations presented in Table 6.1, in predicting the in-plane shear strength of fully grouted reinforced masonry walls. The accuracy of each equation is assessed by comparing the predicted strengths to the experimental data from independent research sources.

6.3.1 Experimental Data Sets

The experimental data sets used in this part of the study are limited to those of fully grouted reinforced concrete and clay brick masonry walls that were subjected to reverse cyclic lateral loads and failed in shear. The data sets selected are from the following experimental programmes:

1. Tests conducted by Shing et al. (1990) at the University of Colorado as part of the U.S. Coordinated Programme for Masonry Building Research;
2. Tests conducted by Matsumura (1987) at Kanagawa University;
3. Tests conducted by Okamoto et al. (1987) at Japan's Building Research Institute, Ministry of Construction;
4. Tests conducted by Sveinsson et al. (1985) at the University of California at Berkeley;
5. Tests conducted at the University of Auckland as reported in Chapter 4.

Of the data sets selected, three of them were obtained from tests in which the top and bottom surfaces were rotationally fixed, while the remainders were of the cantilever type tested at the University of Colorado and University of Auckland. Each experimental study used displacement controlled tests consisting of multiple cycles of reversed loadings. The loading procedures are described in detail in the cited references, and consisted of predefined load-displacement histories characterised by increasing amplitude until failure. The use of a common loading procedure and similar loading rates in each study produced a comparable experimental data.

It is noted that only the Berkeley data from the 1985 series of tests (Sveinsson et al., 1985) is included here. This is because in some of the other data there is doubt about the magnitude of axial compression load at failure, which had a tendency to increase during the tests because of the test set-up arrangement.

The maximum shear strength of each wall is defined as the average of the two peak shear forces achieved in the two opposite directions of cyclic loading. Shear strength is calculated using the net cross-sectional area based on actual dimensions (length x wall thickness). Only data from specimens that were reported to have failed in shear were selected, while others that were reported to have failed in bending or sliding were eliminated. Consequently, a total of sixty-four data are included here for comparison. The data subsets finally selected from the studies listed above are identified in the text by the letters S, M, O, B and A, corresponding to 1-5 respectively, for convenience.

Relevant properties of the specimens are listed in Appendix E. Of the sixty-four specimens presented in Table E.1, there are 10S, 18M, 8O, 21B and 7A. Nineteen of these specimens were single-wythe walls constructed of hollow brick units, see shaded rows in Table E.1.

Table E.1 details the geometric and material properties of the tested specimens, as well as the reinforcement ratios and axial compressive stress applied. As shown in Table E.1, experimental testing conducted at the University of Auckland was intended to investigate the shear strength of concrete masonry walls when subjected to low axial compression stresses ($0 \leq \sigma_n \leq 0.5$ MPa) and low shear reinforcement ratios ($\rho_h \leq 0.062\%$). Experimental studies conducted in U.S. and Japan involved masonry walls that were constructed with higher shear reinforcement ratios ($\rho_h \leq 0.668\%$) and subjected to higher axial compression stress levels ($\sigma_n \leq 5.87$ MPa).

The masonry compressive strength, f'_m , listed in Table E.1 was obtained from prism tests. Shing et al. and Matsumura used three course prism tests. Sveinsson et al. used two types of prism test: three course prisms with h/t ratios of 2 and six course prisms with h/t ratios of 4, and the average values of the two were used as the masonry compressive strength for the Sveinsson et al. specimens. Okamoto et al. did not report the type of prism used. The yield strength of the reinforcement used in each test was obtained by employing tension tests. The U.S. customary units adopted by Shing et al., and Sveinsson et al. are converted to SI units for convenience.

6.3.2 Correlation between Predicted and Measured Response

Each equation listed in Table 6.1 was used to predict the maximum shear capacity of all 64 test specimens, using appropriate specimen characteristics, such as wall dimensions, reinforcing steel ratios, masonry compression strength (f'_m) and the axial load (σ_n). Table 6.2 lists the predicted strengths (v_m , v_s , v_p and the sum v_n) and the actual shear strength (v_{max}) determined from the tests of all 64 specimens. Also included in Table 6.2 is the v_{max}/v_n for all specimens.

Normalised plots (experimentally obtained shear stress, v_{max} , versus predicted shear stress, v_n) are presented in Figures 6.4–6.10 to investigate the accuracy of each equation with respect

Table 6.2 Measured and predicted strength of fully grouted masonry walls

Specimen no.	Specimen label	v_m (MPa)							v_s (MPa)						
		NZS 4230	AS3700	NEHPR	UBC	Matsumura	Shing et al.	Anderson & Priestley	NZS 4230	AS3700	NEHPR	UBC	Matsumura	Shing et al.	Anderson & Priestley
1	1-S	0.58	1.00	0.85	0.45	1.09	1.12	1.09	0.38	0.38	0.24	0.47	0.28	0.31	0.22
2	2-S	0.43	1.00	0.79	0.42	1.01	1.04	1.02	0.38	0.38	0.24	0.47	0.26	0.31	0.22
3	3-S	0.58	1.00	0.79	0.42	1.01	1.04	1.02	0.38	0.38	0.24	0.47	0.26	0.31	0.22
4	4-S	0.58	1.00	0.88	0.47	1.13	1.16	1.13	0.38	0.38	0.24	0.47	0.29	0.31	0.22
5	5-S	0.58	1.00	0.88	0.47	0.93	0.96	1.13	0.38	0.38	0.24	0.47	0.29	0.31	0.22
6	6-S	0.58	1.00	0.90	0.48	1.05	1.05	1.15	0.87	0.87	0.55	1.09	0.45	0.73	0.51
7	7-S	0.58	1.00	0.90	0.48	1.05	0.93	1.15	0.38	0.38	0.24	0.47	0.29	0.31	0.22
8	8-S	0.58	1.00	0.77	0.41	0.99	1.02	0.99	0.87	0.87	0.55	1.09	0.38	0.73	0.51
9	9-S	0.58	1.00	0.96	0.51	1.13	1.16	0.61	0.40	0.40	0.25	0.49	0.32	0.33	0.23
10	10-S	0.58	1.00	0.96	0.51	1.13	1.16	0.61	0.40	0.40	0.25	0.49	0.32	0.33	0.23
11	1-M	0.58	0.93	1.17	0.71	1.43	1.14	1.12	0.36	0.36	0.23	0.45	0.47	0.29	0.21
12	2-M	0.58	0.74	1.04	0.58	1.15	1.14	1.12	0.36	0.36	0.23	0.45	0.46	0.23	0.21
13	3-M	0.58	0.74	1.04	0.58	1.15	1.14	1.12	0.36	0.36	0.23	0.45	0.46	0.23	0.21
14	4-M	0.58	0.36	0.78	0.47	0.85	1.22	1.12	0.36	0.36	0.23	0.45	0.44	0.12	0.20
15	5-M	0.58	0.74	1.05	0.58	0.98	1.01	1.13	0.00	0.00	0.00	0.00	0.00	0.00	0.00
16	6-M	0.58	0.74	1.05	0.58	0.98	1.01	1.13	0.51	0.51	0.32	0.64	0.55	0.32	0.30
17	7-M	0.58	0.74	1.05	0.58	0.98	1.01	1.13	1.03	1.03	0.64	1.29	0.78	0.86	0.59
18	8-M	0.58	0.74	1.05	0.58	1.17	1.16	1.13	1.03	1.03	0.64	1.29	0.78	0.86	0.59
19	9-M	0.58	0.74	1.05	0.58	1.17	1.16	1.13	2.06	2.06	1.29	2.57	1.10	1.73	1.18
20	10-M	0.58	0.74	1.20	0.66	1.33	1.33	1.29	1.03	1.03	0.64	1.29	0.89	0.86	0.59
21	11-M	0.58	0.74	1.13	0.63	1.26	1.26	1.23	1.03	1.03	0.64	1.29	0.84	0.86	0.59
22	12-M	0.58	0.74	1.16	0.65	1.29	1.29	1.26	1.23	1.23	0.77	1.54	0.94	1.04	0.71
23	13-M	0.58	0.74	1.14	0.63	1.29	1.29	1.23	1.09	1.09	0.68	1.36	0.87	0.91	0.63
24	14-M	0.58	0.74	1.24	0.69	1.38	1.38	1.34	1.03	1.03	0.64	1.29	0.92	0.86	0.59
25	15-M	0.58	0.73	1.18	0.64	1.10	1.16	0.64	0.00	0.00	0.00	0.00	0.00	0.00	0.00
26	16-M	0.58	0.73	1.18	0.64	1.10	1.16	0.64	0.51	0.51	0.32	0.64	0.61	0.29	0.29
27	17-M	0.58	0.73	1.18	0.64	1.10	1.16	0.64	1.03	1.03	0.64	1.29	0.86	0.81	0.58
28	18-M	0.58	0.73	1.18	0.64	1.10	1.16	0.64	2.06	2.06	1.29	2.57	1.22	1.62	1.16
29	1-O	0.43	1.05	1.13	0.72	1.10	0.88	1.02	0.47	0.47	0.30	0.59	0.49	0.42	0.28
30	2-O	0.58	0.75	1.07	0.59	0.99	1.06	1.15	0.47	0.47	0.30	0.59	0.53	0.30	0.27
31	3-O	0.43	0.38	0.79	0.42	0.69	1.01	1.02	0.47	0.47	0.30	0.59	0.45	0.16	0.26
32	4-O	0.58	0.75	1.07	0.59	0.99	1.06	1.15	0.47	0.47	0.30	0.59	0.53	0.30	0.27
33	5-O	0.58	0.75	1.07	0.59	0.99	1.06	1.15	0.47	0.47	0.30	0.59	0.53	0.30	0.27
34	6-O	0.58	1.05	1.38	0.88	1.34	1.07	0.62	0.47	0.47	0.30	0.59	0.60	0.42	0.28
35	7-O	0.58	0.75	1.12	0.62	1.05	1.11	0.60	0.47	0.47	0.30	0.59	0.56	0.30	0.27
36	8-O	0.51	0.38	0.86	0.46	0.76	1.10	0.56	0.47	0.47	0.30	0.59	0.49	0.16	0.26
37	1-B	0.58	0.92	1.19	0.72	0.88	0.88	1.15	0.93	0.93	0.58	1.17	0.77	0.75	0.55
38	2-B	0.58	0.92	1.19	0.72	0.88	0.88	1.15	0.93	0.93	0.58	1.17	0.77	0.75	0.55
39	3-B	0.58	0.92	0.98	0.60	0.97	0.81	0.95	1.38	1.38	0.86	1.72	0.77	1.11	0.81
40	4-B	0.58	0.92	0.98	0.60	0.70	0.82	0.95	1.38	1.38	0.86	1.72	0.77	1.11	0.81
41	5-B	0.58	0.92	0.96	0.58	0.95	0.79	0.93	0.69	0.69	0.43	0.86	0.53	0.42	0.40

Table 6.2 (continued)

Specimen no.	Specimen label.	v_m (MPa)							v_s (MPa)						
		NZS 4230	AS3700	NEHPR	UBC	Matsumura	Shing et al.	Anderson & Priestley	NZS 4230	AS3700	NEHPR	UBC	Matsumura	Shing et al.	Anderson & Priestley
42	6-B	0.58	0.92	0.96	0.58	0.68	0.80	0.93	0.69	0.69	0.43	0.86	0.53	0.42	0.40
43	7-B	0.58	0.92	0.96	0.58	0.95	0.79	0.93	0.26	0.26	0.16	0.33	0.33	0.23	0.15
44	8-B	0.58	0.92	0.96	0.58	0.95	0.79	0.93	0.95	0.95	0.60	1.19	0.63	0.65	0.56
45	9-B	0.58	0.92	0.96	0.58	0.95	0.79	0.93	0.69	0.69	0.43	0.86	0.53	0.42	0.40
46	10-B	0.58	0.92	0.96	0.58	0.95	0.79	0.93	0.69	0.69	0.43	0.86	0.53	0.42	0.40
47	11-B	0.58	0.92	1.11	0.67	1.09	0.91	0.54	0.68	0.68	0.43	0.85	0.61	0.42	0.40
48	12-B	0.58	0.92	1.11	0.67	1.09	0.91	0.54	1.70	1.70	1.07	2.13	0.97	1.45	1.00
49	13-B	0.58	0.92	1.11	0.67	1.09	1.00	0.54	0.69	0.69	0.43	0.86	0.61	0.42	0.40
50	14-B	0.58	0.92	1.11	0.67	0.90	0.94	0.54	1.70	1.70	1.07	2.13	0.97	1.45	1.00
51	15-B	0.58	0.92	1.11	0.67	0.79	0.92	0.54	0.69	0.69	0.43	0.86	0.61	0.42	0.40
52	16-B	0.58	0.92	1.11	0.67	0.79	0.92	0.54	1.70	1.70	1.07	2.13	0.97	1.45	1.00
53	17-B	0.58	0.92	1.11	0.67	1.09	0.80	0.54	0.69	0.69	0.43	0.86	0.61	0.42	0.40
54	18-B	0.58	0.92	1.11	0.67	1.09	0.91	0.54	1.70	1.70	1.07	2.13	0.97	1.45	1.00
55	19-B	0.58	0.92	1.11	0.67	1.09	0.91	0.54	0.82	0.82	0.51	1.03	0.67	0.66	0.48
56	20-B	0.58	0.92	1.11	0.67	1.09	0.92	0.54	2.08	2.08	1.30	2.61	1.07	2.00	1.22
57	21-B	0.58	0.92	1.30	0.79	1.28	1.07	0.63	0.35	0.35	0.22	0.44	0.51	0.31	0.21
58	1-A	0.42	1.00	0.78	0.42	0.96	0.88	1.01	0.13	0.13	0.08	0.17	0.15	0.11	0.08
59	2-A	0.42	1.00	0.78	0.42	0.96	0.88	1.01	0.00	0.00	0.00	0.00	0.00	0.00	0.00
60	3-A	0.41	1.00	0.77	0.41	0.94	0.86	0.99	0.15	0.15	0.10	0.19	0.16	0.09	0.09
61	4-A	0.56	1.00	0.80	0.43	0.98	0.90	1.03	0.13	0.13	0.08	0.17	0.16	0.11	0.08
62	5-A	0.50	1.00	0.80	0.43	0.98	0.90	1.03	0.13	0.13	0.08	0.17	0.16	0.11	0.08
63	6-A	0.58	0.50	0.92	0.49	0.81	1.39	1.18	0.13	0.13	0.08	0.17	0.18	0.11	0.08
64	7-A	0.58	1.20	1.21	0.74	1.30	1.02	1.18	0.13	0.13	0.08	0.17	0.18	0.13	0.08

Table 6.2 (continued)

Specimen no.	v_p (MPa)							v_n (MPa)							V_{max} (MPa)
	NZS 4230	AS3700	NEHPR	UBC	Matsumura	Shing et al.	Anderson & Priestley	NZS 4230	AS3700	NEHPR	UBC	Matsumura	Shing et al.	Anderson & Priestley	
1	0.00	0.00	0.47	0.00	0.31	0.18	0.47	0.95	1.38	1.51	0.92	1.67	1.61	1.78	1.74
2	0.00	0.00	0.00	0.00	0.00	0.00	0.00	0.81	1.38	1.03	0.89	1.27	1.35	1.24	1.35
3	0.00	0.00	0.17	0.00	0.11	0.06	0.17	0.95	1.38	1.20	0.89	1.39	1.42	1.41	1.47
4	0.00	0.00	0.17	0.00	0.11	0.07	0.17	0.95	1.38	1.29	0.94	1.54	1.55	1.53	1.65
5	0.00	0.00	0.47	0.00	0.31	0.19	0.47	0.95	1.38	1.57	0.94	1.53	1.46	1.82	1.63
6	0.00	0.00	0.47	0.00	0.31	0.19	0.47	1.45	1.87	1.59	1.57	1.80	1.97	2.13	1.92
7	0.00	0.00	0.47	0.00	0.31	0.19	0.47	0.95	1.38	1.59	0.95	1.65	1.43	1.84	1.78
8	0.00	0.00	0.47	0.00	0.31	0.17	0.47	1.45	1.87	1.37	1.37	1.68	1.91	1.97	2.05
9	0.00	0.00	0.48	0.00	0.32	0.21	0.48	0.97	1.40	1.68	1.00	1.77	1.71	1.33	1.79
10	0.00	0.00	0.17	0.00	0.11	0.08	0.17	0.97	1.40	1.37	1.00	1.57	1.57	1.02	1.56
11	0.00	0.00	0.12	0.00	0.08	0.05	0.12	0.94	1.30	1.52	1.17	1.97	1.48	1.46	1.60
12	0.00	0.00	0.12	0.00	0.08	0.05	0.12	0.94	1.11	1.39	1.03	1.69	1.43	1.45	1.72
13	0.00	0.00	0.12	0.00	0.08	0.05	0.12	0.94	1.11	1.39	1.03	1.69	1.43	1.45	1.87
14	0.00	0.00	0.12	0.00	0.08	0.05	0.12	0.94	0.72	1.13	0.92	1.37	1.39	1.44	1.61
15	0.00	0.00	0.49	0.00	0.32	0.20	0.49	0.58	0.74	1.54	0.58	1.30	1.21	1.62	1.70
16	0.00	0.00	0.49	0.00	0.32	0.20	0.49	1.09	1.26	1.57	1.22	1.85	1.53	1.92	1.89
17	0.00	0.00	0.49	0.00	0.32	0.20	0.49	1.60	1.77	1.57	1.57	2.07	2.07	2.21	2.28
18	0.00	0.00	0.49	0.00	0.32	0.20	0.49	1.60	1.77	1.57	1.57	2.26	2.23	2.21	2.29
19	0.00	0.00	0.49	0.00	0.32	0.20	0.49	2.40	2.80	1.57	1.57	2.58	3.09	2.81	2.93
20	0.00	0.00	0.49	0.00	0.32	0.23	0.49	1.60	1.77	1.79	1.79	2.53	2.42	2.37	2.59
21	0.00	0.00	0.49	0.00	0.32	0.22	0.49	1.60	1.77	1.70	1.70	2.42	2.34	2.31	2.24
22	0.00	0.00	0.49	0.00	0.32	0.22	0.49	1.81	1.98	1.74	1.74	2.55	2.55	2.45	2.63
23	0.00	0.00	0.49	0.00	0.32	0.22	0.49	1.66	1.83	1.71	1.71	2.47	2.42	2.35	2.43
24	0.00	0.00	0.49	0.00	0.32	0.24	0.49	1.60	1.77	1.86	1.86	2.62	2.48	2.43	2.59
25	0.00	0.00	0.49	0.00	0.31	0.23	0.49	0.58	0.73	1.67	0.64	1.41	1.39	1.13	2.18
26	0.00	0.00	0.49	0.00	0.31	0.23	0.49	1.09	1.25	1.78	1.29	2.02	1.68	1.42	1.95
27	0.00	0.00	0.49	0.00	0.31	0.23	0.49	1.60	1.76	1.78	1.78	2.27	2.20	1.71	1.71
28	0.00	0.00	0.49	0.00	0.31	0.23	0.49	2.40	2.79	1.78	1.78	2.63	3.01	2.30	2.04
29	0.00	0.00	0.00	0.00	0.00	0.00	0.00	0.90	1.52	1.40	1.31	1.58	1.30	1.30	2.67
30	0.00	0.00	0.49	0.00	0.32	0.20	0.49	1.05	1.22	1.59	1.19	1.84	1.56	1.91	1.96
31	0.00	0.00	0.00	0.00	0.00	0.00	0.00	0.90	0.85	1.09	1.01	1.14	1.16	1.28	2.04
32	0.00	0.00	0.98	0.00	0.63	0.41	0.98	1.05	1.22	1.59	1.19	2.16	1.76	2.40	2.40
33	0.00	0.00	1.47	0.00	0.95	0.61	1.47	1.05	1.22	1.59	1.19	2.47	1.97	2.89	2.61
34	0.00	0.00	0.00	0.00	0.00	0.00	0.00	1.05	1.52	1.67	1.47	1.93	1.49	0.90	3.12
35	0.00	0.00	0.00	0.00	0.00	0.00	0.00	1.05	1.22	1.42	1.22	1.61	1.41	0.87	2.32
36	0.00	0.00	0.00	0.00	0.00	0.00	0.00	0.99	0.85	1.16	1.05	1.25	1.26	0.82	2.04
37	0.00	0.00	0.47	0.00	0.31	0.20	0.47	1.51	1.85	1.60	1.60	1.95	1.83	2.17	1.95
38	0.00	0.00	0.75	0.00	0.49	0.31	0.75	1.51	1.85	1.60	1.60	2.14	1.94	2.45	2.38
39	0.00	0.00	0.69	0.00	0.45	0.24	0.69	1.96	2.30	1.32	1.32	2.19	2.15	2.45	2.46
40	0.00	0.00	0.69	0.00	0.45	0.24	0.69	1.96	2.30	1.32	1.32	1.92	2.16	2.45	2.46
41	0.00	0.00	0.69	0.00	0.45	0.23	0.69	1.27	1.61	1.29	1.29	1.93	1.44	2.03	2.36

Table 6.2 (continued)

Specimen no.	v_p (MPa)							v_n (MPa)							v_{max} (MPa)
	NZS 4230	AS3700	NEHPR	UBC	Matsumura	Shing et al.	Anderson & Priestley	NZS 4230	AS3700	NEHPR	UBC	Matsumura	Shing et al.	Anderson & Priestley	
42	0.00	0.00	0.69	0.00	0.45	0.23	0.69	1.27	1.61	1.29	1.29	1.67	1.45	2.03	2.23
43	0.00	0.00	0.69	0.00	0.45	0.23	0.69	0.84	1.18	1.29	0.91	1.73	1.26	1.78	1.92
44	0.00	0.00	0.69	0.00	0.45	0.23	0.69	1.53	1.87	1.29	1.29	2.03	1.68	2.18	2.43
45	0.00	0.00	0.44	0.00	0.29	0.15	0.44	1.27	1.61	1.29	1.29	1.77	1.36	1.77	1.96
46	0.00	0.00	0.69	0.00	0.45	0.23	0.69	1.27	1.61	1.29	1.29	1.93	1.44	2.03	2.40
47	0.00	0.00	0.69	0.00	0.45	0.27	0.69	1.26	1.60	1.49	1.49	2.16	1.60	1.63	1.84
48	0.00	0.00	0.69	0.00	0.45	0.27	0.69	2.28	2.62	1.49	1.49	2.51	2.63	2.23	1.92
49	0.00	0.00	0.69	0.00	0.45	0.27	0.69	1.27	1.61	1.49	1.49	2.16	1.69	1.63	2.35
50	0.00	0.00	0.69	0.00	0.45	0.27	0.69	2.28	2.62	1.49	1.49	2.32	2.66	2.23	2.40
51	0.00	0.00	0.69	0.00	0.45	0.27	0.69	1.27	1.61	1.49	1.49	1.85	1.61	1.63	2.03
52	0.00	0.00	0.69	0.00	0.45	0.27	0.69	2.28	2.62	1.49	1.49	2.21	2.64	2.23	2.20
53	0.00	0.00	0.69	0.00	0.45	0.27	0.69	1.27	1.61	1.49	1.49	2.16	1.49	1.63	2.18
54	0.00	0.00	0.69	0.00	0.45	0.27	0.69	2.28	2.62	1.49	1.49	2.51	2.63	2.23	2.14
55	0.00	0.00	0.69	0.00	0.45	0.27	0.69	1.40	1.74	1.49	1.49	2.22	1.84	1.71	2.25
56	0.00	0.00	0.69	0.00	0.45	0.27	0.69	2.40	3.00	1.49	1.49	2.62	3.19	2.45	2.27
57	0.00	0.00	0.69	0.00	0.45	0.31	0.69	0.93	1.27	1.74	1.22	2.25	1.69	1.53	2.69
58	0.00	0.00	0.00	0.00	0.00	0.00	0.00	0.56	1.13	0.87	0.58	1.11	0.99	1.09	0.83
59	0.00	0.00	0.00	0.00	0.00	0.00	0.00	0.42	1.00	0.78	0.42	0.96	0.88	1.01	0.74
60	0.00	0.00	0.00	0.00	0.00	0.00	0.00	0.56	1.15	0.87	0.60	1.10	0.95	1.08	0.84
61	0.00	0.00	0.13	0.00	0.08	0.05	0.13	0.70	1.13	1.01	0.59	1.22	1.06	1.24	1.04
62	0.00	0.00	0.06	0.00	0.04	0.02	0.06	0.64	1.13	0.95	0.59	1.18	1.03	1.17	0.98
63	0.00	0.00	0.06	0.00	0.04	0.03	0.06	0.71	0.63	1.07	0.66	1.03	1.53	1.32	0.82
64	0.00	0.00	0.06	0.00	0.04	0.03	0.06	0.71	1.33	1.35	0.91	1.53	1.18	1.33	1.39

Table 6.2 (continued)

Specimen no.	V_{max}/V_n						
	NZS 4230	AS3700	NEHPR	UBC	Matsumura	Shing et al.	Anderson & Priestley
1	1.83	1.27	1.15	1.89	1.04	1.08	0.98
2	1.67	0.98	1.32	1.51	1.06	1.00	1.09
3	1.55	1.07	1.23	1.65	1.06	1.04	1.05
4	1.74	1.20	1.28	1.76	1.08	1.07	1.08
5	1.71	1.19	1.04	1.73	1.07	1.12	0.90
6	1.32	1.02	1.20	1.22	1.06	0.97	0.90
7	1.87	1.30	1.12	1.88	1.08	1.25	0.97
8	1.42	1.10	1.50	1.50	1.22	1.08	1.04
9	1.84	1.28	1.06	1.79	1.01	1.05	1.35
10	1.60	1.12	1.13	1.55	0.99	0.99	1.53
11	1.70	1.23	1.05	1.37	0.81	1.08	1.10
12	1.83	1.56	1.24	1.67	1.02	1.21	1.19
13	1.99	1.69	1.35	1.81	1.11	1.31	1.29
14	1.72	2.23	1.43	1.75	1.18	1.16	1.12
15	2.95	2.29	1.11	2.92	1.31	1.41	1.05
16	1.73	1.50	1.20	1.54	1.02	1.23	0.98
17	1.42	1.29	1.45	1.45	1.10	1.10	1.03
18	1.43	1.29	1.46	1.46	1.01	1.03	1.03
19	1.22	1.05	1.87	1.87	1.14	0.95	1.04
20	1.61	1.46	1.45	1.45	1.02	1.07	1.09
21	1.40	1.26	1.32	1.32	0.93	0.96	0.97
22	1.46	1.33	1.51	1.51	1.03	1.03	1.07
23	1.46	1.33	1.43	1.43	0.98	1.01	1.04
24	1.61	1.46	1.39	1.39	0.99	1.04	1.07
25	3.78	2.97	1.30	3.39	1.55	1.57	1.92
26	1.79	1.56	1.10	1.52	0.97	1.16	1.37
27	1.06	0.97	0.96	0.96	0.75	0.78	1.00
28	0.85	0.73	1.15	1.15	0.78	0.68	0.89
29	2.96	1.75	1.90	2.04	1.69	2.06	2.06
30	1.87	1.60	1.24	1.66	1.07	1.26	1.03
31	2.26	2.40	1.88	2.01	1.78	1.75	1.60
32	2.29	1.97	1.52	2.03	1.11	1.36	1.00
33	2.49	2.13	1.65	2.20	1.06	1.33	0.90
34	2.97	2.05	1.86	2.13	1.61	2.09	3.46
35	2.21	1.89	1.64	1.90	1.44	1.64	2.65
36	2.07	2.40	1.76	1.94	1.63	1.62	2.50
37	1.29	1.05	1.22	1.22	1.00	1.07	0.90
38	1.57	1.28	1.49	1.49	1.11	1.22	0.97
39	1.26	1.07	1.86	1.86	1.12	1.14	1.00
40	1.26	1.07	1.86	1.86	1.28	1.14	1.00
41	1.86	1.47	1.83	1.83	1.22	1.63	1.16

Specimen no.	V_{max}/V_n						
	NZS 4230	AS3700	NEHPR	UBC	Matsumura	Shing et al.	Anderson & Priestley
42	1.76	1.39	1.73	1.73	1.34	1.54	1.10
43	2.28	1.62	1.48	2.10	1.11	1.52	1.08
44	1.59	1.30	1.89	1.89	1.20	1.45	1.12
45	1.55	1.22	1.52	1.52	1.11	1.45	1.11
46	1.90	1.50	1.86	1.86	1.24	1.67	1.19
47	1.46	1.15	1.24	1.24	0.85	1.15	1.13
48	0.84	0.73	1.29	1.29	0.76	0.73	0.86
49	1.86	1.46	1.58	1.58	1.09	1.39	1.44
50	1.05	0.91	1.61	1.61	1.03	0.90	1.08
51	1.61	1.27	1.37	1.37	1.10	1.26	1.25
52	0.97	0.84	1.48	1.48	1.00	0.83	0.99
53	1.72	1.36	1.46	1.46	1.01	1.46	1.33
54	0.94	0.82	1.44	1.44	0.85	0.81	0.96
55	1.61	1.30	1.51	1.51	1.02	1.22	1.32
56	0.95	0.76	1.53	1.53	0.87	0.71	0.93
57	2.91	2.13	1.54	2.20	1.20	1.59	1.77
58	1.50	0.74	0.96	1.43	0.75	0.84	0.77
59	1.75	0.74	0.94	1.77	0.77	0.84	0.73
60	1.50	0.73	0.97	1.39	0.76	0.89	0.78
61	1.49	0.92	1.03	1.75	0.85	0.98	0.84
62	1.54	0.87	1.03	1.65	0.83	0.95	0.84
63	1.16	1.30	0.77	1.25	0.80	0.54	0.62
64	1.96	1.04	1.03	1.54	0.91	1.18	1.05

to different parameters. For example, Figure 6.4(a) examines the accuracy of the shear strength provisions of NZS4230:1990 when variation is set on f'_m appropriate to each test result. The line of unity represents perfect correlation. The spread of points above and below the line of unity demonstrates the tendency to over- or under-predict the shear strength of the masonry walls, as well as the scatter in the test results. Because New Zealand masonry design standard recommends a shear strength reduction factor, ϕ , to be taken as 0.75, correlation for ϕv_n is also included in Figures 6.4–6.10.

Figure 6.4 presents masonry shear prediction using NZS4230:1990. It shows that the NZS4230:1990 approach for masonry shear strength does not provide a particularly good estimate. The figure shows v_{max}/v_n varies from 0.84 to 3.78, with an average v_{max}/v_n of 1.72. The normalised plots show that NZS4230:1990 over-predicts the shear strength of 5 specimens (about 8% of total), but under-predicts the shear strength of 42 specimens by more than 50% of their actual strengths (i.e. $v_{max}/v_n \geq 1.50$). Scatter of results in Figure 6.4(b) demonstrates the tendency of Equation 2-28 to under-predict the contribution of shear

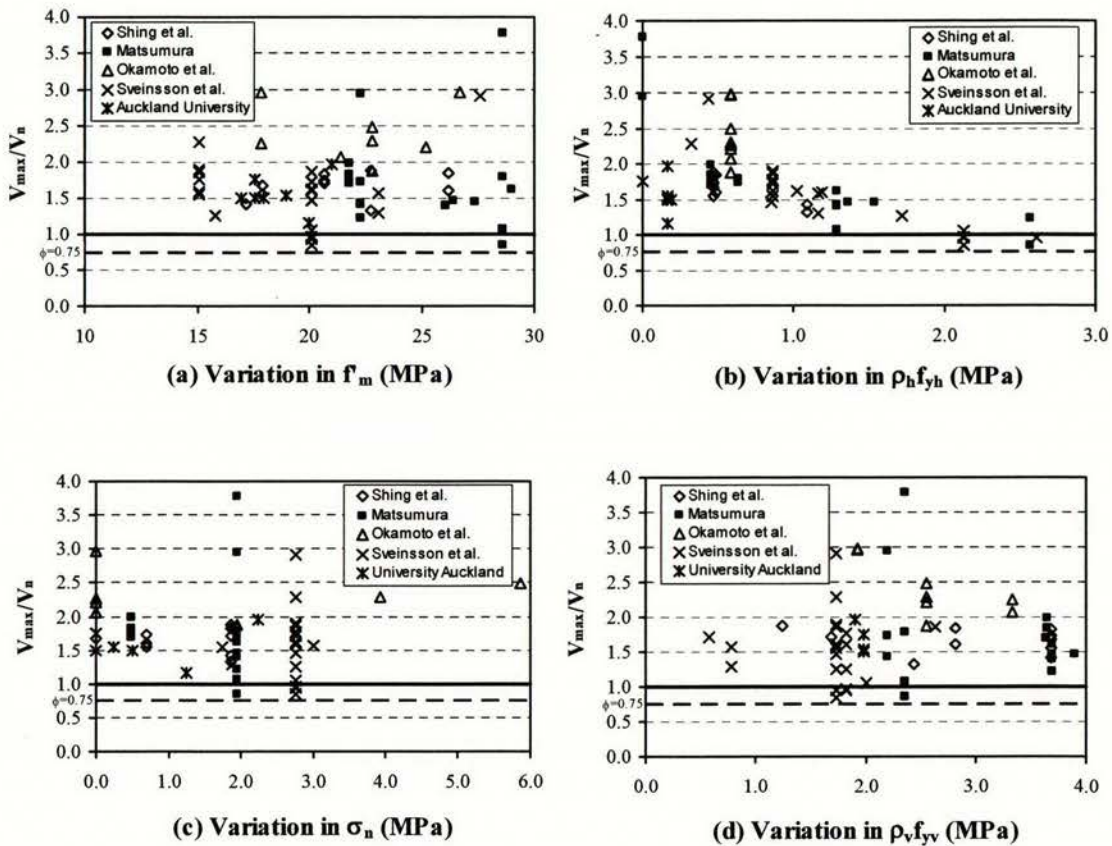


Figure 6.4 Experimental results versus prediction by NZS4230:1990.

reinforcement at low values of $\rho_h f_{yh}$ but over-predicts the results at high value of $\rho_h f_{yh}$. In addition, the scatter of results in Figures 6.4(c) and (d) show that the beneficial effects of axial compression and vertical reinforcement on masonry shear strength are not properly considered by this standard.

The Australian masonry standard is unsuccessful in accurately predicting the masonry shear strength, as shown in Figure 6.5. The figure shows that v_{max}/v_n varies from 0.73 to 2.97. The AS3700 expression over-predicts the shear strength of 13 specimens (about 20% of total), of which 5 specimens have $v_{max}/v_n < 0.75$. When closely studying Figure 6.5(a), it is evident that v_{max}/v_n tends to increase with increasing f'_m . This is most likely to be caused by the absence of the f'_m term in Equation 2-26. In addition, the beneficial effect of vertical reinforcement and axial compressive load is not considered in AS3700, causing the scatter in Figures (c) and (d).

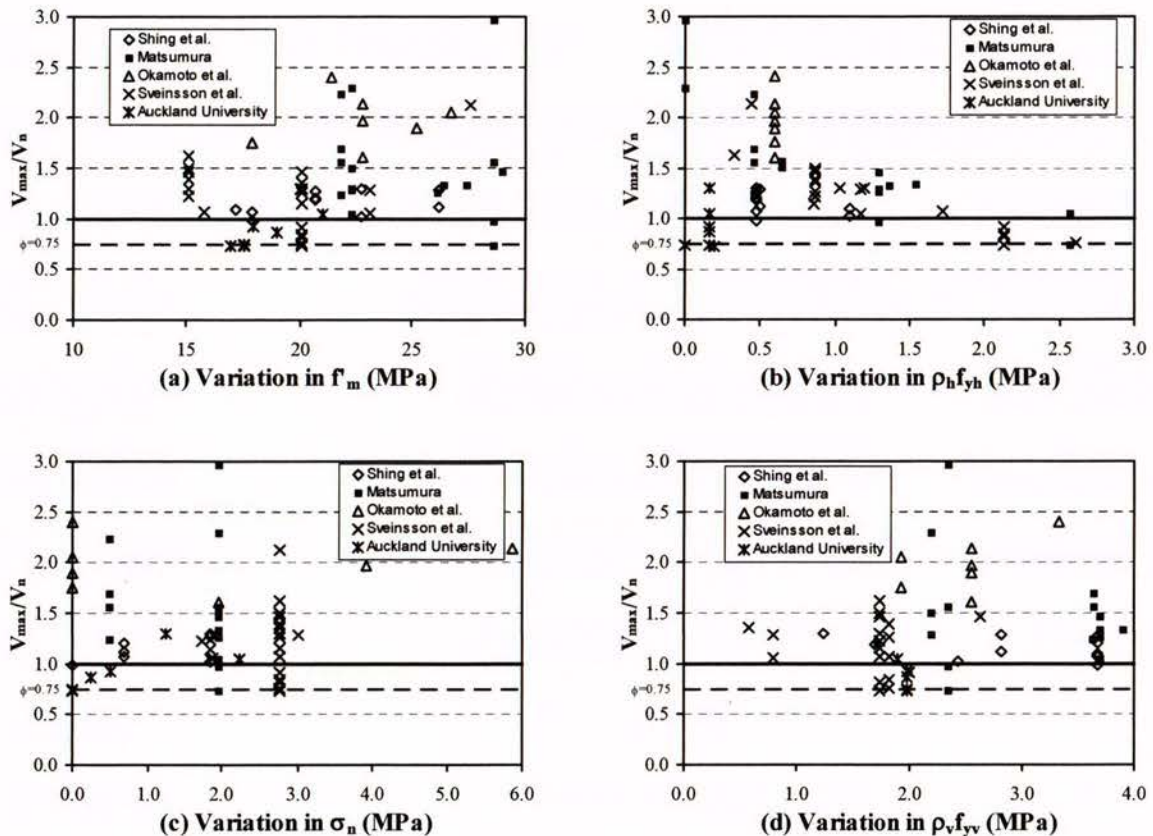


Figure 6.5 Experimental results versus prediction by AS3700.

Despite the simple form of Equation 2-25, NEHPR is capable of providing better shear strength prediction than either the New Zealand or the Australian masonry design standards. Figure 6.6 shows that v_{max}/v_n varies from 0.77 to 1.90, with a mean v_{max}/v_n of 1.39 and a standard deviation of 0.29. The figure shows that NEHPR expression over-predicts the shear strength of 5 specimens (i.e. $v_{max}/v_n < 1.0$) but under-predicts the shear strength of 21 specimens (about 33% of the total) by more than 50% of the test strength (i.e. $v_{max}/v_n > 1.50$).

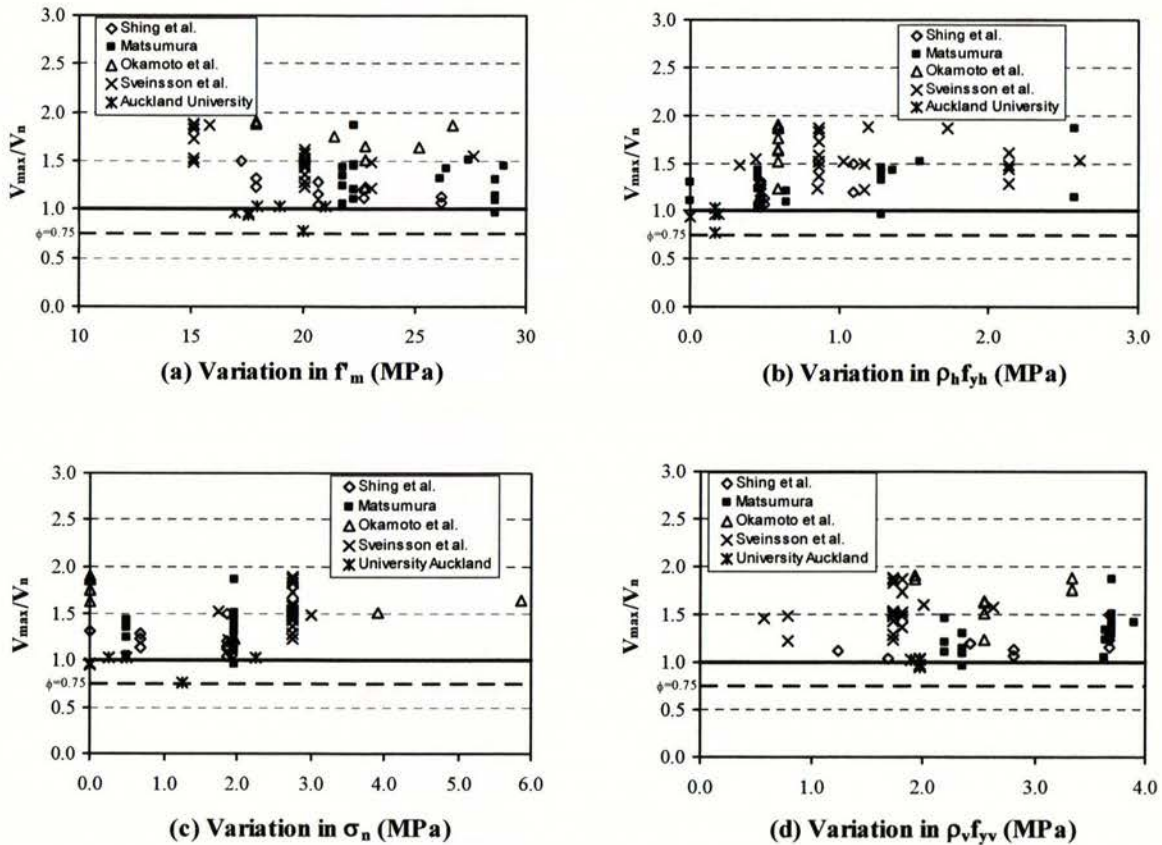


Figure 6.6 Experimental results versus prediction by NEHPR.

Figure 6.7 illustrates the fact that UBC is less successful than NEHPR in predicting masonry shear strength. The scatter shown in Figure 6.7 is most likely due to the neglect of the shear contribution from axial compression load and longitudinal reinforcement, and also over-predicting the contribution of shear reinforcement at high value of $\rho_h f_{yh}$. The normalised plots show that v_{max}/v_n varies from 0.96 to 3.39, with a mean v_{max}/v_n of 1.68.

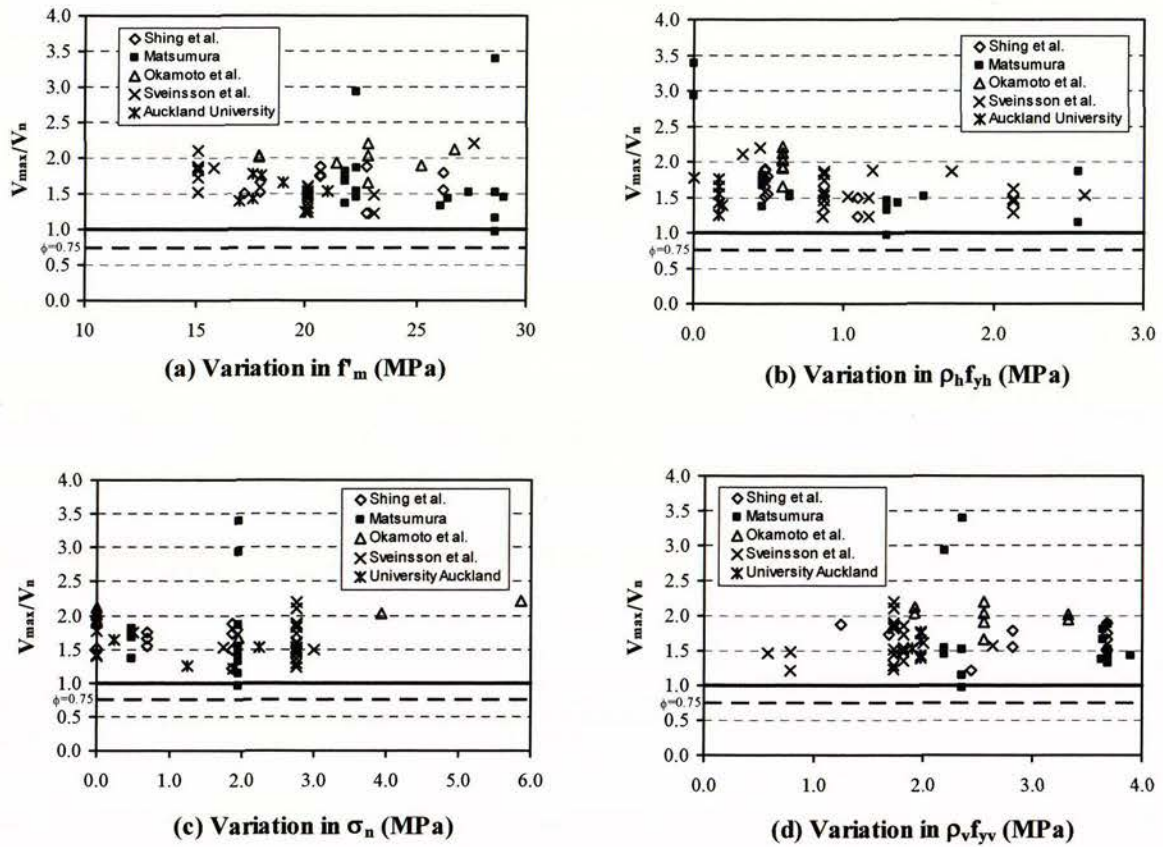


Figure 6.7 Experimental results versus prediction by UBC.

Matsumura developed Equation 2-17 by utilising his test results as well as test results reported by other researchers in Japan. He used regression analysis to determine the appropriate functional forms of the parameters. Overall, Matsumura's equation is successful in predicting the shear strength of most masonry walls, as illustrated in Figure 6.8. However, this equation is unlikely to be adopted into the New Zealand masonry design standard due to

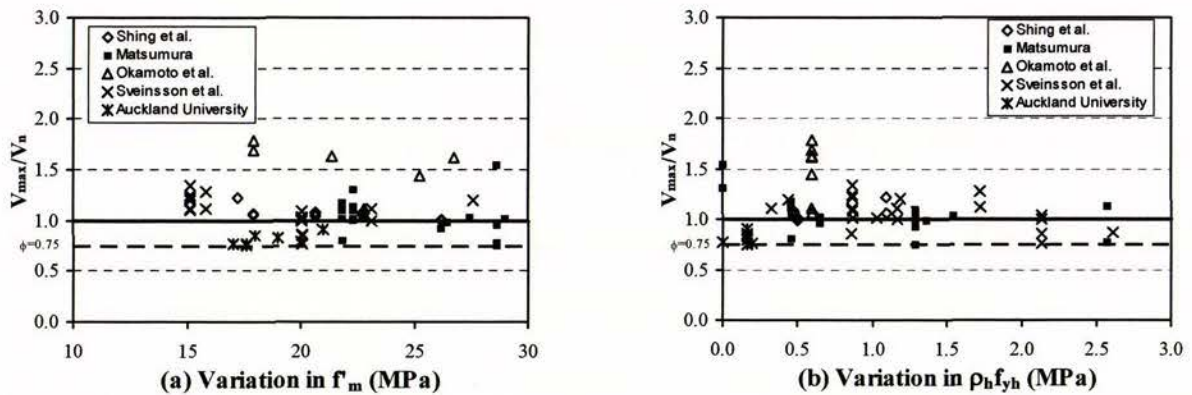


Figure 6.8 Experimental results versus prediction by Matsumura.

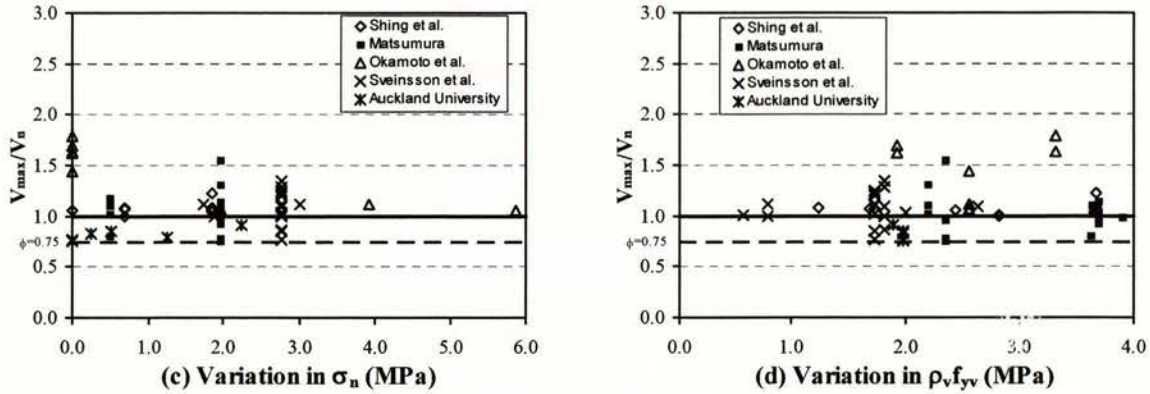


Figure 6.8 Experimental results versus prediction by Matsumura (continued).

the complexity of the equation plus the fact that it has over-predicted the masonry shear strength of all specimens tested at the University of Auckland. The normalised plots shown in Figure 6.8 shows v_{max}/v_n varies from 0.75 to 1.78, with a mean v_{max}/v_n of 1.08.

Figure 6.9 shows masonry shear prediction using the Shing et al. shear expression. Shing et al. concluded from their experimental testing that masonry shear strength depends on the tensile strength of masonry as well as on several other mechanisms, such as aggregate interlocking, the dowel action of longitudinal steel and the action of horizontal shear reinforcement. Due to the complexity in predicting the shear strength of reinforcing masonry walls, a semi-empirical design formula based on the mentioned mechanisms was proposed by Shing et al. This formula was developed to fit the test data of group S ($h_e/\ell_w \approx 1.0$) using regression analysis. Consequently, the results of data set S are better predicted by Equation 2-28 than any of other experimental data (see Figure 6.9). The figure shows that v_{max}/v_n varies

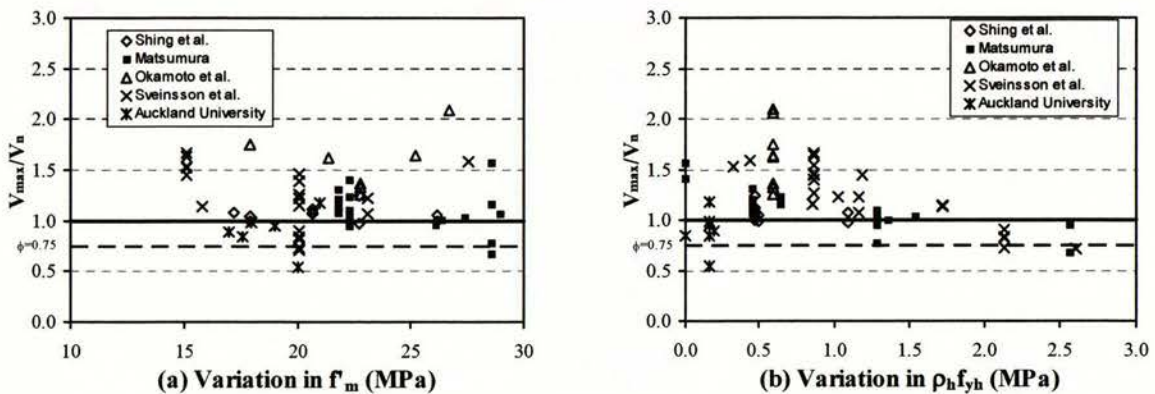


Figure 6.9 Experimental results versus prediction by Shing et al.

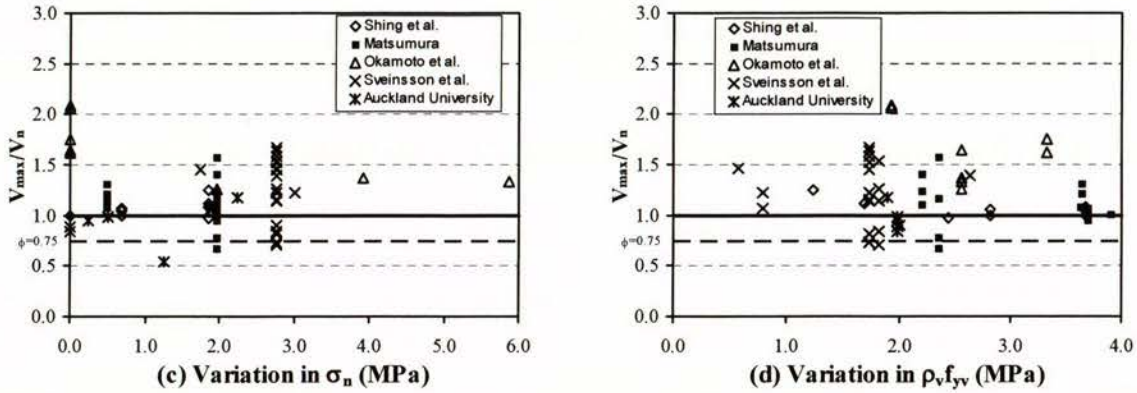


Figure 6.9 Experimental results versus prediction by Shing et al (continued).

from 0.54 to 2.09, with a mean v_{max}/v_n of 1.18. The figure shows that Equation 2-18 over-predicted the shear strength of 18 specimens, of which 6 specimens are experimental results recorded at the University of Auckland. As shown in Figure 6.9, 4 specimens (about 6% of the total) had their measured strength less than $0.75v_n$.

Anderson and Priestley proposed a simple expression to predict masonry shear in 1992. Despite the simple form of Equation 2-21, Figure 6.10 demonstrates that shear predictions using Equation 2-21 provides reasonable agreement with experimental results. However, Equation 2-21 over-predicts the shear strength of 21 specimens (6 of them are specimens recorded at the University of Auckland), of which 2 specimens had their test strengths less than 75% of the predicted strengths. The normalised plots show v_{max}/v_n varies from 0.62 to 3.46, with a mean v_{max}/v_n of 1.18.

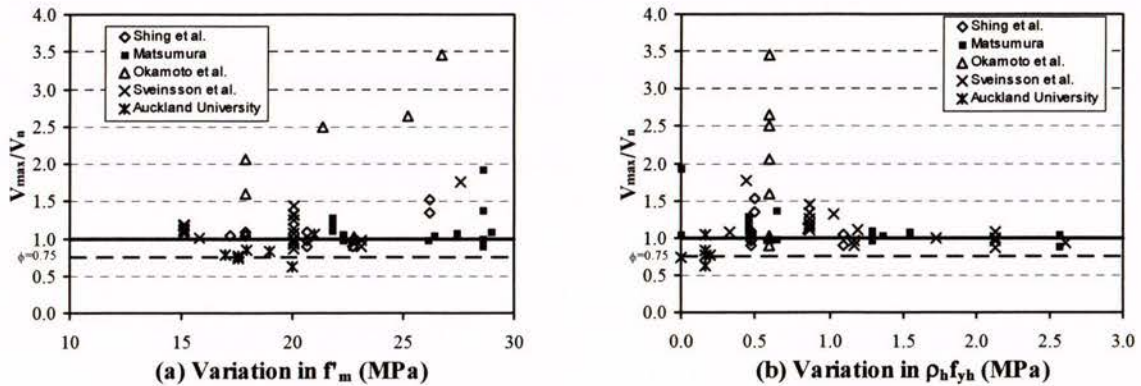


Figure 6.10 Experimental results versus prediction by Anderson and Priestley.

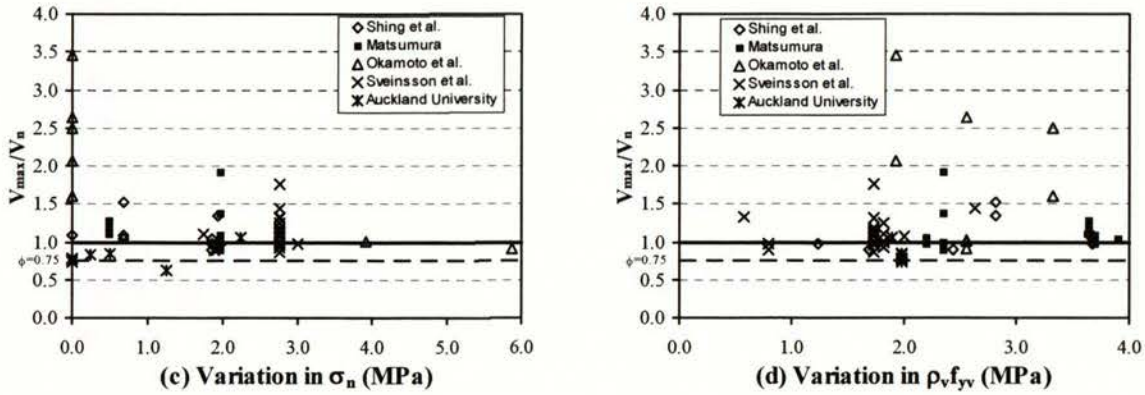


Figure 6.10 Experimental results versus prediction by Anderson and Priestley (continued).

6.3.3 Analysis of Data

Table 6.2 shows that none of the predictive equations can successfully predict the wall strength of data set recorded by Okamoto et al. This consistent under-prediction suggests that the specimens of data set O, for whatever reason, developed higher than normal strengths. To determine if this is indeed the case, comparison is made between Specimen 6-O (specimen no. 34) and Specimen 10-S (specimen no. 10). Specimen 6-O shares similar characteristic to specimen 10-S except for the magnitude of axial compression stress. Specimen 6-O had zero axial compression stress while Specimen 10-S had an axial compression stress of 0.69 MPa. The ultimate shear strength recorded from the actual tests were 3.12 MPa for Specimen 6-O, but only 1.56 MPa for the S specimen. The fact that the O specimen, despite of the absence of axial load, developed about twice the strength as the group S specimen confirms the possibility that specimens of group O may have developed shear strengths that were substantially higher than the specimens of group S of similar construction. Similar comparisons with results from specimen groups O and M indicate the same trend (e.g. compare results of 1-O and 1-M).

Table 6.3 Mean (x_m), standard deviation (s_d) for v_{max}/v_n

v_{max}/v_n	Equations						
	NZS4230	AS3700	NEPHR	UBC	Matsumura	Shing et al.	Anderson & Priestley
x_m	1.716	1.359	1.387	1.675	1.077	1.182	1.182
s_d	0.548	0.472	0.287	0.382	0.227	0.313	0.464

A sample mean, x_m , and standard deviation, s_d , are calculated for each group of comparisons, using the following formulae:

$$x_m = \frac{\sum x_i}{n} \quad s_d = \sqrt{\frac{\sum_1^n (x_i - x_m)^2}{(n-1)}} \quad (6-1)$$

where:

$$x_i = i^{\text{th}} V_{\text{max}}/V_n \text{ value, } n = \text{sample size}$$

The numerical value of standard deviation presented in Table 6.3 cannot be used in statistical analysis because the data points being evaluated do not represent repetitive tests. However, the standard deviation presented here can be useful for making comparisons of the predictive accuracy of each shear equation.

It can be observed from the figures presented in section 6.3.2 and results presented in Tables 6.2 and 6.3, that the New Zealand and Australian masonry standards, and the UBC are conservative in their treatment of masonry shear strength. It is shown in Figure 6.7 and Table 6.3 that the predictive equation proposed by Matsumura is the most successful of those considered. However, due to the complex nature of this equation, it is unlikely to be implemented into the New Zealand masonry design standard.

Despite the simple form of the formula adopted by NEHPR, this equation is capable of predicting masonry shear strength (reinforced-fully grouted walls) with good accuracy. This is illustrated in Figure 6.6 and in Table 6.3. Of particular significance to be observed in Table 6.2 is that the NEHPR shear expression is the only equation that provided close shear predictions to most masonry walls (except Specimen 6-A) tested at the University of Auckland, see shaded column shown in Table 6.2. Specimen 6-A (Wall 9) was built with H/L ratio of 2 and the wall did not develop its maximum shear strength until large displacement ($d_{v\text{max}} = 20 \text{ mm}$). As compared to other masonry walls tested at the University of Auckland, Wall 9 suffered significantly more damage (i.e. more cracking) before it developed its maximum strength at a displacement of 20 mm, therefore resulting in a loss of shear strength capacity. Consequently, NEHPR over-predicted the shear strength of Wall 9 by about 23%, but it closely matched the test results of the six squat fully-grouted concrete masonry walls ($H/L \leq 1$) tested at the University of Auckland, with V_{max}/V_n varying between 0.94 and 1.03.

The NZS4230:1990 and UBC consistently under-predicted the University of Auckland test results by 15-96%, while the other four shear equations over-predicted most of the Auckland test results with v_{\max}/v_n varying between 0.53 and 1.30.

6.4 Partially Grouted Walls

This section compares the accuracy of the predictive equations presented in Table 6.1, in predicting the in-plane shear strength of reinforced partially grouted masonry walls. Accuracy is assessed by comparing the predicted strengths to actual experimental data from independent research sources.

6.4.1 Experimental Data Sets

Yancey (1991) reported a relative scarcity of experimental study to investigate the shear strength of partially grouted masonry wall. More than half of the reported tests of partially grouted masonry walls were conducted in Japan by Matsumura (1987), followed by the University of California at Berkeley by Chen et al. (1985). The data from these two sources reflect construction and reinforcement practices unique to high seismic risk areas.

The experimental data sets included in this part of the study are limited to results of partially-grouted concrete and clay brick masonry walls which were subjected to reverse cyclic lateral loads until shear failure occurred. Due to the scarcity of the test data, only 38 experimental data are included in this study. The selection is based on common aspects and features of the experimental programme, i.e. test set-up, boundary conditions, loading procedure, physical similarities, etc. The data sets selected are from the following experimental programmes:

1. Thirty specimens are selected from tests conducted by Matsumura (1987) at Kanagawa University;
2. Six specimens are selected from tests conducted by Chen et al. (1978) at the University of California at Berkeley;
3. Two specimens tested at the University of Auckland.

The data subsets selected from the studies listed above are identified in the text by the letters MP, BP and AP, corresponding to 1-3 respectively.

All partially grouted masonry specimens selected for this study (except the two specimens tested at the University of Auckland) were tested with the top and bottom surfaces kept rotationally fixed or parallel. The experimental study conducted at the University of Auckland was of the cantilever type. Each specimen was subjected to increasing reverse cyclic lateral displacements until failure. The use of a common loading procedure and similar loading rates in each study produced comparable experimental data.

The maximum lateral force resisted by the wall specimens, after averaging the values from both loading directions, are divided by the net horizontal area to define maximum shear stresses. For partially grouted masonry walls, $A_n = \ell_w x(t - b_f)$, see Figure 2.18.

Relevant properties of the partially grouted specimens are listed in Table E.2 in Appendix E. All walls, except Specimens 29, 30 and 34-36, were constructed of concrete masonry units. The two MP and three BP specimens were constructed of hollow clay brick units.

Table E.2 details the geometric and material properties of the tested specimens, as well as the reinforcement ratios and axial compression stress applied. As shown in Table E.2, the two concrete masonry walls tested at the University of Auckland were aimed to investigate the shear strength of partially grouted masonry walls that had no shear reinforcement and no axial compression load. Experimental studies conducted in U.S. and Japan examined the shear strength of partially grouted masonry walls that were reinforced with shear reinforcement of $0 \leq \rho_h \leq 0.222\%$ and subjected to axial compression loads of $0 \leq \sigma_n \leq 2.08$ MPa. The masonry compressive strength, f'_m , listed in Table E.2 was obtained by prism tests. Both Kanagawa University and University of Auckland used three-course prism tests. Three-course and six-course prisms with h/t ratios of 2 and 4, respectively, were used as the masonry compressive strength for the Berkeley specimens. The yield strength of the reinforcement used in each test was obtained by tension tests. The U.S. customary units used by Chen et al. are converted into S.I units for convenience.

6.4.2 Correlation between Predicted and Measured Response

The equations listed in Table 6.1 were used to predict the maximum shear strength of the 38 test specimen mentioned in section 6.4.1. Appropriate specimen characteristic, such as wall

Table 6.4 Measured and predicted strength of partially grouted masonry walls

Specimen no.	Specimen Label	v_m (MPa)							v_s (MPa)						
		NZS 4230	AS3700	NEPHR	UBC	Matsumura	Shing et al.	Anderson & Priestley	NZS 4230	AS3700	NEPHR	UBC	Matsumura	Shing et al.	Anderson & Priestley
1	1-MP	0.39	0.98	1.04	0.65	0.77	0.90	0.97	0.22	0.22	0.14	0.27	0.19	0.16	0.13
2	2-MP	0.58	0.98	1.33	0.83	1.05	1.22	1.25	0.22	0.22	0.14	0.27	0.25	0.16	0.13
3	3-MP	0.39	0.82	0.94	0.56	0.69	0.96	0.97	0.22	0.22	0.14	0.27	0.19	0.12	0.13
4	4-MP	0.58	0.82	1.21	0.71	0.87	1.20	1.25	0.22	0.22	0.14	0.27	0.24	0.12	0.13
5	5-MP	0.39	0.52	0.77	0.40	0.58	1.40	0.97	0.22	0.22	0.14	0.27	0.19	0.06	0.13
6	6-MP	0.58	0.52	0.99	0.52	0.66	1.62	1.25	0.22	0.22	0.14	0.27	0.24	0.06	0.13
7	7-MP	0.39	0.82	0.94	0.56	0.69	0.96	0.97	0.00	0.00	0.00	0.00	0.00	0.00	0.00
8	8-MP	0.39	0.82	0.94	0.56	0.69	0.96	0.97	0.00	0.00	0.00	0.00	0.00	0.00	0.00
9	9-MP	0.39	0.82	0.94	0.56	0.69	0.96	0.97	0.22	0.22	0.14	0.27	0.19	0.12	0.13
10	10-MP	0.39	0.82	0.94	0.56	0.69	0.96	0.97	0.46	0.46	0.29	0.57	0.27	0.26	0.27
11	11-MP	0.39	0.82	0.94	0.56	0.69	0.96	0.97	0.68	0.68	0.43	0.86	0.34	0.51	0.41
12	12-MP	0.58	0.82	1.21	0.71	0.89	1.23	1.25	0.22	0.22	0.14	0.27	0.24	0.12	0.13
13	13-MP	0.58	0.82	1.21	0.71	0.89	1.23	1.25	0.22	0.22	0.14	0.27	0.24	0.12	0.13
14	14-MP	0.58	0.82	1.21	0.71	0.89	1.23	1.25	0.22	0.22	0.14	0.27	0.24	0.12	0.13
15	15-MP	0.50	0.84	0.89	0.52	0.64	0.88	0.90	0.00	0.00	0.00	0.00	0.00	0.00	0.00
16	16-MP	0.50	0.84	0.89	0.52	0.64	0.88	0.90	0.46	0.46	0.29	0.57	0.25	0.26	0.27
17	17-MP	0.50	0.84	0.89	0.52	0.64	0.88	0.90	0.68	0.68	0.43	0.86	0.31	0.51	0.40
18	18-MP	0.50	0.84	0.89	0.52	0.64	0.88	0.90	1.03	1.03	0.65	1.29	0.38	0.77	0.61
19	19-MP	0.58	0.82	1.21	0.71	0.89	1.51	1.25	0.00	0.00	0.00	0.00	0.00	0.00	0.00
20	20-MP	0.58	0.82	0.87	0.51	0.64	1.09	0.90	0.00	0.00	0.00	0.00	0.00	0.00	0.00
21	21-MP	0.58	0.82	1.21	0.71	0.89	1.51	1.25	0.46	0.46	0.29	0.57	0.35	0.26	0.27
22	22-MP	0.58	0.82	1.21	0.71	0.89	1.51	1.25	0.68	0.68	0.43	0.86	0.43	0.51	0.41
23	23-MP	0.58	1.04	1.38	0.88	1.01	1.13	1.25	0.46	0.46	0.29	0.57	0.35	0.34	0.27
24	24-MP	0.58	1.04	1.38	0.88	1.01	1.13	1.25	0.46	0.46	0.29	0.57	0.35	0.34	0.27
25	25-MP	0.58	0.99	1.34	0.84	0.92	1.11	1.25	0.46	0.46	0.29	0.57	0.35	0.32	0.27
26	26-MP	0.58	0.84	1.23	0.72	0.77	1.10	1.25	0.46	0.46	0.29	0.57	0.35	0.25	0.27
27	27-MP	0.58	0.57	1.02	0.52	0.59	1.12	1.25	0.46	0.46	0.29	0.57	0.34	0.11	0.26
28	28-MP	0.58	0.57	1.02	0.52	0.59	1.12	1.25	0.46	0.46	0.29	0.57	0.34	0.11	0.26
29	29-MP	0.58	0.89	1.41	0.86	1.07	1.35	0.70	0.33	0.33	0.21	0.41	0.33	0.25	0.20
30	30-MP	0.58	0.89	1.36	0.83	1.03	1.30	0.67	0.33	0.33	0.21	0.41	0.32	0.25	0.20
31	1-BP	0.53	0.92	0.88	0.53	0.42	0.66	0.86	0.19	0.19	0.12	0.24	0.16	0.00	0.11
32	2-BP	0.54	0.92	0.90	0.54	0.56	0.76	0.87	0.00	0.00	0.00	0.00	0.00	0.00	0.00
33	3-BP	0.55	0.92	0.90	0.54	0.56	0.76	0.87	0.38	0.38	0.24	0.47	0.22	0.14	0.22
34	4-BP	0.58	0.92	1.07	0.65	0.51	0.80	0.52	0.29	0.29	0.18	0.36	0.23	0.00	0.17
35	5-BP	0.58	0.92	1.10	0.67	0.69	0.94	0.53	0.00	0.00	0.00	0.00	0.00	0.00	0.00
36	6-BP	0.58	0.92	1.07	0.65	0.68	0.92	0.52	0.56	0.56	0.35	0.70	0.32	0.20	0.33
37	1-AP	0.44	1.00	0.80	0.43	0.63	0.90	1.03	0.00	0.00	0.00	0.00	0.00	0.00	0.00
38	2-AP	0.44	1.00	0.80	0.43	0.63	0.82	1.03	0.00	0.00	0.00	0.00	0.00	0.00	0.00

Table 6.4 (continued)

Specimen no.	v_p (MPa)							v_n (MPa)							V_{max} (MPa)
	NZS 4230	AS3700	NEPHR	UBC	Matsumura	Shing et al.	Anderson & Priestley	NZS 4230	AS3700	NEPHR	UBC	Matsumura	Shing et al.	Anderson & Priestley	
1	0.00	0.00	0.00	0.00	0.00	0.00	0.00	0.61	1.20	1.17	0.92	0.96	1.06	1.10	1.14
2	0.00	0.00	0.00	0.00	0.00	0.00	0.00	0.80	1.20	1.47	1.11	1.30	1.38	1.38	1.58
3	0.00	0.00	0.00	0.00	0.00	0.00	0.00	0.61	1.04	1.08	0.83	0.88	1.08	1.10	1.18
4	0.00	0.00	0.00	0.00	0.00	0.00	0.00	0.80	1.04	1.35	0.99	1.11	1.33	1.38	1.54
5	0.00	0.00	0.00	0.00	0.00	0.00	0.00	0.61	0.74	0.91	0.68	0.77	1.45	1.10	1.47
6	0.00	0.00	0.00	0.00	0.00	0.00	0.00	0.80	0.74	1.12	0.79	0.90	1.68	1.37	1.37
7	0.00	0.00	0.00	0.00	0.00	0.00	0.00	0.39	0.82	0.94	0.56	0.69	0.96	0.97	0.76
8	0.00	0.00	0.00	0.00	0.00	0.00	0.00	0.39	0.82	0.94	0.56	0.69	0.96	0.97	0.94
9	0.00	0.00	0.00	0.00	0.00	0.00	0.00	0.61	1.04	1.08	0.83	0.88	1.08	1.10	1.07
10	0.00	0.00	0.00	0.00	0.00	0.00	0.00	0.85	1.27	1.23	1.13	0.97	1.22	1.24	1.16
11	0.00	0.00	0.00	0.00	0.00	0.00	0.00	1.08	1.50	1.34	1.34	1.03	1.47	1.38	1.45
12	0.00	0.00	0.17	0.00	0.11	0.08	0.17	0.80	1.04	1.52	0.99	1.25	1.43	1.55	1.78
13	0.00	0.00	0.35	0.00	0.23	0.16	0.35	0.80	1.04	1.69	0.99	1.37	1.51	1.72	1.86
14	0.00	0.00	0.52	0.00	0.35	0.23	0.52	0.80	1.04	1.73	0.99	1.48	1.59	1.90	2.34
15	0.00	0.00	0.17	0.00	0.11	0.06	0.17	0.50	0.84	1.06	0.52	0.75	0.93	1.07	1.22
16	0.00	0.00	0.17	0.00	0.11	0.06	0.17	0.96	1.30	1.24	1.09	1.01	1.19	1.34	1.91
17	0.00	0.00	0.17	0.00	0.11	0.06	0.17	1.18	1.53	1.24	1.24	1.06	1.44	1.47	2.04
18	0.00	0.00	0.17	0.00	0.11	0.06	0.17	1.53	1.88	1.24	1.24	1.13	1.70	1.68	2.46
19	0.00	0.00	0.35	0.00	0.23	0.16	0.35	0.58	0.82	1.56	0.71	1.12	1.67	1.59	2.07
20	0.00	0.00	0.35	0.00	0.23	0.11	0.35	0.58	0.82	1.22	0.51	0.87	1.20	1.25	1.14
21	0.00	0.00	0.35	0.00	0.23	0.16	0.35	1.03	1.27	1.73	1.28	1.48	1.93	1.87	2.19
22	0.00	0.00	0.35	0.00	0.23	0.16	0.35	1.26	1.50	1.73	1.57	1.55	2.18	2.00	2.41
23	0.00	0.00	0.17	0.00	0.12	0.08	0.17	1.03	1.50	1.73	1.45	1.48	1.55	1.69	2.03
24	0.00	0.00	0.17	0.00	0.12	0.08	0.17	1.03	1.50	1.73	1.45	1.48	1.55	1.69	1.97
25	0.00	0.00	0.17	0.00	0.11	0.08	0.17	1.03	1.45	1.73	1.41	1.39	1.50	1.69	1.91
26	0.00	0.00	0.17	0.00	0.11	0.08	0.17	1.03	1.30	1.68	1.29	1.22	1.42	1.68	1.84
27	0.00	0.00	0.17	0.00	0.11	0.08	0.17	1.03	1.03	1.48	1.09	1.04	1.30	1.67	1.40
28	0.00	0.00	0.17	0.00	0.11	0.08	0.17	1.03	1.03	1.48	1.09	1.04	1.30	1.67	1.41
29	0.00	0.00	0.00	0.00	0.00	0.00	0.00	0.91	1.22	1.62	1.27	1.40	1.60	0.89	2.15
30	0.00	0.00	0.00	0.00	0.00	0.00	0.00	0.91	1.22	1.57	1.24	1.35	1.55	0.87	2.01
31	0.00	0.00	0.24	0.00	0.15	0.07	0.24	0.72	1.11	1.18	0.78	0.73	0.73	1.20	1.59
32	0.00	0.00	0.23	0.00	0.15	0.07	0.23	0.54	0.92	1.13	0.54	0.71	0.83	1.10	1.53
33	0.00	0.00	0.25	0.00	0.16	0.08	0.25	0.93	1.30	1.20	1.02	0.94	0.98	1.34	1.63
34	0.00	0.00	0.49	0.00	0.32	0.18	0.49	0.86	1.20	1.44	1.01	1.06	0.98	1.18	2.81
35	0.00	0.00	0.45	0.00	0.29	0.17	0.45	0.58	0.92	1.48	0.67	0.99	1.11	0.98	1.93
36	0.00	0.00	0.47	0.00	0.31	0.18	0.47	1.14	1.48	1.44	1.35	1.31	1.30	1.32	1.38
37	0.00	0.00	0.00	0.00	0.00	0.00	0.00	0.44	1.00	0.80	0.43	0.63	0.90	1.03	1.20
38	0.00	0.00	0.00	0.00	0.00	0.00	0.00	0.44	1.00	0.80	0.43	0.63	0.82	1.03	0.79

Table 6.4 (continued)

Specimen no.	V_{max}/v_n						
	NZS 4230	AS3700	NEPHR	UBC	Matsumura	Shing et al.	Anderson & Priestley
1	1.86	0.95	0.97	1.24	1.19	1.09	1.03
2	1.99	1.32	1.08	1.43	1.21	1.16	1.15
3	1.93	1.14	1.09	1.42	1.34	1.12	1.07
4	1.94	1.48	1.14	1.56	1.39	1.20	1.12
5	2.40	1.98	1.62	2.17	1.92	1.33	1.34
6	1.72	1.85	1.22	1.73	1.54	1.12	1.00
7	1.93	0.93	0.81	1.37	1.10	0.82	0.78
8	2.39	1.15	1.00	1.69	1.36	1.01	0.97
9	1.75	1.03	0.99	1.29	1.21	0.99	0.97
10	1.36	0.91	0.94	1.03	1.20	0.98	0.93
11	1.34	0.96	1.08	1.08	1.41	1.00	1.05
12	2.24	1.72	1.17	1.80	1.43	1.27	1.15
13	2.34	1.79	1.10	1.89	1.37	1.26	1.08
14	2.94	2.26	1.36	2.37	1.58	1.51	1.23
15	2.44	1.45	1.16	2.33	1.62	1.34	1.14
16	2.00	1.47	1.54	1.75	1.90	1.64	1.43
17	1.72	1.34	1.64	1.64	1.92	1.44	1.39
18	1.61	1.31	1.98	1.98	2.18	1.47	1.47
19	3.59	2.53	1.33	2.90	1.85	1.53	1.30
20	1.98	1.39	0.94	2.22	1.31	1.17	0.92
21	2.12	1.72	1.27	1.71	1.49	1.36	1.17
22	1.91	1.60	1.40	1.54	1.56	1.29	1.20
23	2.06	1.35	1.57	1.65	1.79	1.63	1.47
24	2.00	1.31	1.52	1.60	1.73	1.58	1.43
25	1.94	1.32	1.48	1.59	1.78	1.58	1.39
26	1.87	1.42	1.42	1.65	1.95	1.63	1.34
27	1.43	1.36	1.15	1.46	1.74	1.40	1.03
28	1.44	1.37	1.15	1.47	1.76	1.41	1.04
29	2.37	1.76	1.33	1.69	1.54	1.35	2.41
30	2.22	1.64	1.28	1.62	1.49	1.30	2.32
31	2.19	1.43	1.34	2.05	2.18	2.18	1.32
32	2.86	1.67	1.36	2.82	2.15	1.83	1.39
33	1.75	1.26	1.35	1.60	1.73	1.67	1.22
34	3.26	2.34	1.95	2.79	2.64	2.85	2.39
35	3.36	2.11	1.31	2.90	1.96	1.74	1.97
36	1.21	0.93	0.96	1.02	1.06	1.06	1.04
37	2.70	1.20	1.49	2.80	1.91	1.33	1.16
38	1.78	0.79	0.98	1.84	1.26	0.96	0.77

dimensions, reinforcing steel ratios, masonry compression strength (f'_m) and the axial load (σ_n) were used as the inputs in the predictive equations. Table 6.4 lists the predicted strength (v_m , v_s , v_p and the sum v_n) obtained from each predictive equation, and the actual shear strength (v_{max}) determined from the tests of all 38 specimens.

Normalised plots (v_{max}/v_n) are presented in Figures 6.11 to 6.17 to investigate the accuracy of each equation with respect to different parameters. For examples, Figure (a) of each plot examines the accuracy of each predictive equation when variation is set on f'_m appropriate to each test result, and Figure (b) examines the accuracy of the predictive equation when variation is set on $\rho_h f_{yh}$.

The line of unity represents perfect correlation. Points deviating from this line indicate both the scatter in the test results and approximations in the predictive formulation. The spread of points above and below the line illustrates the tendency to over- and under-predict the shear strength of the masonry walls, as well as the general scatter in the test results. The corresponding value accounting for the strength reduction factor (ϕ) is also shown in Figures 6.11-6.17.

Figure 6.11 illustrates the fact that the shear provision in the current New Zealand masonry design standard is incapable of accurately predicting the shear strength of partially grouted masonry walls. Scatter of results above the line of unity, as shown in Figures 6.11(a) to (d), clearly demonstrates that the NZS4230 under-predicts the test results by a significant margin. The test strengths of 31 specimens (about 82% of the total) are observed to be at least 50%

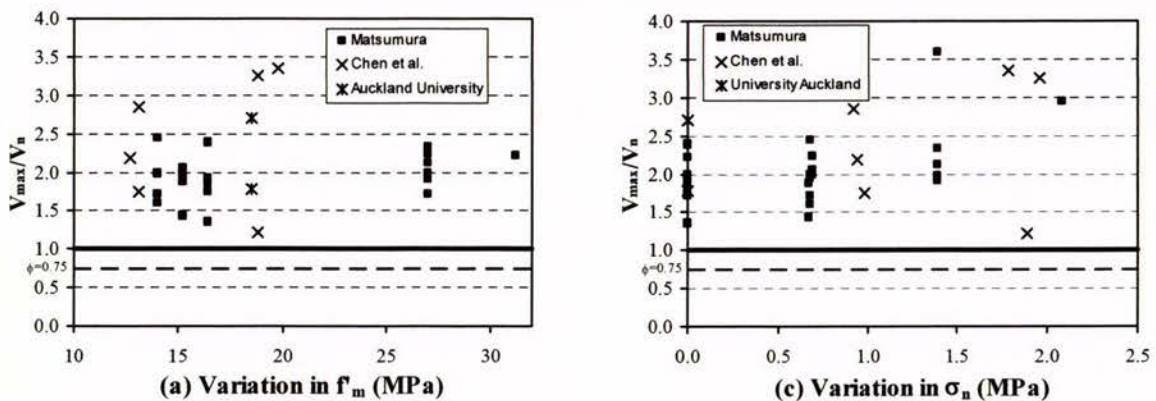


Figure 6.11 Experimental results versus prediction by NZS4230:1990.

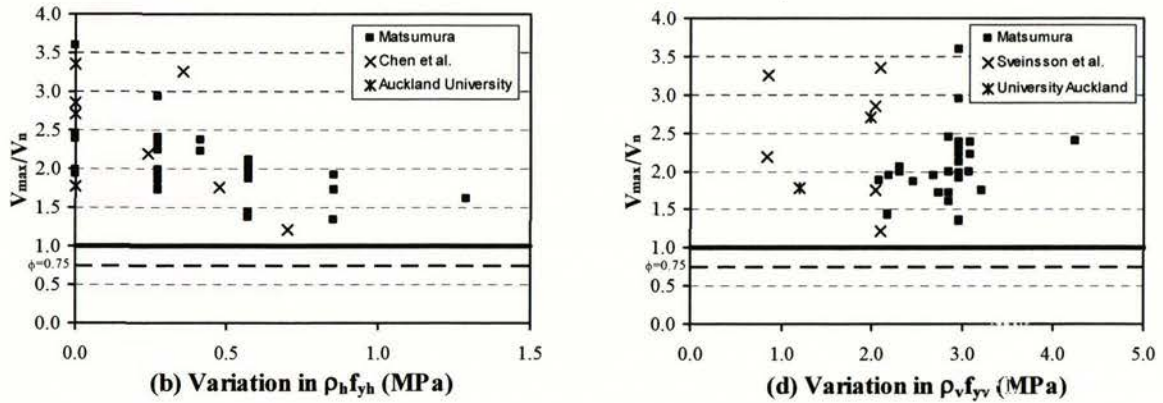


Figure 6.11 Experimental results versus prediction by NZS4230:1990 (continued).

more than those predicted by NZS4230:1990. Figure 6.10(b) vividly shows the tendency of NZS4230:1990 to under-predict the contribution of shear reinforcement at low values of $\rho_h f_{yh}$ but over-predict the results at higher values of $\rho_h f_{yh}$. Figure 6.10 shows v_{max}/v_n varies from 1.21 to 3.75.

Figure 6.12 shows shear predictions using the Australian masonry standard. The AS3700 expression is shown here to be unsuccessful in predicting the masonry shear strength of

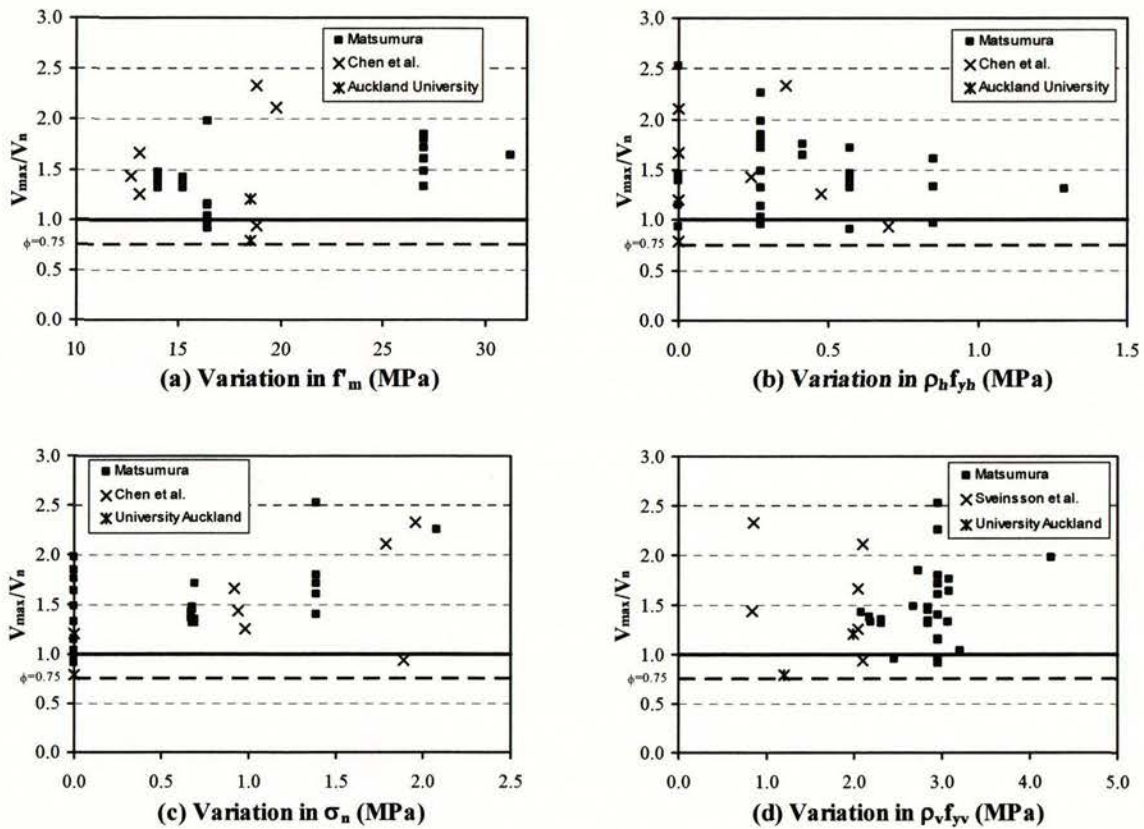


Figure 6.12 Experimental results versus prediction by AS3700.

partially grouted masonry walls. Part of the scatter in the figure is mostly due to the neglect of the influences of f'_m and axial compression load on masonry shear strength, and also the possibility of over-predicting the contribution of reinforcement at high value of $\rho_h f_{yh}$. The normalised plots show shear prediction using AS3700 resulted v_{max}/v_n that varies between 0.79 and 2.53, with a mean v_{max}/v_n of 1.46.

Despite the simple form of the formulation, NEHPR is capable of providing an improved shear strength prediction than either the New Zealand or the Australian masonry design standards. Figure 6.13 illustrates that v_{max}/v_n varies from 0.80 to 1.98, with a mean v_{max}/v_n of 1.28. The NEHPR expression under-predicts the shear strength of 29 specimens, of which 7 specimens have $v_{max}/v_n > 1.5$. The NEHPR expression over-predicts the shear strength of 7 partially grouted specimens, of which 1 specimen (3% of the total) has $v_{max}/v_n < 0.9$.

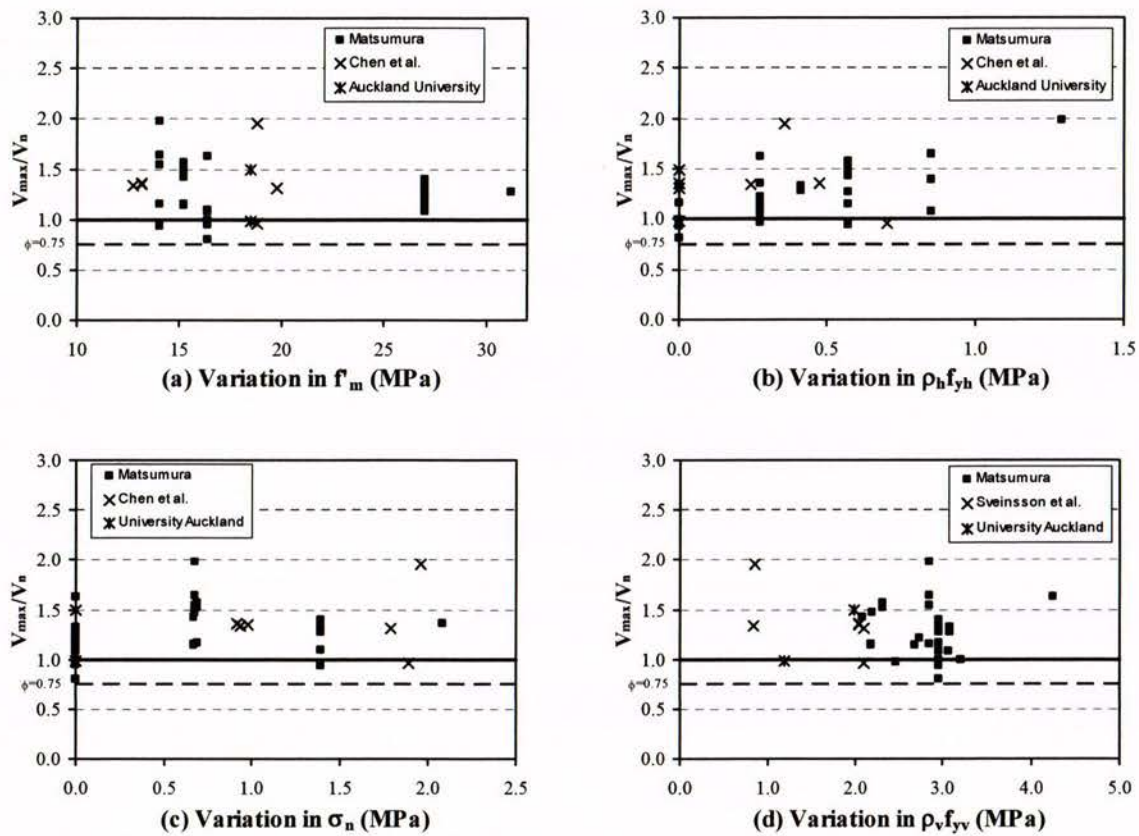


Figure 6.13 Experimental results versus prediction by NEHPR.

Figure 6.14 illustrates the fact that the UBC is unsuccessful in predicting the shear strength of partially grouted masonry walls. The scatter shown in Figure 6.14 is mostly caused by neglect of the contribution of axial compression towards masonry shear strength. Figure 6.14(b) shows that the UBC tends to over-predict the contribution of shear reinforcement at

high values of $\rho_h f_{yh}$. The normalised plots show that v_{max}/v_n varies between 1.02 and 2.90, with 72% of the specimens having $v_{max}/v_n > 1.50$.

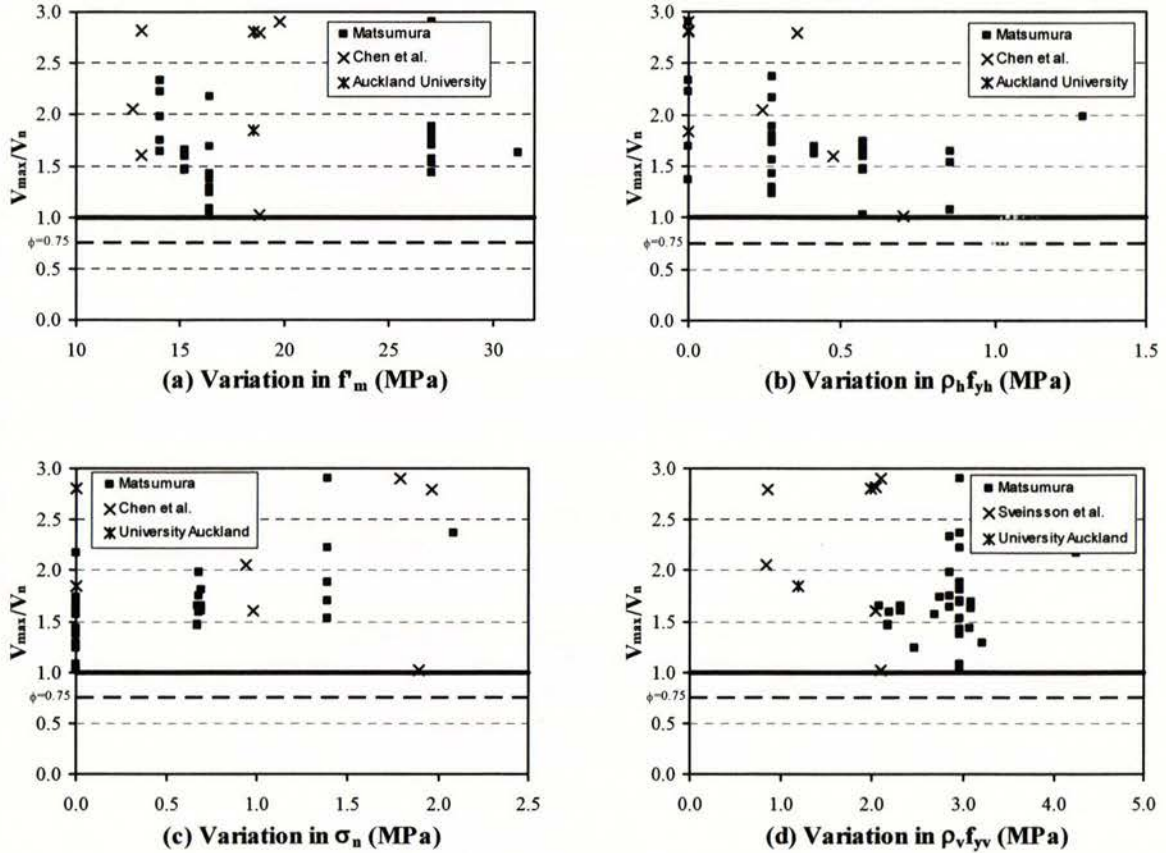


Figure 6.14 Experimental results versus prediction by UBC.

The shear expression proposed by Matsumura (Equation 2-17) was based on the use of gross area. Consequently, it tends to under-predict the shear strength of partially grouted masonry when the shear stress, v_n , is calculated according to net horizontal area, A_n . Figure 6.15 displays the spread of points above the line of unity and v_{max}/v_n varies from 1.06 to 2.64. The test strength of 21 specimens (about 55% of the total) have $v_{max}/v_n > 1.5$.

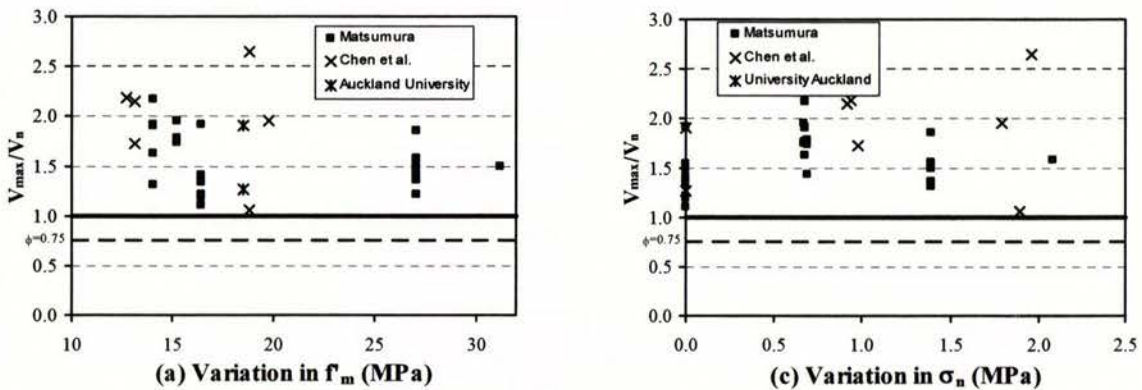


Figure 6.15 Experimental results versus prediction by Matsumura.

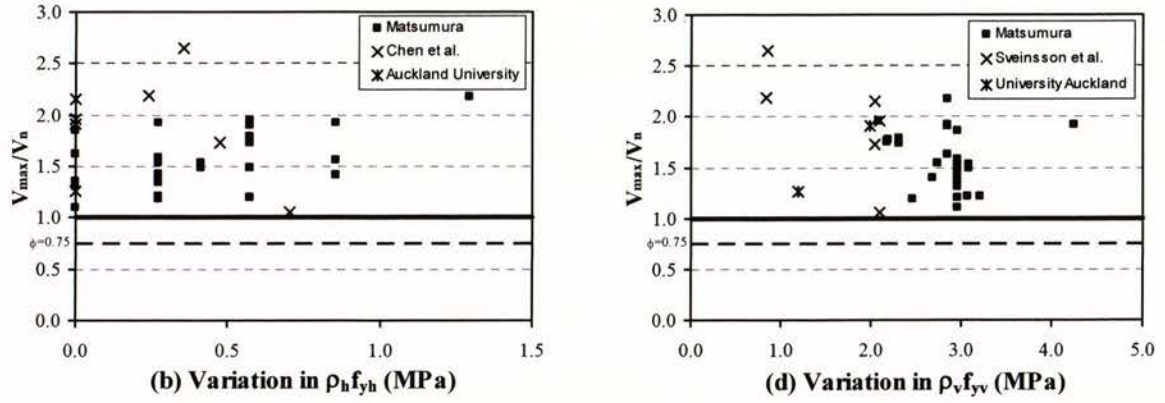


Figure 6.15 Experimental results versus prediction by Matsumura (continued).

The formula proposed by Shing et al. was developed to fit the test data of fully grouted masonry walls tested at the University of Colorado. Consequently, it is unable to precisely predict the shear strength of partially grouted masonry walls. This is shown in the scatter of points above/below the line of unity in Figure 6.16. It is shown that v_{max}/v_n varies from 0.82 to 2.85 with a mean v_{max}/v_n of 1.38.

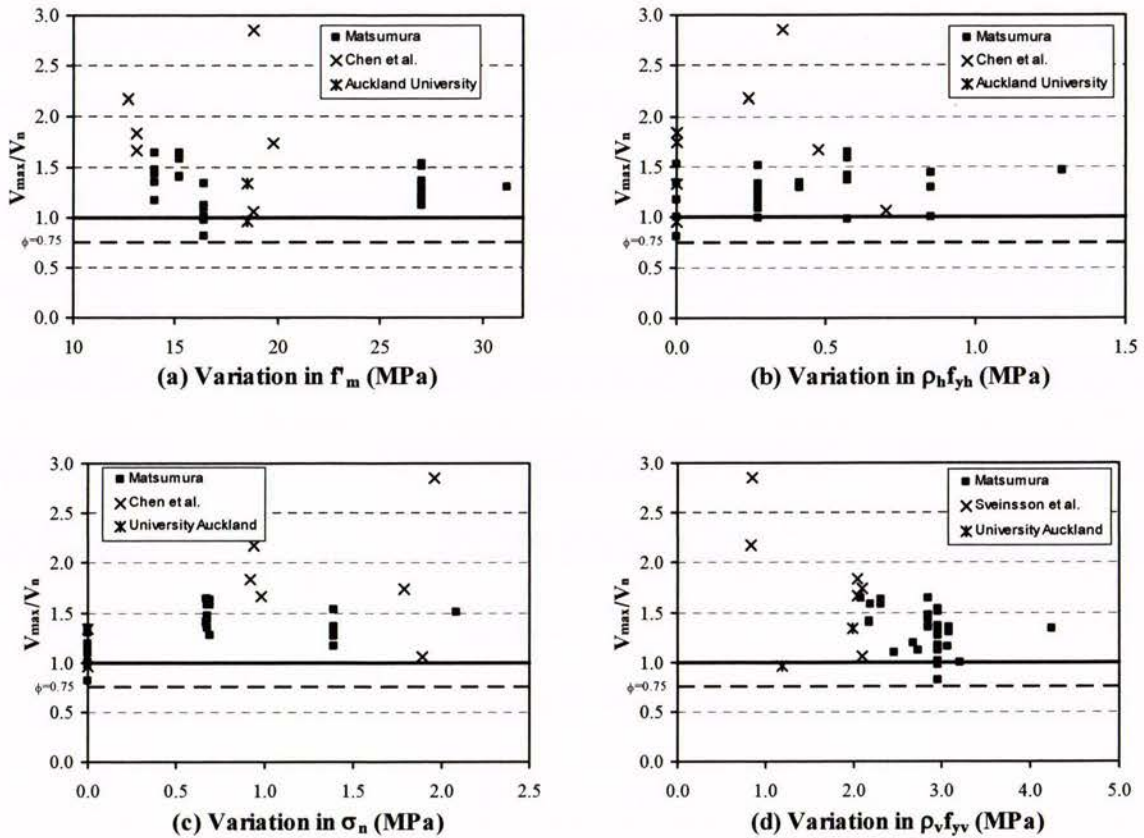


Figure 6.16 Experimental results versus prediction by Shing et al.

Figure 6.17 displays correlation between the test results and shear prediction using the equation proposed by Anderson and Priestley. It is shown that v_{max}/v_n varies from 0.77 to 2.41, and about 50% of the specimens fall outside the range of $0.8 < v_{max}/v_n < 1.2$. The Anderson and Priestley equation over-predicts the shear strength of 6 specimens, of which 1 specimen has its test strength lower than 80% of the predicted strength.

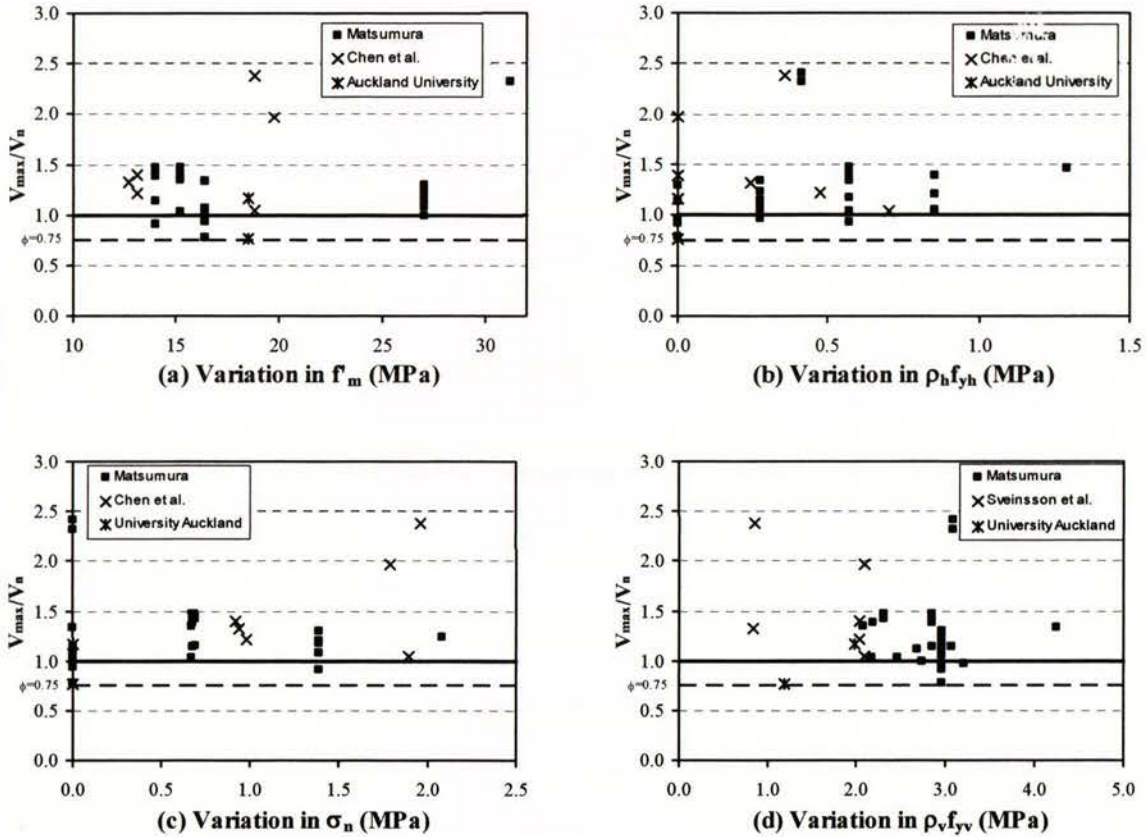


Figure 6.17 Experimental results versus prediction by Anderson and Priestley.

6.4.3 Analysis of Data

Table 6.5 on the following page, presents the calculated sample mean, x_m , and standard deviation, s_d , using Equation 6-1, for each group of comparisons.

It is emphasised that the numerical value of standard deviation presented in Table 6.5 is unsuitable for use in statistical analysis because the data points being evaluated do not represent repetitive tests. However, the standard deviation calculated here can be useful for making comparisons of the predictive accuracy of each shear equation.

Table 6.5 Mean (x_m), standard deviation (s_d) for v_{max}/v_n

v_{max}/v_n	Equations						
	NZS4230	AS3700	NEHPR	UBC	Matsumura	Shing et al.	Anderson & Priestley
x_m	2.104	1.462	1.275	1.808	1.625	1.384	1.278
s_d	0.551	0.412	0.269	0.516	0.353	0.373	0.394

It can be observed from Figures 6.13-6.27 and Table 6.5 that the shear expressions adopted by NEHPR (Equation 2-25) and that proposed by Anderson and Priestley (Equation 2-21) provide the closest shear prediction for the 38 partially grouted specimens. Although the NEHPR expression over-predicted the shear strength of 7 specimens, only 1 specimen has its wall strength less than 90% of the predicted shear strength. The Anderson and Priestley shear expression has similarly over-predicted the shear strength of 6 specimens, of which 1 specimen has $v_{max}/v_n < 0.8$.

Table 6.4 vividly indicates that the shear strength provisions from NZS4230:1990 and UBC significantly under-estimate the shear strength of the two partially grouted masonry walls tested at the University of Auckland. Comparison of the two test results with shear predictions using NEHPR indicates that Equation 2-25 provides good estimate for the partially grouted wall reinforced with 3-D20 vertical reinforcing bars, but under-estimates the shear strength of the second partially grouted wall reinforced with 5-D20 vertical reinforcing bars. Comparison of the two Auckland test results with the remaining shear equations (AS3700, Shing et al., and Anderson and Priestley) indicate mixed results, since the three predictive equations over-estimate the masonry shear strength in the lighter reinforced partially grouted wall, but under-estimate the masonry shear strength for the wall reinforced with 5-D20 vertical reinforcing bars.

The following conclusions can be drawn on the basis of the maximum strength comparisons discussed in Sections 6.3 and 6.4. There is no doubt that the shear expression in NZS430:1990 does not adequately predict the maximum shear strength for the range of parameters represented by the masonry walls included in this study. Of the four equations currently prescribed by codes, the NEHPR shear expression is generally the closest masonry shear strength predictor. However, there are still some deficiencies in the NEHPR shear

equation since it does not address masonry shear strength within potential plastic hinge zone. In addition, the use of $0.5\rho_h f_{yh}$ in its v_s term is contrary to well established split beam theory. Consequently, new shear expression would need to be established (see Chapter 7) to account for the contribution of shear reinforcement and the effect of masonry shear strength within the potential plastic hinge zone.

Chapter 7

Shear Equation Improvement

In Chapter 6, the accuracy of the seven shear equations in predicting masonry shear strength were examined relative to the experimental results of 102 independent wall tests. The comparisons highlighted poor correlation of some equations with the test results. These were mostly due to inconsistencies of the functions describing the effect of different parameters, such as axial compressive stress, masonry compressive strength, shear span ratios, and the effects of horizontal and vertical reinforcement on strength.

This chapter describes a new shear equation proposed by the author for possible inclusion in the New Zealand masonry design standard.

7.1 New Shear Equation

7.1.1 Modification of V_m

There is wide divergence of opinions, design approach, and code equations related to the shear strength of reinforced masonry walls. Due to the complexity of shear mechanisms, no effective theoretical models have yet been proposed. Consequently it is proposed that for practical structural design calculations, the nominal shear strength of a masonry wall panel is given by Equation 2-9:

$$V_n = V_m + V_s + V_p$$

where

$$V_m = v_m b_w d$$

and for shear walls loaded in-plane, d shall be taken as $0.8\ell_w$ (see Figure 2.18)

$$\text{and } v_m = k(C_1 + C_2)\sqrt{f'_m} \quad (7-1)$$

where $C_1 = 0.083[4 - 1.75(h_e/\ell_w)]$ and $C_2 = 0.022\rho_v f_{yv}$, and h_e/ℓ_w need not be taken greater than 1,

$$\text{and } k = \begin{cases} 1.0 & \mu \leq 2.0 \\ 2.0 - 0.5\mu & 2.0 < \mu \leq 4.0 \\ 0 & \mu > 4.0 \end{cases}$$

As shown in Equation 7-1, the v_m term proposed here is similar to the NEHPR expression, but this new equation includes the effects of longitudinal reinforcement and displacement ductility on masonry shear strength. Tests have shown that walls that fail in shear show very poor cyclic response and their strength deteriorates rapidly. Also, walls that initially yield in flexure may fail in shear after several large inelastic cycles, with rapid strength degradation immediately following. Hence, within the plastic hinge region of a wall, it is usually required that the shear reinforcement be designed to carry the entire shear load. A less conservative approach adopted here has assumed that negligible shear strength degradation occurs up to a member ductility ratio of 2, followed by a gradual decrease at higher design ductility values (see Figure 7.1). This behaviour is recognised by the k factor employed in Equation 7-1. Similar to the NEHPR shear equation, the C_1 term in Equation 7-1 accounts for the effect of h_e/ℓ_w on masonry shear strength.

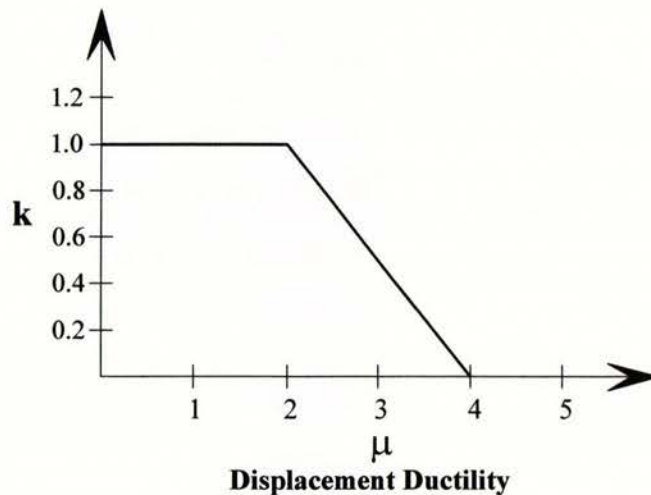


Figure 7.1 Relationship between ductility and masonry shear resisting mechanism.

It was previously reported that part of the shear resistance capacity of masonry is attributed to the dowel action of vertical reinforcement (Shing et al, 1990), and this is represented by the

C_2 term in Equation 7-1. During dowel action of the vertical reinforcing bar, shear force can be transferred along a diagonal crack by the shear, flexural and kinking actions which are activated locally in reinforcing bars due to their relative displacement along a crack. In addition, by helping to control the diagonal cracks, the friction along these cracks would be enhanced, therefore there would be some increase in shear capacity due to vertical reinforcing bars. However, at the onset of the yielding of longitudinal reinforcement, the resistance of the bars essentially diminish. This effect is represented by the k factor shown in Equation 7-1.

7.1.2 Modification of V_s

It has been observed by some researchers that the shear reinforcement has limited efficiency in masonry walls. For example, Anderson and Priestley (1992) proposed Equation 2-21:

$$V_n = C_{ap} \sqrt{f'_m} A_n + 0.5 A_h f_{yh} \frac{d}{s} + 0.25N$$

The above equation has been developed from statistical data fitting, showing that the shear reinforcement does not have full efficiency compared to that assumed in a reinforced concrete member. An explanation by Anderson and Priestley (1992) is as follows: upon initial loading of a wall, all shear is carried by the concrete and the shear reinforcement is essentially unstressed. When diagonal cracking occurs the reinforcing steel at the crack must go into tension, but because of the crack opening the shear carried by the masonry across the crack is reduced. As the crack widens the tension in the shear reinforcing steel increases, increasing the shear carried by the steel, but the shear carried across the crack by the masonry decreases. Hence, as deformation increases, the rate at which the steel increases shear capacity may be less than the rate at which the masonry loses strength, and so a maximum capacity is reached.

In addition to the explanation presented above, the following observations are realised when taking a detailed look at the database presented in Chapter 6:

1. The shear reinforcing steel in the walls had various end anchorage arrangements, with possible different efficiency of the anchorage;
2. Several walls in the database had rather short length, suggesting that in those walls, because of the anchorage details and development length of the shear reinforcing

steel, it was unlikely that the length of shear steel was enough to fully develop their yield strength.

Taking account of the above explanations, a new equation is proposed to account for V_s . Equation 7-2 is proposed base on the hypothesis that the reduced efficiency of shear reinforcement could be evaluated by defining a “dead zone” of the shear reinforcement in which the steel is not efficient. Consequently a reduced effective depth of the section, D_{eff} , is employed in the V_s term. It is assumed that the reduced efficiency of the horizontal reinforcement is due to bar anchorage effects. These effects account for the cover to the longitudinal reinforcement and the development of shear reinforcement.

$$V_s = 0.9A_h f_{yh} \frac{D_{\text{eff}}}{s_h} \quad (7-2)$$

where $D_{\text{eff}} = \ell_w - d' - \ell_{dh}$

7.1.3 Modification of V_p

The shear strength enhancement resulting from axial compression is considered as an independent component of the shear strength, resulting from a diagonal compression strut (Priestley et al., 1994), as shown in Figure 7.2, given by Equation 7-3:

$$V_p = 0.9N \tan \alpha \quad (7-3)$$

where $N \leq 0.1f'_m A_n$

For a cantilever wall, α is the angle formed between the wall axis and the strut from the point of load application to the centre of the flexural compression zone at the wall plastic hinge critical section. For a wall in double bending, α is the angle between the wall axis and the line joining the centres of flexural compression at the top and bottom of the wall (see Figure 7.2). The justification for the abovementioned approach is the simple observation that the axial load must effectively form a compression strut at an angle to the wall axis since it must be transmitted through the flexural compression zone, and that the direction of the horizontal component of the force resists the applied shear force (Priestley et al., 1994).

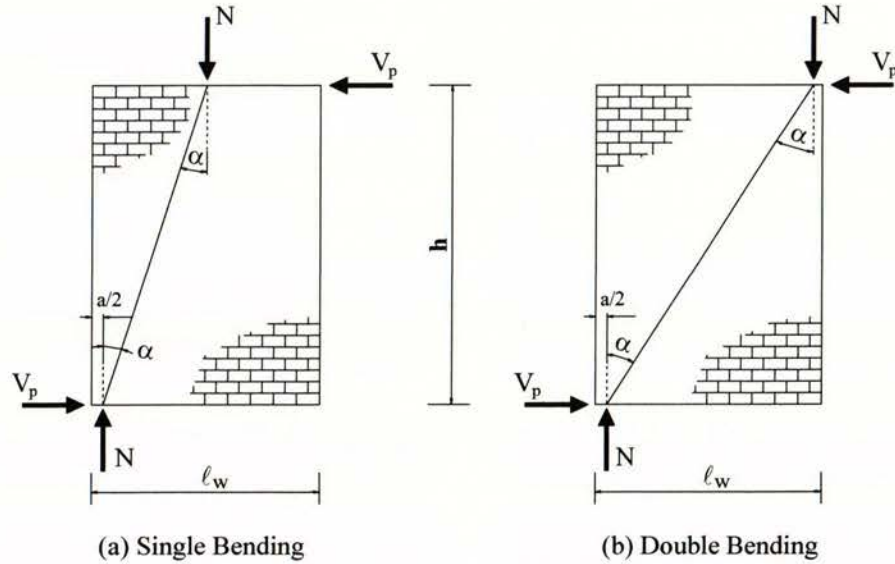


Figure 7.2 Contribution of axial force to masonry shear strength.

The above method implies that the shear strength of squat axially loaded walls should be greater than that of more slender walls. It also implies that as the axial load increases, and hence the depth a of the flexural compression zone increases, the increase in shear strength will become less significant.

Finally, by adding the new V_m , V_s and V_p terms, a new shear expression is developed and shown in Equation 7-4. An upper limit of $0.33\sqrt{f'_m}A_n$ is implemented in Equation 7-4 to prevent this shear equation being less conservative than the NEHPR shear expression.

$$V_n = 0.8k(C_1 + C_2)A_n\sqrt{f'_m} + 0.9A_h f_{yh} \frac{D_{eff}}{s_h} + 0.9N \tan \alpha \leq 0.33A_n\sqrt{f'_m} \quad (7-4)$$

7.2 Correlation between Predicted and Measured Strength

This section of the report compares the suitability of Equation 7-4 in predicting the in-plane shear strength of reinforced masonry walls. As indicated in Sections 6.3.1 and 6.4.1, most of the test data listed in Tables 6.2 and 6.3 are assembled from published conference and journal papers. Consequently, there was difficulty in obtaining sufficient information to evaluate the μ_{vmax} (ductility level of wall at the point when maximum strength developed, i.e. d_{vmax}/Δ_y) of some walls. This is especially the case when working with the experimental data for tests

conducted by the Japanese researchers. As a result, only a portion of the Japanese test data is included in this part of study (see Tables E.1 and E.2)

7.2.1 Fully Grouted Walls

The experimental data sets used in this part of the study are limited to those of fully grout-filled masonry walls, and a total of 47 specimens are included here. The measured and predicted shear strength of the 47 specimens are listed in Table 7.1, where predicted strength (v_m , v_p , v_s and v_n) is based on Equation 7-4, using appropriate specimen characteristics and $\phi = 1.0$. Please refer to Table E.1 for the μ_{vmax} values for each specimen. Although Table 7.1 does not contain all the data listed in Table 6.2, it can indicate the accuracy of Equation 7-4.

Similar to Section 6.3.2, normalised plots (v_{max}/v_n) are presented in Figure 7.3 to investigate the accuracy of Equation 7-4 with respect to different parameters. The data are organised according to masonry compressive strength, shear reinforcement ratio, axial load level and longitudinal reinforcement ratio. Considerable improved representation of the actual shear strength is apparent as compared to the shear predictions using NZS4230:1990 (see Figure 6.4). As shown in Figure 7.3, v_{max}/v_n varies from 0.93 to 1.89, with resulted mean and standard deviation of 1.41 and 0.28. The use of a shear strength reduction factor of $\phi = 0.75$ will effectively provide a lower limit to the data. It is successfully demonstrated in Figure 7.3 that Equation 7-4 produces result similar to that of NEHPR (please refer to Section 6.3.2) but Equation 7-4 has more “engineering meaning” than the NEHPR shear expression.

By observing Table 7.1, it can be seen that Equation 7-4 under-estimates the shear strength of the 5 square ($h_e/\ell_w = 1.0$) masonry walls tested at the University of Auckland, with v_{max}/v_n varying from 1.24 to 1.38, but slightly over-predicts the shear strength of the slender ($h_e/\ell_w = 2.0$) and squat walls ($h_e/\ell_w = 0.6$). However, it is observed that the shear prediction of Specimen 6-A (Wall 9) is significantly improved (as compared to the shear prediction using NEHPR, see Table 6.2) by the introduction of k term in Equation 7-4. The v_{max}/v_n ratio of Specimen 6-A is improved from 0.77 when using the NEHPR shear expression to 0.94 when calculated using Equation 7-4.

Table 7.1 Shear prediction of fully grouted masonry walls using Equation 7-4

Specimen no.	Specimen label	MPa				V_{max}/V_n
		V_m	V_s	V_p	V_n	
1	1-S	0.00	0.35	0.66	1.02	1.71
2	2-S	0.53	0.35	0.00	0.88	1.53
3	3-S	0.68	0.35	0.26	1.28	1.15
4	4-S	0.39	0.35	0.25	0.99	1.67
5	5-S	0.83	0.35	0.71	1.50	1.09
6	6-S	0.94	0.62	0.70	1.57	1.22
7	7-S	0.94	0.36	0.70	1.57	1.13
8	8-S	0.00	0.61	0.59	1.20	1.71
9	9-S	0.86	0.38	0.73	1.69	1.06
10	10-S	1.01	0.38	0.28	1.67	0.94
11	5-M	1.02	0.00	1.08	1.56	1.09
12	6-M	1.02	0.40	1.08	1.56	1.21
13	7-M	0.33	0.81	1.08	1.56	1.46
14	8-M	1.14	0.81	1.07	1.56	1.47
15	9-M	0.98	1.40	1.07	1.56	1.88
16	15-M	1.16	0.00	1.08	1.76	1.23
17	16-M	0.60	0.40	1.08	1.76	1.10
18	17-M	1.16	0.80	1.08	1.76	0.97
19	18-M	1.14	1.41	1.08	1.76	1.16
20	1-B	0.00	0.70	1.38	1.59	1.23
21	2-B	0.00	0.70	1.64	1.59	1.50
22	3-B	0.00	0.90	1.09	1.31	1.88
23	4-B	0.82	0.90	1.06	1.31	1.88
24	5-B	0.00	0.44	1.04	1.28	1.84
25	6-B	0.00	0.44	1.01	1.28	1.74
26	7-B	0.00	0.24	1.04	1.28	1.50
27	8-B	0.00	0.66	1.04	1.28	1.89
28	9-B	0.34	0.44	1.08	1.28	1.53
29	10-B	0.77	0.44	1.04	1.28	1.87
30	11-B	0.07	0.48	1.42	1.48	1.24
31	12-B	0.41	1.19	1.42	1.48	1.30
32	13-B	0.14	0.48	1.39	1.48	1.59
33	14-B	0.41	1.19	1.39	1.48	1.62
34	15-B	0.00	0.48	1.38	1.48	1.37
35	16-B	0.00	1.19	1.38	1.48	1.49
36	17-B	0.83	0.48	1.42	1.48	1.47
37	18-B	0.67	1.19	1.42	1.48	1.45
38	19-B	0.32	0.65	1.42	1.48	1.52
39	20-B	0.33	1.63	1.42	1.48	1.53
40	21-B	0.68	0.33	1.99	1.73	1.55
41	1-A	0.51	0.13	0.00	0.64	1.30
42	2-A	0.54	0.00	0.00	0.54	1.38
43	3-A	0.53	0.15	0.00	0.68	1.24
44	4-A	0.50	0.13	0.20	0.83	1.25
45	5-A	0.50	0.13	0.10	0.73	1.34
46	6-A	0.69	0.13	0.05	0.87	0.95
47	7-A	1.13	0.14	0.17	1.44	0.97

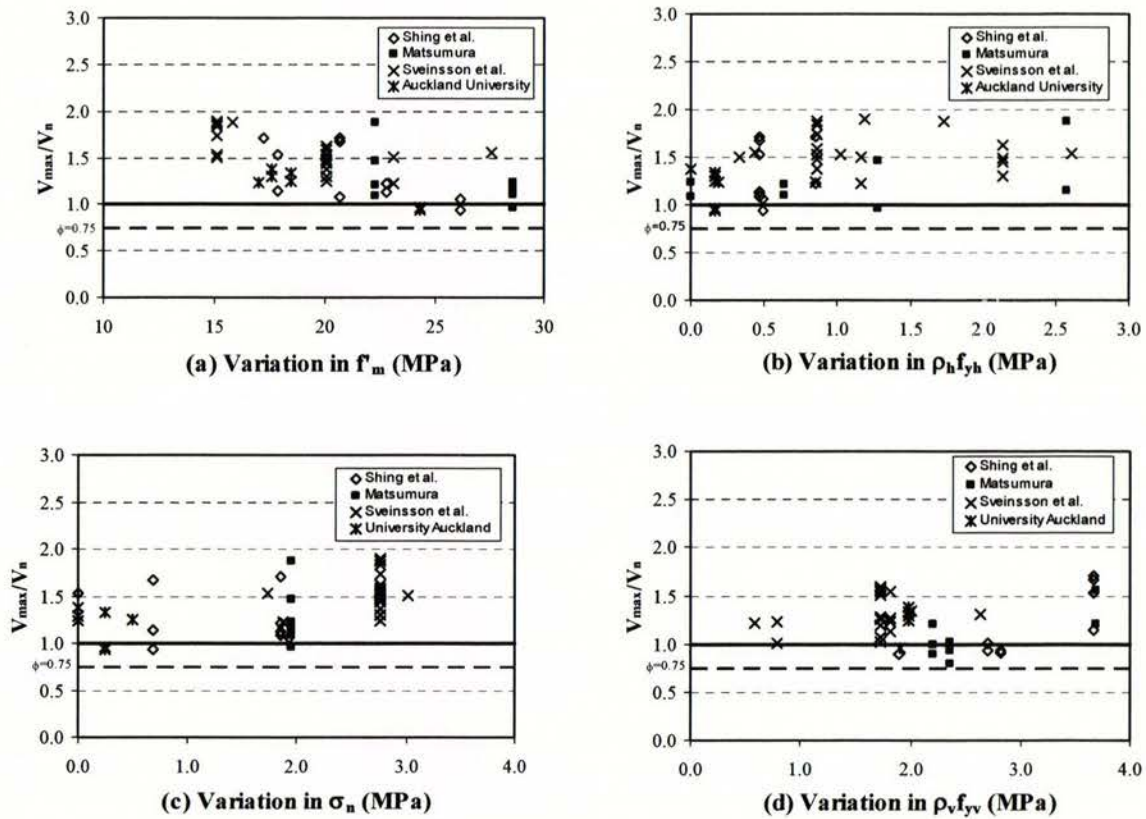


Figure 7.3 Experimental results versus prediction by Equation 7-4.

From the comparison results presented in Table 7.1 and Figure 7.3, it is reasonable to suggest that shear prediction using Equation 7-4 produces satisfactory accuracy for fully grout-filled masonry walls.

7.2.2 Partially Grouted Walls

The experimental data sets used in this part of the study are limited to those of partially grout-filled masonry walls. As reported earlier, difficulty arose when trying to obtain sufficient information of the test data. Consequently, only 20 specimens are included in this part of the study. Table 7.2 lists the actual shear strength (v_{max}) of the 20 specimens, and the predicted strength (v_m , v_s , v_p and v_n) obtained from Equation 7-4. The μ_{vmax} values for each specimen are included in Table E.2.

Table 7.2 Shear prediction of partially grouted masonry walls using Equation 7-4

Specimen no.	Specimen label	MPa				V_{max}/V_n
		V_m	V_s	V_p	V_n	
1	7-MP	0.97	0.00	0.00	0.97	0.79
2	9-MP	0.75	0.19	0.00	0.94	1.14
3	10-MP	0.99	0.37	0.00	1.34	0.87
4	11-MP	0.99	0.55	0.00	1.34	1.09
5	12-MP	1.27	0.20	0.44	1.71	1.04
6	13-MP	1.27	0.20	0.88	1.71	1.08
7	14-MP	1.27	0.20	1.31	1.71	1.36
8	19-MP	1.50	0.00	0.88	1.71	1.21
9	21-MP	1.50	0.39	0.88	1.71	1.28
10	22-MP	0.98	0.59	0.88	1.71	1.41
11	29-MP	0.69	0.31	0.00	1.00	2.15
12	30-MP	1.39	0.31	0.00	1.70	1.18
13	1-BP	0.76	0.14	0.70	1.18	1.35
14	2-BP	0.85	0.00	0.67	1.19	1.28
15	3-BP	0.85	0.27	0.72	1.19	1.36
16	4-BP	0.92	0.18	1.39	1.43	1.96
17	5-BP	1.04	0.00	1.32	1.47	1.32
18	6-BP	0.96	0.37	1.38	1.43	0.96
19	1-AP	0.79	0.00	0.00	0.79	1.52
20	2-AP	0.73	0.00	0.00	0.73	1.08

Normalised plots (experimentally obtained shear stress, v_{max} , versus predicted shear stress, v_n) are presented in Figure 7.4 to investigate the accuracy of Equation 7-4 in predicting the shear strength of partially grout-filled masonry walls. It shows predicted strength varies from -21% to +115% of the measured strength (i.e. $0.79 \leq v_{max}/v_n \leq 2.15$). Equation 7-4 over-predicts the shear strength of 3 specimens, of which 1 specimen has $v_{max}/v_n < 0.8$. This comparison shows a standard deviation 0.33 and a mean v_{max}/v_n of 1.27 for the 20 specimens. Consequently, it is shown here that shear prediction of partially grouted masonry walls using Equation 7-4 produced similar results to that of NEHPR (refer to section 6.4.2).

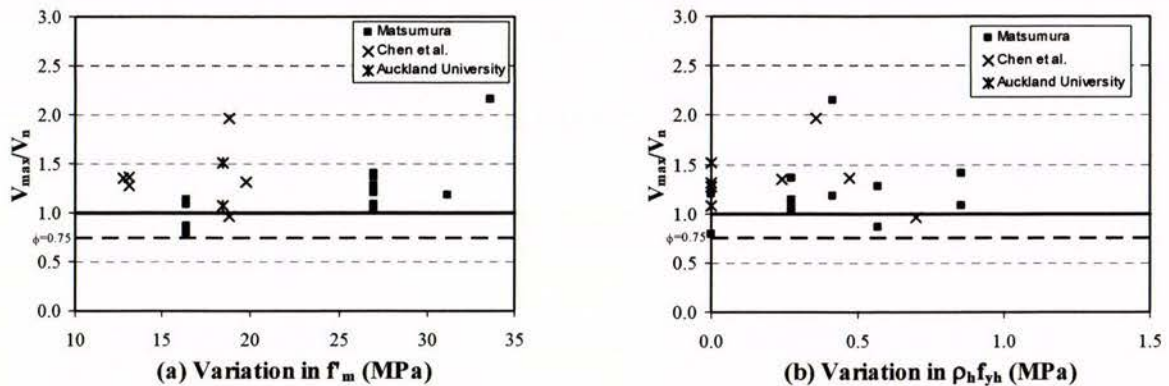


Figure 7.4 Experimental results of partially grouted walls versus prediction by Equation 7-4.

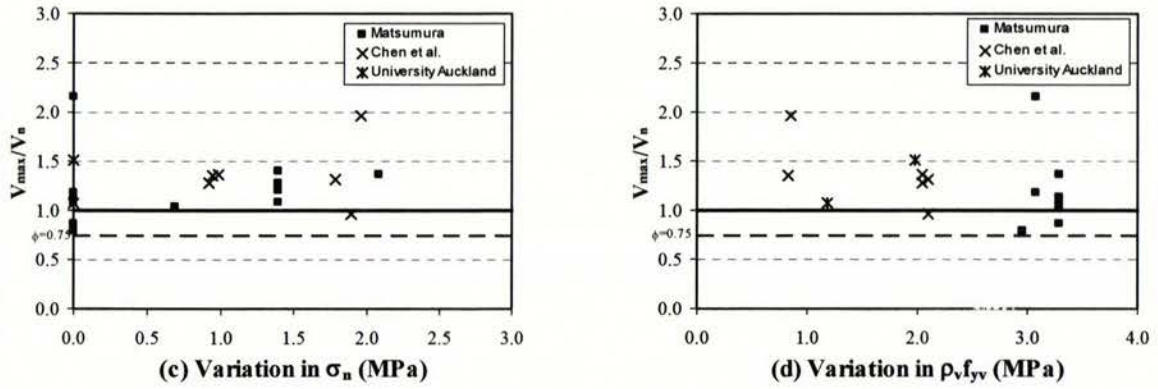


Figure 7.4 Experimental results of partially grouted walls vs prediction by Equation 7-4 (continued).

The following conclusion can be drawn on the basis of the maximum strength comparisons presented in Sections 7.2 and 7.3. It has been shown that Equation 7-4 provides significantly improved masonry shear prediction compared to the NZS4230:1990 shear expression. In addition, it has been successfully shown that shear prediction using Equation 7-4 produced similar results as the NEHPR. Consequently, it is recommended to replace the shear expression in the current New Zealand masonry standard (NZS4230:1990) by Equation 7-4.

Chapter 8

Conclusion

This chapter is comprised of two sections, with section 8.1 summarising conclusions from this research study and section 8.2 listing recommendations for future research on topics associated with this report.

8.1 Summary of Findings

Conclusions reported herein are separated into two sections. Sections 8.1.1 summarises the findings from the experimental results reported in Chapters 4 and 5, and section 8.1.2 presents findings obtained from the comparison of shear equations reported in Chapters 6 and 7.

8.1.1 Experimental Results

It is concluded that valuable information about masonry shear strength was captured in the testing of full scale masonry walls reported in Chapter 4. The test matrix allowed for meaningful comparison of test specimens, and provided important information for the parameters being investigated in this study.

As mentioned immediately above, the following conclusions are based on the experimental results reported in Chapter 4:

1. The shear resistance of reinforced masonry walls is the result of complex mechanisms, such as tension of horizontal reinforcement, dowel action of vertical reinforcement, as well as aggregate interlocking along diagonal cracks. However, due to the complexity of these mechanisms, no effective theoretical models have yet been proposed to predict the shear strength of a masonry wall panel. Hence, the nominal

shear strength of reinforced masonry walls is evaluated as sum of contributions from masonry, shear reinforcement and applied axial compression load during practical calculation.

2. Horizontal reinforcement is effective in providing additional shear resistance to masonry walls. However, a change in the amount of horizontal reinforcement results in relatively little change in the maximum shear strength of the walls. Furthermore, the amount of horizontal reinforcement does not appear to influence the rate at which the wall stiffness degrades.
3. The ductility capacity of a masonry shear wall is improved by evenly distributing the horizontal reinforcement up the height of the wall.
4. Axial compression load has a significant influence on the in-plane shear performance of masonry shear walls, mainly because it suppresses the tensile field in a material inherently weak in tension. As the axial compression load increases, so does the ability of masonry walls to offer shear resistance. It was observed from experimental study that an increase in axial compression stress delays the initiation of cracking. It was shown in the experimental study that the post-cracking deformation capacity of a masonry wall is significantly reduced with increasing axial compression stress. This is because the failure type becomes more brittle as the axial compressive stress increases.
5. Masonry shear strength decreases inversely in relation to the h_e/l_w ratio.
6. The stiffness of a masonry wall increases when the axial compression stress level increases. However, the stiffness degradation rate appears to be independent of the axial compression stress.
7. The effect of grouting is insignificant as far as the net shear stress is concerned. It was shown in experimental results that the post-cracking deformation capacity is reduced for walls with more grouting. The stiffness degradation rate is independent of the type of grouting.

8.1.2 Masonry Shear Equation

The suitability of shear equations in predicting the maximum in-plane shear strength of masonry walls is reported in Chapters 6 and 7. The following conclusions can be drawn:

1. The New Zealand and Australian masonry standards, and UBC are conservative in their treatment of masonry shear strength.
2. The predictive equations proposed by Matsumura and Shing et al. are effective in predicting the shear strength of fully grouted masonry walls but these two equations are unsuccessful in capturing the shear strength of partially grouted masonry walls.
3. Of the seven existing equations examined in Chapter 6, the NEHPR shear expression provides the closest shear prediction for both the fully and partially grouted masonry walls. However, the NEHPR shear expression does not address masonry shear strength within the potential plastic hinge zone. Also, the use of $0.5\rho_h f_{yh}$ in its v_s term is contrary to well established split beam theory. Consequently, a new shear equation was developed and presented in Chapter 7.
4. It was successfully shown that the newly proposed shear equation provided significant improved masonry shear prediction when compared to the NZS4230:1990 shear expression. It was also shown that shear prediction using the newly proposed equation produced results similar to the NEHPR expression. Consequently, it is recommended to implement this newly proposed shear equation into the future New Zealand masonry design standard.

8.2 Recommendation for Future Research

In order to further the rationalisations that could be made to the shear strength provisions in the New Zealand masonry design standard, the following areas of research could be undertaken:

1. The study reported in this report has concentrated on wall with simple geometry. Therefore, further structural testing may be necessary to address the effect of complex geometries, such as Tee-sections and corners, and wall with penetrations for doors and windows.
2. In this study, only reinforced masonry walls were considered. In lieu of the development of prestressed masonry, it is deemed appropriate to investigate the shear strength capacity of unreinforced prestressed masonry walls.
3. A study of the suitability of the developed expression to predict the out-of-plane shear strength is required.

Chapter 9

References

Anderson, D. L., and Priestley, M. J. N. (1992), "In Plane Shear Strength of Masonry Walls", Proceedings of the 6th Canadian Masonry Symposium, Saskatoon, Saskatchewan, pp. 223-234.

AS 3700—1998, "Masonry Structures", Standards Association of Australia, Homebush, NSW, Australia.

Beck, J. K., Curtin, W. G., and Shaw, G. (1988), "Design of Reinforced and Prestressed Masonry", Thomas Telford, London.

Brammer, D. R. (1995), "The Lateral Force-Deflection Behaviour of Nominally Reinforced Masonry Walls", ME Thesis, Department of Civil and Resource Engineering, University of Auckland, New Zealand.

Brunner, J. D., and Shing, P. B. (1996), "Shear Strength of Reinforced Masonry Walls", TMS Journal, Vol. 14, No. 1, pp. 65-77.

BSSC (1998), "NEHRP Recommended Provisions for Seismic Regulations for New Buildings and other Structures", Building Seismic Safety Council for the Federal Emergency Management Agency, Washington, D.C, Report No. FEMA-302.

Cavalheiro, O. P., and Pedroso, G. M. (2000), "Experimental Data on Hollow Block Prisms Using Direct Shear Test", Proceedings of the 12th International Brick/Block Masonry Conference, Madrid, Spain, pp. 433-440.

Chen, Shi-Wen J., Hidalgo, P. A., Mayes, R. L., Clough, R. W., and McNiven, H. D. (1978), "Cyclic Loading Tests of Masonry Single Piers, Volume 2-Height to Width Ratio of 1", Report No. UCB/EERC-78/28, Earthquake Engineering Research Centre, University of California, Berkeley, CA.

Christie, N. J. R., and Isaac, H. P. (1976), "Australian Concrete Masonry—Design and Construction Volume 1", Concrete Masonry Association of Australia, Sydney, Australia.

Crisafulli, F. J., Carr, A. J., and Park, R. (1995), "Shear Strength of Unreinforced Masonry Panels", Proceedings of the Pacific Conference on Earthquake Engineering, Vol. 3, Melbourne, Australia, pp. 77-86.

Davidson, B. J. (1996), "In-Plane Cyclic Loading of Nominally Reinforced Masonry Walls with Openings", New Zealand Concrete Society Conference, Wairakei, New Zealand, pp. 120-129.

Davidson, B. J., and Brammer, D. R. (1995), "Cyclic Performance of Nominally Reinforced Masonry Walls", Technical Conference of NZSEE, New Plymouth, New Zealand, pp. 120-129.

Hansen, K. F., Nykanen, E., and Gottfredsen, F. R. (1998), "Shear Behaviour of Bed Joints at Different Levels of Precompression", Danish Building Research Institute-VTT Building Research, Vol. 12, No. 2, pp. 70-78.

Hendry, A. W. (1991), "Reinforced and Prestressed Masonry", Longman Scientific & Technical, England.

Hidalgo, P. A., Mayes, R. L., McNiven, H. D., and Clough, R.W. (1978), "Cyclic Loading Tests of Masonry Single Piers", Volume 1, Report No. UCB/EERC-78/27, Earthquake Engineering Research Centre, University of California, Berkeley, CA.

Hidalgo, P. A., Mayes, R. L., McNiven, H. D., and Clough, R.W. (1979), "Cyclic Loading Tests of Masonry Single Piers", Volume 3, Report No. UCB/EERC-79/12, Earthquake Engineering Research Centre, University of California, Berkeley, CA.

Hiraishi, H. (1985), "Flexural Behaviour of Reinforced Masonry Walls", First Meeting of the U.S.-Japan Joint Technical Coordinating Committee on Masonry Research, Tokyo, Japan.

Hiraishi, H. (1984), "Evaluation of Shear and Flexural Deformation of Flexural Type Shear Walls", Bulletin NZSEE, Vol. 17, No. 2, pp. 135-144.

Kaminosono, T., Teshigowara, M., Hiraishi, H., Fujisawa, M., and Nakaoka, A. (1988), "Experimental Study on Seismic Performance of Reinforced Masonry Walls", Proceedings of the 9th World Conference on Earthquake Engineering, Tokyo-Kyoto, Japan, pp. 109-114.

Larbi, A., and Harris, H. (1990), " Seismic Behaviour of Reinforced Block Masonry Shear Walls using 1/3 Scale Direct Models", Proceedings of the 5th North America Masonry Conference, University of Illinois, Urbana-Champaign, pp. 321-332.

Laursen, P. T., and Ingham, J. M. (2000a), "Cyclic In-Plane Structural Testing of Prestressed Concrete Masonry Walls. Phase 1: Simple Wall Configurations. Volume A: Evaluation of Wall Structural Performance", School of Engineering Report No. 599, University of Auckland.

Laursen, P. T., and Ingham, J. M. (2000b), “Cyclic In-Plane Structural Testing of Prestressed Concrete Masonry Walls. Phase 1: Simple Wall Configurations. Volume B: Data Resource”, School of Engineering Report No. 600, University of Auckland.

Mann, W. and Muller, H. (1982), “Failure of Shear-Stressed Masonry-An Enlarged Theory, Tests and Application to Shear Walls”, Proceedings of the British Ceramic Society, pp. 223-235.

Matsumura, A. (1985), “Effectiveness of Shear Reinforcement in Concrete Masonry Walls”, First Joint Technical Coordinating Committee on Masonry Research-U.S.-Japan Coordinated Earthquake Research Programme, Tokyo, Japan.

Matsumura, A. (1987), “Shear Strength of Reinforced Hollow Unit Masonry Walls”, Proceedings of the 4th North America Masonry Conference, Paper No. 50, Los Angeles, CA, pp. 50-1—50-16.

Matsumura, A. (1988), “Shear Strength of Reinforced Masonry Walls”, Proceedings of the 9th World Conference on Earthquake Engineering, Vol. 7, Tokyo, Japan, pp. 121-126.

Matsumura, A. (1990), “Planar Shear Loading Test on Reinforced Fully Grouted Hollow Clay Masonry Walls”, Proceedings of the 5th North America Masonry Conference, University of Illinois, Urbana-Champaign, pp. 347-356.

Mayes, R. L., Omote, Y., and Clough, R. W. (1976a), “Cyclic Shear Tests on Masonry Piers, Volume 1: Test Results”, Report No. UCB/EERC-76/8, Earthquake Engineering Research Centre, University of California, Berkeley, CA.

Mayes, R. L., Omote, Y., and Clough, R. W. (1976b), "Cyclic Shear Tests of Masonry Piers, Volume 2, No. EERC 76-16, Earthquake Engineering Research Centre, University of California, Berkeley, CA.

NZS 4230:1990, "Code of Practice for The Design of Masonry Structures", Standards Association of New Zealand, Wellington.

NZS 4230:Part2:1990, "Commentary on the Design of Masonry Structures", Standards Association of New Zealand, Wellington.

Okamoto, S., Yamazaki, Y., Kaminosono, T., Teshigawara, M., and Hirashi, H. (1987), "Seismic Capacity of Reinforced Masonry Walls and Beams", Proceedings of the 18th Joint Meeting of the U.S.-Japan Cooperative Program in Natural Resource Panel on Wind and Seismic Effects, NBSIR 87-3540, National Institute of Standards and Technology, Gaithersburg, pp. 307-319.

Page, A. W. (1989), "A Parameter Study of The Behaviour of Masonry Shear Walls", Proceedings of the 5th Canadian Masonry Symposium, Vancouver, pp. 341-352.

Park, R. (1986), "Design of Building Structures of Limited Ductility", Bulletin NZSEE, Vol. 19, No. 4, pp. 285-338.

Park, R. (1989), "Evaluation of Ductility of Structures and Structural Assemblages for Laboratory Testing", Bulletin NZSEE, Vol. 22, No. 3, pp. 155-166.

Paulay, T. and Loeber, P. J. (1974), "Shear Transfer by Aggregate Interlock", Shear in Reinforced Concrete, Volume 1, American Concrete Institute, Detroit, pp. 1-15.

Paulay, T., and Priestley, M. J. N. (1992), "Seismic Design of Reinforced Concrete and Masonry Buildings", John Wiley and Sons, U.S.

Priestley, M. J. N. (1976), "Cyclic Testing of Heavily Reinforced Concrete Masonry Shear Walls", Department of Civil Engineering, University of Canterbury, New Zealand, Research Report 76-12.

Priestley, M. J. N. (1977), "Seismic Resistance of Reinforced Concrete Masonry Shear Walls with High Steel Percentages", Bulletin NZSEE, Vol. 10, No. 1, pp. 1-16.

Priestley, M. J. N. (1980), "Seismic Design of Masonry Buildings-Background to the Draft Masonry Design Code DZ4210", Bulletin NZSEE, Vol. 13, No. 4, pp. 329-346.

Priestley, M. J. N., and Elder, D.McG. (1982), "Cyclic Loading Tests of Slender Concrete Masonry Shear Walls", Bulletin NZSEE, Vol. 15, No. 1, pp. 3-21.

Priestley, M. J. N., Seible, S., and Calvi, G. M. (1996), "Seismic Design and Retrofit of Bridges", John Wiley and Sons, New York.

Priestley, M. J. N., Verma, R., and Xiao, Y. (1994), "Seismic Shear Strength of Reinforced Concrete Column", Journal of Structural Engineering, Vol. 120, No. 8.

Schultz, A. E. (1996), "Seismic Performance of Partially-Grouted Masonry Shear Walls", Proceedings of the 11th World Conference on Earthquake Engineering, CD-Rom Paper No. 1221, Acapulco, Mexico, pp. 246-256.

Scott, E. F. (1999), "A Report of The Relief Organisation in Hastings Arising out of the [Magnitude 7.8] Earthquake in Hawke's Bay [New Zealand] on February 3, 1931", Bulletin NZSEE, Vol. 32, No. 4, pp. 246-256.

Shing, P. B., Brunner, J. D., and Lotfi, H. R. (1993), "Evaluation of Shear Strength of Reinforced Masonry Walls", TMS Journal, Vol. 12, No. 1, pp. 65-77.

Shing, P. B., Klamerua, E., Spaeh, H., and Noland, J. L. (1988), "Seismic Performance of Reinforced Masonry Shear Walls", Proceedings of the 9th World Conference on Earthquake Engineering, Vol. 7, Tokyo, Japan, pp. 103-108.

Shing, P. B., Noland, J. L., Klamerus, E., and Schuller, M. (1989), "Inelastic Behaviour of Concrete Masonry Shear Walls", ASCE Journal of Structural Engineering, Vol. 15, pp. 2204-2225.

Shing, P. B., Noland, J. L., Spaech, H., Klamerus, E., and Schuller, M. (1991), "Response of Single-Storey Reinforced Masonry Shear Walls to In-Plane Lateral Loads", TCCMAR Report 3.1(a)-2.

Shing, P. B., Schuller, M., and Hoskere, V. S. (1990a), "In-Plane Resistance of Reinforced Masonry Shear Walls", ASCE Journal of Structural Engineering, Vol. 116, No. 3, pp. 619-640.

Shing, P. B., Schuller, M., and Hoskere, V. S. (1990b), "Strength and Ductility of Reinforced Masonry Shear Walls", Proceedings of the 5th North America Masonry Conference, University of Illinois, Urbana-Champaign, pp. 309-320.

Singh, S. S., Cooke, N., and Bull, D. K. (1999), "Out-of-Plane Performance of a Partially Filled Reinforced Concrete Masonry Wall with Ribraft™ Floor", *Bulletin NZSEE*, Vol. 32, No. 2, pp. 90-101.

Sucuoglu, H., and McNiven, H. D. (1991), "Seismic Shear Capacity of Reinforced Masonry Piers", *ASCE Journal of Structural Engineering*, Vol. 117, No. 7, pp. 2166-2186.

Sveinsson, B. I., Mayes, R. L., and McNiven, H. D. (1985), "Cyclic Loading of Masonry Single Piers", *Volume 4, Report No. UCB/EERC-85/15*, Earthquake Engineering Research Centre, University of California, Berkeley.

Tomažević, M. (1999), "Earthquake-Resistance Design of Masonry Buildings", Imperial College Press, London.

Tomažević, M., Lutman, M., Velechovsky, T., and Zarnic, R. (1986), "Seismic Resistance of Reinforced Masonry Walls, Volume 1: Test Results, Part One", Report ZRMK/IKPI-86/04, Institute for Testing and Research in Material and Structures, Ljubljana, Yugoslavia.

Tomažević, M., Lutman, M., Velechovsky, T., and Zarnic, R. (1987), "Seismic Resistance of Reinforced Masonry Walls, Volume 2: Test Results, Part two", Report ZRMK/IKPI-87/06, Institute for Testing and Research in Material and Structures, Ljubljana, Yugoslavia.

Tomažević, M., Lutman, M. (1988), "Seismic Resistance of Reinforced Masonry Walls", *Proceedings of the 9th World Conference on Earthquake Engineering*, Vol. 6, Tokyo, Japan, pp97-102.

Voon, K. C., and Ingham, J. M. (2001), "Towards Suitable Shear Strength Provisions for inclusion in the New Zealand Masonry Design Standard", *Proceedings of the 6th Australasian Masonry Conference*, Adelaide, South Australia, pp. 393-402.

Woodward, K., and Rankin, F. (1985a), "Influence of Block and Mortar Strength on Shear Resistance of Concrete Block Masonry Walls", NBSIR 85-3143, National Bureau of Standards, Gaithersburg, MD.

Woodward, K., and Rankin, F. (1985b), "Influence of Aspect Ratio on Shear Resistance of Concrete Block Masonry Walls", NBSIR 84-2993, National Bureau of Standards, Gaithersburg, MD.

Yancey, C. W., Fattal, S. G., and Dikkers, R. D. (1991), "Review of Research Literature on Masonry Shear Walls", NISTIR 4512, National Bureau of Standards, Gaithersburg, MD.

Yokel, F. Y., and Fattal, S. G. (1975), "A Failure Hypothesis for Masonry Shear Walls", NBSIR 75-703, National Bureau of Standards, Gaithersburg, MD.

Yokel, F. Y., and Fattal, S. G. (1976), "Failure Hypothesis for Masonry Shear Walls", ASCE Journal of Structural Engineering, Vol. 102, pp. 515-531.

Zhang, X. D. (1998), "Out-of-Plane Performance of Partially Grouted Reinforced Concrete Masonry Walls under Simulated Seismic Loading", ME Thesis, University of Canterbury.

Appendix A-Experimental Results

This section briefly reports the experimental results of the two reinforced concrete masonry walls of Series A. These two walls served as a trial run to investigate the appropriateness of the test set-up and loading procedure presented in section A.1. The results presented in section A.4 were not considered when formulating the conclusions presented in Chapter 8 as both walls reported here failed to fully develop their wall strengths.

A.1 Test Set-up

The test set-up adopted for the testing of the two walls in Series A is shown in Figure A.1, with the reinforcement details shown in Figure A.2. The steel channel section was attached to the masonry walls by five D20 cast-in bars, spaced at 400 mm c/c.

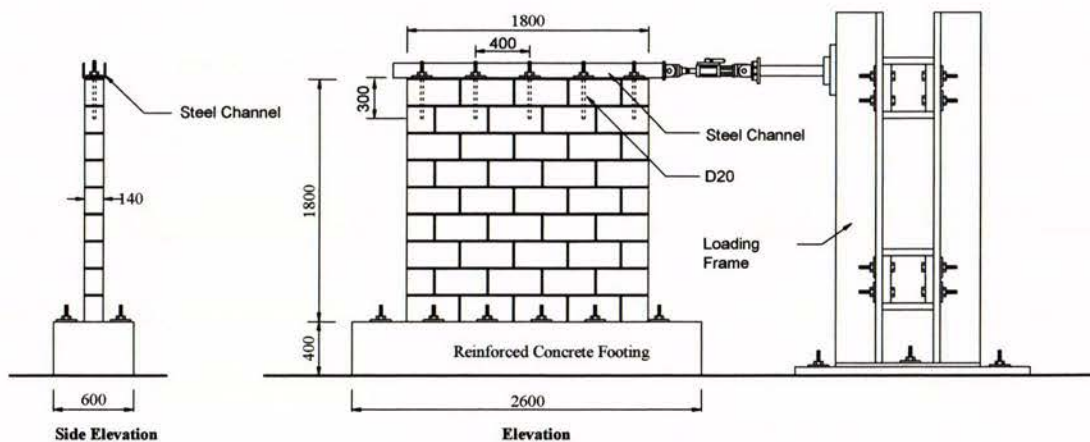


Figure A.1 Series A, test set-up.

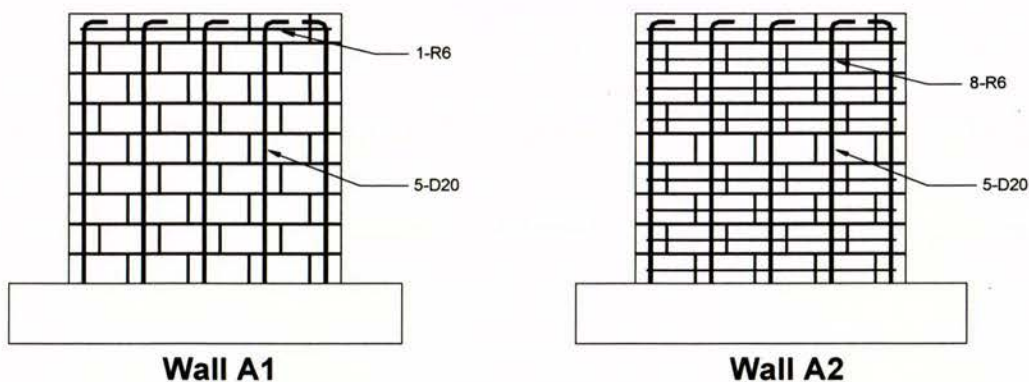


Figure A.2 Reinforcement details of masonry walls in Series A.

The two walls were constructed on the re-usable reinforced concrete footing shown in Figure 3.2. The concrete base had DH32 starter bars spaced at 400 mm centres that were drilled and tapped to accommodate D20 vertical wall reinforcement. The concrete base was stressed down to the laboratory floor with high strength steel rods so that sufficient shear friction was provided to eliminate any slip between the base and the floor. Before wall construction, the vertical reinforcement bars were first tapped at the straight ends, then threaded into the pre-tapped DH32 starters that protruded from the reinforced concrete footing.

A.2 Testing Procedure

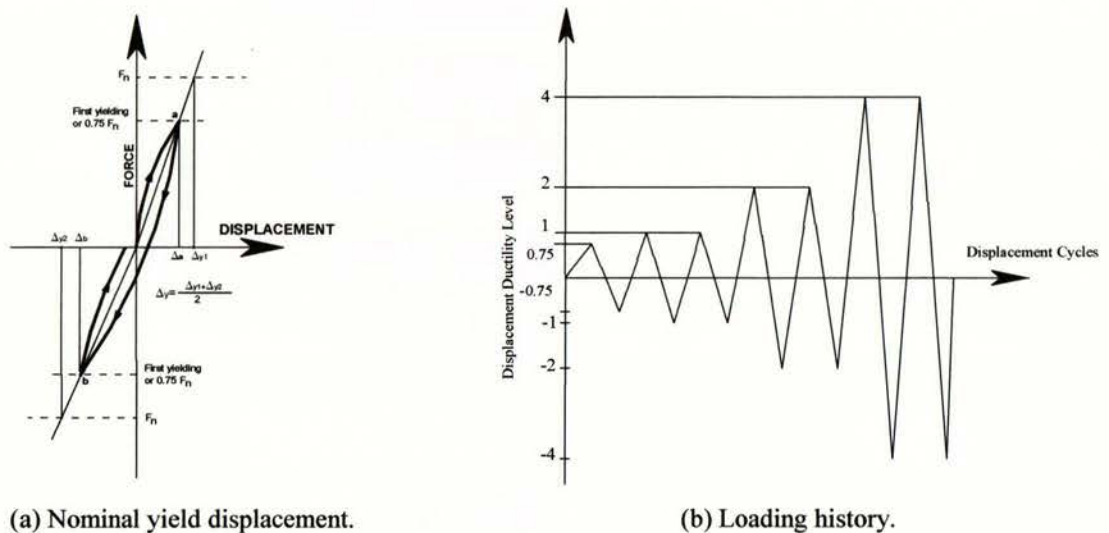


Figure A.3 Test procedure.

The two masonry walls in Series A were tested using a procedure similar to that outlined by Park (1989). This procedure consists of determining the nominal yield displacement Δ_y by measuring the displacement Δ_{y1} and Δ_{y2} . The steps in the procedure are:

1. Apply a lateral force equal to $\frac{3}{4}$ of F_n in one direction and record the displacement of the wall Δ_a .
2. Unload the wall and repeat step (1) in the reverse direction to obtain Δ_b . Extrapolate straight lines from the origin of the force/displacement plot through the points $(\frac{3}{4} F_n, \Delta_a)$ and $(-\frac{3}{4} F_n, \Delta_b)$ and find their intersection with the nominal lateral force. This step is illustrated in Figure A.3(a). The displacement Δ at a ductility value of μ is defined as $\mu * \Delta_y$.

3. Apply lateral force slowly in a sequence so that the top of the wall is displaced to the ductility levels shown in Figure A.3(b).

A.3 Material Properties

The properties (average strength) of the respective materials used in both wall constructions are as follows:

Yield strength of vertical reinforcing steels, f_{yv}	= 318 MPa
Yield strength of R6 horizontal reinforcing steel, f_{yh}	= 325 MPa
Masonry compressive strength, f'_m	= 17.2 MPa
Compressive grout strength, f'_g	= 16.1 MPa
Compressive mortar strength, f'_j	= 9.3 MPa

The nominal flexural and shear strength of the two tested walls (A1 and A2) was calculated before experimental testing was conducted. The wall nominal flexural strength was calculated using Equation 2-6, while the shear strength of the two masonry walls was calculated using shear provisions adopted by NEHPR and NZS 4230:1990 respectively.

A.4 Experimental Results

A.4.1 Wall A1

The nominal flexural strength, F_n , and the wall shear strength, V_n , were calculated for a fully grouted concrete masonry wall, with the results presented in Table A.1.

Table A.1 Wall A1, strength prediction

F_n (kN)	V_n (kN)	
	NZS 4230	NEHPR
229	162	231

The masonry wall failed prematurely due to rapid deterioration of the bond beam. During the early stages of testing (less than $\pm \frac{3}{4}F_n$), most structural damage concentrated at the bond beam, with some minor flexural and diagonal shear cracks being identified. However, the wall failed at the end of the first ductility 1 pull cycle (about -3.6 mm) when significant damage occurred at the bond beam (see Figure A.5), accompanied by the formation of three diagonal cracks. Maximum push and pull direction strengths of +162 kN/-184 kN were recorded.

The force-displacement (F-D) plot is presented in Figure A.4. As can be seen in the figure, abrupt strength degradation and significant increase in lateral displacement took place in the pull direction after significant damage occurred at the bond beam.

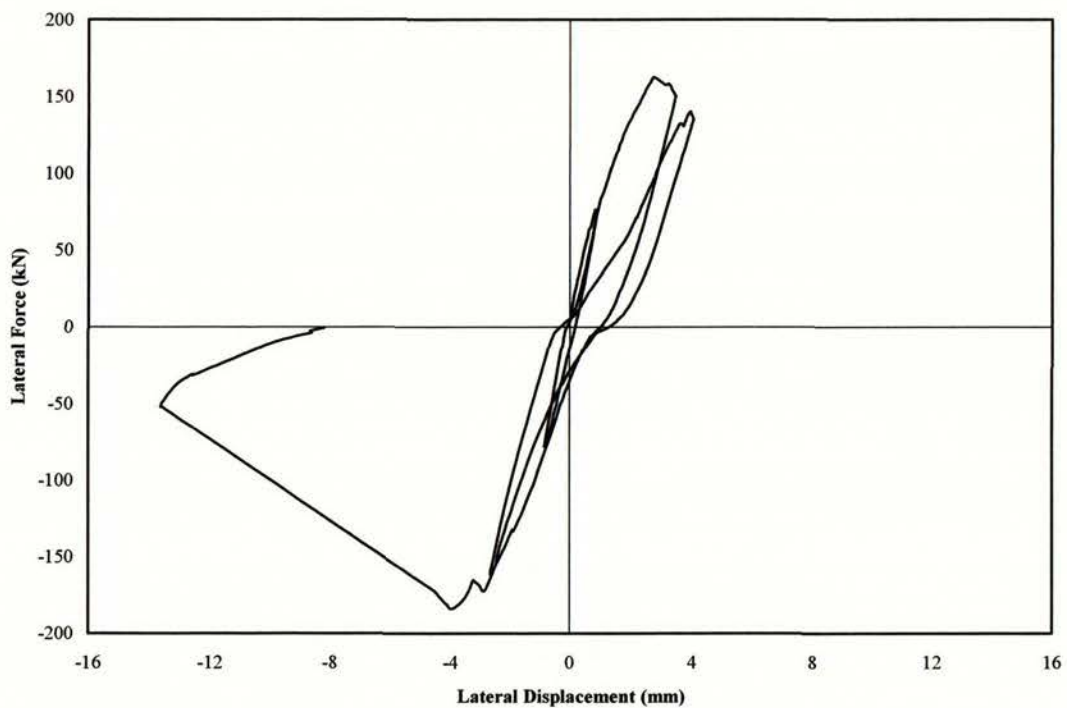


Figure A.4 Force-displacement behaviour for Wall A1.

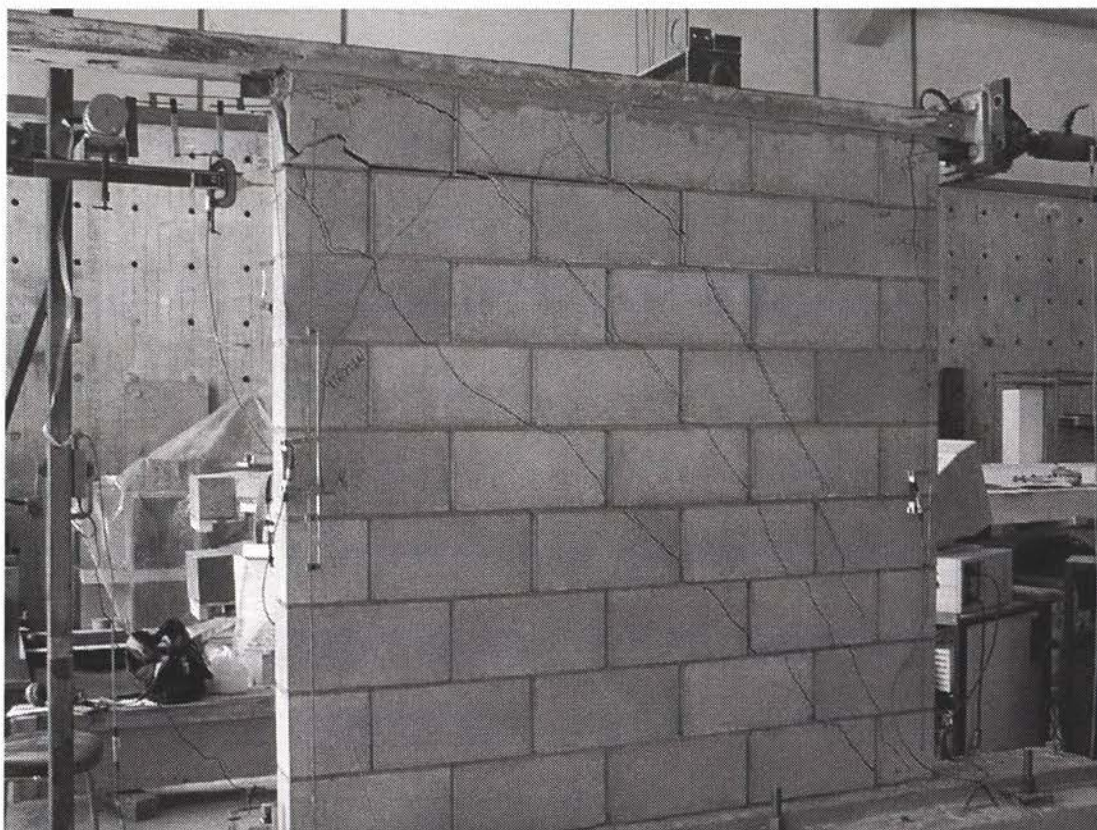


Figure A.5 Structural damage at the bond beam accompanied by diagonal cracks after ductility 1 displacement.

A.4.2 Wall A2

The nominal flexural strength, F_n , and the wall shear strength, V_n , were calculated for a fully grouted concrete masonry wall, with the results presented in Table A.2.

Table A.2 Wall A2, strength prediction

F_n (kN)	V_n (kN)	
	NZS4230	NEHPR
229	104	195

Similar to Wall A1, Wall A2 suffered premature failure caused by inability of the bond beam to properly transfer shear stress to the entire masonry wall. The force-displacement (F-D) plot presented in Figure A.6 shows that rapid loss of strength took place after degradation of the bond beam (see Figure A.7) at ductility 1 displacement (about 5.5 mm). The maximum strengths of +162 kN and -148 kN were measured during the first cycle to ductility ± 1 displacement.

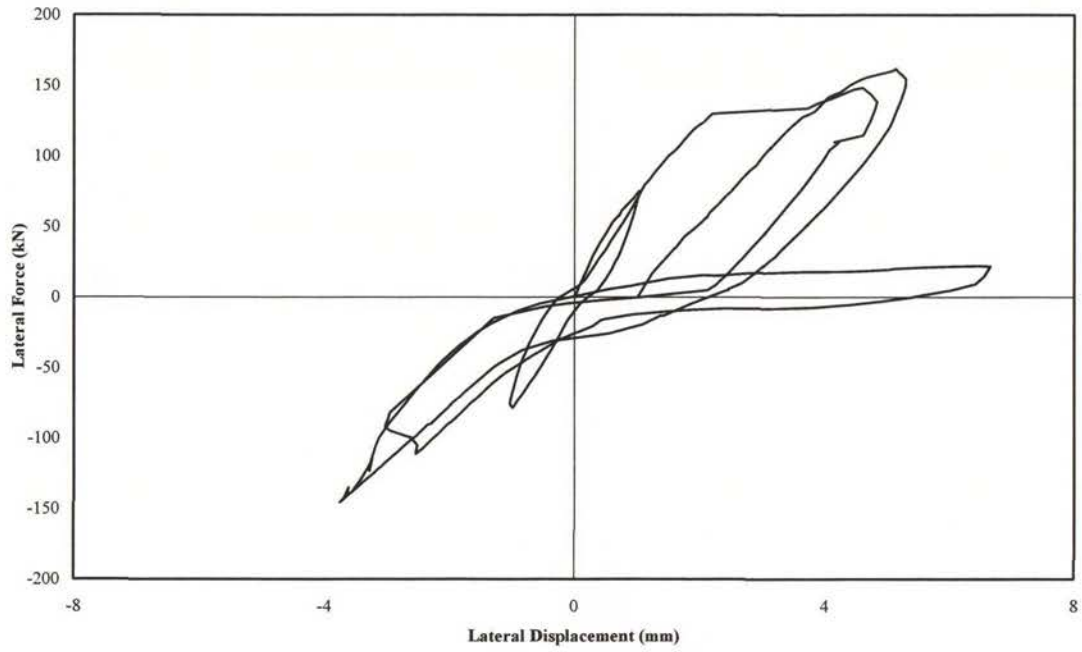


Figure A.6 Force-displacement behaviour for Wall A2.



Figure A.7 Structural damage at bond beam causing significant steel channel-masonry wall slippage.

A.5 Conclusion

Following the testing of Walls A1 and A2, it was concluded that inadequate strength of the bond beam had prevented the behaviour of the two masonry walls to be properly evaluated. It was therefore concluded that there was a need to modify the test set-up shown in Figure A.1 for future test.

Appendix B

Experimental Results-Series B

Appendix B presents experimental results for the eight reinforced concrete masonry walls of Series B, tested at the University of Auckland. These results played a significant role in formulating the conclusions of this report.

All eight concrete masonry walls in Series B, were constructed of 15 series CMUs (nominal thickness of 15 cm), which resulted in an effective wall thickness of 140 mm for a fully grout-filled masonry wall and about 63 mm for a partially grout-filled wall. All eight masonry walls had the same dimensions: length of 1.8 m and height of 1.8 m. The parameters investigated in this part of the study included: (1) the influence of horizontal shear reinforcement towards masonry shear strength, (2) the influence of shear reinforcement on wall behaviour, (3) the effect of two types of grouting: full grouting and partial grouting, and (4) the effect of axial compression load in enhancing masonry shear strength.

For information about wall construction, test set-up, testing procedure and data reduction please refer to Chapter 3. This report defines displacement in the push direction as positive while displacement in the pull direction as negative.

B.1 Wall 1

This section describes the laboratory test of Wall 1, which served as a trial run of the test set-up described in section 3.2. The reinforcement details are shown in Figure B.1.1, with the shear reinforcement consisting of R6 spaced vertically at 400 mm c/c. The nominal flexural strength, F_n , and the wall shear strength, V_n , were calculated according to section 3.7 for a fully grouted concrete masonry wall and the results are presented in Table B.1.1.

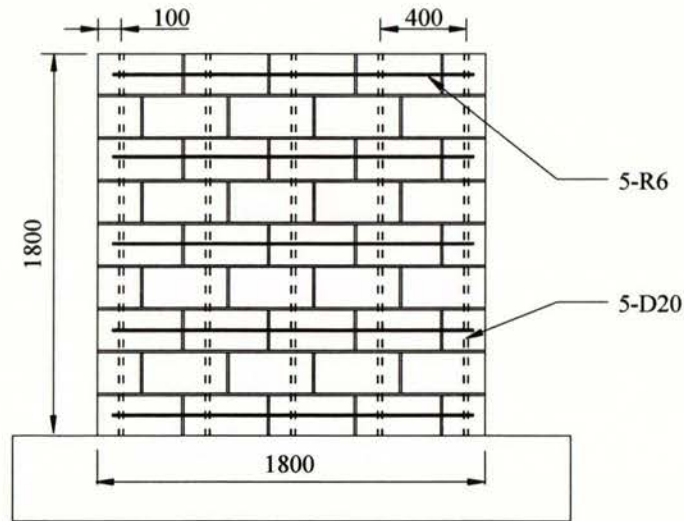


Figure B.1.1 Wall 1 reinforcement details.

Table B.1.1 Wall strength predictions

Masonry strength	Nom. Flexural strength	Masonry shear strength V_n	
f'_m	F_n	NZS4230	NEHPR
17.6	229	142	219
MPa	kN	kN	kN

B.1.1 Pre-test

The masonry wall was tested on the 53rd days after construction. Instrumentation was attached to the wall according to section 3.5.1. Prior to wall testing the wall was inspected, with no cracks or structural defects being identified.

B.1.2 Testing

0.5 mm push, 1st cycle

No clear evidence of cracking. An applied force of 49 kN was recorded with corresponding displacement of 0.49 mm.

0.5 mm pull, 1st cycle

A maximum strength of -60 kN was recorded at the target displacement. No cracking was noted.

0.5 mm push, 2nd cycle

On the second cycle to this displacement, the wall developed a maximum strength of 49 kN. The wall responded similar to the previous push cycle and no cracking was identified.

0.5 mm pull, 2nd cycle

The wall developed a maximum strength of –54 kN for this displacement cycle. The wall response mirrored that of the previous pull cycle and no cracking was identified.

1.0 mm push, 1st cycle

A maximum strength of 72 kN was measured at the conclusion of this displacement cycle. An uplift of 0.28 mm was measured at the tension toe, creating a base crack approximately 0.5 m long.

1.0 mm pull, 1st cycle

A single hairline horizontal crack was identified along a mortar joint at wall mid-height on the tension side. A maximum strength of –80.5 kN was recorded. No base crack was identified.

According to the procedure outlined in section 3.8, the measured lateral force for the two directions of loading resulted in an average yield displacement of:

$$\Delta_y = \frac{229}{\frac{1}{2}(72 - (-80.5))} = 3.0 \text{ mm}$$

1.0 mm push, 2nd cycle

The wall response mirrored that of the previous pull cycle. A maximum strength of 70 kN was measured at the target displacement. No cracking was identified.

1.0 mm pull, 2nd cycle

A maximum strength of –75 kN was measured with no cracking identified for this direction of loading.

2.0 mm push, 1st cycle

An uplift of about 0.5 mm was measured at the tension toe, extending the crack to approximately 800 mm along the base. No other cracking was identified on the wall. A maximum strength of 117 kN was measured at the displacement of 1.98 mm.

2.0 mm pull, 1st cycle

Four new hairline horizontal (flexure) cracks were identified on mortar joints at the wall edge on the tension side. A maximum strength of -121 kN was measured at a displacement of -1.96 mm.

2.0 mm push, 2nd cycle

The wall responded similarly to observations made in the previous push cycle. A maximum strength of 107 kN was measured, and no new cracking was identified.

2.0 mm pull, 2nd cycle

Minor elongations to previously formed horizontal cracks were observed. A maximum strength of -116 kN was measured.

4.0 mm push, 1st cycle (see Photo 9, Appendix G)

The first diagonal (shear) crack initiated from the edge of the wall when the wall was displaced to about 2.5 mm. This crack inclined at an angle of approximately 45° to the horizontal. The formation of this diagonal crack did not reduce wall strength. The second diagonal crack formed at about 3.2 mm, resulting in significant increase in displacement and a corresponding loss in strength. Maximum strengths of 150 kN and 141 kN were measured at displacements of 3.2 mm and 4.1 mm respectively.

4.0 mm pull, 1st cycle (see Photo 9)

New diagonal cracks and elongations to previously formed flexural cracks were identified. Unlike the previous push cycle, there was no loss in strength during the formation of shear cracks. A maximum strength of -176 kN was measured.

4.0 mm push, 2nd cycle

No new cracks were observed, but minor extensions to horizontal cracks were noted. The maximum force achieved in this cycle was 135 kN.

4.0 mm pull, 2nd cycle

No new cracks were identified. The wall reached a maximum strength of -165 kN at the conclusion of this load cycle.

6.0 mm push, 1st cycle

Small extensions to previously formed diagonal cracks were observed, accompanied by two new shear cracks when the wall was displaced to the target displacement. Diagonal cracks that formed in the previous load steps were observed to widen to approximately 2.0 mm. No crushing or spalling of masonry was observed at this stage. A maximum strength of 198 kN was measured.

6.0 mm pull, 1st cycle

A significant amount of new diagonal cracks were identified at the conclusion of this load step. Small extensions to cracks that formed in the previous pull cycle were also observed. An uplift of approximately 0.7 mm at the wall heel and a maximum force of -205 kN were measured.

6.0 mm push, 2nd cycle (see Photo 10)

A maximum strength of 179 kN was measured for this load cycle, and no new cracks or crack extensions were identified.

6.0 mm pull, 2nd cycle (see Photo 10)

No new cracks or crack extensions were identified. A maximum strength of -197 kN was measured.

8.0 mm push, 1st cycle

A maximum strength of 205 kN was measured at this load step. Further development of new diagonal cracks were observed, accompanied by significant uplift (about 2 mm) at the tension toe.

8.0 mm pull, 1st cycle

Further formation of new diagonal cracks was observed at the completion of this load cycle. A maximum strength of –193 kN was measured. There was no sign to indicate crushing or spalling of masonry at this stage.

8.0 mm push, 2nd cycle

A maximum strength of 194 kN was measured. No new cracks or crack elongation were observed.

8.0 mm pull, 2nd cycle

A maximum strength of –187 kN was measured. Again no new cracking was detected.

10 mm push, 1st cycle (see Photo 11)

The wall responded similarly to observations made in the previous push cycle. First sign of compression toe distress due to masonry crushing was observed. A maximum strength of 217 kN was measured, accompanied by an uplift of 3.1 mm at the tension toe.

10 mm pull, 1st cycle

The wall behaved similarly to observations made in the previous push cycle, where splitting of the concrete masonry block took place at the compression toe. A maximum strength of –194 kN was measured.

10 mm push, 2nd cycle

The wall reached a maximum strength of 195 kN at the end of this loading cycle. No new cracking was identified. An uplift of about 3.5 mm was measured at the tension toe.

10 mm pull, 2nd cycle

Sign of mortar being crushed at compression toe and started to fall off. A maximum strength of –180 kN was measured. No new cracks were identified.

12 mm push, 1st cycle

The wall behaved similarly to observations made in the previous push cycle, with further crushing of masonry at the compression toe that eventually caused spalling of the face shells. A maximum strength of 198 kN was measured.

12 mm pull, 1st cycle

The wall responded similarly to observations made in the previous pull cycle. A maximum strength of -190 kN was measured.

12 mm push, 2nd cycle

Significant strength loss was observed, and a maximum strength of 156 kN was recorded for this loading cycle. The strength measured in this cycle corresponded to about 72% of the maximum strength achieved in the push direction. Hence, the wall was defined as failing according to the test procedure outlined in section 3.8.

Instead of forming new cracks, most damage was represented by the crushing of masonry in the compression toe. Severe crushing of the compression toe reduced the wall's capacity to transfer shear load to the base. An uplift of about 3.6 mm was measured at the tension toe.

12 mm pull, 2nd cycle

A maximum strength of -180 kN was measured at the end of this load step. Further crushing of the compression toe caused spalling of the face shell.

14 mm push, 1st cycle

The maximum strength recorded for this load step was 138 kN. The rapid strength degradation was caused by severe crushing of the wall compression toe as mentioned previously. Further widening of diagonal cracks was observed.

14 mm pull, 1st cycle

The wall achieved a maximum strength of -167 kN for this cycle. The wall behaved similarly to observations made in the previous pull cycle, and no new shear cracking was identified.

14 mm push, 2nd cycle (see Photo 12)

The wall achieved a maximum strength of 107 kN for this cycle. Crushing of the grout core at the compression toe was sufficient to expose the extreme vertical reinforcing bar, and it was observed that the extreme vertical reinforcement was buckled under compression force.

14 mm pull, 2nd cycle (see Photo 12)

A maximum strength of -159 kN was measured. Apart from crushing of the compression toe, no new cracks were identified. The strength measured in this load cycle corresponded to 77% of the maximum strength recorded in the pull direction.

B.1.3 Summary Behaviour

The maximum push direction strength of +217 kN was measured during the first cycle to +10 mm displacement, and the maximum pull direction strength of -205 kN was measured during the first cycle to -6 mm displacement. The force-displacement (F-D) plot is presented in Figure B1.2. As can be seen in Figure B1.2, strength degradation took place in the push direction after the wall reached its maximum strength. The wall was defined as failing during the second push cycle to +12 mm displacement when the wall strength dropped below $0.8V_{\max}$.

The wall had a flexure-shear type of failure mode. This was characterised by the initiation of visible horizontal (flexural) cracking along the mortar joints at a low displacement level. As the wall was being pushed/pulled to further lateral displacement, initiation of cracking along the wall diagonals occurred when the principal tensile stresses exceeded the tensile strength of masonry under the increasing imposed lateral displacements. This type of failure was expected for Wall 1 since the predicted wall flexural strength was slightly higher than the predicted shear strength. Final failure was due to crushing of the masonry at the compression toes.

The yield displacement for Wall 1 was evaluated to be 3.0 mm. The wall was defined as failing during the second cycle to 12 mm displacement.

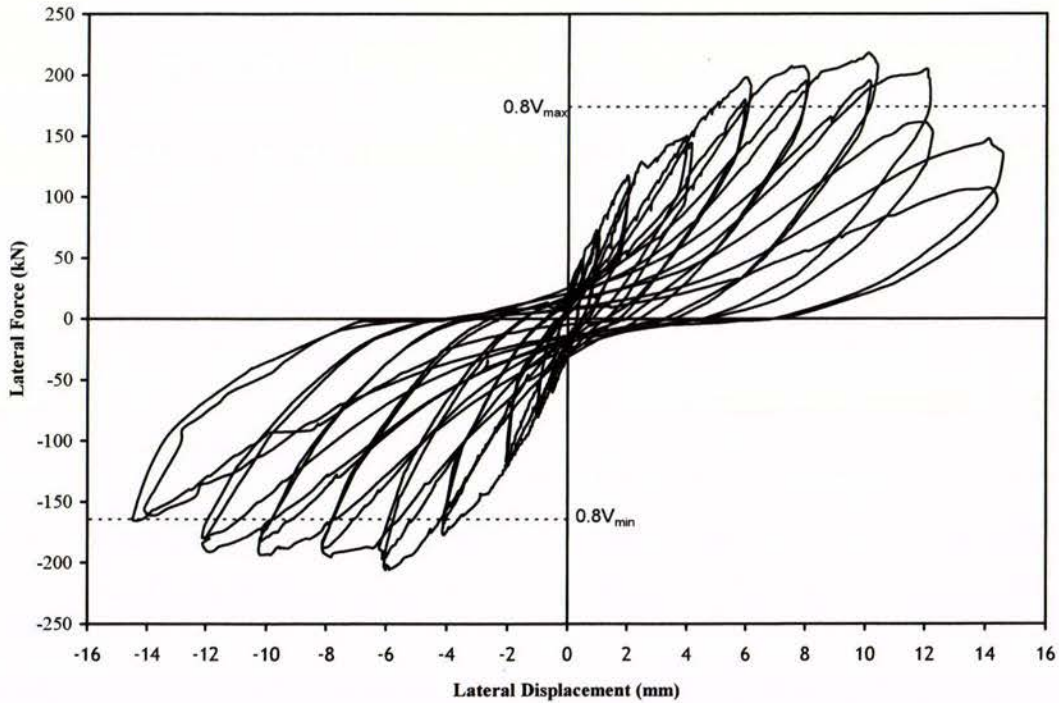


Figure B.1.2 Force-displacement behaviour for Wall 1.

As can be observed in Figure B.1.2, abrupt strength degradation did not take place. It was therefore possible to classify Wall 1 as having a flexure-shear type of failure. This type of failure was made possible for Wall 1 due to the adoption of 400 mm spaced R6 shear reinforcement. The shear reinforcement enables the redistribution of stresses throughout the wall diagonals after the initiation of shear cracking. Accordingly, the initial diagonal cracks did not widen significantly under increasing horizontal forces, but instead new sets of diagonal cracks formed and gradually spread over the wall diagonals, accompanied by high energy dissipation and ductile behaviour. Failure occurred gradually in this case as the strength of the wall deteriorated under cyclic horizontal loading. Finally, partial crushing of masonry at the position of compression toes and severely cracked portions of the wall diagonals took place at larger imposed lateral displacement. Due to the significant amount of diagonal shear cracking and the absence of abrupt loss of strength, Wall 1 could also be classified as having a “ductile shear failure”.

B.1.4 Force-displacement Envelope

Figure B.1.3 shows the force-displacement envelope for the test. The plot was constructed from the peak force recorded in the first cycle for each displacement level. It is seen that wall

strength degraded significantly after 10 mm displacement in the push direction, but strength degradation in the pull direction happened more gradually. It is clearly shown in the figure that the maximum strength developed by Wall 1 was less than the calculated flexural strength, therefore indicating that the wall failed in shear. It is also shown in Figure B.1.3 that the shear strength predicted by NZS4230:1990 was significantly lower than the actual shear strength achieved by the masonry wall. The shear strength predicted by NEHPR closely matched the measured wall shear strength.

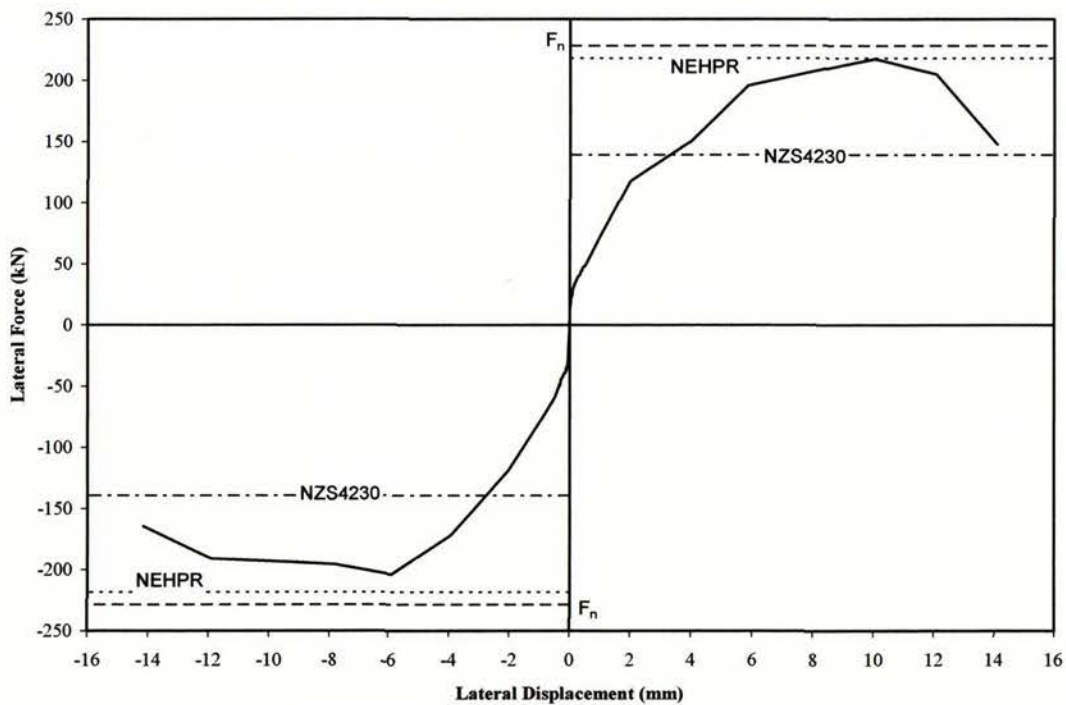


Figure B.1.3 Force-displacement envelope of Wall 1.

B.1.5 Panel Displacement Components

The total horizontal displacement of the wall was decomposed into four components according to the procedure outlined in section 3.9. These were the horizontal displacement due to shear displacement, flexural displacement, rocking displacement and sliding of the wall on its base. It is noted that the summed up displacement (shear + flexural + rocking + sliding) does not add up to match the overall displacement measured at the loading beam. Ideally the line representing the sum of components should coincide with the line representing the lateral displacement measured at the loading beam. Figure B.1.4 provides an indication of the relative size of each component for various stages of the displacement envelope until the displacement of ± 12 mm.

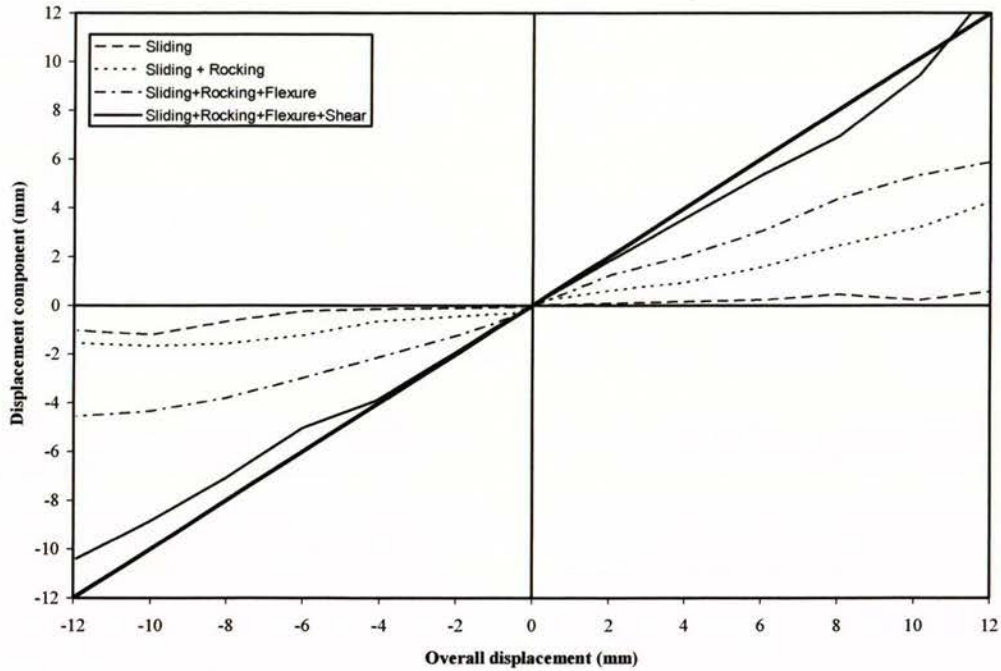


Figure B.1.4 Components of displacement.

B.1.6 Stiffness Degradation

The stiffness degradation curves for Wall 1 are presented in Figures B.1.5 and B.1.6. The stiffness during a loading cycle was obtained by dividing the extreme positive and negative lateral forces by the corresponding displacements in each loading cycle. The stiffness values obtained from the first cycle of loading were averaged and plotted against the corresponding average (absolute) lateral force measured during testing (Figure B.1.5). The stiffness values were also plotted against the average (absolute) lateral displacement, see Figure B.1.6. These relationships provide an indication of the sensitivity of the wall with respect to the level of horizontal force, or lateral displacement. The stiffness degradation curve was truncated at the stage when the maximum shear strength was attained.

A wall stiffness of 108 kN/mm was calculated when the wall was loaded to ± 0.5 mm displacement. The wall stiffness dropped to 22 kN/mm when maximum push direction strength developed during the cycle to +10 mm displacement. As can be seen from Figure B.1.6, significant stiffness degradation was present even at the beginning stages of horizontal loading, much earlier than the development of the first visible crack.

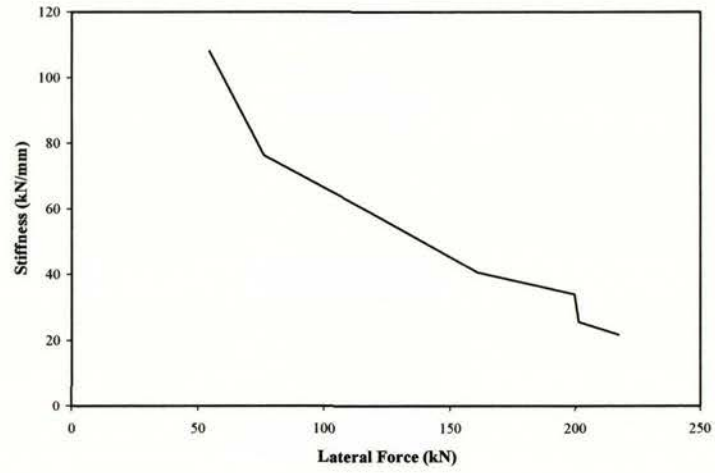


Figure B.1.5 Stiffness vs lateral force.

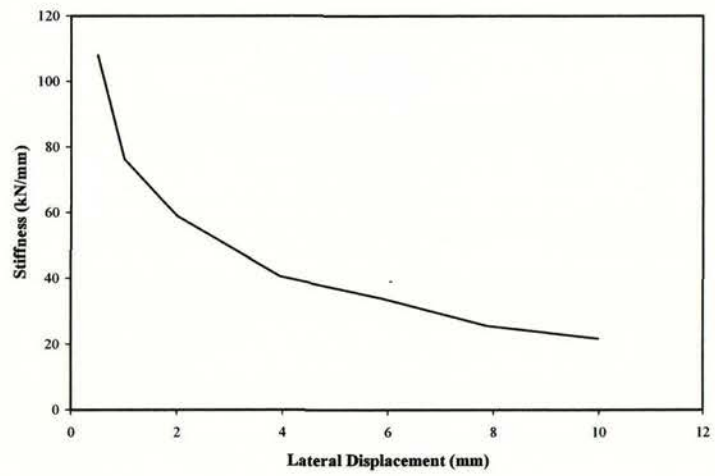


Figure B1.6 Stiffness vs lateral displacement.

B.2 Wall 2

This section describes the laboratory test of Wall 2 on the 60th day after construction. Horizontal shear reinforcement consisted of a single R6 bar embedded in the top of the wall, creating a shallow bond beam. This test had been designed to investigate the shear strength provided purely by the masonry. The shallow bond beam was designed to ensure effective shear transfer from the loading beam to the entire masonry wall. Therefore, the nominal flexural strength, F_n , and the wall shear strength, V_n , were calculated according to section 3.7 for a fully grouted masonry wall, with the results presented in Table B.2.1.

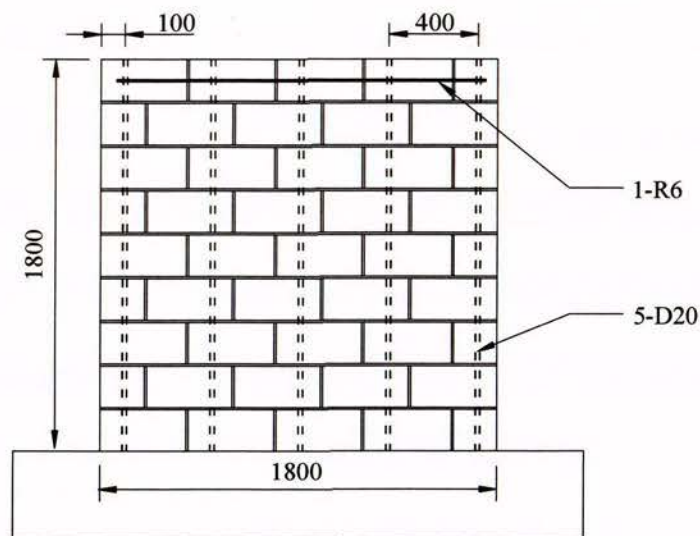


Figure B.2.1 Wall 2 reinforcement details.

Table B.2.1 Wall strength predictions

Masonry strength	Nom. Flexural strength	Masonry shear strength V_n	
f'_m	F_n	NZS4230	NEHPR
17.6	229	105	195
MPa	kN	kN	kN

B.2.1 Pre-test

Instrumentation was attached to the wall according to section 3.5.1. No precondition was noted.

B.2.2 Testing

0.5 mm push, 1st cycle

No clear evidence of cracking. An applied force of 69 kN was recorded.

0.5 mm pull, 1st cycle

A maximum strength of –75 kN was recorded at a displacement of –0.50 mm. No cracking was noted.

0.5 mm push, 2nd cycle

Measured force was 69 kN, and corresponding displacement was 0.49 mm.

0.5 mm pull, 2nd cycle

Measured displacement was –0.51 mm, and corresponding force was –75 kN. No cracking was identified.

1.0 mm push, 1st cycle

A maximum strength of 99 kN was measured at the conclusion of this displacement cycle. Hairline horizontal cracks were identified to initiate from the wall end (tension zone) and extended about 200 mm along the first three courses of mortar joints. The decompressed wall toe was measured to have an uplift of about 0.3 mm.

1.0 mm pull, 1st cycle

The wall behaved similarly to observations made on the previous push cycle and three hairline horizontal cracks were identified. A maximum strength of –96 kN was recorded.

According to the procedure outlined in section 3.8, the measured lateral forces for the two directions of loading resulted in an average yield displacement of:

$$\Delta_y = \frac{229}{\frac{1}{2}(99 - (-96))} = 2.3 \text{ mm}$$

1.0 mm push, 2nd cycle

No new cracks or extensions of cracks were identified. A maximum strength of 87 kN was recorded.

1.0 mm pull, 2nd cycle

A maximum strength of -96 kN was measured with no new cracks identified.

2.0 mm push, 1st cycle

The first diagonal crack (inclined at an angle of approximately 45° to the horizontal) was identified, accompanied by two new horizontal cracks. An uplift of about 0.5 mm was measured, creating a crack at the base that extended approximately 500 mm along the base. A maximum force of 132 kN was measured.

2.0 mm pull, 1st cycle

A diagonal crack with a measured width of about 0.3 mm was identified, although no accurate measurement was taken. A maximum strength of -128 kN was measured, accompanied by an uplift of 0.25 mm at the tension side.

2.0 mm push, 2nd cycle

A maximum strength of 125 kN was measured, and no new cracking or extensions of cracks were identified.

2.0 mm pull, 2nd cycle

No new cracks were noted. A maximum strength of -125 kN was measured.

4.0 mm push, 1st cycle (see Photo 13)

The lateral force resisted by the wall increased gradually to a maximum of 177 kN at a displacement of 3.65 mm. This was followed by a sudden loss in strength (accompanied by a “splitting” noise) and sudden increase in displacement (from 3.65 mm to 4.90 mm) when a new diagonal crack formed suddenly and propagated across the entire wall. The maximum crack width was about 1 mm. The wall strength finally settled at 132 kN. No further development of horizontal cracks were observed at this stage.

4.0 mm pull, 1st cycle (see Photo 13)

The wall behaved similarly to observations made for the previous push cycle. A maximum lateral force of -166 kN was measured at a displacement of -3.3 mm. The load then dropped suddenly, followed by an abrupt increase in displacement when a diagonal crack opened up

suddenly. The wall strength finally settled at -154 kN at a displacement of -4.0 mm. The diagonal cracks developed up to this stage had a pattern of x-shaped form.

4.0 mm push, 2nd cycle

No new cracks were observed, but widening of existing diagonal cracks (maximum crack width about 2.5mm) was noted. The maximum strength achieved in this cycle was 127 kN.

4.0 mm pull, 2nd cycle

The wall responded similarly to the previous push cycle. No new cracks were identified. The wall reached a maximum strength of -152 kN at the conclusion of this load cycle.

6.0 mm push, 1st cycle

A new diagonal crack (about 600 mm long) was identified to initiate from the bond beam. The face shells along the previously formed diagonal crack showed sign of crushing. The maximum crack width of previously formed diagonal cracks was measured to be approximately 4 mm. A maximum strength of 177 kN and an uplift of about 1.1 mm at the tension toe were measured.

6.0 mm pull, 1st cycle

A maximum strength of -195 kN was measured at a displacement of -5.9 mm. This was then followed by a sudden increase in displacement (from -5.9 mm to -6.6 mm) when the diagonal cracks widened suddenly (about 3.5 mm). The wall strength finally settled at -183 kN at the displacement of -6.6 mm.

6.0 mm push, 2nd cycle

A maximum force of 148 kN was measured for this load cycle. No new cracking was identified, but there was continued widening and crushing along the main diagonal crack.

6.0 mm pull, 2nd cycle

No new cracks or extensions of cracks were identified. A maximum force of -147 kN was measured.

8.0 mm push, 1st cycle

A maximum strength of 160 kN and an uplift of 2.0 mm were measured for this load step. Further crushing of face shells along the main diagonal crack was noted.

8.0 mm pull, 1st cycle

A maximum strength of -160 kN was measured at the conclusion of this loading cycle. No new cracks were identified.

8.0 mm push, 2nd cycle (see Photo 14)

A maximum force of 127 kN was measured. This force corresponded to about 72% of the maximum strength achieved in the push direction. Therefore Wall 2 was defined as failing according to the test procedure outlined in section 3.8.

No new cracks were identified, but face shells spalling (both sides of wall) occurred at the centre of the wall, coincided with the position of the mounted measuring point, influencing the accuracy of deformation measurements.

8.0 mm pull, 2nd cycle

A maximum strength of -138 kN was measured. This force corresponded to 71% of the maximum strength achieved in the pull direction. No new cracking was detected.

10 mm push, 1st cycle

The wall responded with a sudden increase in displacement to 12.0 mm when force loading stopped at the displacement of 10 mm. A maximum force of 131 kN was measured at +10 mm displacement, but dropped significantly to 82 kN during the abrupt increased displacement to +12 mm. The x-shaped diagonal crack was significantly widened to cause further spalling of face shells along the diagonal crack.

10 mm pull, 1st cycle

The wall behaved similarly to observations made in the previous push cycle where widening of diagonal cracks was observed. A maximum force of -122 kN was recorded.

10 mm push, 2nd cycle

The wall reached a maximum strength of 62 kN at the end of this loading cycle. Further deterioration was observed to take place along the diagonal cracks.

10 mm pull, 2nd cycle (see Photo 15)

The grout core at the centre of the wall was crushed and subsequently removed. The exposed centre vertical reinforcing bar buckled when the wall reached a maximum strength of -97 kN at the conclusion of this loading cycle.

12 mm push, 1st cycle

The wall behaved similarly to observations made in the previous push cycle, and further spalling and crushing along the diagonal crack continued. A maximum strength of +63 kN was measured.

12 mm pull, 1st cycle

The wall achieved a maximum strength of -99 kN for this load step. Wall behaviour was dominated by widening of the diagonal crack and crushing of the wall compression toe.

12 mm push, 2nd cycle

The grout core at the centre of wall was significantly crushed and spalled off. Also noted was the significant crushing at the compression toe. A maximum strength of 50 kN was recorded for this load step.

12 mm pull, 2nd cycle (see Photo 16)

A maximum force of -94 kN was recorded at the conclusion of this load cycle. Testing was terminated at completion of this load cycle since the wall had lost significant strength in the push direction.

B.2.3 Summary Behaviour

The maximum push and pull direction strengths of 177 kN and -195 kN were measured during the first cycle to ± 6 mm displacement. The force-displacement (F-D) plot is presented in Figure B2.2. Significant strength degradation took place in both directions after the wall reached its maximum strength. The wall had a shear type of failure mode, as expected because the predicted nominal flexural strength was larger than the predicted shear strength. The shear mode of failure was characterised by the initiation of visible horizontal cracks at low displacement levels (less than ± 2 mm displacement for this wall). As the wall was pushed/pulled to further displacement, initiation of diagonal crackings occurred when the principal stresses due to the applied lateral force exceeded the tensile strength of masonry.

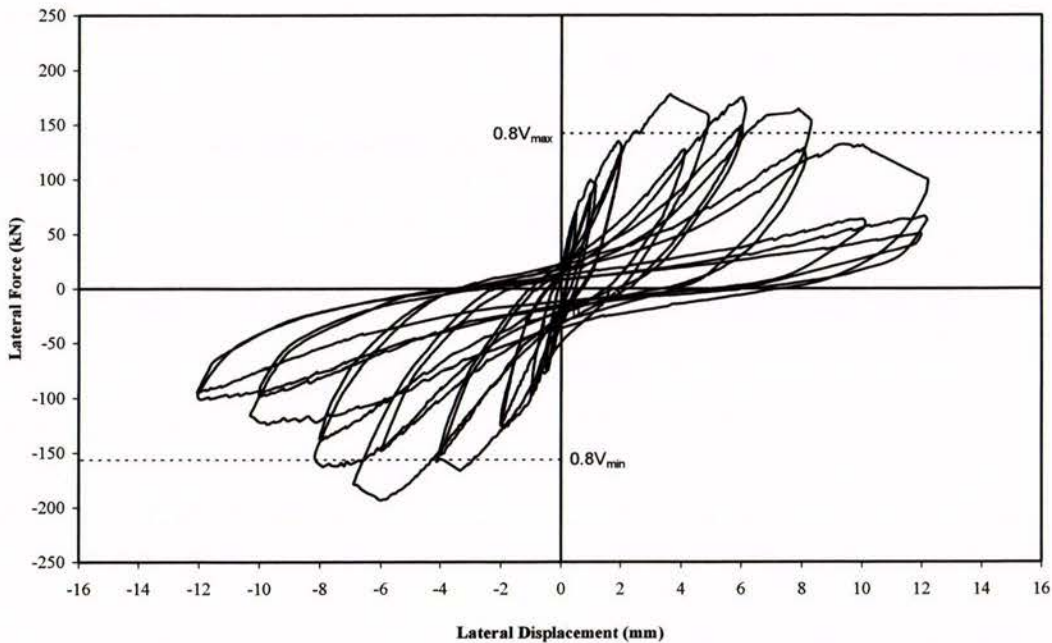


Figure B2.2 Force-displacement history of Wall 2.

As can be observed in Figure B2.2, rapid strength degradation took place immediately after the wall reached its maximum strength. Failure of the wall occurred during the first push cycle to +8.0 mm displacement. Wall 2 could be classified as having a “brittle shear failure”. This type of failure was due to the lack of adequate shear reinforcement to provide the proper transfer of tensile stresses across the diagonal cracks. Therefore the initial cracks opened extensively, with poor energy dissipation capacity. Finally, the formation of a major x-shaped diagonal crack pair caused rapid strength deterioration at larger imposed lateral displacement.

The yield displacement for Wall 2 was evaluated to be 2.3 mm. The wall was defined as failing during the second cycle to 8 mm displacement.

B.2.4 Force-displacement Envelope

Figure B.2.3 shows the force-displacement envelope for the test. The plot was constructed from the peak force recorded in the first cycle for each displacement level. It is shown in Figure B.2.3 that rapid strength degradation took place after the wall developed its maximum strength at ± 6 mm displacement. It was observed that the maximum strength developed by Wall 2 was less than the calculated flexural strength, therefore indicating the wall failed in shear. Figure B.2.3 shows that the shear strength predicted by NZS4230:1990 was significantly lower than the actual shear strength achieved by the tested masonry wall, and that the shear strength predicted by NEHPR more closely matched the measured wall shear strength.

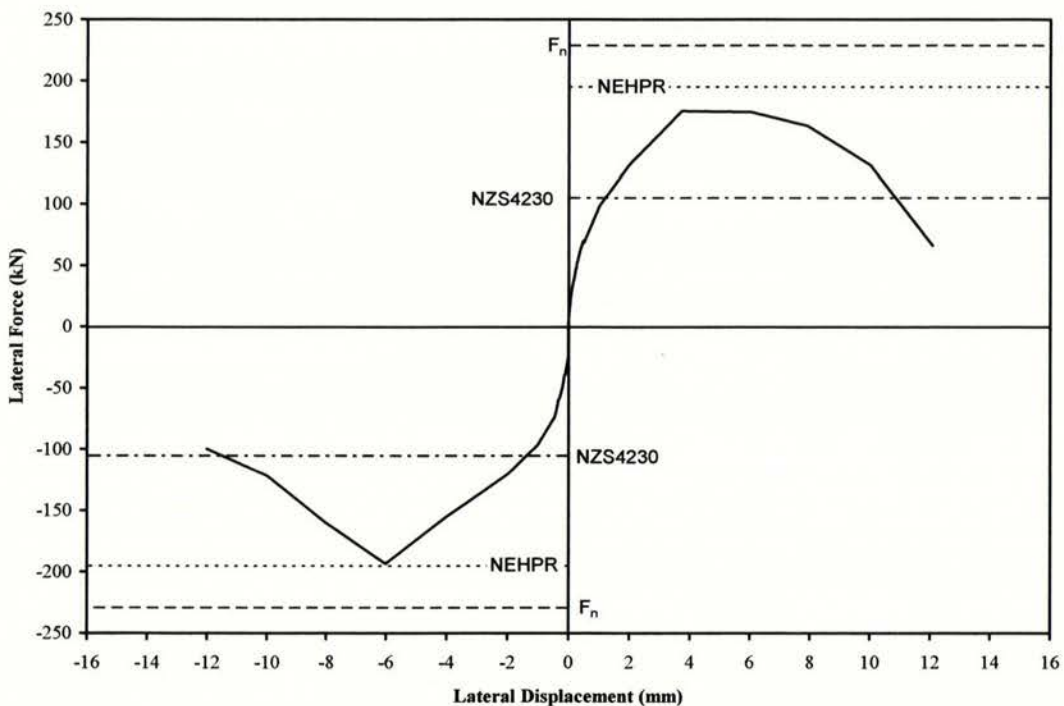


Figure B.2.3 Force-displacement envelope for Wall 2.

B.2.5 Panel Displacement Components

The total horizontal displacement of the wall was decomposed into four components according to the procedure outlined in section 3.9. These were shear displacement, flexural

displacement, rocking displacement and sliding of the wall on its base. It is noted in Figure B.2.4 that the summed up displacement (shear + flexural + rocking + sliding) does not add up to match the overall displacement measured at the loading beam. It is seen that rocking and flexure were the dominant modes for displacements up to ± 2 mm displacement, and beyond that the shear displacement component increased significantly, becoming the most significant displacement component at later stage of testing. Figure B.2.4 was plotted up to 8 mm displacement, due to severe face shell spalling that occurred at this displacement level, which subsequently caused faulty reading in the displacement transducers.

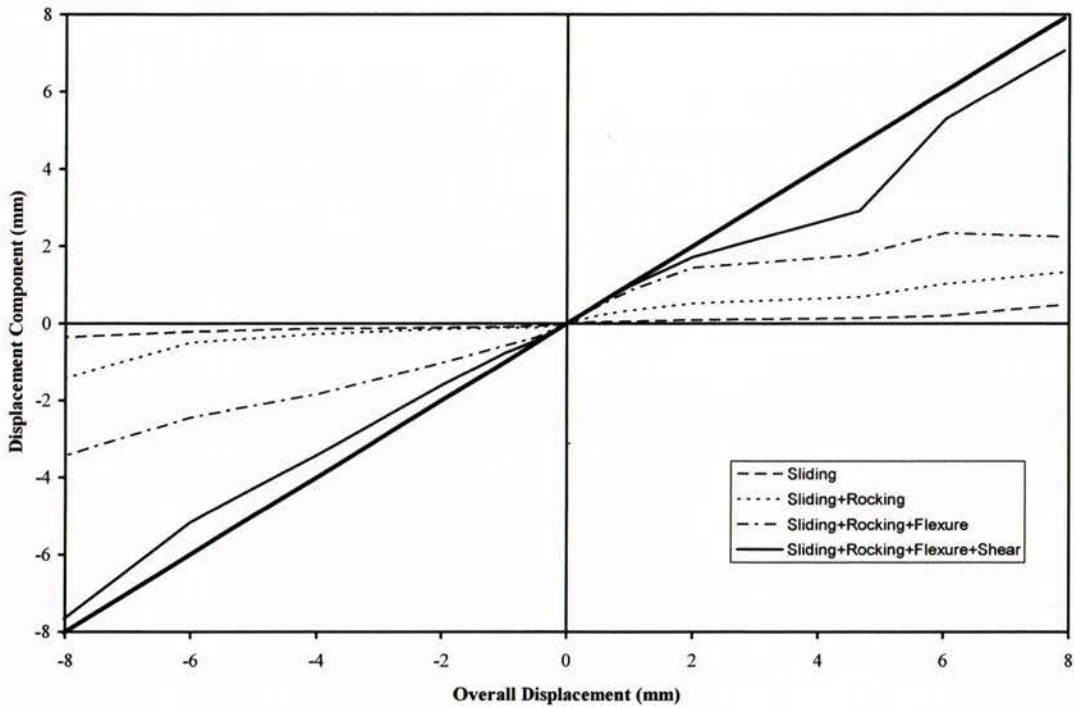


Figure B.2.4 Components of displacement.

B.2.6 Stiffness Degradation

The stiffness degradation curves for Wall 2 are presented in the two following figures. The stiffness during a loading cycle was obtained by dividing the extreme positive and negative lateral forces by the corresponding displacements in each load cycle. The stiffness values obtained from the first cycle of loading were averaged and plotted against the corresponding average absolute lateral force and lateral displacement. These relationships provided an indication of the sensitivity of wall stiffness with respect to the level of horizontal force, or lateral displacement. The stiffness degradation was truncated when the maximum shear strength was attained.

A wall stiffness of 144 kN/mm was calculated when the wall was loaded to ± 0.5 mm displacement. The wall stiffness dropped to 30 kN/mm when maximum strength developed during the cycle to ± 6 mm displacement.

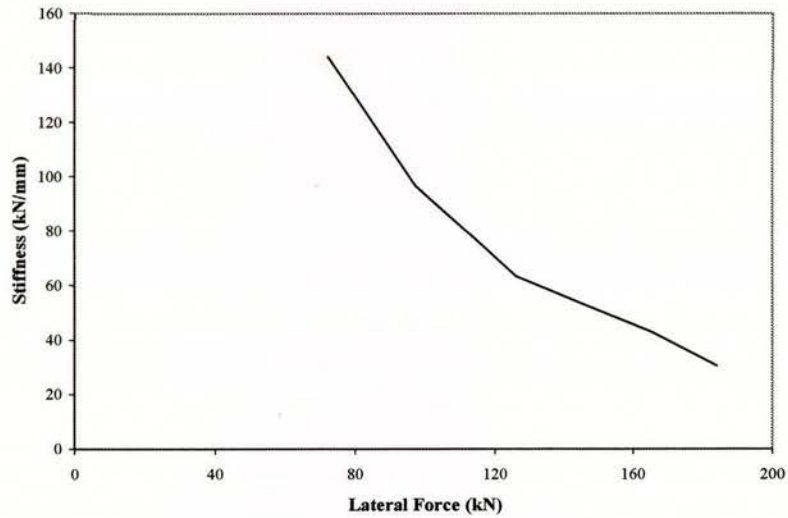


Figure B.2.5 Stiffness vs lateral force.

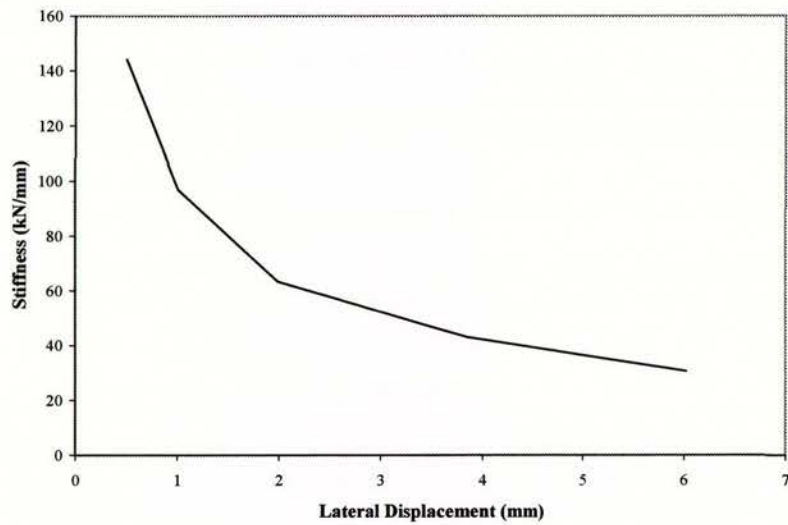


Figure B.2.6 Stiffness vs lateral displacement.

B.3 Wall 3

Testing of Wall 3 is described in this section. Reinforcement details shown in Figure B.3.1 indicates the shear reinforcement, consisting of D10 bars, were embedded at 400mm c/c. As shown in Table B.3.1, V_n predicted by NEHPR was higher than the expected F_n . Consequently, the wall was expected to exhibit a predominantly flexural type of response.

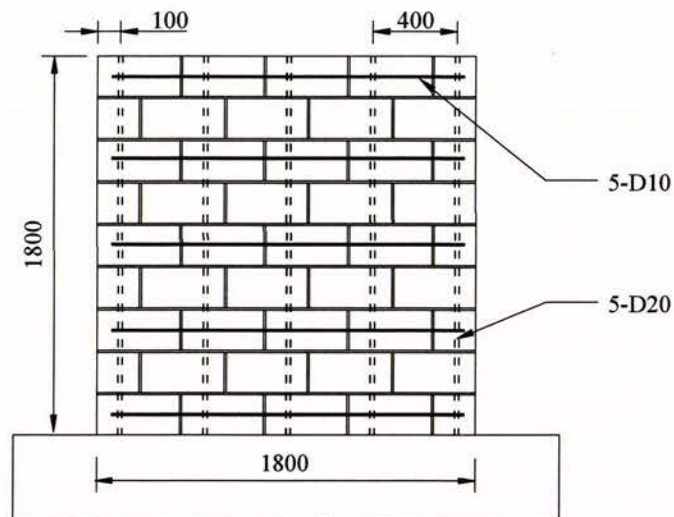


Figure B.3.1 Wall 3 reinforcement details.

Table B.3.1 Wall strength predictions

Masonry strength	Nom. Flexural strength	Masonry shear strength V_n	
f'_m	F_n	NZS4230	NEHPR
17.0	229	191	250
MPa	kN	kN	kN

B.3.1 Pre-test

Instrumentation was attached to the wall according to section 3.5.1. Wall 3 was tested approximately 19 days after construction. Prior to wall testing the wall was inspected, with no cracks or structural defects being identified.

B.3.2 Testing

0.5 mm push, 1st cycle

The wall developed a maximum strength of 67 kN at this displacement. No cracking or other damage of the masonry wall was identified.

0.5 mm pull, 1st cycle

A maximum force of –47 kN was reached at this displacement level. No cracking was identified.

0.5 mm push, 2nd cycle

No cracking was identified when the wall developed a maximum strength of 64 kN for this load step.

0.5 mm pull, 2nd cycle

A maximum force of –45 kN was recorded. No cracking was identified.

1.0 mm push, 1st cycle

A maximum strength of 104 kN was recorded. Hairline horizontal (flexural) cracks were identified on three courses of mortar joints with a maximum length of about 800 mm, the cracks had a maximum width of approximately 0.1 mm, although no accurate measurements were taken.

1.0 mm pull, 1st cycle

The response of the wall mirrored that of the previous push cycle. A maximum strength of –82 kN was recorded.

According to the procedure outlined in section 3.8, the measured lateral forces for the two directions of loading resulted in an average yield displacement of:

$$\Delta_y = \frac{229}{\frac{1}{2}(104 - (-82))} = 2.46 \text{ mm}$$

1.0 mm push, 2nd cycle

No new crack or extensions of cracks were identified. A maximum force of 98 kN was recorded.

1.0 mm pull, 2nd cycle

The wall developed a maximum strength of -75 kN, and no new crack was identified.

2.0 mm push, 1st cycle (see Photo 17)

New horizontal cracks developed on mortar joints on the tension side. A maximum strength of 152 kN was recorded.

2.0 mm pull, 1st cycle (see Photo 17)

As shown in Photo 17, the wall's response mirrored that of the previous push cycle. The wall developed a maximum strength of -135 kN for this load step.

2.0 mm push, 2nd cycle

A maximum strength of 140 kN was measured, and no new cracking was identified.

2.0 mm pull, 2nd cycle

Minor elongation of horizontal cracks that had formed in the previous pull cycle. A maximum force of -130 kN was measured. All cracks that had formed in the previous cycles closed when unloaded, suggesting that the wall was still behaving elastically at this stage of testing.

4.0 mm push, 1st cycle (see Photo 18)

The wall developed a maximum strength of 198 kN at the completion of this loading step. Two diagonal cracks (approximately 45° to the horizontal) were identified on the wall panel, with a maximum crack width of approximately 0.55 mm (although no accurate measurement was taken). Visible uplift measuring 0.88 mm was also noted at the wall tension toe.

4.0 mm pull, 1st cycle (see Photo 18)

The response of the wall mirrored that of the previous push cycle. A maximum strength of -185 kN was achieved in this load step.

4.0 mm push, 2nd cycle

No new cracking but minor elongation of existing diagonal cracks were noted. The maximum force achieved in this cycle was 180 kN.

4.0 mm pull, 2nd cycle

The response was the same as for the previous cycle. The wall reached a maximum strength of -174 kN at the conclusion of this load cycle.

6.0 mm push, 1st cycle

A minor bond splitting crack (vertical cracking) was identified on top of the wall at the position of the outermost vertical tension bar. The diagonal crack was noted to extend to the compression toe, and mortar in the path of diagonal cracks was severely crushed and started to fall off. A maximum strength and uplift of 215 kN and 1.4 mm were measured respectively. Wall sliding at the base was measured to be about 0.51 mm.

6.0 mm pull, 1st cycle

The response of the wall mirrored that of the previous push cycle. A maximum strength of –203 kN and an uplift of 1.75 mm were measured. No new cracking was identified. Wall sliding of about -0.78 mm was measured.

6.0 mm push, 2nd cycle

No new cracking or extension of cracks was identified. A maximum strength of 186 kN was measured.

6.0 mm pull, 2nd cycle

Now new cracks or crack extensions were identified. The maximum strength achieved in this load step was –186 kN, which was the same as for the previous push cycle.

8.0 mm push, 1st cycle

A maximum strength of 215 kN was measured at this load step. There was further development of diagonal cracks. Sliding of the wall along the base was measured to be about 1.05 mm, accompanied by an uplift of 2.0 mm.

8.0 mm pull, 1st cycle

The wall developed a maximum strength of –199 kN at the completion of this load cycle. There was sign of severe masonry crushing at the compression toe. Wall sliding and uplift (at tension toe) were measured to be about 1.4 mm and 2.0 mm respectively.

8.0 mm push, 2nd cycle

A maximum strength of 189 kN was measured. No new cracks or crack elongations were observed. Minor spalling of face shells took place at the tension toe due to masonry crushing, which had occurred in the previous pull cycle.

8.0 mm pull, 2nd cycle

A maximum strength of –178 kN was measured. Further crushing of masonry at the compression toe was observed.

10 mm push, 1st cycle

There was significant spalling of masonry at the tension toe, exposing the outermost vertical bar. No new cracking was identified. There was a slight drop in wall strength (206 kN) compared to the maximum strength developed in the first push cycle of 8 mm displacement. Wall sliding was measured to be about 1.53 mm at the base. The wall uplift was unable to be measured from this stage onwards due to spalling of masonry at the tension toe which subsequently resulted in the removal of a measuring instrument.

10 mm pull, 1st cycle

When the wall was pulled to the displacement of 10.2 mm, the diagonal crack widened up suddenly, resulting in a slight loss of strength but significant increase in displacement. The peak strength reached was –189 kN. At the final displacement of –11.1 mm the strength had dropped to –177 kN. Wall sliding was measured to be about –2.2 mm, accompanied by an uplift of 2.7 mm.

10 mm push, 2nd cycle

The wall reached a maximum strength of 170 kN at the end of this loading cycle. This strength corresponded to 79% of the maximum strength recorded in the push direction.

Therefore the wall was defined as failing according to the test procedure outlined in section 3.8.

Deterioration of the compression toe was evident with the formation of new cracks. Wall sliding was measured to be about 1.6 mm.

10 mm pull, 2nd cycle

The wall strength dropped significantly due to the spalling of compression toe masonry, which had occurred during the previous displacement cycle. A maximum strength of –150 kN was measured at the end of this load step (about 71% of the maximum strength reached in the pull direction). No new cracking was identified. Wall sliding of approximately –2.3 mm was measured.

12 mm push, 1st cycle (see Photo 19)

Deterioration of compression toe continued with the crushing of mortar bed and the widening of cracks at the compression toe region. A maximum strength of 177 kN was measured, accompanied by a wall sliding of 1.95 mm.

12 mm pull, 1st cycle (see Photo 19)

A maximum force of –167 kN was measured for this load step. No new cracking was identified.

12 mm push, 2nd cycle

The wall responded similarly to observations made in the previous push cycle. A maximum force of 149 kN was measured.

12 mm pull, 2nd cycle

The wall responded similarly to observations made in the previous pull cycle. A maximum strength of –153 kN was recorded.

14 mm push, 1st cycle

The wall was accidentally pushed to 16.5 mm instead of the target displacement of 14.0 mm. Significant crushing at the compression toe was noted, resulting in the subsequent spalling of

masonry during unloading. The exposed outermost vertical bar indicated that the bar had been buckled under compression force. A maximum force of 153 kN was recorded at the end of this load step. The wall was measured to slide about 2.3 mm along the base.

14 mm pull, 1st cycle

Significant widening of the main diagonal crack was noted (approximately 4 mm in width), accompanied by the elongation of 3 diagonal cracks. A maximum force of -171 kN was recorded with a corresponding sliding of -3.1 mm.

14 mm push, 2nd cycle

A maximum force of 119 kN was recorded for this loading cycle. No new cracking was noted.

14 mm pull, 2nd cycle

A maximum strength of -159 kN was measured. Apart from the widening of diagonal cracks, no new cracking was identified.

16 mm push, 1st cycle (see Photo 20)

The wall response similarly to that of the previous push cycle. A maximum strength of 130 kN was reached with a corresponding sliding of 2.5 mm.

16mm pull, 1st cycle

The wall developed a maximum strength of -154 kN. No new cracking was identified.

16mm push, 2nd cycle

The wall developed a maximum strength of 130 kN at the completion of this load step. No new cracking was identified.

16mm pull, 2nd cycle

A maximum strength of -154 kN was recorded. No new cracking was identified.

B.3.3 Summary Behaviour

The force-displacement (F-D) curve is presented in Figure B.3.2. The wall developed a maximum push direction strength of 215 kN during the first cycle to 8 mm displacement, and a maximum pull direction strength of -203 kN during the first cycle to -6 mm displacement.

The maximum strength achieved by the wall was about 94% of the calculated flexural strength. It was observed that a cracking at the wall-foundation base interface had caused significant sliding to take place along wall base. Due to sliding displacement that occurred during load reversal, a significant portion of the shear force was transferred primarily by dowel action of the vertical reinforcement. This, in turn, led to a reduction in wall strength, and consequently led to the failure of the wall to develop its predicted flexural strength.

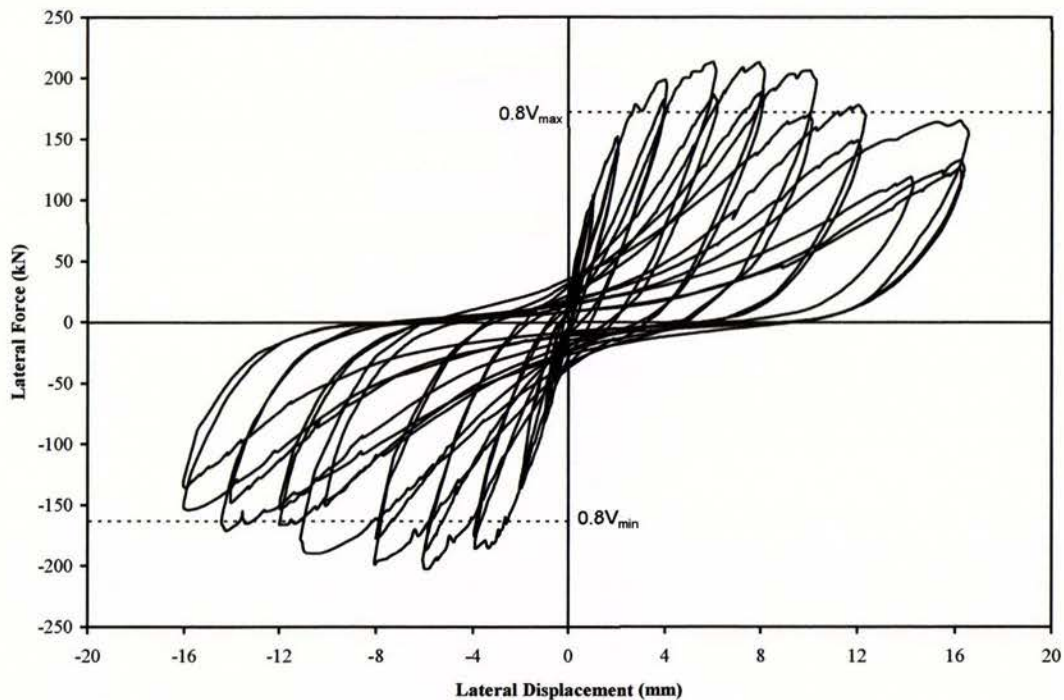


Figure B.3.2 Force-displacement behaviour for Wall 3.

The wall did not exhibit sudden loss of strength after it developed maximum wall strength, but exhibited gradual strength degradation. Although horizontal and diagonal shear cracks were prominent on the wall face, the ultimate failure mode was characterised by face shell spalling and significant sliding at wall's base. It was therefore possible to classify Wall 3 as having a sliding-flexure type of failure.

The yield displacement for Wall 3 was evaluated to be 2.46 mm. The wall was defined as failing during the second cycle to 10 mm displacement.

B.3.4 Force-displacement Envelope

The force-displacement envelope is represented in Figure B.3.3. The plot was constructed from the peak force recorded in the first cycle for each displacement level. As can be seen in the figure, strength degradation occurred gradually after the maximum strength was reached in both directions. It is also shown in Figure B.3.3 that the wall failed to achieve the calculated flexural strength, but that the maximum strength developed exceeded the shear strength predicted by NZS4230:1990, indicating the New Zealand masonry standard is conservative in predicting masonry shear strength.

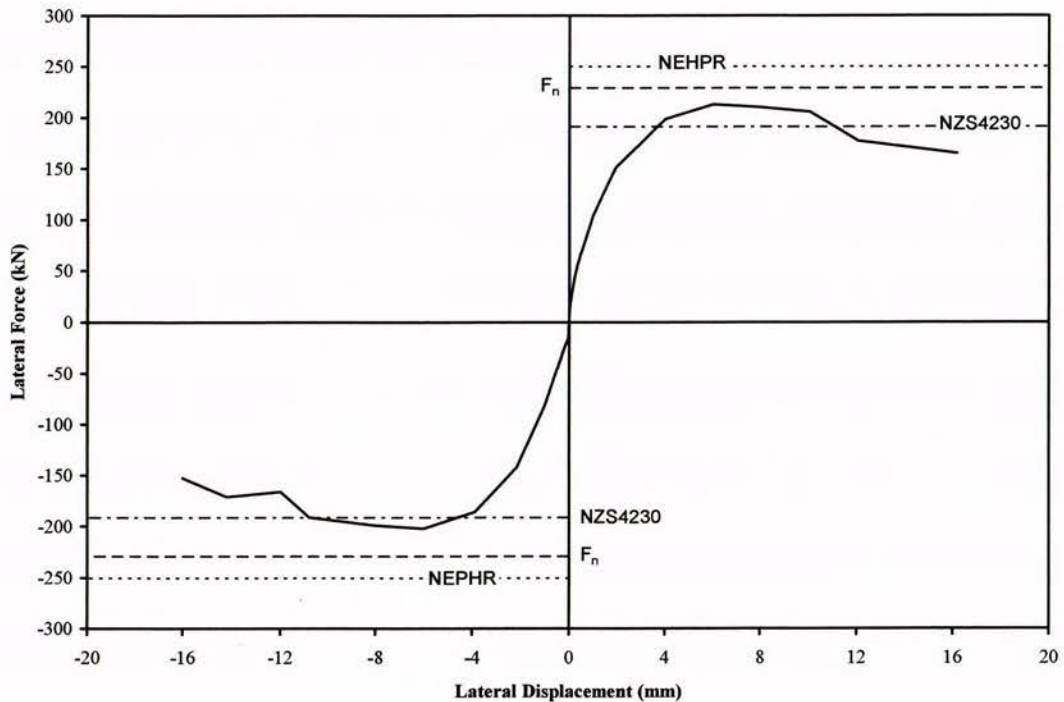


Figure B.3.3 Force-displacement envelope of Wall 3.

B.3.5 Panel Displacement Components

As shown in Figure B.3.4, the total horizontal displacement of the wall was decomposed into four components of displacement according to the procedure outlined in section 3.9. From the sliding, rocking, flexure and shear displacement component plot in Figure B.3.4, it is seen that the shear and sliding displacements were small in magnitude at early stage of testing, but

these two components increased in magnitude as the wall was being loaded to larger displacement. However, the rocking and flexure were the two most dominant displacement modes throughout the test. Figure B.3.4 provides an indication of the relative size of each component for various stages of displacement until ± 8 mm of displacement. Significant errors in the deformation plot when the wall was loaded beyond ± 8 mm of displacement were undoubtedly the result of the profuse cracking (which eventually caused the spalling of face shells) affecting the displacement transducer readings.

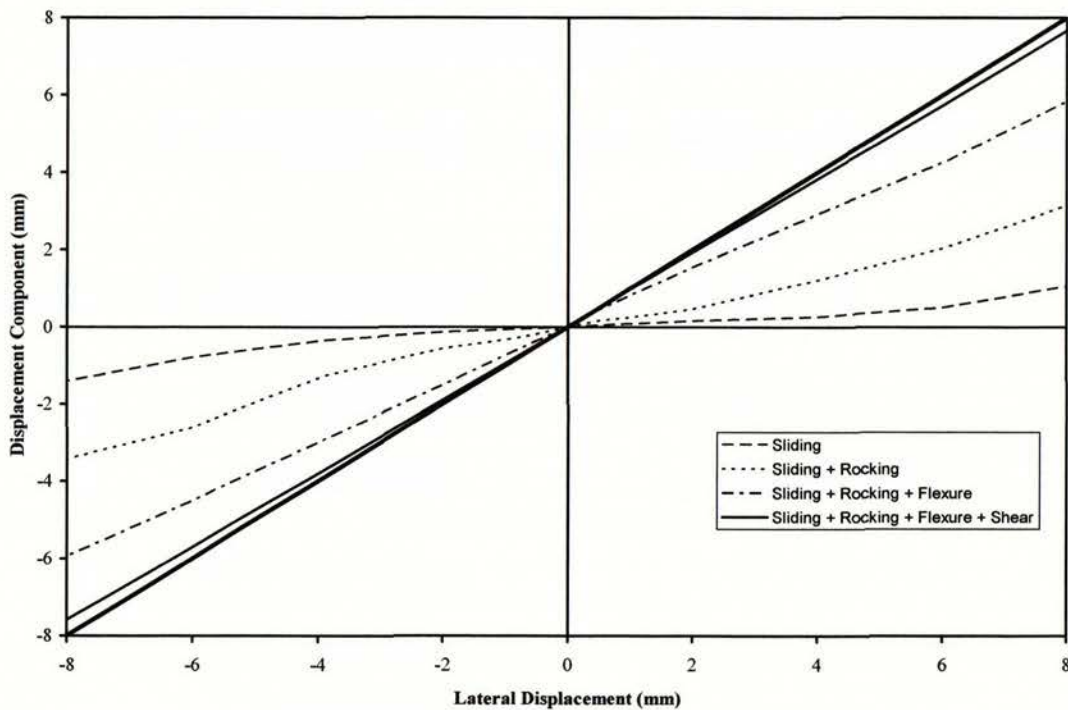


Figure B.3.4 Components of displacement

B.3.6 Stiffness Degradation

The stiffness during a loading cycle was obtained by dividing the extreme positive and negative lateral forces by the corresponding displacements in each load cycle. The stiffness values obtained from the first cycle of loading were averaged and plotted against the corresponding average of the absolute lateral force. This plot is presented in Figure B.3.5. Figure B.3.6 plots the stiffness values against the average of the absolute lateral displacement. The stiffness degradation curve was plotted up to the stage when the maximum lateral force was developed. Similar to the previous Walls 1 and 2, Wall 3 exhibited significant stiffness degradation at the beginning stages of lateral loading.

A wall stiffness of 114 kN/mm was calculated when the wall was loaded to ± 0.5 mm displacement. The wall stiffness dropped to 34 kN/mm when the maximum strength developed during the first cycle to -6 mm displacement.

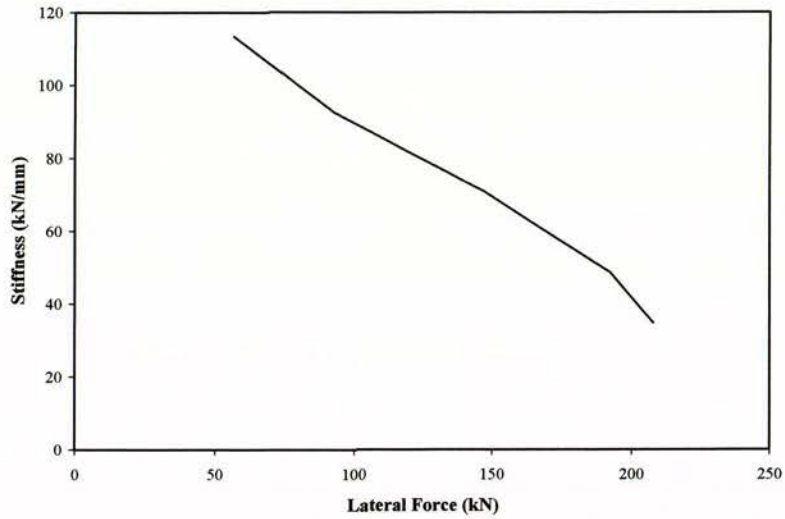


Figure B.3.5 Stiffness vs lateral force.

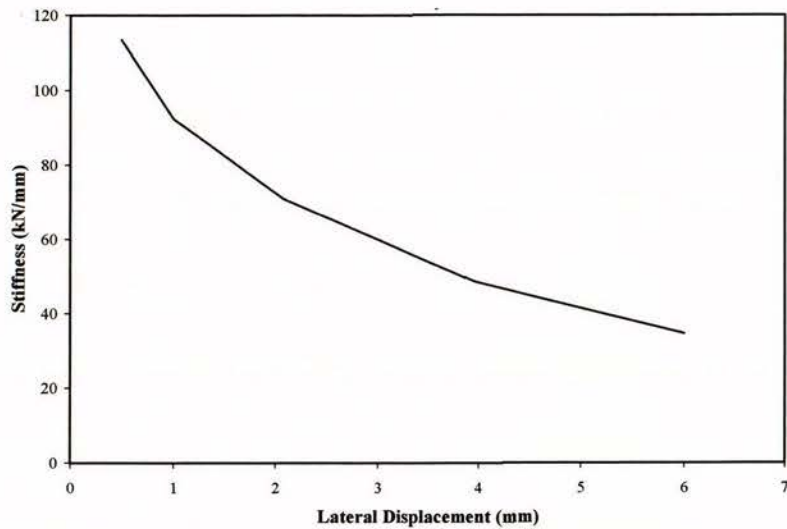


Figure B.3.6 Stiffness vs lateral displacement.

B.4 Wall 4

This section describes the laboratory testing of Wall 4. In order to study the effect of the distribution of shear reinforcement, two combinations of reinforcing bars were used in Walls 1 and 4, each combination contributing approximately the same total cross-sectional area of shear reinforcement. The two combinations were:

Wall	Shear Reinforcement	ΣA_h (mm ²)
1	5-R6	141
4	2-D10	157

The distribution of shear reinforcing bars in Wall 4 is shown in Figure B.4.1 (please see Figure B.1.1 for reinforcement details of Wall 1). The 141 mm² represents about 0.056% of the gross area of the wall. Extensive literature review suggested that closely spaced shear reinforcement (using reinforcing steels with of bar sizes) could result in a more ductile inelastic response. It was therefore expected Wall 4 to have a total shear strength approximately the same as for Wall 1, but exhibited a more rapid strength degradation behaviour.

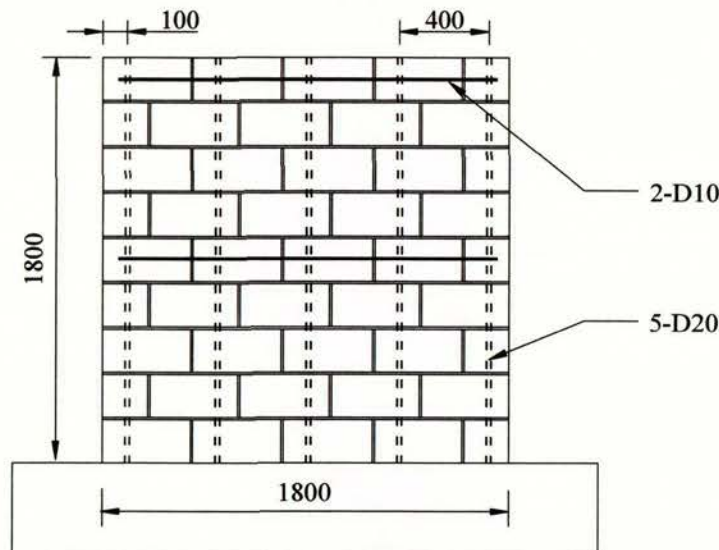


Figure B.4.1 Wall 4 reinforcement details.

Table B.4.2 Wall strength predictions

Masonry strength	Nom. Flexural strength	Masonry shear strength V_n	
f'_m	F_n	NZS4230	NEHPR
17.0	229	152	219
MPa	kN	kN	kN

B.4.1 Pre-test

Instrumentation was attached to the wall according to section 3.5.1. Wall 4 was tested approximately 33 days after construction. The wall was inspected prior to testing, and visible shrinkage cracks were found on mortar joints at the top centre of the wall. However, it was determined that the identified cracks were insignificant to cause structural damage to the wall.

B.4.2 Testing

0.5 mm push, 1st cycle

The wall developed a maximum strength of 58 kN at this displacement level. No cracking was identified.

0.5 mm pull, 1st cycle

The wall developed the same strength as for the previous push cycle when it reached the target displacement of -0.5 mm. No cracking was identified.

0.5 mm push, 2nd cycle

The wall developed a maximum strength of 54 kN for this load step. No cracking was identified.

0.5 mm pull, 2nd cycle

A maximum strength of -59 kN was recorded at a displacement of -0.51 mm. No cracking was identified.

1.0 mm push, 1st cycle

A maximum force of 84 kN was recorded. One fine horizontal crack was identified to initiate from the wall tension edge along the first mortar bed course. The crack width was about 0.15 mm, although no accurate measurement was taken. An uplift of 0.14 mm was measured at the wall heel.

1.0 mm pull, 1st cycle

The wall response mirrored that of the previous push cycle. The wall developed a maximum strength of –83 kN. An uplift of 0.2 mm was recorded.

According to the testing procedure outlined in section 3.8, the measured lateral forces recorded in the two directions of loading resulted in an average yield displacement of:

$$\Delta_y = \frac{229}{\frac{1}{2}(84 - (-83))} = 2.74 \text{ mm}$$

1.0 mm push, 2nd cycle

One new horizontal crack (about 400 mm in length) was identified on the second mortar bed layer. A maximum strength of 88 kN was measured at end of this load step.

1.0 mm pull, 2nd cycle

The wall developed a maximum strength of –85 kN, and no new cracking was identified.

2.0 mm push, 1st cycle

One new horizontal crack and extensions of the two previously formed cracks were observed at the conclusion of this loading cycle. The previously formed cracks were observed to have widened a small extent. The wall developed a maximum strength of 139 kN, accompanied by an uplift of 0.25 mm.

2.0 mm pull, 1st cycle

A maximum strength of –135 kN was measured. Three new hairline horizontal cracks were identified along the mortar bed layers. The cracks identified in the previous pull cycle extended to the centre of the wall and had widened a small extent (maximum cracks width about 0.2 mm). An uplift of 0.25 mm was measured at the tension toe.

2.0 mm push, 2nd cycle

Two new horizontal cracks were noted on the wall. No extensions of previously formed cracks were identified. A maximum strength of 132 kN was recorded.

2.0 mm pull, 2nd cycle

One new horizontal crack was identified. A maximum strength of -131 kN was recorded.

4.0 mm push, 1st cycle (see Photo 21)

The lateral force resisted by the wall increased steadily to a maximum of 183 kN at a displacement of 3.0 mm. This was immediately followed by a loss in strength (accompanied by a “splitting” noise) and an increase in displacement (from 3.0 mm to 3.7 mm) when a diagonal crack opened up suddenly and propagated across the wall. A maximum strength of 191 kN was measured when the wall was further pushed to a displacement of 4.1 mm.

Apart from the formation of the single diagonal crack, few minor extensions of previously formed horizontal cracks were observed. The diagonal crack was measured to have a maximum width of about 1.0 mm, again no accurate measurement was taken. An uplift of 0.65 mm was measured at the end of this load step.

4.0 mm pull, 1st cycle (see Photo 21)

The wall response was similar to observations made in the previous cycle. One diagonal crack initiated from the bond beam when the wall was pulled to a lateral displacement of -3.0 mm. The wall was further pulled to a displacement of -3.95 mm when another diagonal crack developed (a “splitting” noise was heard). This new crack initiated from the wall end, and crossed the centre of the wall, and ended at the wall base (giving a x-shaped diagonal crack). The formations of the second diagonal crack caused a sudden increase in displacement from -3.95 mm to -4.75 mm and a drop in wall strength from the maximum of -199 kN to -183 kN. There was sign of minor spalling of face shells along the diagonal cracks. An uplift of 0.8 mm was measured at the wall tension toe.

4.0 mm push, 2nd cycle

The wall developed a maximum strength of 177 kN at the end of this load cycle. Apart from the extensions of diagonal cracks, no new cracking was identified. The wall was measured to slide about 0.15 mm along the base.

4.0 mm pull, 2nd cycle

The wall developed a maximum strength of -163 kN at the end of this load step. No new crack or extensions of cracks were identified.

6.0 mm push, 1st cycle

The wall reached a maximum strength of 218 kN at the displacement of 6.2 mm. No new cracking was identified. The diagonal crack was measured to have widened to about 2.0 mm. Face shells along the diagonal crack showed sign of deterioration. Wall uplift and sliding were measured to be about 1.35 mm and 0.24 mm respectively.

6.0 mm pull, 1st cycle

New cracks were observed to form adjacent to the main diagonal crack, causing further deterioration of face shells. The wall reached a maximum strength of -201 kN for this load cycle, accompanied by an uplift of 0.95 mm.

6.0 mm push, 2nd cycle

The wall responded similarly to observations made in the previous push cycle. No new cracking was identified, but mortar bed at the compression toe region was noted to have crushed. A maximum strength of 203 kN was measured.

6.0 mm pull, 2nd cycle

The wall responded similarly to observations made in the previous loading cycle. Apart from a drop in strength to -184 kN, no new cracking was identified.

8.0 mm push, 1st cycle

A maximum strength of 223 kN was measured at a displacement of 8.4 mm. Minor spalling of face shells along the diagonal crack was observed. An uplift of 1.4 mm and wall sliding of 0.28 mm were measured.

8.0 mm pull, 1st cycle

The wall responded similarly to observations made in the previous pull cycle. No new cracking was identified, but the diagonal crack width was widened to a small extent. A maximum strength of –190 kN was measured, accompanied by an uplift of 1.2 mm.

8.0 mm push, 2nd cycle

No new cracks or extensions of cracks were identified. A maximum strength of 197 kN was measured for this loading cycle.

8.0 mm pull, 2nd cycle

The wall behaved similarly to observations made in the previous push cycle. The maximum diagonal crack width of about 4.5 mm was measured (although no accurate measurement was taken). A maximum strength of –163 kN was measured.

10 mm push, 1st cycle

The wall was pushed to a displacement of about 9.6 mm when sudden widening of diagonal cracks occurred, resulting in a slight loss in strength. The wall strength was measured to be 215 kN at a lateral displacement of 10.1 mm. An uplift of 1.7 mm was measured.

10 mm pull, 1st cycle

Significant spalling of masonry face shells was observed along the diagonal cracks. The maximum strength reached in this load cycle was measured to be –146 kN, and this strength corresponded to about 72% of the maximum strength achieved in the pull direction. Hence, the wall was defined as failing according to the test procedure outlined in section 3.8.

10 mm push, 2nd cycle (see Photo 22)

The wall strength increased steadily to 167 kN at a displacement of 8.4 mm, but dropped abruptly when the diagonal crack widened significantly, accompanied by a large increase in displacement. The wall finally settled at a lateral displacement of 10.6 mm with measured lateral force of 147 kN (about 66% of the maximum strength recorded in the push direction). Significant crushing of the wall compression toe was observed at the conclusion of this loading cycle.

10 mm pull, 2nd cycle (see Photo 22)

The wall developed a maximum strength of –116 kN at the end of this loading cycle. Further development of diagonal cracks and degradation of compression toe were observed.

12 mm push, 1st cycle (see Photo 23)

The wall strength (138 kN) dropped abruptly when it was push to a displacement of 11.5 mm. The sudden loss in strength was accompanied by an instantaneous increment of wall lateral displacement to 18.0 mm. Inspection of the wall revealed widely open diagonal cracks (maximum crack width about 6 mm) and severe compression toe crushing. The wall strength was measured to be 118 kN at the end of this load step.

12 mm pull, 1st cycle

A maximum strength of –106 kN for this loading cycle. No new cracking or extensions of cracks were identified.

12 mm push, 2nd cycle

The wall responded similarly to observations made in the previous pull cycle. A maximum strength of 59 kN was measured.

12 mm pull, 2nd cycle

A maximum strength of –72 kN was recorded. No new cracking was identified. Further degradation of the wall compression toe was observed. Masonry at the wall tension toe fell off and subsequently removed.

14 mm push, 1st cycle

The wall developed a maximum strength of 67 kN at the end of this loading cycle. No new cracking was identified. Further crushing of the wall compression toe was observed.

14 mm pull, 1st cycle

A maximum strength of –75 kN was recorded for this loading cycle. No new cracking was identified. Further degradation of the wall compression toe was observed.

B.4.3 Summary Behaviour

The force–displacement (F-D) curve for Wall 4 is presented in Figure B.4.2. The maximum push direction strength of 223 kN was measured during the first cycle to 8 mm displacement, and the maximum pull direction strength of –201 kN was measured during the first cycle to –6 mm displacement. As shown in Figure B.4.2, significant strength degradation took place in both directions after the wall reached its maximum strength.

The wall had a shear type of failure, this failure mode was expected because the predicted nominal flexural strength was larger than the predicted shear strength. Shear type of failure was characterised by the initiation of visible horizontal cracks at low displacement levels. As the wall was pushed/pulled to further displacement, initiation of diagonal cracking occurred when the principal stresses due to applied lateral force exceeded the tensile strength of masonry.

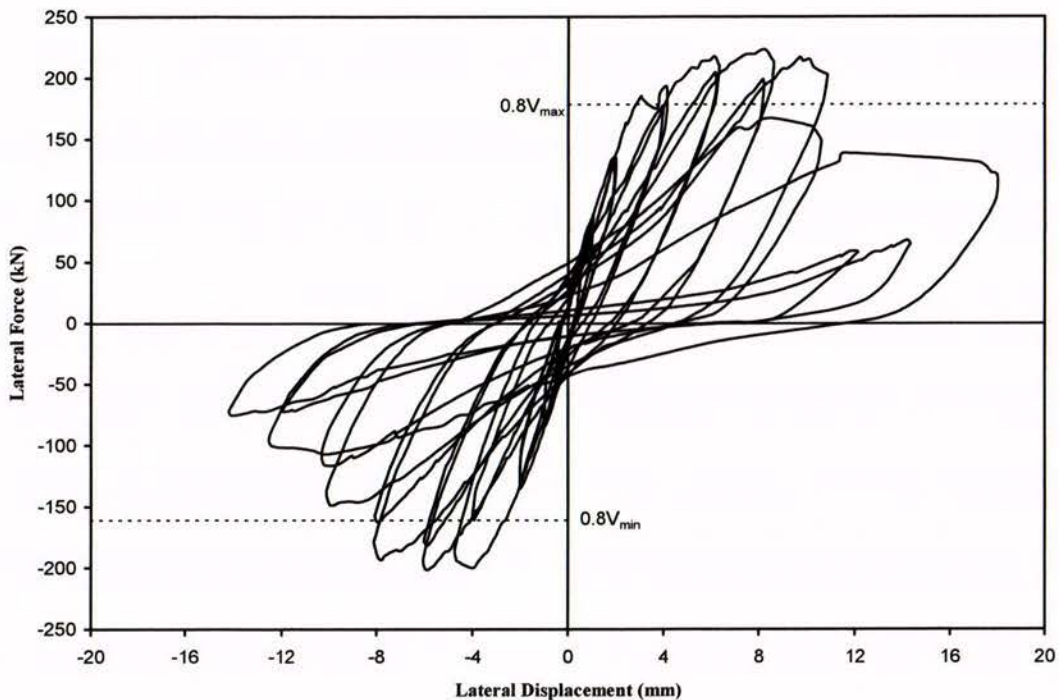


Figure B.4.2 Force-displacement history of Wall 4.

As shown in Figure B.4.2, rapid strength degradation took place immediately after the wall reached its maximum strength. It was therefore possible to classify Wall 4 as having a “brittle shear failure”. This type of shear failure was expected since Wall 4 was designed without closely distributed shear reinforcement (as compared to Wall 1), and consequently the tensile

stress due to applied shear force couldn't be adequately transferred across the diagonal cracks. Hence the cracks opened extensively, resulting in a major x-shaped diagonal crack pair, which led to a relatively sudden and destructive failure.

The yield displacement of Wall 4 was evaluated to be 2.74 mm. The wall was defined as failing during the first cycle to -10 mm displacement.

B.4.4 Force-displacement Envelope

The force-displacement envelope for Wall 4 is presented in Figure B.4.3. The plot was constructed from the peak force recorded in the first cycle for each displacement level. It can be seen that the wall strength degraded rapidly in both directions after the maximum wall strength was developed. Although Wall 4 had approximately the same amount of shear reinforcement as Wall 1, its F-D response after failure was more closely matched to that of a horizontally unreinforced wall, i.e. Wall 2.

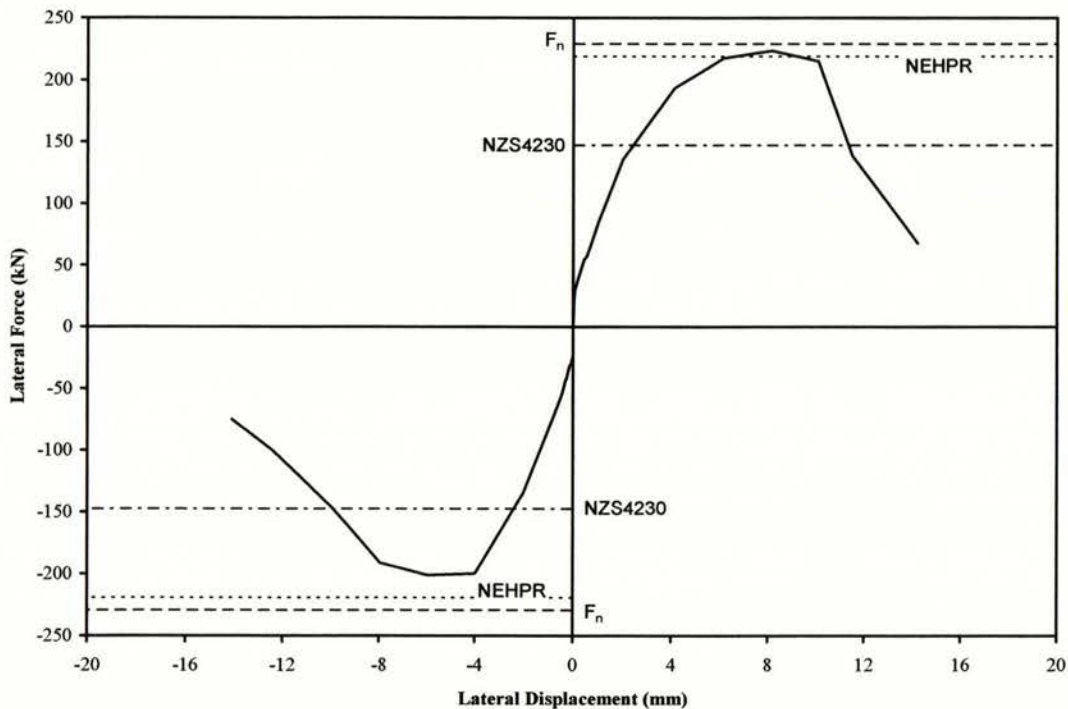


Figure B.4.3 Force-displacement envelope of Wall 4.

Figure B.4.3 shows that the shear strength predicted by NZS4230:1990 was significantly lower than the actual strength reached by the tested masonry wall.

B.4.5 Panel Displacement Components

The wall displacement was decomposed according to the procedure outlined in section 3.9 with the result presented in Figure B.4.4.

From the sliding, rocking, flexure and shear displacement components plotted in Figure B.4.4, it is seen that wall sliding was not a significant feature for this wall's behaviour. Shear displacement component increased significantly when the wall was pulled beyond -6 mm of displacement. For the push direction, the shear component increased in magnitude when the flexure and rocking displacement component remained relatively constant at a larger displacement level. Figure B.4.4 was plotted up to ± 10 mm displacement due to significant face shells spalling that occurred beyond this displacement level, which subsequently influencing the displacement transducer readings.

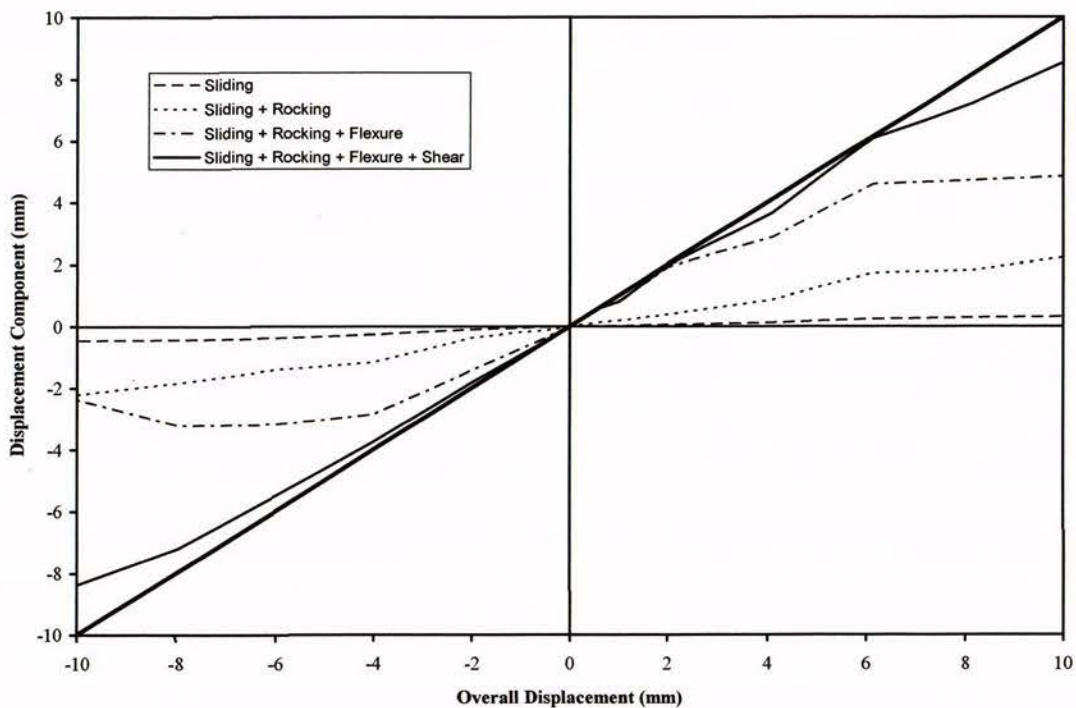


Figure B.4.4 Components of displacement.

B.4.6 Stiffness Degradation

The stiffness degradation curves for Wall 4 are presented in the two following figures. The stiffness during a loading cycle was obtained by dividing the extreme positive and negative forces by the corresponding displacements in each load cycle. The stiffness values obtained

from the first cycle of loading were averaged and plotted against the corresponding average absolute lateral force and lateral displacement. These relationships provided an indication of the sensitivity of wall stiffness with respect to the level of horizontal force, or lateral displacement. The stiffness degradation was truncated when the maximum shear strength was attained.

An initial wall stiffness of 111 kN/mm was calculated from the maximum forces measured during the first cycle to ± 0.5 mm displacement. The wall stiffness dropped to 34 kN/mm when maximum wall strength developed during the cycle to -6 mm displacement.

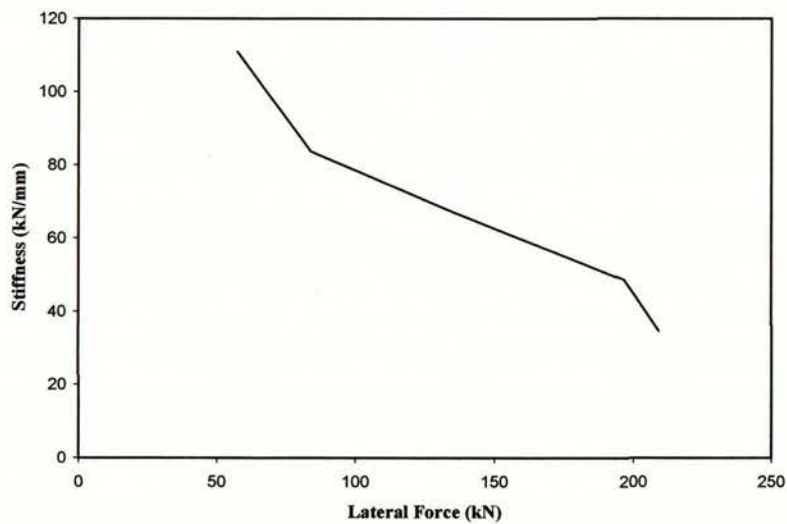


Figure B.4.5 Stiffness vs lateral force.

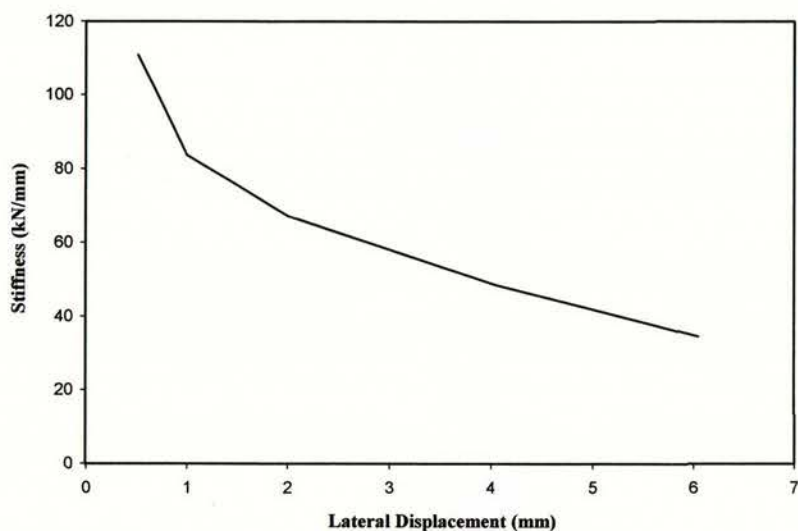


Figure B.4.6 Stiffness vs lateral displacement.

B.5 Wall 5

This section describes the testing of Wall 5, which was constructed to the same overall dimension as those of the previously reported fully grout-filled walls, but was partially grouted. As shown in Figure B.5.1, no shear reinforcement was embedded during construction and only cells containing the wall vertical reinforcing bars were grouted. The effective width of the wall used for shear calculation was about 63 mm, after discounting the width of voids. The wall was expected to exhibit shear dominated behaviour based on relatively low masonry shear strength due to partial grouting and because no horizontal shear reinforcement was employed.

Self-weight of the wall panel was calculated to be 6.8 kN. Information about wall construction, test set-up, testing procedure and data reduction may be found in Chapter 3.

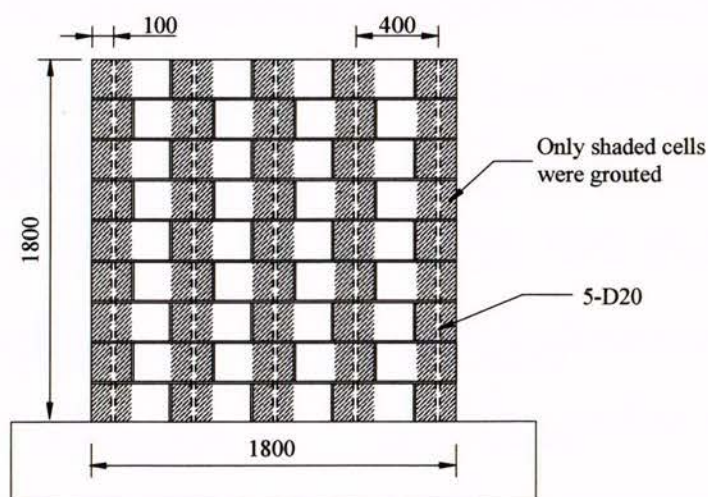


Figure B.5.1 Wall 5 construction details.

Table B.5.1 Wall strength predictions

Masonry strength	Nom. Flexural strength	Masonry shear strength V_n	
f'_m	F_n	NZS4230	NEHPR
18.5	229	50	91
MPa	kN	kN	kN

B.5.1 Pre-test

Instrumentation was attached to the wall according to section 3.5.1. Wall 5 was tested approximately 21 days after construction. The wall was inspected prior to testing. Significant structural damage was noted on the wall, on the side closest to the actuator (see Photo 25 in Appendix G). The damage was caused by accidental falling of heavy material on top of the wall, causing compressive type of cracking. The pre-test cracks were marked in green to avoid confusion with wall response during experimental testing. Due to the significant structural defects on the left side of the wall, it was determined that the wall would have significant less strength in the pull direction than in the push direction. It was therefore decided that the wall would be loaded according to the loading sequence described in section 3.8, but the strength measured in the pull direction was to be considered to be non-representative of the actual wall strength.

B.5.2 Testing

0.5 mm push, 1st cycle

The wall developed a maximum strength of 44 kN at a displacement of 0.61 mm. Fine horizontal cracks were identified along mortar bed joints, initiating from the wall edge on the tension side. The pre-test cracks (marked in green) were widened to small extent.

0.5 mm pull, 1st cycle

A maximum force of -31 kN was reached at the displacement of -0.51 mm. Three hairline horizontal cracks were identified on the mortar bed joints on the tension side.

0.5 mm push, 2nd cycle

A maximum force of 45 kN was measured at a displacement of 0.62 mm. No new crack or extensions of cracks were identified.

0.5 mm pull, 2nd cycle

A maximum strength of -33 kN was recorded at a displacement of -0.60 mm. No new cracking was identified.

1.0 mm push, 1st cycle (see Photo 26)

A maximum strength of 66 kN was recorded at a displacement of 1.35 mm. Three diagonal cracks were identified to follow the path of mortar joints (stepped form). The wall was measured to slide about 0.12 mm along the base.

Due to structural damage suffered by the wall prior to wall testing, the wall yield displacement was evaluated according to strength measured in the push direction:

$$\Delta_y = \frac{229}{66} \times 1.35 = 4.68 \text{ mm}$$

1.0 mm pull, 1st cycle (see Photo 26)

The response of the wall mirrored that of the previous push cycle. A maximum strength of –50 kN was recorded at a displacement of –1.20 mm.

1.0 mm push, 2nd cycle

The wall responded similarly to observations made in the previous push cycle. No new cracking was identified. A maximum strength of 51 kN was recorded at the end of this load step.

1.0 mm pull, 2nd cycle

The wall developed a maximum strength of –47 kN at a displacement of –1.30 mm. No new cracking was identified.

2.0 mm push, 1st cycle

Minor extensions of previously formed diagonal cracks were observed. The wall developed a maximum strength of 93 kN, accompanied by a wall sliding of 0.20 mm.

2.0 mm pull, 1st cycle

Following loading to –2.0 mm displacement, there was a small increase in the number of diagonal cracking, with a maximum crack width of about 0.2 mm (although no accurate measurement was taken). The wall developed a maximum strength of –66 kN.

2.0 mm push, 2nd cycle

The wall responded similarly to observations made in the previous push cycle. No new cracking was identified. A maximum force of 73 kN was measured at the end of this load step.

2.0 mm pull, 2nd cycle

Minor elongations of horizontal cracks that had formed in the previous pull cycle. A maximum strength of -56 kN was measured.

4.0 mm push, 1st cycle

The wall developed a maximum strength of 120 kN, exceeding the calculated shear strength of 91 kN shown in Table B.5.1. Extensions of diagonal cracks were noted to take place at wall centre, with a maximum crack width of about 1.0 mm. Wall sliding of 0.22 mm was measured along the base.

4.0 mm pull, 1st cycle

The wall response mirrored that of the previous loading cycle, and new cracks were identified at wall centre. The wall developed a maximum strength of -88 kN, with a corresponding wall sliding of -0.17 mm.

4.0 mm push, 2nd cycle

The wall responded similarly to observations made in the previous push cycle. No new cracking was detected. A maximum strength of 110 kN was measured.

4.0 mm pull, 2nd cycle

No new cracking was detected at the completion of this loading step. A maximum strength of -83 kN was measured.

6.0 mm push, 1st cycle

More diagonal cracks were observed to form at the centre of the wall, and the diagonal cracks were noted to extend to the wall compression toe. A maximum strength of 141 kN was measured, with a corresponding wall sliding of 0.12 mm.

6.0 mm pull, 1st cycle

On the first cycle to this displacement, there were new diagonal cracks identified at the centre of the wall. The wall developed a maximum strength of -117 kN in this direction of loading, exceeding the calculated shear strength. A wall sliding of -0.24 mm was measured at the end of this load step.

6.0 mm push, 2nd cycle

The wall was pushed to 6.6 mm in the positive direction with a corresponding force of 136 kN. Widening of cracks that formed in the previous cycles was observed, but no new cracks or extensions of cracks were detected.

6.0 mm pull, 2nd cycle

The wall developed a maximum strength of -114 kN at the conclusion of this loading cycle. The diagonal cracks were sufficiently wide to allow the penetration of daylight. No new crack or extensions of cracks were identified.

8.0 mm push, 1st cycle

A maximum strength of 143 kN was measured at this load step. Further widening of diagonal cracks caused degradation of wall compression toe. Sliding of the wall along the base was measured to be about 0.13 mm, accompanied by an uplift of 0.6 mm at the tension toe.

8.0 mm pull, 1st cycle

The first spalling of face shell was observed at the conclusion of this loading cycle, creating a void of about 20 mm. The wall developed a maximum strength of -134 kN for this load step. Wall sliding and uplift (at tension toe) were measured to be about -0.25 mm and 0.4 mm respectively.

8.0 mm push, 2nd cycle

A maximum strength of 124 kN was measured. No new cracks or cracks elongation were observed. Further degradation of masonry along diagonal cracks and degradation of wall compression toe, were observed.

8.0 mm pull, 2nd cycle

A maximum strength of –107 kN was measured. No new cracking was identified, but further widening of diagonal cracks was observed.

10 mm push, 1st cycle

Further widening of diagonal cracks caused significant spalling of masonry face shells. Significant crushing of compression toe was also observed. The wall developed a maximum strength of 124 kN, accompanied by wall sliding and uplift of 0.12 mm and 0.70 mm respectively.

10 mm pull, 1st cycle

In this direction of loading, the wall developed a maximum strength of –111 kN. The diagonal cracks were further widened (maximum crack width about 10 mm), but with little additional new cracking. Further face shells spalling was observed.

10 mm push, 2nd cycle (see Photo 27)

The wall reached a maximum strength of 103 kN at the end of this loading cycle. The widening of diagonal cracks caused further degradation of compression toe and CMUs at the centre of the wall. Immediately after pressure release, significant amount of (ungrouted) face shell spalled off.

The maximum strength reached in this cycle corresponded to 72% of the maximum strength recorded in the push direction. Therefore the wall was defined as failing according to the test procedure outlined in section 3.8.

10 mm pull, 2nd cycle (see Photo 27)

The wall developed a maximum strength of –91 kN for this load cycle (about 68% of the maximum strength recorded in the pull direction). No new cracking was identified, but further widening of diagonal cracks were noted. Masonry in the wall tension toe spalled off at the end of this load excursion cycle.

12 mm push, 1st cycle

The wall behaved similarly to observations made in the previous push cycle. A maximum strength of 109 kN was measured accompanied by a wall sliding of 0.11 mm.

12 mm pull, 1st cycle

A maximum strength of -89 kN. No new cracking was identified.

12 mm push, 2nd cycle (see Photo 28)

During this semi-cycle of loading, there was initially a developed strength of 88 kN (at a displacement of 11.5 mm), until the main diagonal crack widened up suddenly (accompanied by a “splitting” noise), resulting in an instant displacement increase and a corresponding loss in strength. The wall finally settled at 12.9 mm with a corresponding strength of 78 kN. Significant amount of face shell spalling was observed.

12 mm pull, 2nd cycle (see Photo 28)

The wall developed a maximum strength of -69 kN for this load excursion cycle. Further spalling of face shell was observed.

14 mm push, 1st cycle

A maximum wall strength of 84 kN was measured for this load excursion cycle. No new cracking was detected, but significant widening of diagonal cracks was observed.

14 mm pull, 1st cycle

The wall behaved similarly to observations made in the previous push cycle. A maximum strength of -72 kN was recorded.

14 mm push, 2nd cycle

Further widening of diagonal cracks were observed. A maximum strength of 66 kN was recorded for this loading cycle.

14 mm pull, 2nd cycle

A maximum strength of -53 kN was recorded. No new cracking was identified.

B.5.3 Summary Behaviour

The force-displacement history of Wall 5 is shown in Figure B.5.2. The wall exhibited shear response, signified by the opening of large diagonal shear cracks across the wall face. The diagonal cracks were initiated by tension splitting of masonry in the compression strut that formed in the wall. Horizontal cracking (flexural response) was observed at lower displacement levels, before the onset of shear cracking. The wall was expected to exhibit shear dominated behaviour based on relatively low masonry shear strength, due to partial grouting and no because horizontal shear reinforcement was employed

Diagonal cracking initiated at the displacement level of ± 2 mm. The initiation of diagonal cracking did not cause immediate strength loss. The wall strength continued to develop until a maximum push direction strength of 143 kN and maximum pull direction strength of -134 kN were measured during the first cycle of ± 8 mm displacement. As shown in Figure B5.2, rapid strength degradation took place after the wall developed its maximum strength. This phenomenon is particularly obvious in the pull direction.

The yield displacement (Δ_y) for this partially grouted wall was evaluated to be 4.68 mm. The wall was defined as failing during the second push cycle to 10 mm displacement.

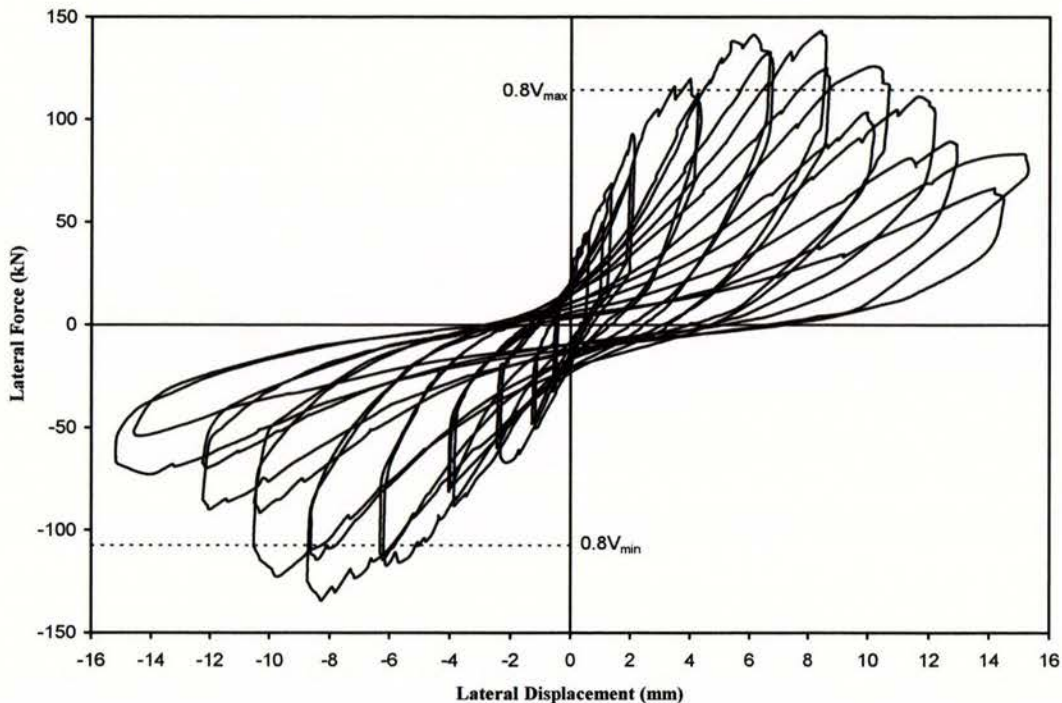


Figure B.5.2 Force-displacement behaviour of Wall 5.

B.5.4 Force-displacement Envelope

Figure B.5.3 shows the force-displacement envelope of the tested wall. The plot was constructed from the peak force recorded in the first cycle for each displacement level. It is seen that the wall strength degraded rapidly after maximum strength was attained at ± 8 mm displacement in both directions of loading.

It is clearly shown in Figure B.5.3 that the masonry shear strength predicted by the New Zealand masonry design standard, NZS4230:1990, was significantly lower than the actual shear strength achieved by the masonry wall.

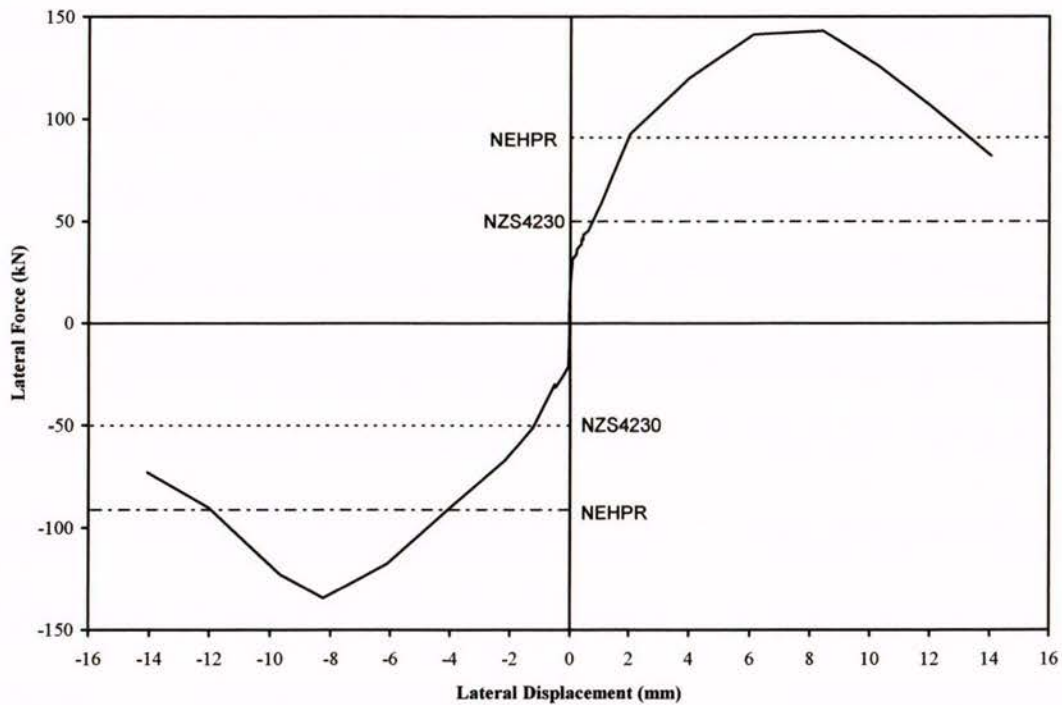


Figure B.5.3 Force-displacement envelope of Wall 5.

B.5.5 Panel Displacement Components

The total horizontal displacement was decomposed into four deformation components according to procedure outlines in section 3.9 with the results shown in Figure B.5.4.

From the sliding, rocking, flexure and shear displacement components plotted in Figure B.5.4, it is seen that shear displacement was the most dominant deformation mode at large displacement levels. The flexural and rocking displacement constituted about 40% of the total

horizontal displacement when the wall was loaded to ± 8 mm displacement, while the sliding displacement mode was negligible throughout the test.

Figure B.5.4 provides an indication of the relative size of each component for various stages of the displacement envelope until the displacement of ± 8 mm. It is noted that the summed up deformation (sliding + rocking + flexure + shear) nearly add up to match the overall displacement measured at the top of the wall.

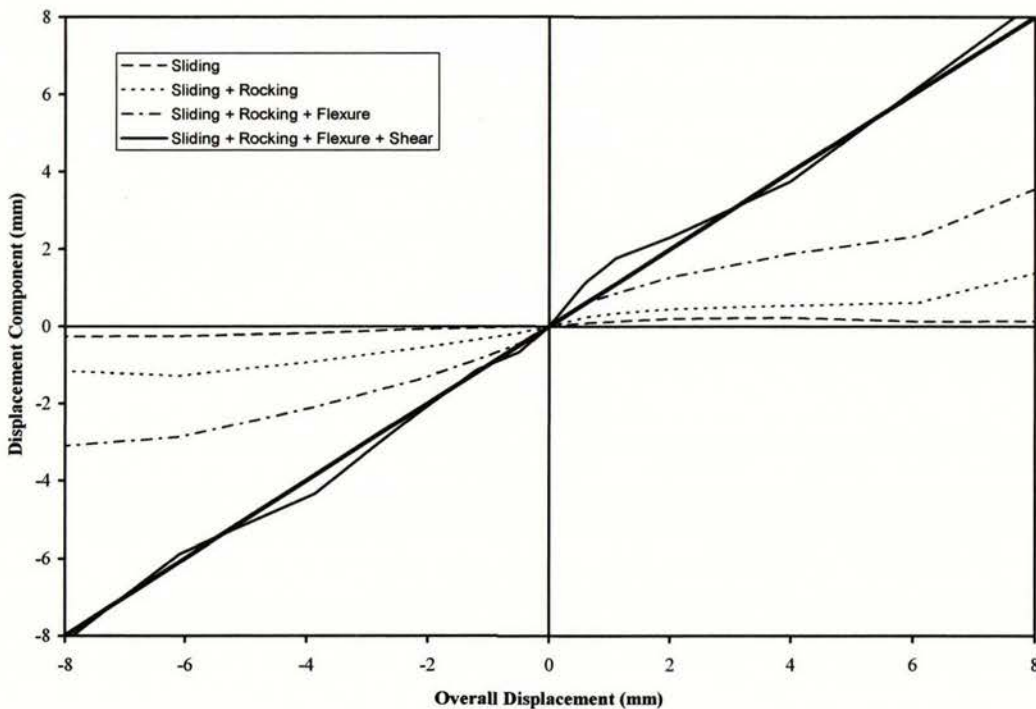


Figure B.5.4 Components of displacement.

B.5.6 Stiffness Degradation

Figures B.5.5 and B.5.6 plot the stiffness values obtained from the first cycle of loading against the lateral force and displacement respectively. The stiffness during a loading cycle was obtained by dividing the extreme positive lateral force by the corresponding displacement in each load cycle. Both stiffness degradation curves in Figures B.5.5 and B.5.6 were truncated when the maximum shear strength was attained.

A wall stiffness of 74 kN/mm was calculated during the first cycle to positive 0.5 mm displacement. However, the stiffness dropped to 17 kN/mm when the wall developed its maximum strength during the first push cycle to 8 mm displacement.

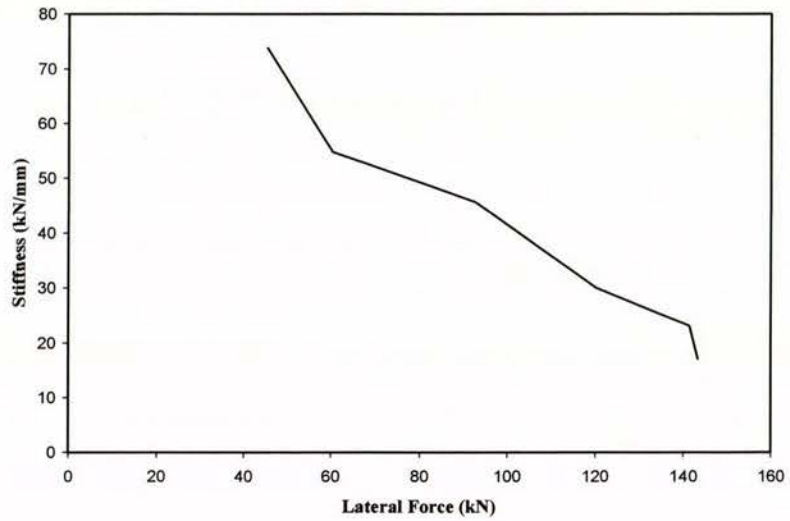


Figure B.5.5 Stiffness vs lateral force.

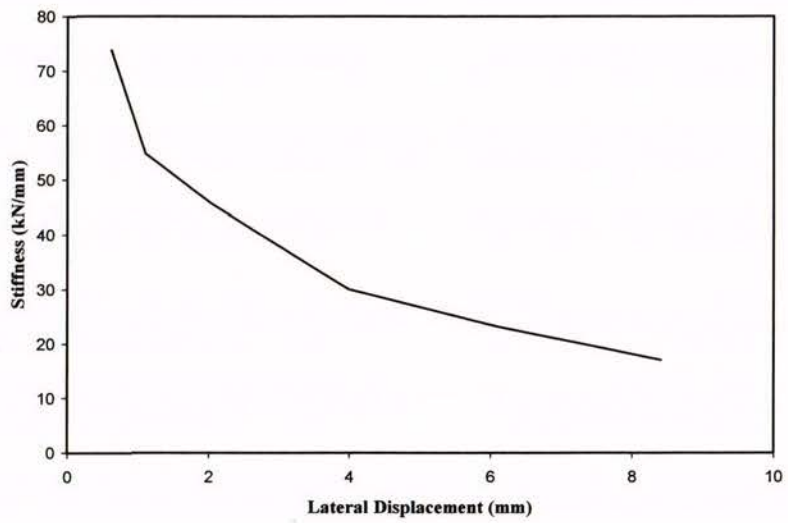


Figure B.5.6 Stiffness vs lateral displacement.

B.6 Wall 6

This section describes the testing of Wall 6 which was constructed similar to the partially grout-filled Wall 5, but was reinforced with 3-D20 oriented vertically and spaced at 800 mm c/c. As shown in Figure B.6.1, no shear reinforcement was embedded during construction and only cells containing the wall vertical reinforcing bars were grouted. The effective width of the wall used for shear calculation was about 63 mm, after discounting the width of voids. The wall was expected to exhibit shear dominated behaviour based on relatively low masonry shear strength due to partial grouting and because no horizontal shear reinforcement was employed.

Self weight of the wall panel was calculated to be 5.2 kN. Information about wall construction, test set-up, testing procedure and data reduction may be found in Chapter 3. Prism testing confirmed masonry compressive strength, $f'_m = 18.5$ MPa. It was noted that f'_m is only valid for the grouted cells, i.e. both end cells and the centre cell shown in Figure B.6.1. The f'_m applies to calculation of flexural strength, but was also used for shear strength calculation.

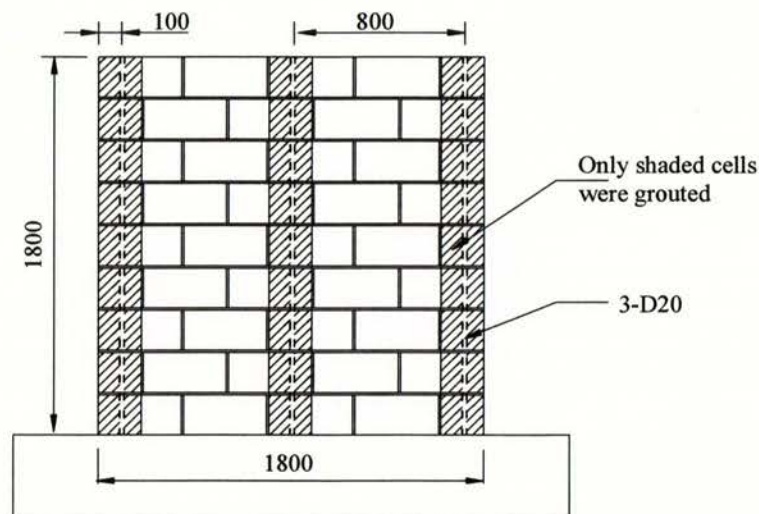


Figure B.6.1 Wall 6 construction details.

Nominal flexural and masonry shear strength were predicted according to section 3.5 for a partially grout-filled concrete masonry wall with the results presented in Table B.6.1:

Table B.6.1 Wall strength predictions

Masonry strength	Nom. Flexural strength	Masonry shear strength V_n	
f'_m	F_n	NZS4230	NEHPR
18.5	142	50	91
MPa	kN	kN	kN

B.6.1 Pre-test

Instrumentation was attached to the wall according to section 3.5.1. Wall 6 was tested approximately 26 days after construction. The wall was inspected prior to testing, with no cracks or structural defect being identified.

B.6.2 Testing

0.5 mm push, 1st cycle

The wall developed a maximum strength of 19 kN when it was pushed to a displacement of 0.53 mm. No cracking was identified.

0.5 mm pull, 1st cycle

A maximum strength of -21 kN was reached at the displacement of -0.60 mm. No cracking was detected.

0.5 mm push, 2nd cycle

A maximum strength of 19 kN was measured at a displacement of 0.52 mm. Again no cracking was identified.

0.5 mm pull, 2nd cycle

A maximum strength of -20 kN was recorded at a displacement of -0.62 mm. There was no evidence of any cracking.

1.0 mm push, 1st cycle

A maximum strength of 35 kN was recorded at the displacement of 1.20 mm. Three hairline horizontal cracks were identified along the mortar joints on the tension side.

1.0 mm pull, 1st cycle

The wall developed a maximum strength of -29 kN at the displacement of -1.0 mm. Significant diagonal cracking (maximum crack width about 0.50 mm) initiated with the cracks following the mortar joints, giving the stepped form shape. These diagonal cracks initiated from the upper left and ended at the wall centre. This crack pattern suggested that the cracking was arrested to a certain degree by the grouted cell at the wall centre.

According to procedure outlined in section 3.8, the measured lateral force for the two directions of loading resulted in an average yield displacement of:

$$\Delta_y = \frac{1}{2} \left[\left(\frac{142}{35} \times 1.3 \right) + \left(\frac{142}{-29} \times -1 \right) \right] = 5.09 \text{ mm}$$

1.0 mm push, 2nd cycle

The wall responded mirrored that in the previous pull cycle. Four new diagonal cracks were identified when the wall was accidentally pushed to a displacement of 1.6 mm. A maximum strength of 39 kN was measured.

1.0 mm pull, 2nd cycle

The wall developed a maximum strength of -27 kN at the end of this load step. No new cracking was identified.

2.0 mm push, 1st cycle

Minor extensions of diagonal cracks were identified. A maximum strength of 46 kN was recorded with a corresponding wall sliding of 0.11 mm. The diagonal cracks were widened to a small extent.

2.0 mm pull, 1st cycle

Two new diagonal cracks were identified, accompanied by the widening of previously formed cracks. The mortar showed first sign of crushing. A maximum strength of -46 kN was recorded for this load excursion cycle.

2.0 mm push, 2nd cycle

The wall responded similarly to observations made in the previous push cycle. No new crack was identified. A maximum strength of 44.5 kN was recorded.

2.0 mm pull, 2nd cycle

On the second cycle to this displacement level there was no new crack identified. A maximum wall strength of -43 kN was recorded.

4.0 mm push, 1st cycle (see Photo 29)

Significant amount of new diagonal cracks developed when the wall was pushed to a displacement of 3.6 mm. The crack pattern now had the form of descending from the top right corner (tension side) to the bottom left (compression side). The wall developed a maximum strength of 68 kN when loading stopped at a displacement of 4.1 mm. Cracks on mortar joints were sufficiently wide to permit the penetration of daylight. The compression zone remained undamaged indicating that strength loss was still premature at this stage.

4.0 mm pull, 1st cycle (see Photo 29)

The wall response mirrored that of the previous pull cycle with further opening of diagonal cracks. No new crack was identified. The wall developed a maximum strength of -65 kN for this loading cycle. The wall condition at this stage is shown in Photo 29.

4.0 mm push, 2nd cycle

The wall developed a maximum strength of 62 kN at a displacement of 4.3 mm. No new cracking was identified.

4.0 mm pull, 2nd cycle

No new cracking was detected at the completion of this loading step. A maximum strength of -61 kN was measured.

6.0 mm push, 1st cycle

A maximum strength of 85 kN was measured in the first cycle to this displacement level. The diagonal crack pattern identified in the previous push excursion cycle developed further with

crack width up to 2 mm. Minor sliding of horizontal bed joints was observed. Wall sliding at the base was measured to be about 0.15 mm.

6.0 mm pull, 1st cycle

On the first cycle to this displacement level, no new cracking was identified. It was however noticed that the diagonal cracks formed in the previous pull cycles were widened to small extent. A maximum strength of -82 kN was measured with a corresponding wall sliding of -0.12 mm.

6.0 mm push, 2nd cycle

The wall responded similarly to observations made in the previous push cycle and further opening of diagonal cracks were observed. A maximum strength of 79 kN was measured for this load excursion cycle.

6.0 mm pull, 2nd cycle

The wall developed a maximum strength of -71 kN at the conclusion of this loading cycle. The wall response mirrored that of the previous pull cycle with further widening of the diagonal cracks up to 4 mm.

8.0 mm push, 1st cycle

A maximum force of 93 kN was measured for this load step, exceeding the estimated shear strengths presented in Table B.6.1. Further development of diagonal cracks were noted. Tapping of face shell in the compression toe region gave a “solid” sound, indicating that the toe was still “strong”. A wall sliding of 0.15 mm was measured.

8.0 mm pull, 1st cycle

The response of the wall mirrored that of the previous push cycle. The wall developed a maximum strength of -91 kN with a corresponding wall sliding of -0.15 mm. Further opening of diagonal cracks were observed, with crack width up to 4.5 mm (although no accurate measurement was taken).

8.0 mm push, 2nd cycle

The wall developed a maximum strength of 83 kN on the second cycle to this displacement. No new cracking was identified.

8.0 mm pull, 2nd cycle

A maximum strength of -82 kN was measured. No new cracking was identified, but further widening of diagonal cracks was observed.

10 mm push, 1st cycle

There was spalling of the crushed mortar due to grinding action. The diagonal cracks opened up further to approximately 6.2 mm. A maximum strength of 92 kN was measured with a corresponding wall sliding of 0.15 mm. There was no clear sign of distress in the compression toe.

10 mm pull, 1st cycle

In this direction, the wall developed a maximum strength of -93 kN. The diagonal cracks formed in the previous cycles were further widened, and few new cracking were observed. The overall wall performance was still very satisfactory at this stage.

10 mm push, 2nd cycle

The wall responded similarly to observations made in the previous push cycle. Significant amount of mortar spalled off due to grinding action. A maximum strength of 75 kN was measured.

10 mm pull, 2nd cycle

The wall strength dropped to -80 kN for this load cycle. No new cracking was identified, but further widening of diagonal cracks and crushing of mortar were observed.

12 mm push, 1st cycle

The wall behaved similarly to observations made in the previous push cycle. A maximum force of 88 kN was measured, accompanied by a wall sliding of 0.15 mm.

12 mm pull, 1st cycle

A maximum force of -88 kN was measured for this load step. The first sign of face shells spalling along the diagonal cracks were observed. The compression toe region remained relatively intact at this stage.

12 mm push, 2nd cycle

The wall responded similarly to observations made in the previous pull cycle. There was no evidence to indicate any significant distress in the compression toe region. A maximum strength of 77 kN was recorded.

12 mm pull, 2nd cycle

The wall developed a maximum strength of -73 kN for this load excursion cycle. No new cracking, but further widening of diagonal cracks was identified.

14 mm push, 1st cycle

On the first cycle to this displacement level, the wall developed a maximum strength of 83 kN. Little strength degradation was observed when compared to the maximum strength recorded in the first push cycle to 12 mm displacement. Further opening of diagonal cracks and continue degradation of face shells was observed.

14 mm pull, 1st cycle

The wall behaved similarly to observations made in the previous push cycle. Additionally, further crushing of mortar beds due to grinding action was observed. A maximum strength of -76 kN was recorded.

14 mm push, 2nd cycle

The wall response mirrored that of the previous push cycle. Further opening of diagonal cracks caused significant spalling of face shells. A maximum strength of 74 kN was recorded for this load cycle.

14 mm pull, 2nd cycle

A maximum strength of -66 kN was recorded for this load cycle. This strength corresponded to about 73% of the maximum strength measured in the pull direction. Therefore the wall was

defined as failing according to the test procedure outlined in section 3.8. The wall responded similarly to observations made in the previous push cycle, spalling of face shells along the diagonal cracks was observed.

16 mm push, 1st cycle (see Photo 30)

During this semi-cycle of loading, the diagonal cracks grew in width when lateral loading was stopped at 16 mm displacement (with a measured force of 60 kN). The opening of diagonal cracks resulted in a significant displacement increase and a corresponding loss in strength. The wall finally settle at a displacement of 18 mm with a corresponding strength of 50 kN (this strength corresponded to about 54% of the maximum strength recorded in the push direction). Inspection of wall revealed a maximum crack width of approximately 8 mm.

16 mm pull, 1st cycle (see Photo 30)

The response was similarly to that of the previous pull excursion with further spalling of face shells. A maximum load of -64 kN was measured.

16 mm push, 2nd cycle A maximum strength of 49 kN was measured for this load excursion. The wall responded similar to that of the previous pull cycle.

16 mm pull, 2nd cycle

A maximum strength of -53 kN was recorded. Further widening of diagonal cracks was observed. The test was terminated at this stage since the wall strength had significantly degraded.

B.6.3 Summary Behaviour

The hysteresis response of Wall 6 is presented in Figure B.6.2. The wall exhibited shear response, signified by the opening of large diagonal shear cracks across the wall face. These diagonal cracks initiated when the principal tensile stresses exceeded the tensile strength of masonry under increasing imposed horizontal displacements. Similar to Wall 5, Wall 6 was expected to exhibit shear dominated behaviour based on relatively low masonry shear strength due to partial grouting and because no horizontal shear reinforcement was employed

Diagonal cracking initiated during the first displacement cycle to -1 mm. The initiation of diagonal cracking did not cause immediate loss of strength. The wall strength continued to develop until a maximum push direction strength of 93 kN and maximum pull direction strength of -93 kN were measured in the first cycle to +8 mm and -10 mm displacements.

The yield displacement of Wall 6 was evaluated to be 5.09 mm. The wall was defined as failing during the second cycle to -14 mm displacement.

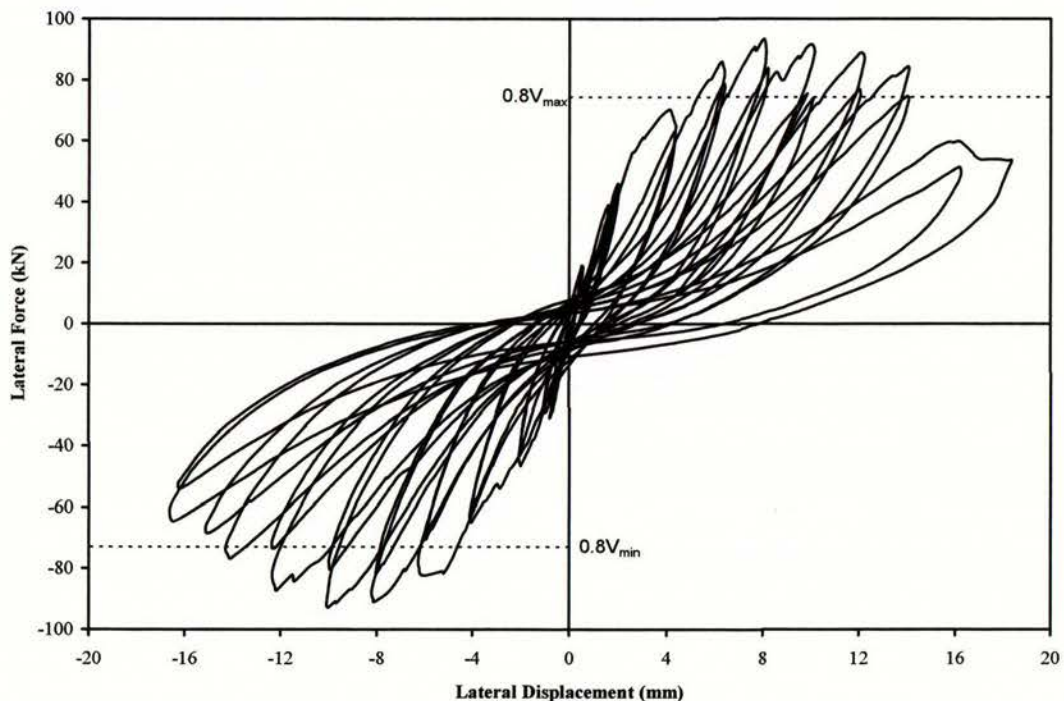


Figure B.6.2 Force-displacement behaviour of Wall 6.

B.6.4 Force-displacement Envelope

Figure B.6.3 shows the force-displacement envelope of the tested wall. The plot was constructed from the peak force recorded in the first cycle for each displacement level. The figure shows that the maximum shear strength achieved by the wall was almost twice the strength allowed by NZS4230:1990. This further proves that the current New Zealand masonry standard is conservative in predicting masonry shear strength.

Additionally, Figure B.6.3 shows the shear strength predicted by NEHPR was closely matched with the actual strength developed by the partially grouted-filled masonry wall.

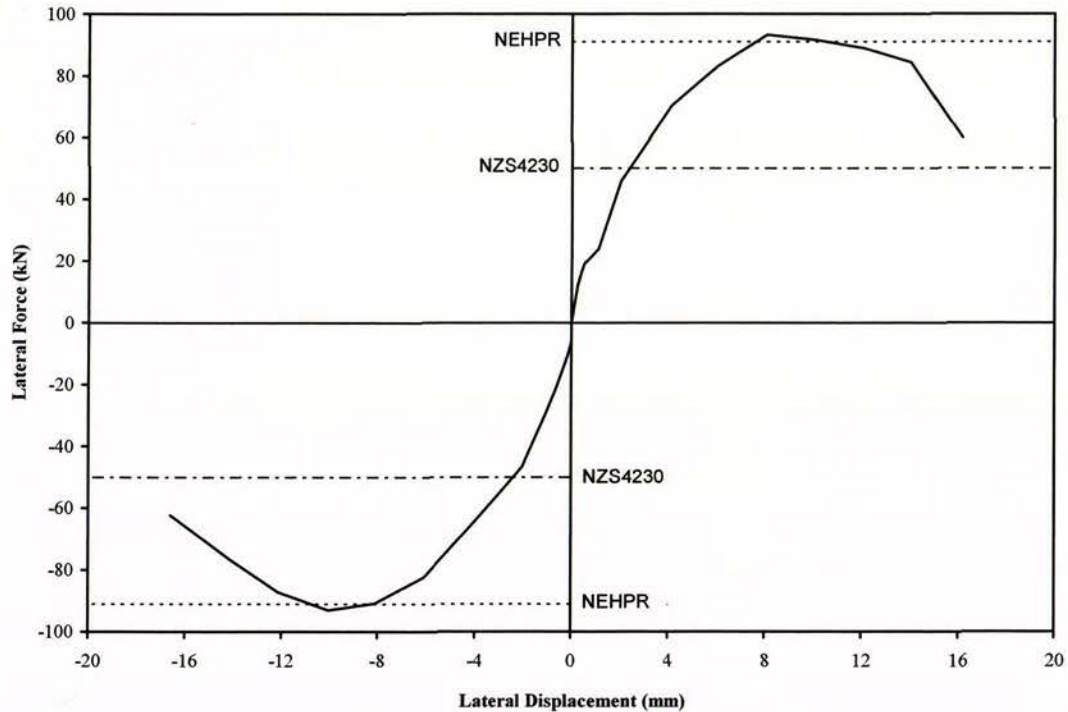


Figure B.6.3 Force-displacement envelope of Wall 6.

B.6.5 Panel Displacement Components

The total horizontal displacement was decomposed into four displacement components according to procedure outlines in section 3.9 with the results shown in Figure B.6.4.

From the sliding, rocking, flexure and shear displacement components plotted in Figure B.6.4, it is seen that shear deformation was the most dominant displacement mode at large displacement levels, and the sliding and rocking displacements were negligible throughout the test. The shear mode of displacement accounted for about 75% of the total horizontal displacement when the wall was loaded to ± 12 mm displacement. Sliding and rocking modes of deformation were insignificant throughout the test.

It is noted the summed up displacement (sliding + rocking + flexure + shear) did not add up to match the overall displacement measured at the top of the wall.

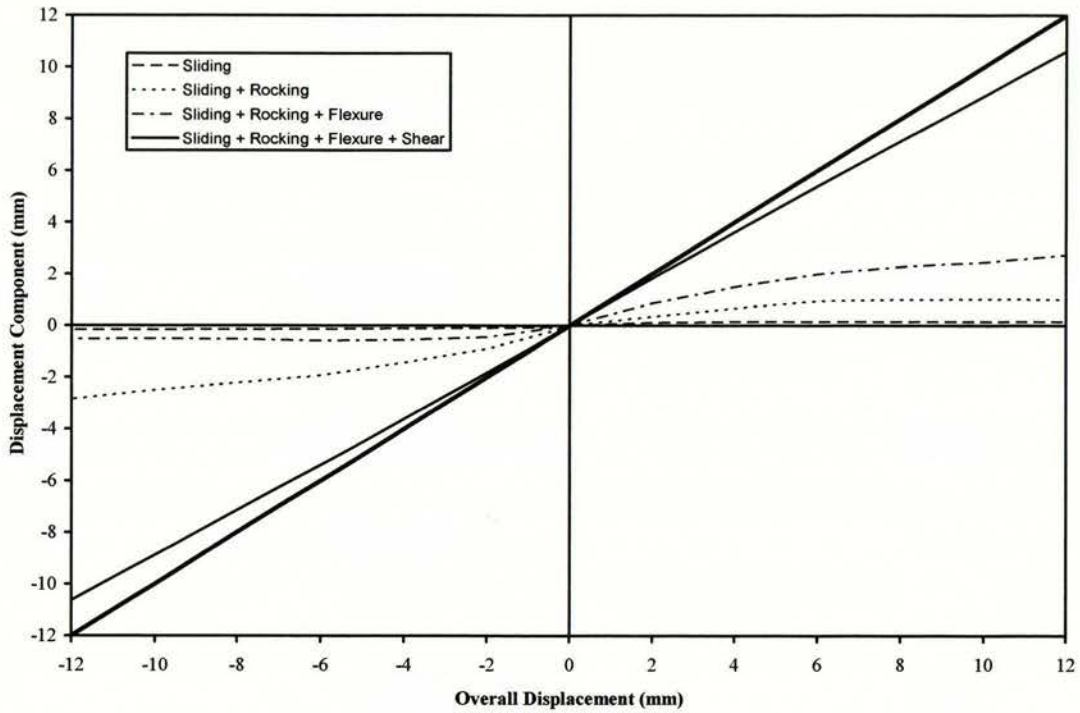


Figure B.6.4 Components of displacement.

B.6.6 Stiffness Degradation

The stiffness during a loading cycle was obtained by dividing the extreme positive and negative lateral forces by the corresponding displacements in each load cycle. The stiffness values obtained from the first cycle of loading were averaged and plotted against the corresponding average absolute lateral force, this plot is presented in Figure B.6.5. Figure B.6.6 plots the stiffness values against the average absolute lateral displacements. Stiffness degradation curve was plotted up to the stage when the maximum strength was developed.

A wall stiffness of 35 kN/mm was calculated at the first cycle to ± 0.5 mm displacement. However, the stiffness dropped to 11 kN/mm when the wall developed its maximum strength in the first push cycle to +8 mm displacement.

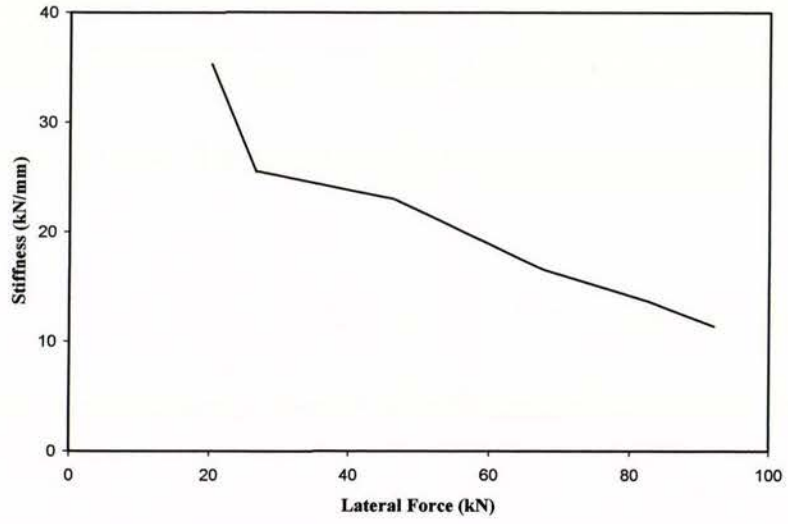


Figure B.6.5 Stiffness vs lateral force.

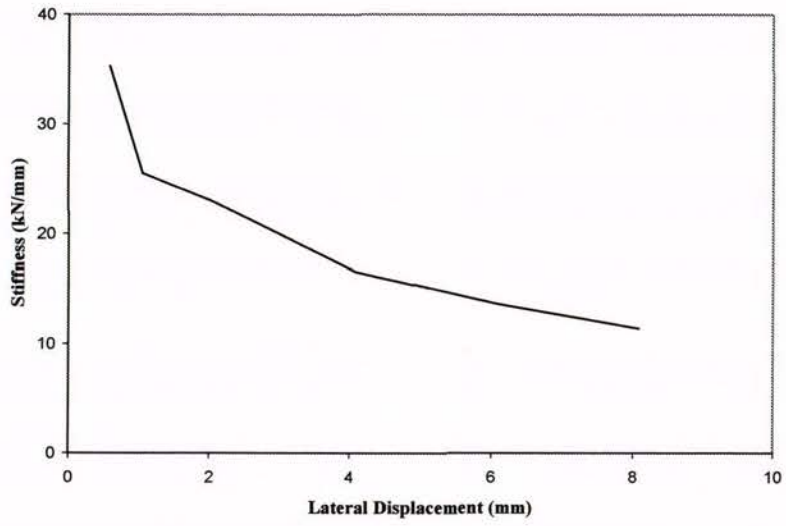


Figure B.6.6 Stiffness vs lateral displacement.

B.7 Wall 7

This section describes the testing of Wall 7 that was constructed to the same overall dimensions as Wall 1, but was subjected to an axial compression stress of 0.5 MPa. As shown in Figure B.7.1, shear reinforcement consisting of R6 steel bars were embedded during construction with a vertical spacing of 400 mm c/c. The wall was fully grout-filled and constructed of 15 series CMUs which resulted in an effective wall thickness of 140 mm.

Self weight of the wall panel was calculated to be 8.4 kN. Information about wall construction, testing procedure and data reduction may be found in Chapter 3. The test set-up adopted in the testing of Wall 7 was similar to that described in Chapter 3, but with two 1.5 m long 250 x 90 steel channels (hereinafter called strong beam), attached and tightened together using M20 bolts, and sat on top of the loading beam in order to provide proper transfer of axial compressive stress of 0.5 MPa (126 kN) into the entire wall. The axial compression force was applied to the wall through the action of 2 pairs of high strength 23 mm diameter VSL prestressing bars incorporated at the locations shown in Figure B.7.2 (or see Photo 31 in Appendix G). The rocker beam which was balanced across the strong beam ensured that the pull down force in the prestressing bars on either side of the wall were equal. Each prestressing bar passed through a 1 kN/mm coil spring placed between the rocker beam and a load cell. The load cells enabled the magnitude of tension forces in the prestressing bars to be monitored throughout the test. The prestressing bars were tensioned by tightening nuts above the load cells. The primary objective of using springs in the test set-up was to maintain an approximately constant vertical force during the test, when the wall was displaced horizontally.

The wall flexural and shear strength were predicted according to section 3.5 for a fully grout-filled concrete masonry wall with results presented in Table B.7.1. The wall was expected to exhibit a shear dominated behaviour since the wall had a shear strength that was lower than its flexural strength.

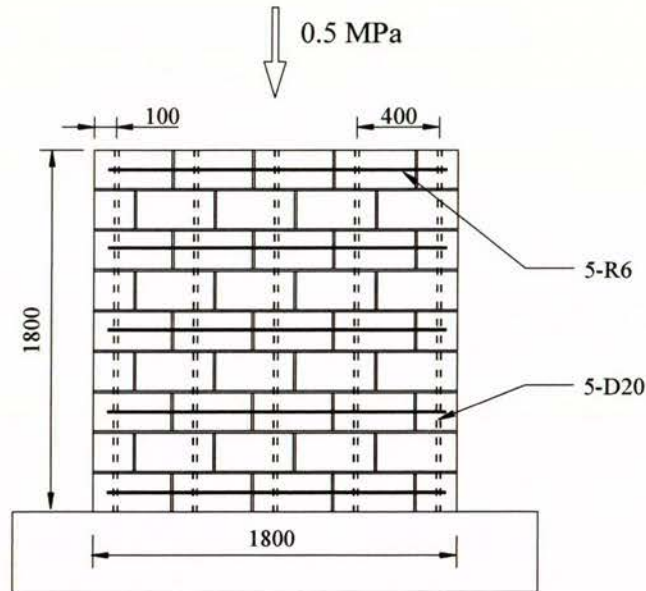


Figure B.7.1 Wall 7 construction details.

Table B.7.1 Wall strength predictions

Masonry strength	Nom. Flexural strength	Masonry shear strength V_n	
f'_m	F_n	NZS4230	NEHPR
18.8	282	176	256
MPa	kN	kN	kN

B.7.1 Pre-test

Instrumentation was attached to the wall according to section 3.5.1. Wall 7 was tested approximately 19 days after construction. The wall was inspected prior to testing. No severe cracks or structural defects were identified.

B.7.2 Testing

0.5 mm push, 1st cycle

The wall developed a maximum strength of 69 kN at a displacement of 0.61 mm. No cracking was identified.

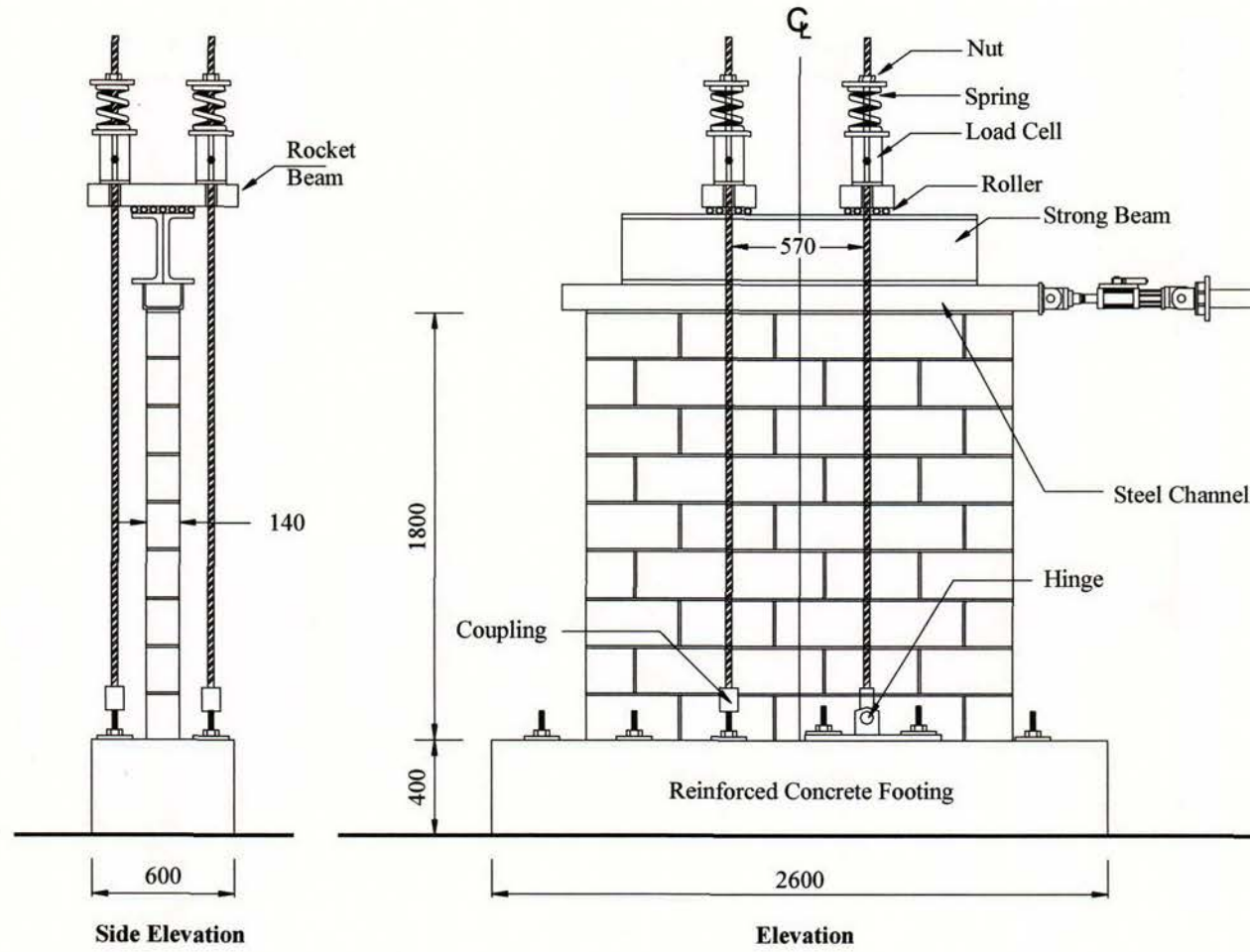


Figure B.7.2 Test set-up for Wall 7.

0.5 mm pull, 1st cycle

A maximum force of -75 kN was reached at the displacement of -0.48 mm. No cracking of any kind was identified at this stage.

0.5 mm push, 2nd cycle

A maximum force of 70 kN was measured at a displacement of 0.51 mm. Again no cracking was identified.

0.5 mm pull, 2nd cycle

A maximum force of -75 kN was recorded at the completion of this load step. No cracking was identified.

1.0 mm push, 1st cycle

A maximum force of 126 kN was recorded for the first push cycle to 1.0 mm displacement. No cracking of any kind was identified. The wall returned to its original position upon unloading.

1.0 mm pull, 1st cycle

The response of the wall mirrored that of the push cycle. A maximum strength of -130 kN was recorded at the conclusion of this load cycle. No cracking was identified, the wall returned to its original position upon unloading.

According to test procedure outlined in section 3.8, the measured lateral force for the two directions of loading resulted in an average yield displacement of:

$$\Delta_y = \frac{282}{\frac{1}{2}(126 - (-130))} = 2.20 \text{ mm}$$

1.0 mm push, 2nd cycle

The wall responded similarly to observations made in the previous push cycle. No cracking was identified. A maximum strength of 126 kN was recorded at the end of this load step.

1.0 mm pull, 2nd cycle

The wall developed a maximum strength of -125 kN. No cracking was identified.

2.0 mm push, 1st cycle

Three hairline horizontal cracks were identified to initiate from the edge of the wall on the tension side, following the mortar joints. The cracks had a maximum length of approximately 600 mm. Also noted was the uplift at the heel that caused a crack at the base which extended to the centre of the wall. A maximum strength of 187 kN was measured for this push cycle. The wall had a permanent deformation of 0.27 mm upon unloading.

2.0 mm pull, 1st cycle

The wall responded similarly to observations made in the previous push cycle with the observation of three fine horizontal cracks and base crack. The wall developed a maximum strength of -196 kN for this pull cycle. The wall returned to its original position upon unloading.

2.0 mm push, 2nd cycle

First sign of diagonal cracks were observed at the completion of this load step. A maximum strength of 162 kN was measured for this load cycle.

2.0 mm pull, 2nd cycle

A single diagonal crack of about 500 mm long was identified to initiate from the bond beam. The wall developed a maximum strength of -186 kN for the second cycle to this displacement level.

4.0 mm push, 1st cycle (see Photo 32)

The wall developed a maximum strength of 235 kN at a displacement of 4.7 mm. Significant diagonal cracking was identified to descend from the top right of the wall towards the bottom left. This was originated from the thrust of the diagonal compression strut, attempting to push the wall end away from the main body of the wall (towards the left). The horizontal cracks formed in the previous push cycle were widened to a small extent. A permanent displacement of 1.0 mm was recorded upon unloading.

4.0 mm pull, 1st cycle (see Photo 32)

The wall responded similarly to observations made in the previous push cycle with the formation of x-shaped diagonal crack (about 0.5 mm wide, although no accurate

measurement was taken). Sign of distress in the compression toe was observed with the commencement of mortar crushing, accompanied by further widening of horizontal cracks formed in the previous pull cycle. A maximum strength of -250 kN was measured at a displacement of -4.5 mm.

4.0 mm push, 2nd cycle

The wall responded similarly to observations made in the previous push cycle. The diagonal cracks identified in the previous push cycle developed further with crack widths up to 1.0 mm. The maximum force of 208 kN was measured for the second push cycle to this displacement level.

4.0 mm pull, 2nd cycle

No new cracking was detected at the completion of this loading step. A maximum strength of -225 kN was measured.

6.0 mm push, 1st cycle

A maximum force of 263 kN was recorded at the peak displacement. The response of the wall was similar to those observed in the previous push cycle with further development of diagonal cracks, and maximum crack width up to about 2 mm was measured. Additionally, first sign of distress (cracks) of face shells in the compression zone was observed. Wall sliding was measured to be about 0.14 mm for this push cycle.

6.0 mm pull, 1st cycle

On the first cycle to this displacement, the wall developed a maximum strength of -261 kN. The wall response was similar to that of the last pull cycle with maximum crack width of about 1.6 mm being identified. Wall sliding was measured to be about -0.23 mm.

6.0 mm push, 2nd cycle

The wall response was similar to observations made in the previous push cycle. No new cracking was identified. The wall developed a maximum strength of 202 kN at the end of this load step. This strength corresponded to about 77% of the maximum strength recorded in the push direction. Therefore the wall was defined as failing according to the test procedure outlined in section 3.8.

6.0 mm pull, 2nd cycle

The wall developed a maximum strength of –236 kN at the conclusion of this loading cycle. The response mirrored that of the first pull cycle. No new cracks or extensions of cracks were identified.

8.0 mm push, 1st cycle

A maximum strength of 232 kN was achieved in the first push cycle to 8 mm displacement. New diagonal cracks were identified accompanied by the widening of previously formed cracks, with crack width up to 3 mm (although no accurate measurement was taken). Additionally, degradation of compression toe continued signified by the compressive splitting of face shell. Wall sliding of 0.3 mm was measured at peak displacement.

8.0 mm pull, 1st cycle

In the pull excursion towards the target displacement of –8 mm, significant widening of the main x-shaped diagonal crack (maximum crack width up to 5 mm) occurred abruptly at a displacement of approximately –7.4 mm resulting in significant loss of strength and a sudden increase in lateral displacement. Additionally, significant crushing of the wall compression toe was observed. The peak strength measured was –235 kN at a lateral displacement of –7.4 mm. At the final displacement of –8.9 mm the strength dropped to –200 kN, this drop of strength constituted a strength loss of more than 20%. A “hollow” sound was heard when tapping on the face shells in the toe region upon unloading, indicating the onset of face shell delamination.

8.0 mm push, 2nd cycle (see Photo 33)

The lateral force increased steadily until the x-shaped diagonal cracks opened up abruptly (accompanied by “bang” noise) at a displacement of 7.8 mm, resulted in a significant loss of strength and a sudden increase in lateral displacement. The peak strength measured was 200 kN at a lateral displacement of 7.8 mm, but at the final displacement of 8.7 mm the strength had dropped to 170 kN. Further degradation of compression toe was observed.

8.0 mm pull, 2nd cycle (see Photo 33)

A maximum strength of –173 kN was measured in the second pull cycle to this displacement level. No new cracking was identified, but further widening of diagonal cracks was evident.

Additionally, the compression toe was further crushed resulting in face shell spalling upon unloading.

10 mm push, 1st cycle

Further widening of diagonal cracks, accompanied by significant crushing of compression toe were observed. The wall developed a maximum strength of 170kN, accompanied by a wall sliding of 0.34 mm.

10 mm pull, 1st cycle

In this direction of loading, the wall developed a maximum strength of -145 kN. The diagonal cracks were further widened (maximum crack width about 7 mm), but with little additional new cracking. Further crushing of wall compression toe resulted in the spalling of grout core.

10 mm push, 2nd cycle (see Photo 34)

The wall responded similarly to observations made in the previous push cycle. Further crushing of compression toe resulted in the spalling of face shells in the toe region. A maximum strength of 151 kN was measured at the end of this load cycle.

10 mm pull, 2nd cycle (see Photo 34)

The wall developed a maximum strength of -123 kN for this load cycle. The wall responded similarly to that of the previous pull cycle. Significant crushing of grout core at compression toe region was observed.

12 mm push, 1st cycle

The wall developed a maximum strength of 145 kN for this load cycle. Further widening of the diagonal cracks resulted in the spalling of face shells at the middle section of the wall. Also, significant amount of grout core fallen off at the tension toe exposing the wall outermost vertical reinforcing bar. Wall sliding of 0.33 mm was measured at the peak lateral displacement.

12 mm pull, 1st cycle

A maximum strength of –121 kN was measured at the conclusion of this loading cycle. The wall response was similar to observations made in the previous pull cycle and further crushing of the wall compression toe was observed.

12 mm push, 2nd cycle

During this semi-cycle of loading, a maximum force of 126 kN was recorded. The wall response mirrored that of the previous pull cycle. Further widening of diagonal cracks was evident with maximum crack width up to 6.8 mm. Significant crushing of compression toe was sufficient to expose the wall outermost vertical compression bar.

12 mm pull, 2nd cycle

The wall developed a maximum strength of –100 kN for this load excursion cycle. The wall response was similar to the previous loading cycle. Further degradation of compression toe region and further spalling of face shells along the diagonal cracks were observed. The maximum crack width was measured to be approximately 7.5 mm.

14 mm push, 1st cycle

The wall developed a maximum strength of 114 kN for this load excursion. The wall response was dominated by further widening of the x-shaped diagonal crack and further crushing of the wall compression toe.

-14 mm pull, 1st cycle

The wall response was similar to observations made in the previous loading cycle. The wall developed a maximum strength of –96 kN for this load cycle.

14 mm push, 2nd cycle (see Photo 35)

A maximum force of 103 kN was recorded for this load cycle. The wall response was similar to observations made in the previous push cycle. No new cracking was identified.

-14 mm pull, 2nd cycle (see Photo 35)

Further crushing of compression toe was observed. The wall developed a maximum strength of –84 kN for this load cycle.

B.7.3 Summary Behaviour

The force-displacement (F-D) curve for Wall 7 is presented in Figure B.7.3. The wall exhibited flexure response for displacement of up to ± 1 mm, signified by the formation of horizontal (flexure) cracks on the mortar joints. The first diagonal crack initiated when the wall was loaded towards -2 mm. As shown in Figure B.7.3, the wall exhibited near symmetrical response throughout the test.

The wall resistance built up to a maximum of about $+263$ kN/ -261 kN during the first cycle to ± 6 mm displacement. Significant strength degradation took place in both loading directions after the maximum strengths were reached. These were coincided with the significant widening of x-shaped diagonal cracks.

The failure mode was characterised by diagonal shear cracking forming on the wall and the crushing of compression toes. The observed failure could therefore be categorised as a shear type of failure. This type of failure was expected because the predicted shear strength was lower than the predicted flexural strength, as shown in Table B.7.1.

The yield displacement of Wall 7 was evaluated to be 2.20 mm. The wall was defined as failing during the second cycle to $+8$ mm displacement.

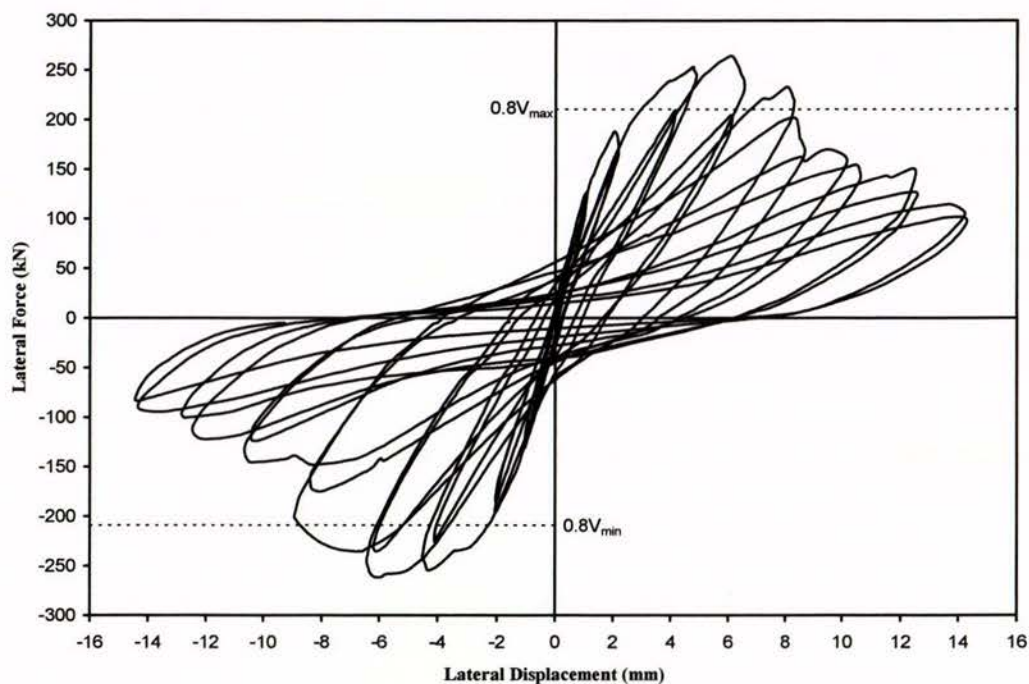


Figure B.7.3 Force-displacement behaviour of Wall 7.

B.7.4 Force-displacement Envelope

Figure B.7.4 shows the force-displacement envelope of the tested wall. The plot was constructed from the peak force recorded in the first cycle for each displacement level. It can be seen that wall strength degraded rapidly in both loading directions after the maximum strengths were developed at ± 6 mm displacement. The figure shows that the maximum shear strength achieved by the wall was about 50% more than that allowed by NZS4230:1990. This further proves that the current New Zealand masonry standard is conservative in predicting masonry shear strength. The masonry shear strength predicted by NEHPR closely matched the actual strength reached by the wall.

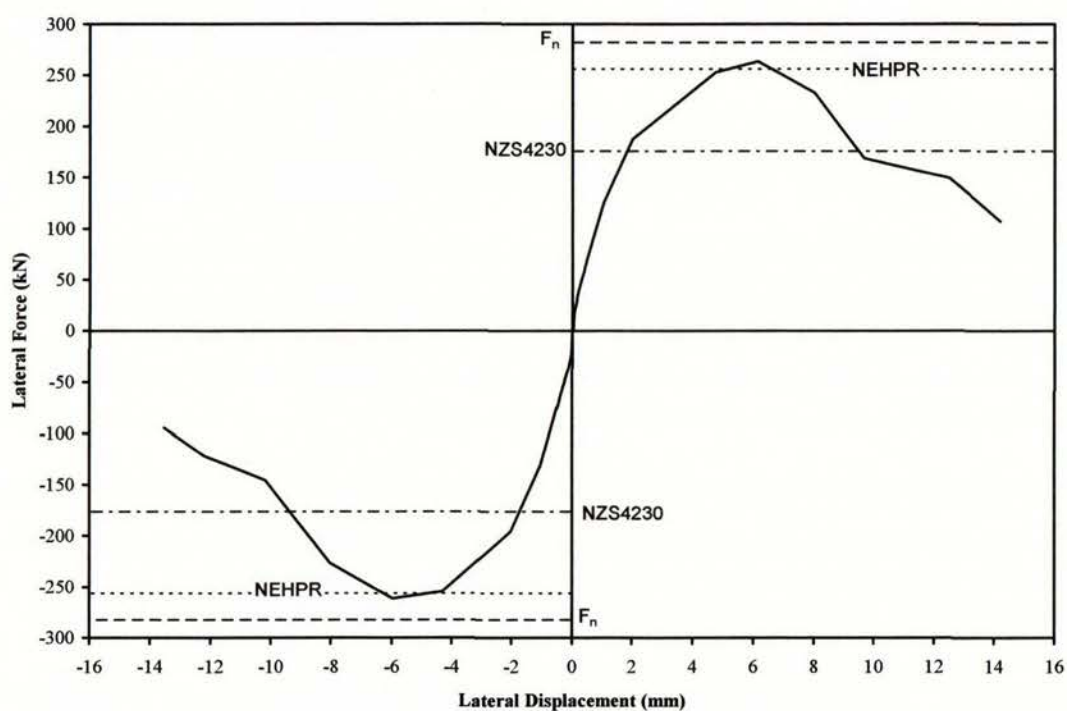


Figure B.7.4 Force-displacement envelope of Wall 7.

B.7.5 Panel Displacement Components

The total horizontal displacement was decomposed into four displacement components according to procedure outlines in section 3.9, with the results shown in Figure B.7.5.

From the sliding, rocking, flexure and shear displacement components plotted in Figure B.7.5, it is seen that sliding deformation was negligible throughout the entire test. Beyond

± 2 mm displacement, the shear deformation component increased significantly. This observation confirms the development of severe shear cracking during the test.

It is noted that the summed up deformations (sliding + rocking + flexure + shear) does not add up to match the overall displacement the overall displacement measured at the top of wall. It is also noted that the rocking deformation was unrealistically high at large imposed displacement level in the pull direction, it was most likely due to the significant damage at the wall toe regions affecting the reading of displacement transducer.

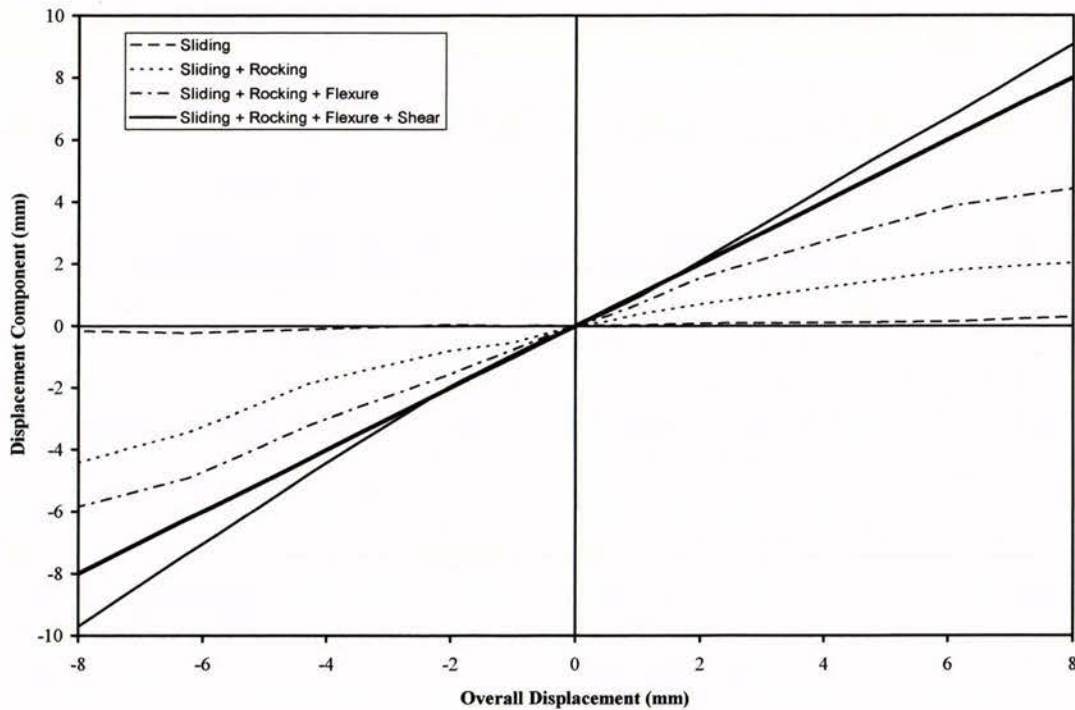


Figure B.7.5 Components of displacement.

B.7.6 Stiffness Degradation

The stiffness during a loading cycle was obtained by dividing the extreme positive and negative lateral forces by the corresponding displacements in each load cycle. The stiffness values obtained from the first cycle of loading were averaged and plotted against the corresponding average absolute lateral force, see Figure B.7.6. Figure B.7.7 plots the stiffness values against the average absolute lateral displacement. Stiffness degradation curve was plotted up to the stage when the maximum lateral force was developed.

A wall stiffness of 147 kN/mm was calculated at the first cycle to ± 0.5 mm displacement. However, the stiffness dropped to 43 kN/mm when the wall developed its maximum strength in the first cycle to ± 6 mm displacement.

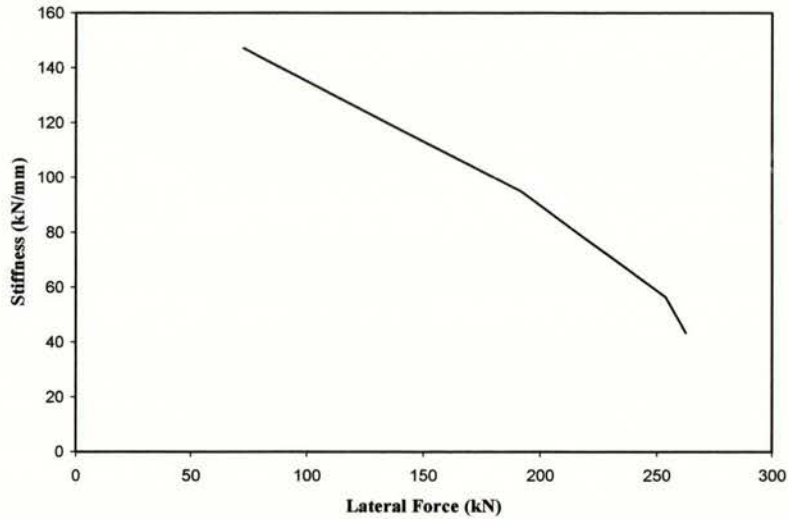


Figure B.7.6 Stiffness vs lateral force.

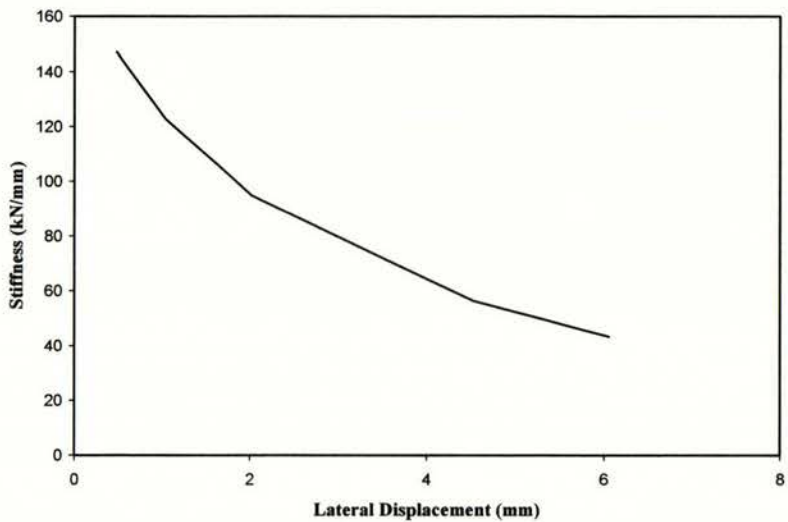


Figure B.7.7 Stiffness vs lateral displacement.

B.7.7 Axial Compression Force

Figure B.7.8 plots the axial compression force acted on top of the wall at the time of testing. It is shown that the variation of total axial compression force was less than 5% throughout the

test, therefore concluding the effectiveness of the springs in maintaining an approximately constant vertical force when the wall was displaced horizontally during testing.

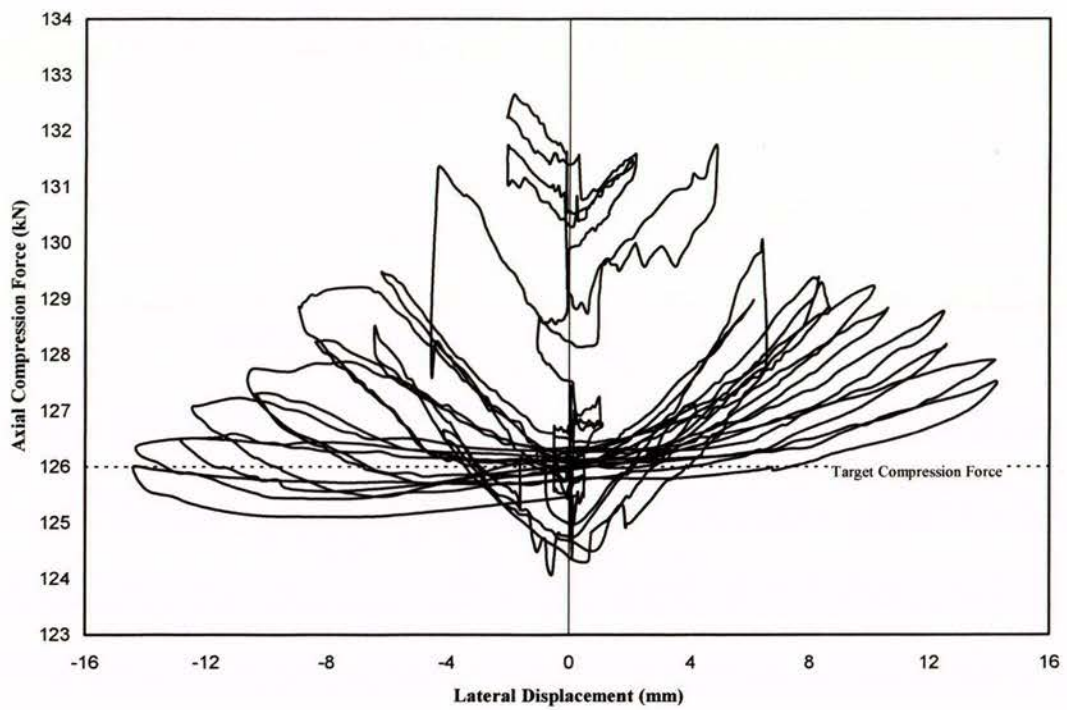


Figure B.7.8 Axial compression force history.

B.8 Wall 8

This section describes the testing of Wall 8 which was constructed with the same overall dimensions and reinforcement details as Walls 1 and 7, but was subjected to an axial compression stress of 0.25 MPa. As shown in Figure B.8.1, shear reinforcement consisted of R6 steel bars were embedded during construction and spaced vertically at 400 mm c/c. The wall was constructed of 15 series CMUs which resulted in an effective wall thickness of 140 mm. The wall was expected to exhibit shear dominated behaviour based on lower masonry shear strength as compared to the wall's flexural strength.

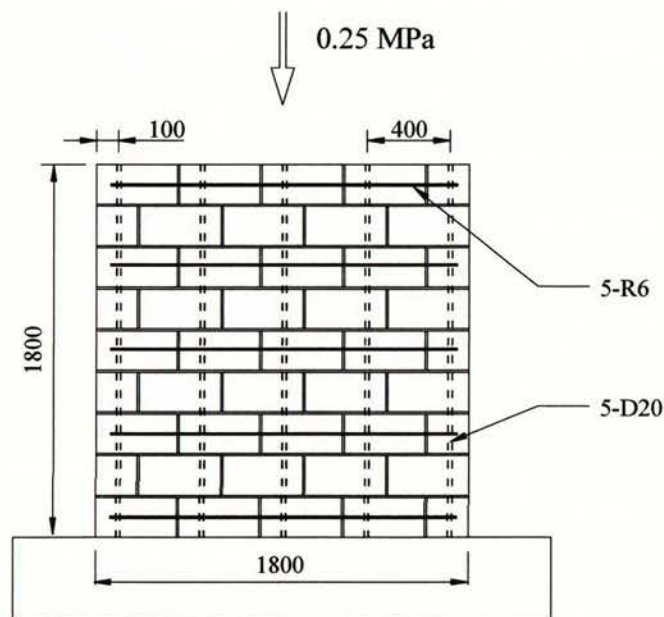


Figure B.8.1 Wall 8 reinforcement details.

Self weight of the wall panel was calculated to be 8.4 kN. Information about wall construction, testing procedure and data reduction may be found in Chapter 3. The test set-up used in the testing of Wall 8 was identical to that shown in Figure B.7.2.

The wall flexural and shear strength were predicted according to section 3.5 for a fully grout-filled concrete masonry wall, with the results presented in Table B.8.1. The wall was expected to exhibit a shear dominated behaviour since the wall had a shear strength that was lower than its flexural strength.

Table B.8.1 Wall strength predictions

Masonry strength	Nom. Flexural strength	Masonry shear strength V_n	
f'_m	F_n	NZS4230	NEHPR
18.8	256	161	240
MPa	kN	kN	kN

B.8.1 Pre-test

Instrumentation was attached to the wall according to section 3.5.1. Wall 8 was tested approximately 26 days after construction. The wall was inspected prior to testing. Horizontal crack (approximately 500 mm long) was identified on the last course of mortar bed (top of wall), on the side closest to actuator. It was expected that the crack was insignificant to cause structural defect to the wall.

B.8.2 Testing

0.5 mm push, 1st cycle

The wall developed a maximum strength of 73 kN when it reached the target displacement. No cracking was identified.

0.5 mm pull, 1st cycle

A maximum force of -69 kN was reached at a displacement of -0.53 mm. No cracking of any kind was identified at this stage.

0.5 mm push, 2nd cycle

A maximum force of 83 kN was measured at a displacement of 0.55 mm. Again no cracking was identified.

0.5 mm pull, 2nd cycle

A maximum force of -60 kN was recorded when the wall reached the target displacement. No cracking was identified at this stage.

1.0 mm push, 1st cycle

The wall developed a maximum strength of 123 kN for this load cycle. Apart from a visible base cracking, two hairline horizontal cracks were identified along the mortar joints on the tension side. An uplift of 0.35 mm was measured at the tension toe. The wall returned to its original position upon unloading.

1.0 mm pull, 1st cycle

The wall responded similarly to observations made in the previous push cycle, with fine horizontal cracks identified on the tension side. A maximum strength of -110 kN was recorded at the end of this load step.

According to procedure outlined in section 3.8, the measured lateral forces for the two directions of loading resulted in an average yield displacement of:

$$\Delta_y = \frac{256}{\frac{1}{2}(123 - (-110))} = 2.20 \text{ mm}$$

1.0 mm push, 2nd cycle

The wall responded similarly to observations made in the previous push cycle and a maximum strength of 123 kN was recorded for this load cycle. No new cracking was identified.

1.0 mm pull, 2nd cycle

The wall developed a maximum strength of -99 kN at the conclusion of this load cycle. The wall response mirrored that of the previous pull cycle, no new cracking was identified.

2.0 mm push, 1st cycle

A maximum strength of 170 kN was recorded in the first push cycle to this displacement level. Diagonal cracks were identified, accompanied by the elongations of horizontal cracks. Wall uplift of 0.47 mm was measured at the tension toe. The wall returned to its original position upon unloading.

2.0 mm pull, 1st cycle

The wall responded similarly to observations made in the previous push cycle and a diagonal crack was identified. A maximum strength of –163 kN was recorded at the completion of this loading cycle.

2.0 mm push, 2nd cycle

The wall responded similarly to observations made in the previous push cycle. The wall developed a maximum strength of 154 kN for this load step. No new cracking was identified.

2.0 mm pull, 2nd cycle

The wall responded similarly to observations made in the previous pull cycle. No new cracking was identified. A maximum strength of –156 kN was recorded for this load step.

4.0 mm push, 1st cycle (see Photo 36)

The wall developed a maximum strength of 215 kN for this load cycle. A new diagonal crack was identified to initiate from the bond beam and descended at about 45° to the right. The cracks formed in the previous cycle were widened to a small extent. A permanent displacement of 1 mm was recorded upon unloading.

4.0 mm pull, 1st cycle (see Photo 36)

One new diagonal crack developed at the centre of the wall when the wall was pulled to a displacement of approximately –2.5 mm. The crack pattern can be easily identified in Photo 36. The diagonal crack did not result in loss of strength but an abrupt increase in lateral displacement to –3 mm. The wall was further pulled to the target displacement and a maximum strength of –225 kN was recorded. Apart from the newly developed diagonal crack, no other new cracking was identified.

4.0 mm push, 2nd cycle

The wall responded similarly to observations made in the previous push cycle. The diagonal cracks identified in the previous push cycle developed further with crack widths grew to a maximum of 0.6 mm. A maximum force of 195 kN was measured for the second push cycle to this displacement level. A permanent displacement of 1 mm was recorded upon unloading.

4.0 mm pull, 2nd cycle

No new cracking was detected at the completion of this loading step. A maximum strength of -218 kN was measured.

6.0 mm push, 1st cycle

A new diagonal crack was identified. This new crack initiated from the wall end and descended at about 45° towards the compression toe. A maximum crack width of about 1 mm was measured. The wall developed a maximum strength of 244 kN for loading cycle.

6.0 mm pull, 1st cycle (see Photo 37)

During this semi-cycle of loading, a major diagonal shear crack grew abruptly at the edge of the wall (crack width of about 5.5 mm) when the wall was pulled to -6 mm, resulting in large displacement increase and a corresponding loss in strength. A maximum strength of -250 kN was recorded at -6 mm displacement. The strength dropped to -231 when the wall settled at a displacement of -8.5 mm. The diagonal crack was resulted from the thrust of the diagonal compression strut, attempting to pull the wall end away (towards the left) from the main body of the wall. It was expected a significant drop in strength for the subsequently load cycles. A permanent displacement of -4 mm was recorded upon unloading.

6.0 mm push, 2nd cycle

The wall suffered a significant loss of strength due to the damage occurred in the previous pull cycle. A maximum strength of 116 kN (about 46% of maximum load) was measured for this load cycle. The wall was therefore defined as failing according to the test procedure outlined in section 3.8. No new cracking was identified.

6.0 mm pull, 2nd cycle

The wall developed a maximum strength of -130 kN at the conclusion of this loading cycle. Further widening of diagonal crack near the wall edge was observed, but no new cracking was identified.

8.0 mm push, 1st cycle

A maximum strength of 122 kN was achieved in the first push cycle to 8 mm displacement. Further widening of previously formed cracks were observed, but no new cracking was identified. There was no evidence of compression toe distress at this stage of testing.

8.0 mm pull, 1st cycle

A maximum strength of -130 was measured for this load cycle. No new cracking was identified.

8.0 mm push, 2nd cycle

The wall response mirrored that of the previous push cycle. A maximum strength of 112 kN was measured, no new cracking of any type was identified.

8.0 mm pull, 2nd cycle

A maximum strength of -110 kN was measured in the second pull cycle to this displacement level. No new cracking was identified, but further widening of diagonal cracks (maximum width about 7 mm) was evident.

B.8.3 Summary Behaviour

The force-displacement (F-D) curve for Wall 8 is presented in Figure B.8.2. The wall exhibited flexure response at low displacement level, signified by the formation of horizontal (flexure) cracks on the mortar joints. The first diagonal crack initiated when the wall was loaded to ± 2 mm displacement. As shown in Figure B.8.2, the wall exhibited near symmetrical response throughout the test.

The wall resistance built up to the maximums of about +244 kN/-250 kN during the first cycle to ± 6 mm displacement. Rapid strength degradation took place in both the push and pull directions after the wall reached the maximum strength.

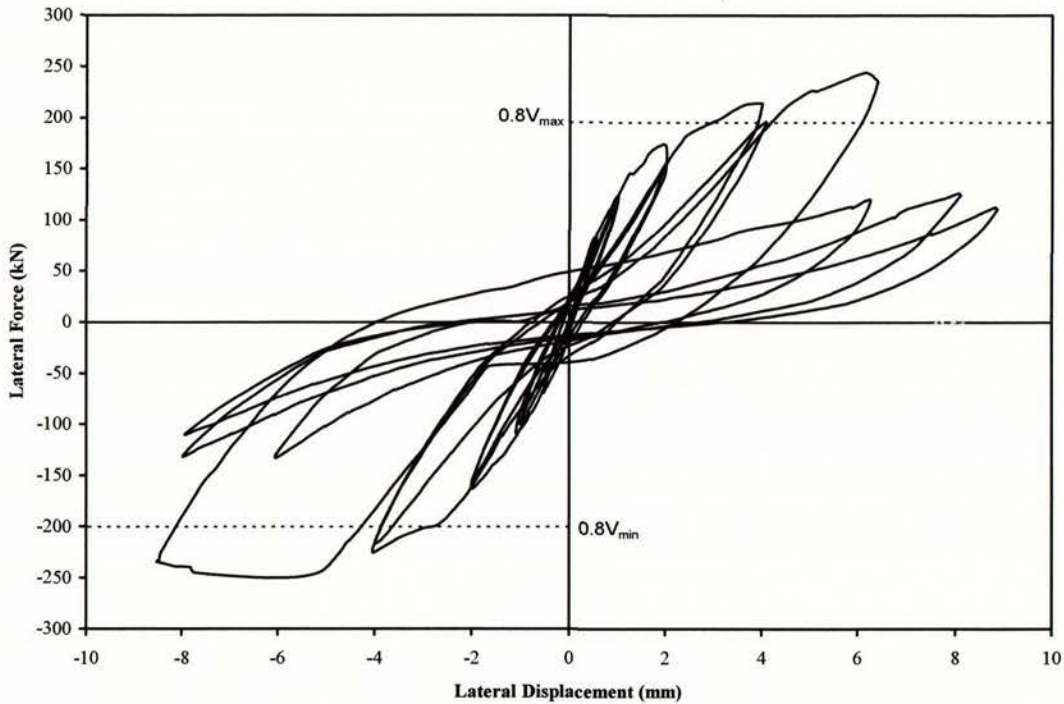


Figure B.8.2 Force-displacement behaviour for Wall 8.

The failure mode was characterised by significant diagonal shear cracking forming on the wall. The observed failure could therefore be categorised as a shear type of failure. This type of failure was expected because the predicted shear strength was lower than the predicted flexural strength as shown in Table B.8.1.

The yield displacement of Wall 8 was evaluated to be 2.20 mm. The wall was defined as failing during the second cycle to 6 mm displacement.

B.8.4 Force-displacement Envelope

Figure B.8.3 shows the force-displacement envelope of the tested wall. The plot was constructed from the peak force recorded in the first cycle for each displacement level. It can be seen that wall strength degraded rapidly in both loading directions after the maximum strengths were developed at ± 6 mm. The figure shows that the maximum shear strength achieved by the wall was about 53% more than that allowed by NZS4230:1990. This further proves that the current New Zealand masonry standard is conservative in predicting masonry shear strength. The shear strength predicted by NEHPR was closely matched with the actual wall strength recorded during testing.

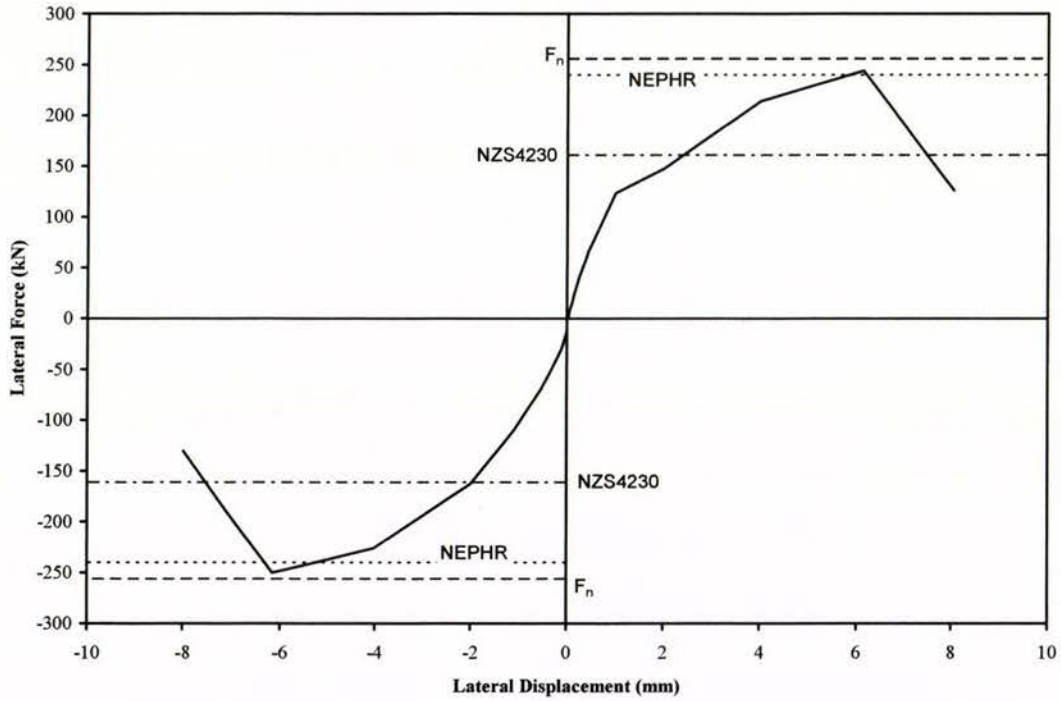


Figure B.8.3 Force-displacement envelope of Wall 8.

B.8.5 Panel Displacement Components

The total horizontal displacement was decomposed into four deformation components according to procedure outlines in section 3.9 with the results shown in Figure B.8.4.

From the sliding, rocking, flexure and shear deformation components plotted in Figure B.8.4, it is seen that sliding deformation was negligible throughout the test. Beyond ± 2 mm displacement, the shear deformation component increased significantly. This observation confirms the development of severe shear cracking.

It is noted that the summed up deformations (sliding + rocking + flexure + shear) does not add up to match the overall displacement the overall displacement measured at the top of wall.

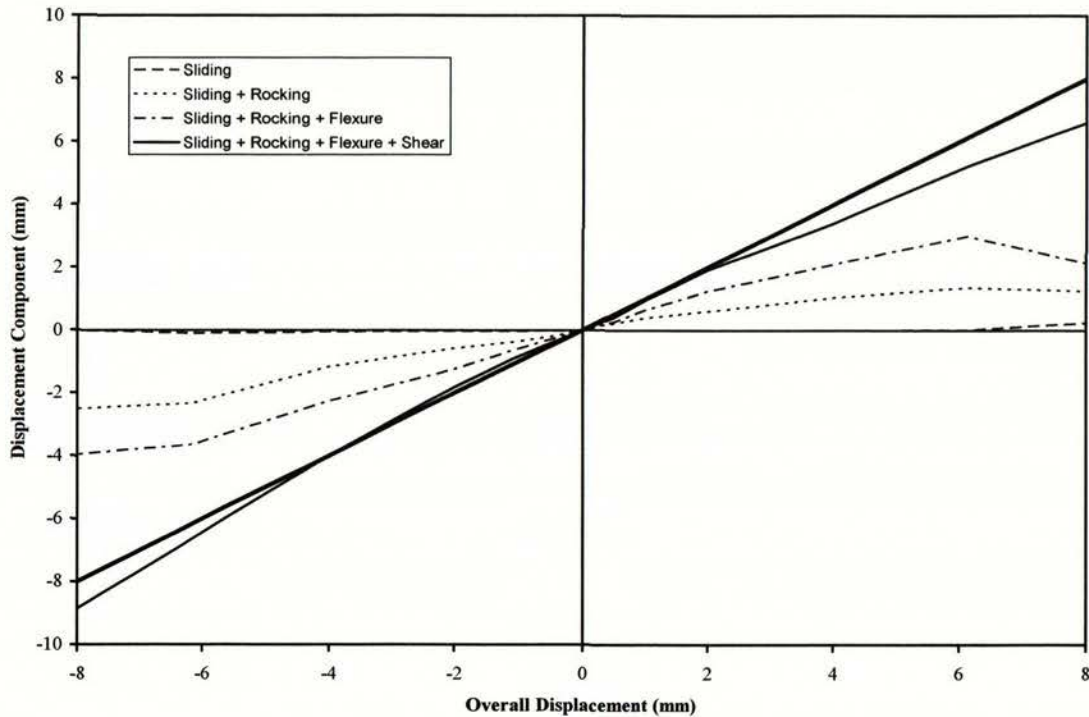


Figure B.8.4 Components of displacement.

B.8.6 Stiffness Degradation

The stiffness during a loading cycle was obtained by dividing the extreme positive and negative lateral forces by the corresponding displacements in each loading cycle. The stiffness values obtained from the first cycle of loading were averaged and plotted against the corresponding average absolute lateral force, this plot is presented in Figure B.8.5. Figure B.8.6 plots the stiffness values against the average absolute lateral displacement. Stiffness degradation curve was plotted up to the stage when the maximum lateral load was developed.

A wall stiffness of 138 kN/mm was calculated at the first cycle to ± 0.5 mm displacement. The wall stiffness dropped to 40 kN/mm when maximum strength developed at ± 6 mm displacement.

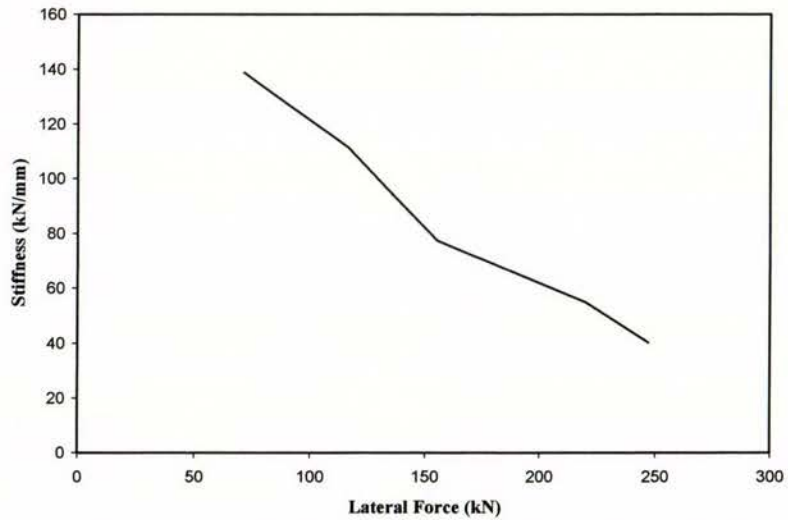


Figure B.8.5 Stiffness vs lateral force.

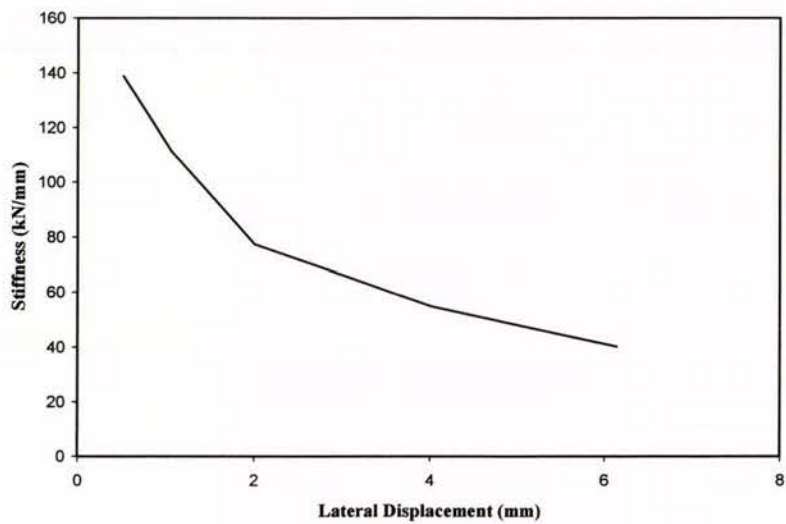


Figure B.8.6 Stiffness vs lateral displacement.

B.8.7 Axial Compression Force

Figure B.8.7 plots the axial compression force acted on top of the wall during the time of testing. It is shown that less than $\pm 5\%$ variation of total axial compression force was presented throughout the test.

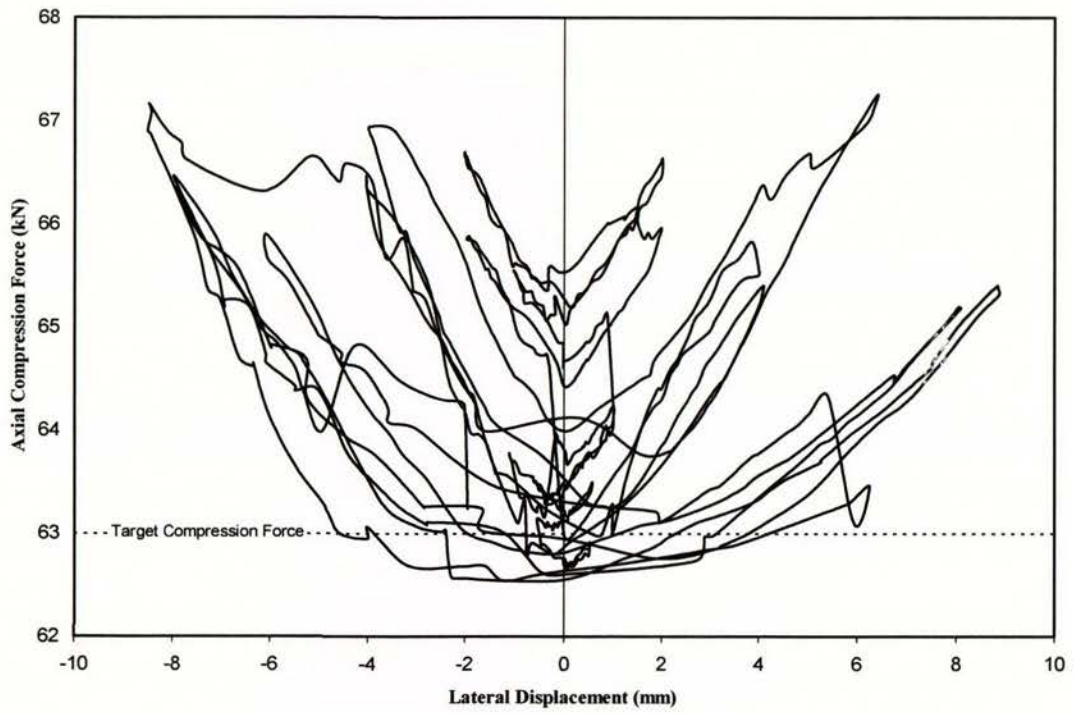


Figure B.8.7 Axial compression force history.

Appendix C

Additional Experiment Testing-Series C

After successful testing of the eight Walls reported in Appendix B, the researchers felt there was a need to investigate the shear strength of concrete masonry walls with H/L ratio other than 1. Subsequently two additional fully grout-filled concrete masonry walls with H/L ratios of 2.0 and 0.6 were tested at the University of Auckland. Details of the two walls are reported in conjunction with test observations in this section of the report. Similar to the eight concrete masonry walls reported in Appendix B, the test results of these two walls played significant role in formulating the conclusions of this report. The test set-up employed for the two additional wall tests were slightly different to that described in section 3.2. Consequently, the set-up for each of the two walls will be individually described in this appendix.

C.1 Wall 9

This section describes the testing of Wall 9 that was constructed to a height and length of 3.6 m and 1.8m respectively, resulting a height to length ratio of 2.0. Wall 9 was constructed on a purpose-built reinforced concrete footing with cast-in DH25 vertical reinforcement spaced at 400 mm centres. As shown in Figure C.1.1, shear reinforcement consisting of R6 steel bars were embedded during construction with a vertical spacing of 400 mm c/c. The wall was constructed of 15 CMUs which resulted in an effective wall thickness of 140 mm. Self weight of the wall panel was calculated to be 16.8 kN.

Test set-up adopted in the testing of Wall 9 was similar to that described for Walls 7 and 8, where a strong beam was sat on top of the loading beam in order to provide proper transfer of axial compression stress of 0.25 MPa (63 kN) into the entire wall. The axial compression force was applied to the wall through the action of a pair of high strength 23 mm diameter VSL prestressing bars incorporated at the centre position of the wall (see Photo 38 in

Appendix G). The rocker beam which was placed across the strong beam ensured that the pull down force in the prestressing bars on either side of the wall were equal.

The wall flexural and shear strength were predicted according to section 3.5 for a fully grout-filled concrete masonry wall with results presented in Table C.1.1. The wall was expected to exhibit a shear dominated behaviour since the wall had a shear strength that was lower than its flexural strength.

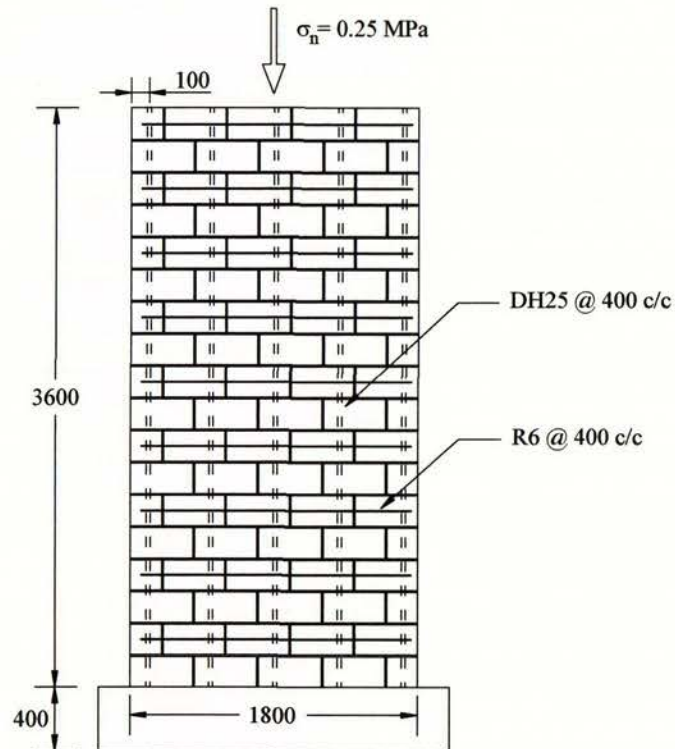


Figure C.1.1 Wall 9 construction details.

Table C.1.1 Wall strength predictions

Masonry strength	Nom. Flexural strength	Masonry shear strength V_n	
f'_m	F_n	NZS4230	NEHPR
24.3	272	178	268
MPa	kN	kN	kN

C.1.1 Pre-test and Testing Procedure

The masonry wall was tested on the 53rd days after construction. Instrumentation was attached to the wall according to section 3.5.1. Prior to wall testing the wall was inspected, with no cracks or structural defects being identified.

A slightly modified cyclic loading sequence, as shown in Figure C.1.2, was adopted for the testing of Wall 9. This new loading sequence was employed so that Wall 9 could be loaded to the same drift ratios as those experienced by the eight walls reported in Series B. Similar to that described in section 3.8, the wall was defined as failing when its strength reduced to 80% of the maximum strength recorded.

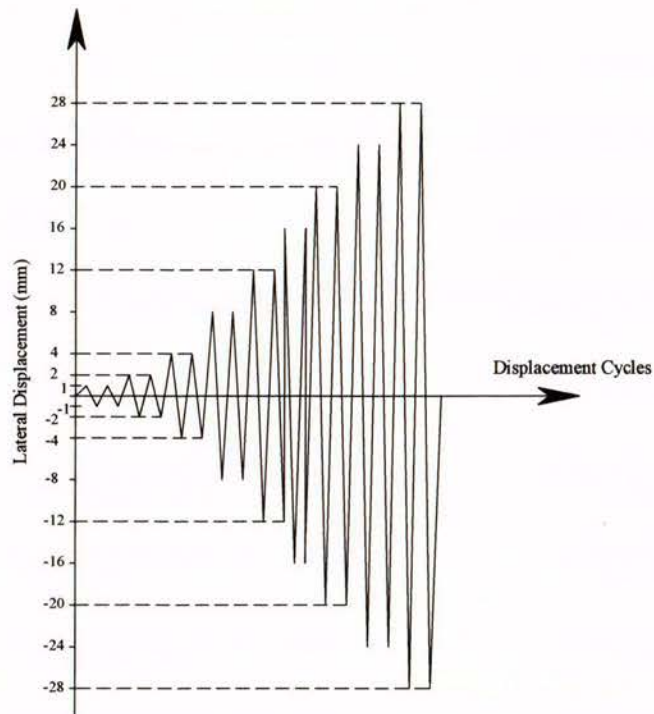


Figure C.1.2 Imposed displacement history.

C.1.2 Testing

1.0 mm push, 1st cycle

No clear evidence of cracking. An applied force of 42.9 kN was recorded with corresponding displacement of 1.27 mm.

1.0 mm pull, 1st cycle

A maximum strength of -52.2 kN was recorded at the target displacement. No cracking was identified.

1.0 mm push, 2nd cycle

The wall developed a maximum strength of 44.6 kN when it reached a displacement of 1.20 mm. No cracking was identified.

1.0 mm pull, 2nd cycle

A maximum force of -55.7 kN was measured at a displacement of -1.31 mm. Again no cracking was identified.

2.0 mm push, 1st cycle

On the first push cycle to this displacement, the wall developed a maximum strength of 75.9 kN. No cracking of any kind was identified.

2.0 mm pull, 1st cycle

The wall response mirrored that of the previous push cycle. A maximum strength of -78.1 kN was recorded at the conclusion of this load cycle. No cracking was identified.

Similar to the procedure outlined in section 3.8, the measured lateral force for the two directions of loading resulted in an average yield displacement of:

$$\Delta_y = \frac{272}{\frac{1}{2}(75.9 - (-78.1))} \times 2.0 = 7.0 \text{ mm}$$

2.0 mm push, 2nd cycle

A maximum strength of 73 kN was measured at a displacement of 2.15 mm. No cracking was identified.

2.0 mm pull, 2nd cycle

The wall response mirrored that of the previous push cycle. A maximum strength of -78.4 kN was measured at a displacement of -2.33 mm. No cracking was identified.

4.0 mm push, 1st cycle

Five hairline horizontal cracks were identified to initiate from the wall tension edge, following the mortar joints. The cracks had a maximum length of approximately 700 mm. A maximum strength of 93 kN was measured at a displacement of 4.16 mm.

4.0 mm pull, 1st cycle

The wall responded similarly to observations made in the previous push cycle. Eight new hairline horizontal cracks were identified along mortar joints on the tension side of the wall. The cracks had a maximum length of about 800 mm. A maximum strength of -107 kN was measured at a displacement of -4.22 mm. All cracks closed when unloaded.

4.0 mm push, 2nd cycle

Minor elongations to previously formed horizontal cracks were observed. A maximum force of 89 kN was measured.

4.0 mm pull, 2nd cycle

Similar to previous push cycle, minor elongations of horizontal cracks were observed. A maximum strength of -94 kN was measured at the end of this load cycle.

8.0 mm push, 1st cycle

The wall developed a maximum strength of 139 kN at a displacement of 8.15 mm. Seven new horizontal cracks and five diagonal cracks (maximum diagonal crack length about 100 mm) were identified. All cracks closed when the wall was unloaded, therefore suggesting the wall was still behaving elastically at this stage of testing.

8.0 mm pull, 1st cycle

The wall response mirrored that of the previous push cycle. A maximum strength of -147 kN and an uplift of 0.30 mm were measured.

8.0 mm push, 2nd cycle

No new cracks were observed, but minor extensions to diagonal cracks formed in the previous push cycle were noted. The maximum force achieved in this cycle was 130 kN.

8.0 mm pull, 2nd cycle

Minor extensions of diagonal cracks formed in the previous pull cycle were noted. The wall reached a maximum strength of -144 kN at the conclusion of this load cycle.

12.0 mm push, 1st cycle (see Photo 39, Appendix G)

The wall developed a maximum strength of 163 kN at the target displacement. Significant amount of new diagonal cracks were identified from the top right of the wall towards the bottom left. This was originated from the thrust of diagonal compressive strut that attempted to push the wall end away from the main body of the wall. Diagonal cracks formed in the previous push cycles were observed to have elongated and widened to a maximum crack width of about 1.0 mm. No crushing or spalling of masonry was observed at this stage. An uplift of 0.32 mm was measured at the tension heel, accompanied by a wall sliding of 0.22 mm.

12.0 mm pull, 1st cycle (see Photo 39)

The wall responded similarly to observations made in the previous push cycle with the formation of new diagonal cracks. The maximum diagonal crack width was measured to be about 0.7 mm. A maximum strength of -189 kN was measured at a displacement of -12.19 mm, accompanied by an uplift of 0.48 mm at the tension toe.

12.0 mm push, 2nd cycle

No new or extension of cracks were identified. A maximum strength of 151 kN was measured for this load cycle.

12.0 mm pull, 2nd cycle

The wall responded similarly to observations made in the previous push cycle. No new cracks or crack extensions were identified. A maximum strength of -164 kN was measured.

16.0 mm push, 1st cycle

A maximum force of 186 kN was measured at a lateral displacement of 16.35 mm. The wall behaved similarly to observations made in the previous push cycle, with further development of diagonal cracks and a maximum crack width of about 2.3 mm was measured. Sign of

distress in the compression toe was observed with the commencement of mortar crushing. Wall uplift and sliding were measured to be about 0.35 mm and 0.26 mm respectively.

16.0 mm pull, 1st cycle

Further extensions of previously formed diagonal cracks were observed, accompanied by few new shear cracks when the wall was displaced to the target displacement. Diagonal cracks formed in previous load steps were observed to have widened to a maximum of approximately 2.0 mm. Similar to previous push cycle, sign of distress was observed in the compression toe with the commencement of mortar crushing, this was accompanied by face shells crushing along diagonal cracks in the compression toe. A maximum force of -185 kN was measured.

16.0 mm push, 2nd cycle

A maximum strength of 178 kN was measured. No new cracks or crack extensions were observed.

16.0 mm pull, 2nd cycle

A maximum strength of -181 kN was measured. Again no new cracking was detected.

20 mm push, 1st cycle (see Photo 40)

The lateral force resisted by the wall increased steadily to a maximum of 204 kN at the target displacement. This was immediately followed by a slight loss in strength (accompanied by a “splitting” noise) and a sudden increase in displacement (from 20.2 mm to 21.5 mm) when a diagonal crack with a measured maximum width of about 5 mm, opened up suddenly and propagated across the wall. The wall strength settled at 197 kN at the lateral displacement of 21.5 mm. New diagonal cracks were observed to form adjacent to previously formed cracks, causing further deterioration and spalling of face shells. Further degradation of compression toe was observed, this was evident by mortar crushing and compressive splitting of face shell.

20 mm pull, 1st cycle (see Photo 40)

Significant amount of new diagonal cracks were observed at the conclusions of this load step, this was accompanied by spalling of face shells along diagonal cracks. A maximum strength of -208 kN was measured for this load cycle.

20 mm push, 2nd cycle

The wall reached a maximum strength of 177 kN at the end of this loading cycle. No new cracking was identified. Further deterioration of face shells were observed to take place along the diagonal cracks.

20 mm pull, 2nd cycle

The wall responded similarly to observations made in the previous push cycle. No new cracking was identified. A maximum strength of -178 kN was measured for this load cycle.

24 mm push, 1st cycle (see Photo 41)

A maximum strength of 185 kN was measured in the first push cycle to 24 mm displacement. Further widening of diagonal cracks and crushing of wall compression toe were observed. A “hollow” sound was heard when tapping on the face shells in the toe region indicated the onset of face shell delamination.

24 mm pull, 1st cycle (see Photo 41)

In this pull excursion, significant widening of the diagonal cracks occurred when loading stopped at a displacement of approximately -24 mm, resulting in significant loss of strength and a sudden increase in lateral displacement. Significant crushing of wall compression toe was observed, and a “hollow” sound was heard when tapping on the face shells, indicating the onset of delamination of face shell in the toe region. The peak strength measured was -191 kN at a lateral displacement of -24 mm. Wall strength dropped to -130 kN at the final displacement of -28.5 mm. This strength corresponded to about 63% of the maximum strength recorded in the pull direction. The wall was therefore defined as failing according to the test procedure outlined in section 3.8.

24 mm push, 2nd cycle

The lateral force increased steadily until the diagonal cracks opened up abruptly (accompanied by a “splitting” noise) at a displacement of 23.6 mm, resulted in a significant loss of strength and a sudden increase in lateral displacement. The peak strength measured was 149 kN at a lateral displacement of 23.6 mm, but at the final displacement of 26.9 mm the strength dropped to 132 kN. This drop of strength constituted a strength loss of about 35% in the push direction. No new cracks were identified, but significant face shells spalling

occurred along the diagonal cracks, coincided with the positions of the mounted measuring point, therefore influencing the accuracy of deformation measurements. The compression toe was further crushed resulting in face shell spalling upon unloading.

24 mm pull, 2nd cycle

A maximum strength of -98 kN was measured in the second pull cycle to this displacement level. No new cracking was identified. Further degradation of compression toe was observed.

28 mm push, 1st cycle

The wall developed a maximum strength of 98 kN for this load cycle. Further widening of cracks resulted in the spalling of face shells along the diagonal cracks. Significant crushing of grout core at the compression toe region was also observed.

28 mm pull, 1st cycle

A maximum strength of -90 kN was measured at the conclusion of this loading cycle. Further degradation/crushing of compression toe region resulted in the spalling of face shell upon unloading. Also, significant amount of grout core fallen off at the tension toe exposing the wall outermost vertical reinforcing bar.

28 mm push, 2nd cycle

The wall achieved a maximum strength of 85 kN for this cycle. The wall response was dominated by further widening of diagonal cracks and the spalling of face shells. It also revealed the buckling of the exposed extreme vertical reinforcing bar under compression force.

28 mm pull, 2nd cycle

A maximum strength of -85 kN was measured. Further widening of diagonal cracks were observed. Significant crushing of compression toe was sufficient to cause the spalling of grout core and exposing the wall outermost vertical compression bar.

32 mm push, 1st cycle (see Photo 42)

The wall developed a maximum strength of 81 kN for this load excursion. The wall response was dominated by the widening of diagonal cracks and further crushing of compression toe region.

32 mm pull, 1st cycle (see Photo 42)

The wall response was similar to observations made in the previous loading cycle. A maximum strength of -71 kN was measured for this load cycle.

32 mm push, 2nd cycle

A maximum strength of 67 kN was recorded for this load cycle. The wall response was similar to observations made in the previous push cycle. No new cracking was identified.

32 mm pull, 2nd cycle

Further crushing of compression toe region was observed. The wall developed a maximum strength of -66 kN for this load cycle.

C.1.3 Summary Behaviour

The force-displacement (F-D) curve for Wall 9 is presented in Figure C.1.2. The wall exhibited flexure response for displacements of up to ± 4 mm, signified by the formation of horizontal cracks on the mortar joints. The first diagonal crack initiated when the wall was pushed to +8 mm displacement. As shown in Figure C.1.2, Wall 9 exhibited near symmetrical response throughout the test.

The wall strength built up to a maximum of +204 kN and -207 kN during the first cycle to ± 20 mm displacement. As shown in Figure C1.2, significant strength degradation took place in both directions after the wall reached its maximum strength. These were coincided with the significant widening of diagonal cracks. The wall was defined as failing during the first pull cycle to -24 mm displacement when the wall strength dropped below $0.8V_{\max}$.

Wall 9 displayed a shear type of failure. This was characterised by early flexural horizontal cracks along the mortar joints at low displacement level and later augmented with diagonal

cracks that extended across the wall. The shear failure took place after the wall developed its maximum strength, which was followed by rapid strength degradation characterised by the opening of diagonal cracks and the crushing of the compression toe. A shear failure was expected for Wall 9 since it had flexural strength which was higher than its shear strength.

The yield displacement for Wall 9 was evaluated to be 7.0 mm. The wall was defined as failing during the first cycle to -24 mm displacement.

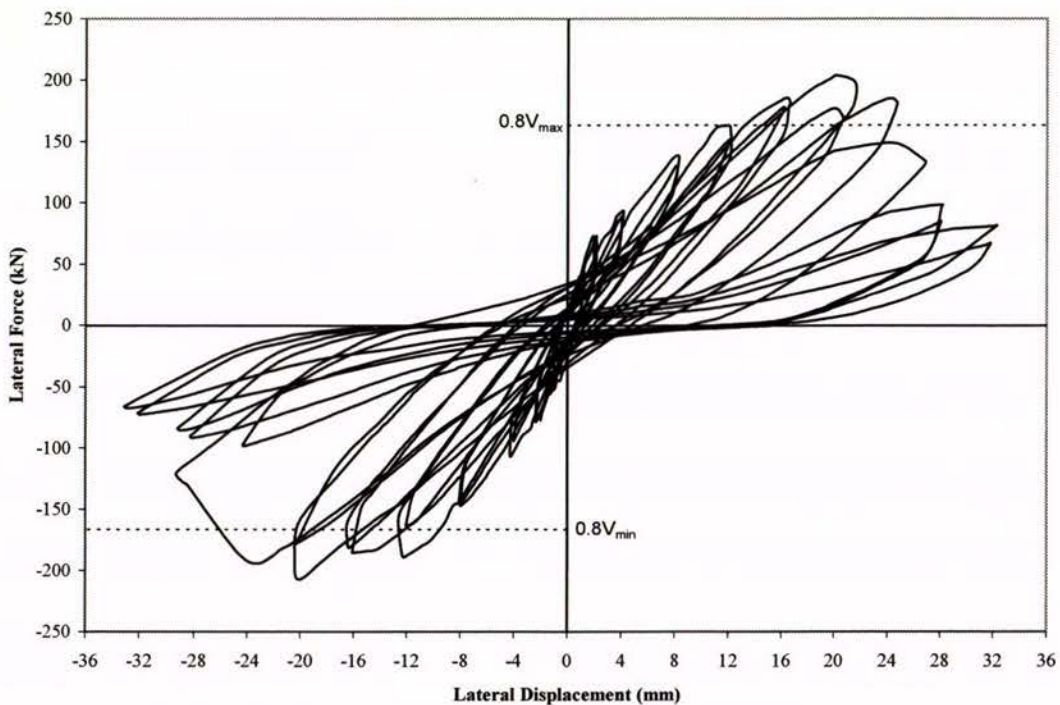


Figure C.1.2 Force-displacement behaviour for Wall 9.

C.1.4 Force-displacement Envelope

Figure C.1.3 shows the force-displacement envelope for the test. The plot was constructed from the peak force recorded in the first cycle for each displacement level. It is seen that wall strength degraded significantly after the wall was loaded to ± 24 mm displacement level. It is clearly shown in the figure that the maximum strength developed by Wall 9 was significantly less than the calculated flexural strength, therefore strongly indicated the wall failed in shear. It is also shown in Figure C.1.3 that the shear strength predicted by NZS4230:1990 was only slightly lower than the actual shear strength achieved by the masonry wall. However, the NEHPR expression had over-predicted the actual shear strength of this slender masonry wall by 23%. Consequently, the test result of this 3.6 m tall masonry wall indicated the possible

likelihood of NEHPR to unsafely over-estimate the shear strength of masonry walls which have H/L ratios of more than 1.

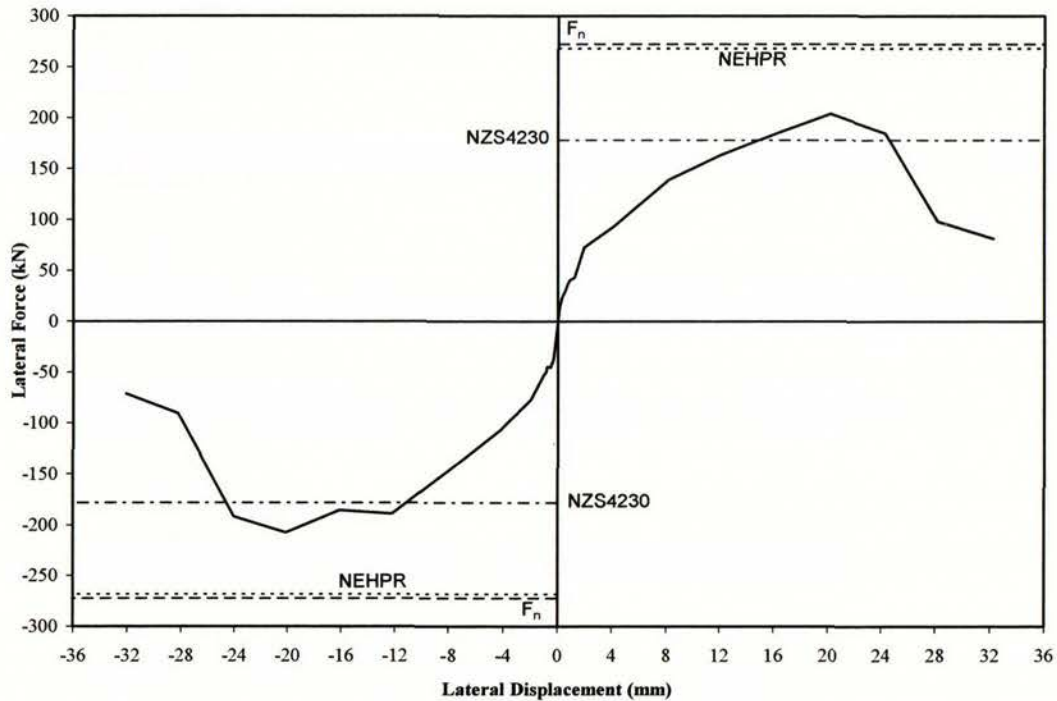


Figure C.1.3 Force-displacement envelope of Wall 9.

C.1.5 Panel Displacement Components

The plot of components of displacement in Figure C.1.4 shows a good agreement between the calculated composite displacement and the measured displacement up to the displacement of ± 24 mm. The error increased considerably beyond ± 24 mm when cracking passed through the wall's measuring point.

As shown in Figure C.1.4, the sliding deformation was small in magnitude relative to other components. Flexural displacement was the dominant deformation mode before the onset of shear deformation at ± 12 mm displacement level. Considerable increase in shear displacement occurred with the concurrent increase in diagonal cracking and widening of diagonal cracks. Shear displacement constituted about 50% of the total horizontal displacement when the wall was loaded to ± 24 mm displacement.

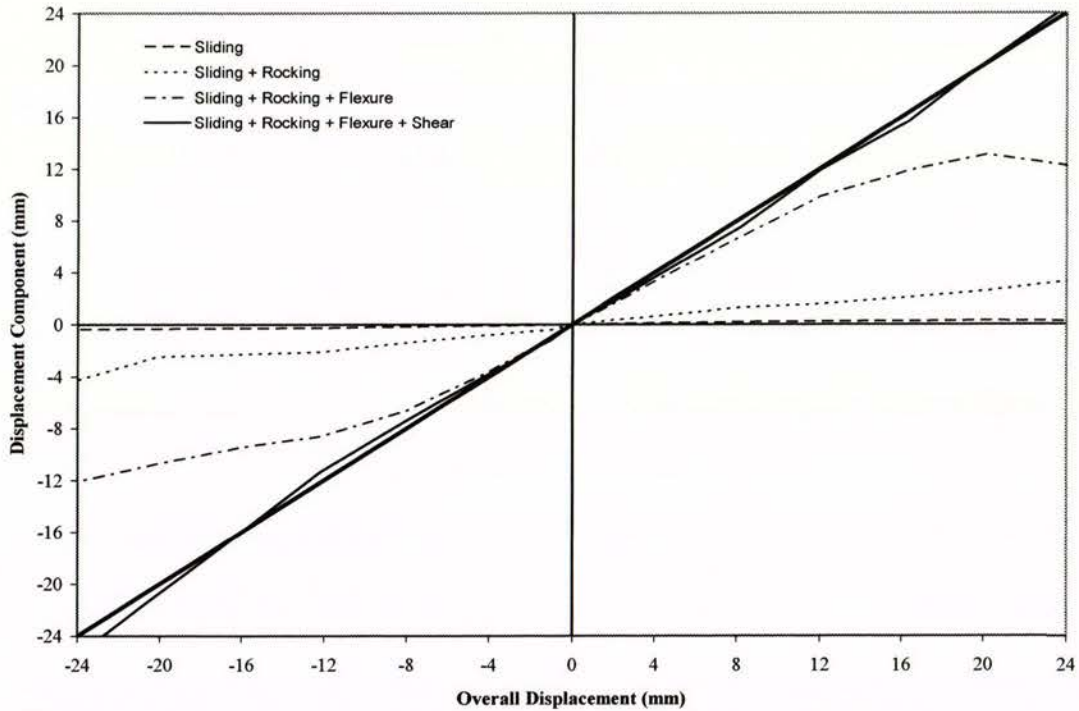


Figure C.1.4 Components of displacement.

C.1.6 Stiffness Degradation

The stiffness degradation curves for Wall 9 are presented in Figures C.1.5 and C.1.6. The stiffness during a loading cycle was obtained by dividing the extreme positive and negative lateral forces by the corresponding displacements in each loading cycle. The stiffness values obtained from the first cycle of loading were averaged and plotted against the corresponding average absolute lateral force and lateral displacement. These relationships provide an indication of the sensitivity of the wall with respect to the level of horizontal force, or lateral displacement. The stiffness degradation curve was truncated at the stage when the maximum shear strength was attained.

A wall stiffness of 43 kN/mm was calculated when the wall was loaded to ± 1.0 mm displacement. The wall stiffness dropped to 10 kN/mm when maximum strength developed at ± 20 mm displacement. As shown in Figure C.1.6, significant stiffness degradation was present even at the beginning stages of horizontal loading, much earlier than the development of the first visible crack.

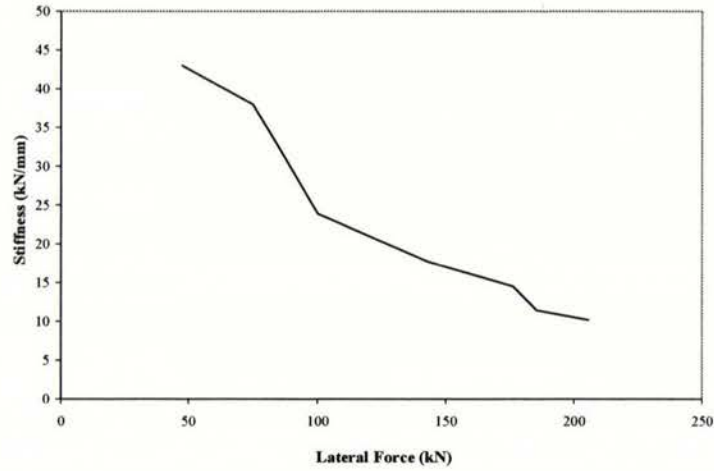


Figure C.1.5 Stiffness vs lateral force.

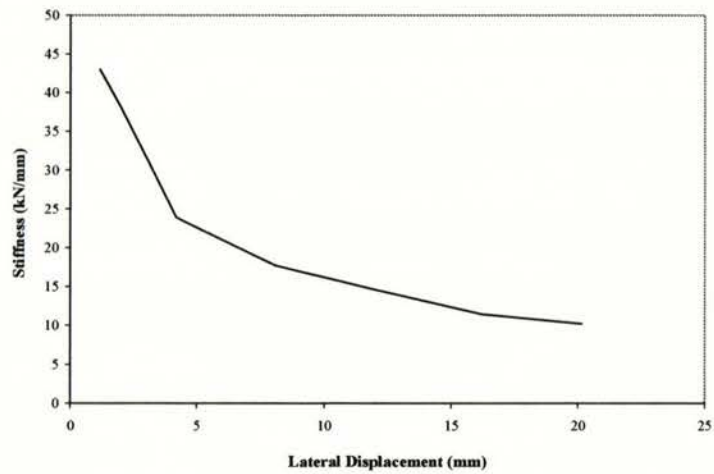


Figure C.1.6 Stiffness vs lateral displacement.

C.1.7 Axial Compression Force

Figure C.1.7 shows the axial compression force history plotted against the overall displacement. It is seen from this figure that the total compression force approached 67 kN when the wall developed its maximum strength at about ± 20 mm displacement. It is also noted that the total compression force at all excursion peak exceeded the target compression force of 63 kN.

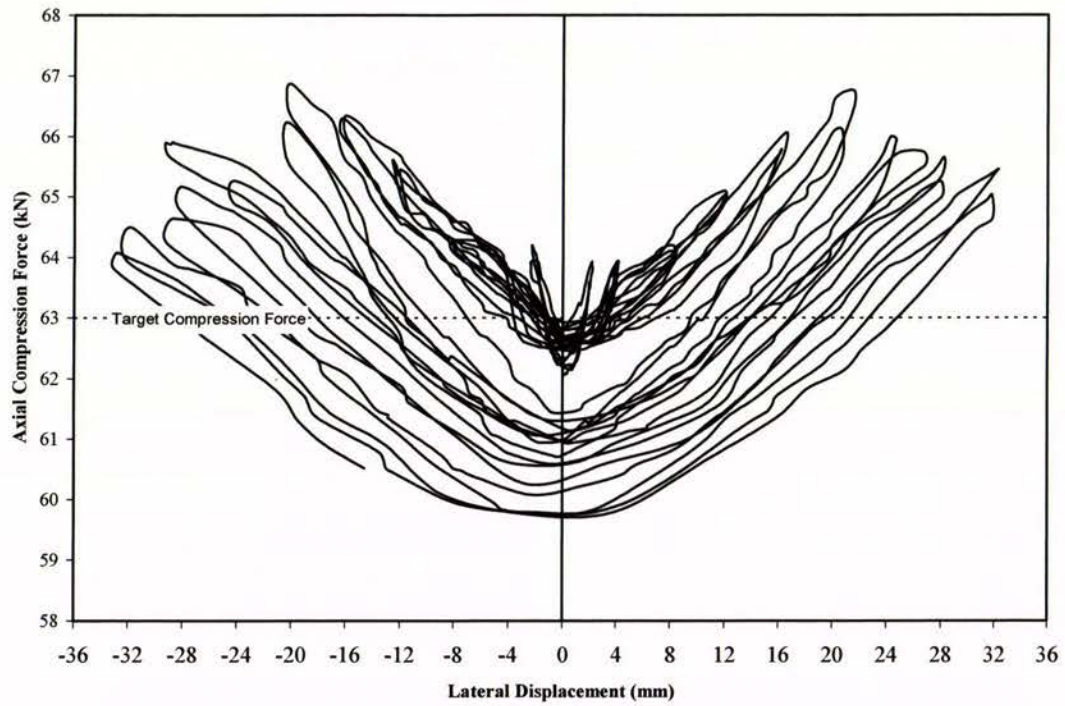


Figure C.1.7 Axial compression force history.

C.2 Wall 10

This section describes the testing of Wall 10 which was constructed to a height and length of 1.8 m and 3.0 m respectively, resulting a H/L ratio of 0.6. The two 2.6 m long reinforced concrete footing detailed in section 3.2 were jointed to create a 5.2 m long footing to accommodate the construction of Wall 10. The 5.2 m long footing had all DH32 starter bars spaced at 400 mm centres to accommodate the D20 vertical reinforcement. As shown in Figure C.2.1, shear reinforcement consisting of R6 steel bars were embedded during construction with a vertical spacing of 400 mm c/c. The wall was constructed of 15 series CMUs, therefore resulted in an effective wall thickness of 140 mm. Self weight of the wall panel was calculated to be 14.0 kN. Information about wall construction, testing procedure and data reduction may be found in Chapter 3.

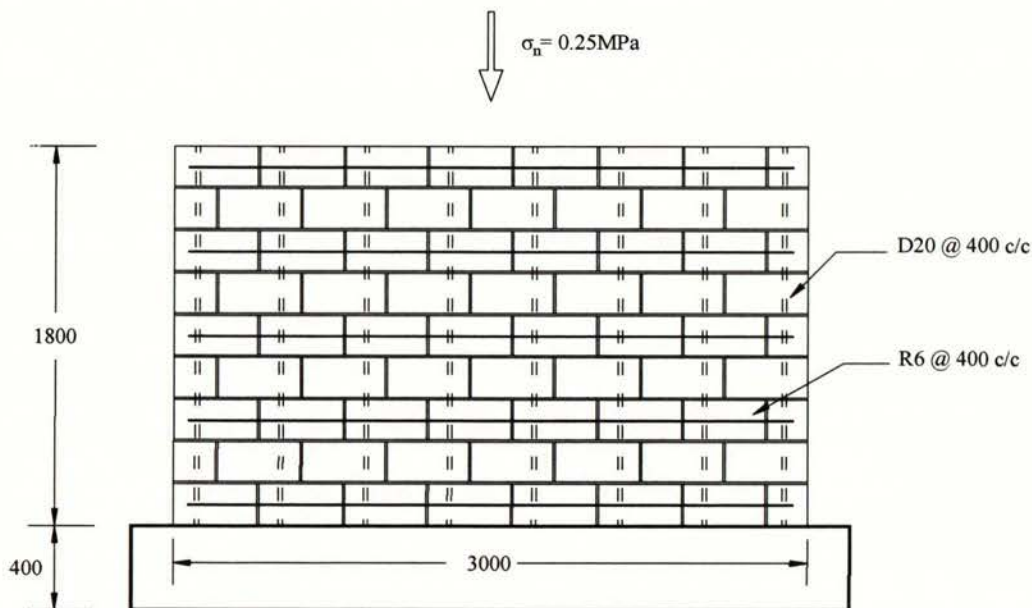


Figure C.2.1 Wall 10 construction details.

The test set-up reported earlier was slightly modified for this wall test. The 150 x 75 steel channel loading beam used in previously reported wall tests was replaced with a 180 x 75 steel channel since it was considered the 150 x 75 steel channel section would be inappropriate to properly transfer the expected large lateral force to the wall. Furthermore, two hydraulic actuators were used to provide the required lateral force. A 3 m long strong beam was placed on top of the loading beam in order to provide proper transfer of axial compression stress of 0.25 MPa (105 kN) into the entire wall. The axial compression force

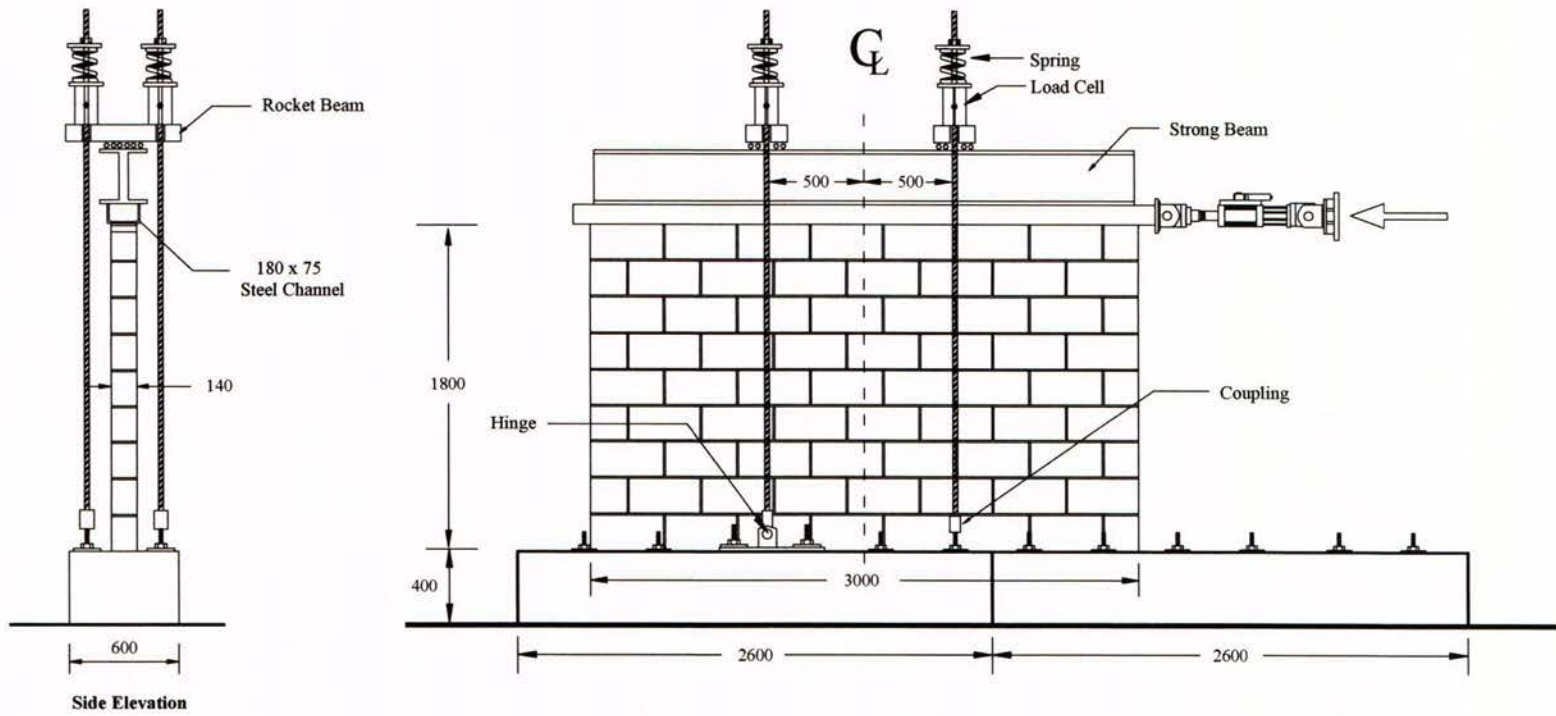


Figure C.2.2 Test set-up for Wall 10

was applied to the wall through the action of two pairs of high strength 23 mm diameter VSL prestressing bars.

The wall flexural and shear strength were predicted according to section 3.5 for a fully grout-filled concrete masonry wall with results presented in Table C.2.1. The wall was expected to exhibit a shear dominated behaviour since the wall had a shear strength that was lower than its flexural strength.

Table C.2.1 Wall strength predictions

Masonry strength	Nom. Flexural strength	Masonry shear strength V_n	
f'_m	F_n	NZS4230	NEHPR
24.3	672	297	568
MPa	kN	kN	kN

C.2.1 Pre-test

Instrumentation was attached to the wall according to section 3.5.1. Prior to wall testing the wall was inspected, no cracks or structural defects were identified.

C.2.2 Testing

0.5 mm push, 1st cycle

No clear evidence of cracking. An applied force of 154 kN was recorded with corresponding displacement of 0.54 mm.

0.5 mm pull, 1st cycle

A maximum strength of -139 kN was recorded at the target displacement. No cracking of any kind was identified at this stage.

0.5 mm push, 2nd cycle

On the second cycle to this displacement, the wall developed a maximum strength of 148 kN. The wall responded similar to the previous push cycle and no cracking was identified.

0.5 mm pull, 2nd cycle

The wall developed a maximum strength of -128 kN for this displacement cycle. The wall response mirrored that of the previous pull cycle and no cracking was identified.

1.0 mm push, 1st cycle

The wall developed a maximum strength of 225 kN for this load cycle. Three hairline horizontal and a single diagonal cracks were identified on the wall. The three horizontal cracks were observed to initiate from the wall edge (tension side) and extended about 300 mm along the mortar joints. The diagonal crack width was measured to be about 0.1 mm. The decompressed wall toe was measured to have uplifted about 0.25 mm.

1.0 mm pull, 1st cycle

The wall responded similarly to observations made in the previous push cycle. Two horizontal and one hairline diagonal cracks were identified on the tension side of the wall. A maximum strength of -221 kN was measured, accompanied by an uplift of 0.16 mm.

According to the procedure outlined in section 3.8, the measured lateral force for the two directions of loading resulted in an average yield displacement of:

$$\Delta_y = \frac{672}{\frac{1}{2}(225 - (-223))} = 3.0 \text{ mm}$$

1.0 mm push, 2nd cycle

No new crack or extensions of cracks were identified. A maximum strength of 199 kN was recorded.

1.0 mm pull, 2nd cycle

A maximum strength of -182 kN was measured, no new cracking identified for this direction of loading.

2.0 mm push, 1st cycle

The wall developed a maximum strength of 352 kN for this load cycle. One new diagonal crack was identified on the wall; this was accompanied by elongations to previously formed

cracks. Maximum diagonal crack width at this stage of testing was measured to be about 0.5 mm. An uplift of 0.35 mm was measured at the tension toe.

2.0 mm pull, 1st cycle

The wall developed a maximum strength of -310 kN for this load cycle. Two new diagonal cracks and elongations to previously formed cracks were identified. Maximum crack width of about 1.0 mm was measured. An uplift of 0.28 mm was measured at the tension toe.

2.0 mm push, 2nd cycle

The wall responded similarly to observations made in the previous push cycle. A maximum strength of 307 kN was measured. No new cracks or crack extensions were identified.

2.0 mm pull, 2nd cycle

No new cracks or cracks extensions were identified. The wall developed a maximum strength of -307 kN at the conclusion of this load cycle.

4.0 mm push, 1st cycle

The wall developed a maximum strength of 571 kN in this push cycle. Three new diagonal cracks were identified to initiate from the bond beam and descended towards the wall base at about 45°. Sign of distress in the compression toe was observed with the commencement of mortar crushing. The diagonal cracks identified in the previous push cycle were observed to develop further with crack width up to 1 mm. An uplift of 0.36 mm was measured at the tension toe.

4.0 mm pull, 1st cycle

During this semi cycle of loading, a major diagonal shear crack grew abruptly near the edge of the wall (crack width about 4.5 mm) when the wall was pulled to about -4.1 mm. This resulted in large displacement increase and a corresponding loss in strength. A maximum strength of -598 kN was measured at -4.1 mm displacement, and the wall strength dropped to -547 kN when the wall settled at a displacement of -6.9 mm.

Apart from the widely opened diagonal crack mentioned above, four new diagonal cracks were identified on the wall. Some of the cracks identified in previous cycles were observed to have elongated and widened further.

4.0 mm push, 2nd cycle

Significant loss of strength was observed for this load cycle. A maximum strength of 336 kN (about 59% of maximum load) was measured for this load cycle. The wall was therefore defined as failing according to test procedure outlines in section 3.8. No new cracking was identified.

4.0 mm pull, 2nd cycle

No new cracking was identified. The wall reached a maximum strength of -352 kN at the conclusion of this load cycle.

6.0 mm push, 1st cycle

A maximum strength of 350 kN was recorded in the first push cycle to 6 mm displacement. Significant deterioration of face shells caused by new crackings and widening of previously formed cracks.

6.0 mm pull, 1st cycle

The wall developed a maximum strength of -401 kN for this load cycle. No new cracking or crack extensions were observed.

6.0 mm push, 2nd cycle

A maximum strength of 313 kN was measured for this load cycle, no new cracking or crack extensions were identified.

6.0 mm pull, 2nd cycle

The wall responded similar to observations made in the previous push cycle. No new cracking or crack extensions were identified. A maximum strength of -337 kN was measured.

8.0 mm push, 1st cycle

A maximum strength of 275 kN was measured for this load step. Further widening of diagonal cracks caused the spalling of face shells. Also observed was the degradation of bond beam that caused significant slippage between the masonry wall and the steel loading channel.

8.0 mm pull, 1st cycle

The wall developed a maximum strength of -306 kN. The wall response mirrored that of the previous push cycle, no new cracking of any type was identified.

8.0 mm push, 2nd cycle

A maximum strength of 246 kN was measured. No new crack or crack elongations were observed.

8.0 mm pull, 2nd cycle

A maximum strength of -187 kN was measured. Again no new cracking was detected.

10 mm push, 1st cycle

The wall developed a maximum strength of 251 kN. Further widening of diagonal cracks (maximum crack width about 6.8 mm) were observed. Further degradation of bond beam was observed to cause the crushing of masonry adjacent to vertical reinforcing bars. Spalling of face shells took place at the bond beam.

10 mm pull, 1st cycle

The wall developed a maximum strength of -260 kN for this load cycle. The wall responded similarly to observations made in the previous push cycle. Further degradation of the bond beam was sufficient to cause the crushing of grout core and exposing the reinforcing bars. No new cracking was identified.

10 mm push, 2nd cycle

The wall developed a maximum strength of 223 kN. No new cracking was identified.

10 mm pull, 2nd cycle.

A maximum strength of -223 kN was measured in the second pull cycle to this displacement level. No new cracking was identified. Further widening of diagonal crack and degradation of bond beam were evident.

12 mm push, 1st cycle

A maximum strength of 209 kN was measured for this load cycle. Further widening of previously formed cracks were observed, no new cracking was identified. No sign of compression toe distress was observed at this stage of testing.

12 mm pull, 1st cycle

The wall behaved similarly to observations made in the previous push cycle where widening of diagonal cracks were observed. Also observed was the buckling of R6 shear reinforcing bar at bond beam layer. A maximum force of -215 kN was recorded.

12 mm push, 2nd cycle

The wall developed a maximum strength of 177 kN at the end of this loading cycle. Further deterioration of the bond beam was observed.

12 mm pull, 2nd cycle

Continue degradation of bond beam caused further spalling and crushing of masonry. A maximum strength of -184 kN was measured.

C.2.3 Summary Behaviour

The force-displacement (F-D) history of Wall 10 is shown in Figure C.2.3. The wall exhibited shear response, characterised by significant diagonal shear cracking. These diagonal cracks were initiated by tension splitting of masonry in the compression strut that formed in the wall. Similar to other tested walls, horizontal cracking was observed at low displacement level (up to ± 0.5 mm) before the onset of shear cracking.

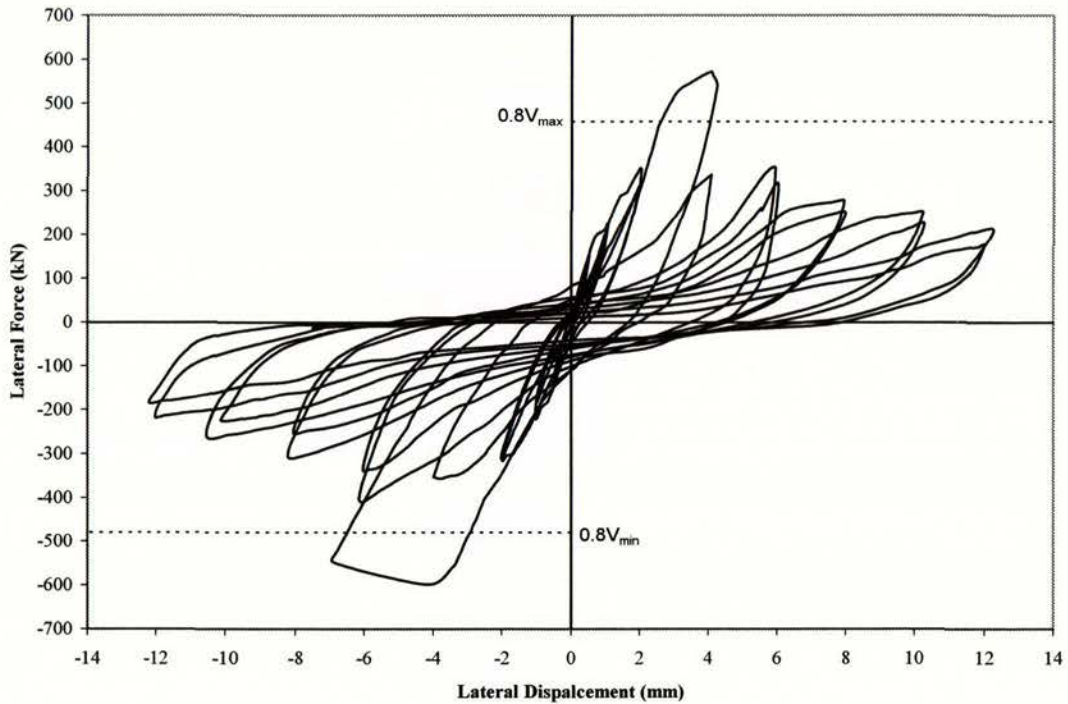


Figure C.2.3 Force-displacement behaviour for Wall 10.

The maximum push and pull direction strengths of +572kN and -598kN were measured during the first cycle to ± 4 mm displacement. Rapid strength degradation took place immediately after a wide diagonal crack grew abruptly near the wall edge when the wall was pulled to -4 mm.

The failure mode was characterised by significant diagonal shear cracking forming on the wall. The observed failure could therefore be categorised as a shear type of failure. This type of failure was expected because the predicted shear strength was lower than the predicted flexural strength, as shown in Table C.2.1.

The yield displacement of Wall 10 was evaluated to be 3.0 mm. The wall was defined as failing during the second push cycle to 4 mm displacement.

C.2.4 Force-displacement Envelope

Figure C.2.4 shows the force-displacement envelope for the test. The plot was constructed from the peak force recorded in the first cycle for each displacement level. It can be seen that wall strength degraded rapidly in both directions after the maximum strengths were

developed at ± 4 mm. The figure shows that the maximum strength developed by Wall 10 was significantly less than the calculated flexural strength, therefore indicating the wall failed in shear.

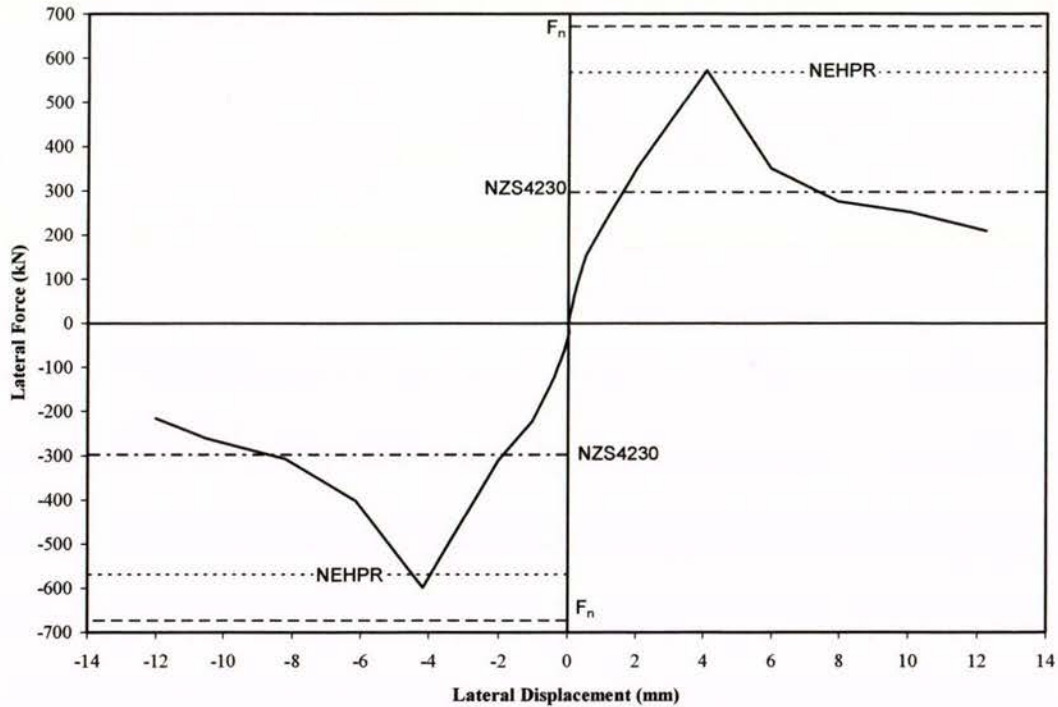


Figure C.2.4 Force-displacement envelope of Wall 10.

Figure C.2.4 undoubtedly shows the conservative shear prediction when using NZS4230:1990 as the maximum shear strength achieved by the wall was about double that allowed by the NZS4230:1990. This was mostly due to the low v_m that is being allowed by NZS4230:1990 ($v_m \leq 0.72$ MPa) despite of the high f'_m value obtained from prism testing. The figure also illustrates the shear strength predicted by NEHPR closely matched the actual wall strength recorded during testing.

C.2.5 Panel Displacement Components

The plot of displacement components in Figure C.2.5 shows the calculated composite displacement correlated reasonably well with the measured displacement up to the displacement of ± 8 mm. The error increased considerably beyond ± 8 mm when cracking passed through the wall's measuring point. Consequently, the displacement components beyond ± 8 mm are not shown in this plot.

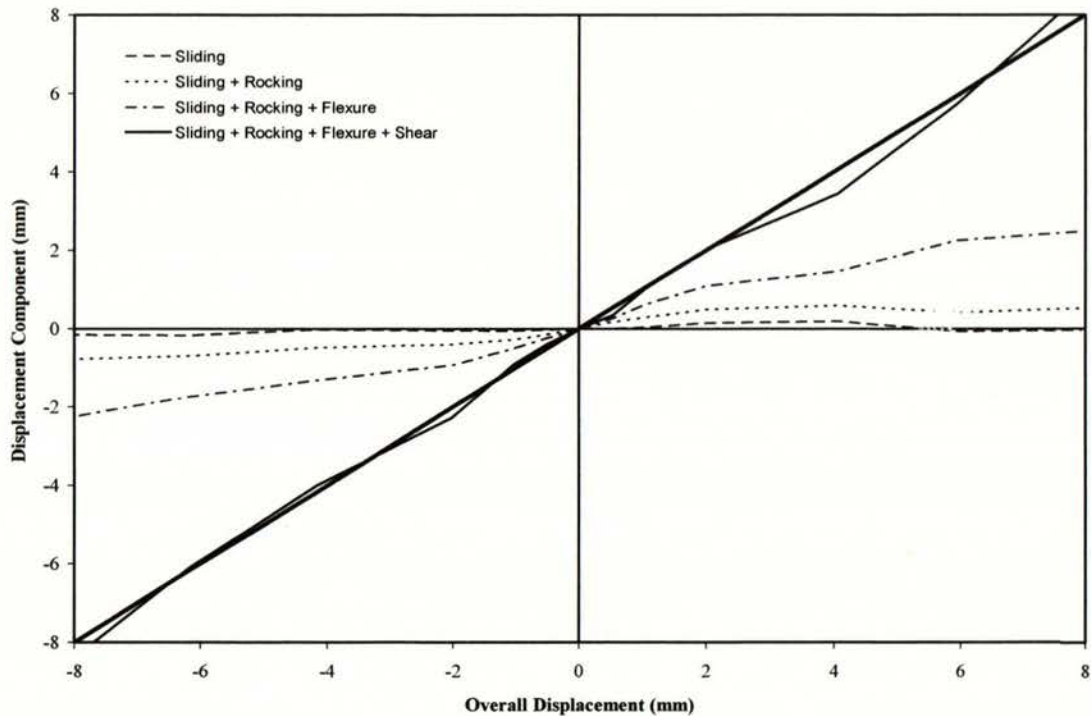


Figure C.2.5 Components of displacement.

As shown in Figure C.2.5, sliding deformation was insignificant throughout the test. The significance of rocking and flexure deformations reduced when the wall was displaced to larger displacement. For example, rocking and flexure deformations constituted about 66% of the total displacement when the wall was displaced to ± 0.5 mm. Their contribution was however reduced significantly to about 27% when the wall was displaced to ± 8 mm. Shear deformation increased considerably when the wall was pushed/pulled beyond ± 2 mm, this was coincided with the increase in diagonal cracking and widening of diagonal cracks. Shear displacement constituted about 72% of the total horizontal displacement when the wall was loaded to ± 8 mm displacement.

C.2.6 Stiffness Degradation

The stiffness degradation curves for Wall 10 are presented in Figures C.2.6 and C.2.7. The stiffness during a loading cycle was obtained by dividing the extreme positive and negative lateral forces by the corresponding displacements in each loading cycle. The stiffness values obtained from the first cycle of loading were averaged and plotted against the corresponding average absolute lateral force and lateral displacement. These relationships provide an indication of the sensitivity of the wall with respect to the level of horizontal force, or lateral

displacement. The stiffness degradation curve was truncated at the stage when the maximum shear strength was attained.

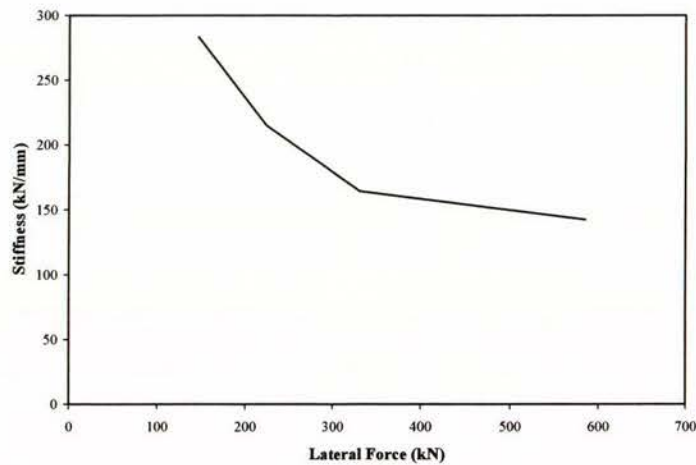


Figure C.2.6 Stiffness vs lateral force.

A wall stiffness of 283 kN/mm was calculated when the wall was loaded to ± 0.5 mm displacement. The wall stiffness dropped to 142 kN/mm when maximum push direction strength developed during the cycle to ± 4 mm displacement.

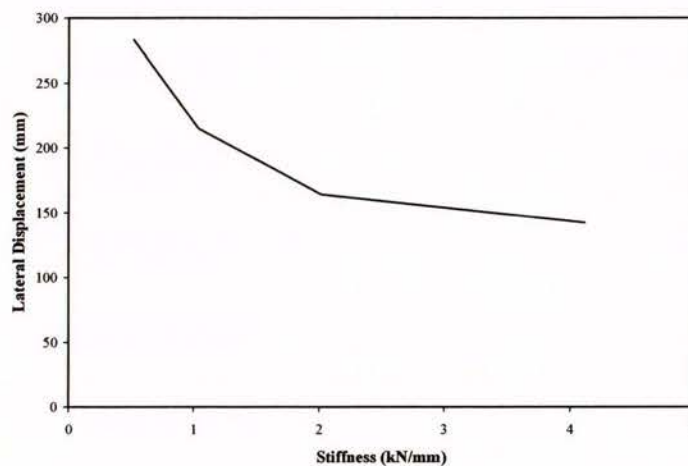


Figure C.2.7 Stiffness vs lateral displacement.

C.2.7 Axial Compression Force

Figure C.2.8 shows the axial compression force history plotted against the overall displacement. It is noted that the total compression force peaked during the first cycle to ± 4 mm displacement. The subsequent unloading reveals that the total axial compression force reduced after this point, this is particularly evident in the push direction of loading.

Consequently, the figure shows the loss of axial compression force coincided with the deterioration of the masonry wall that was caused by significant diagonal cracking and the widening of diagonal cracks.

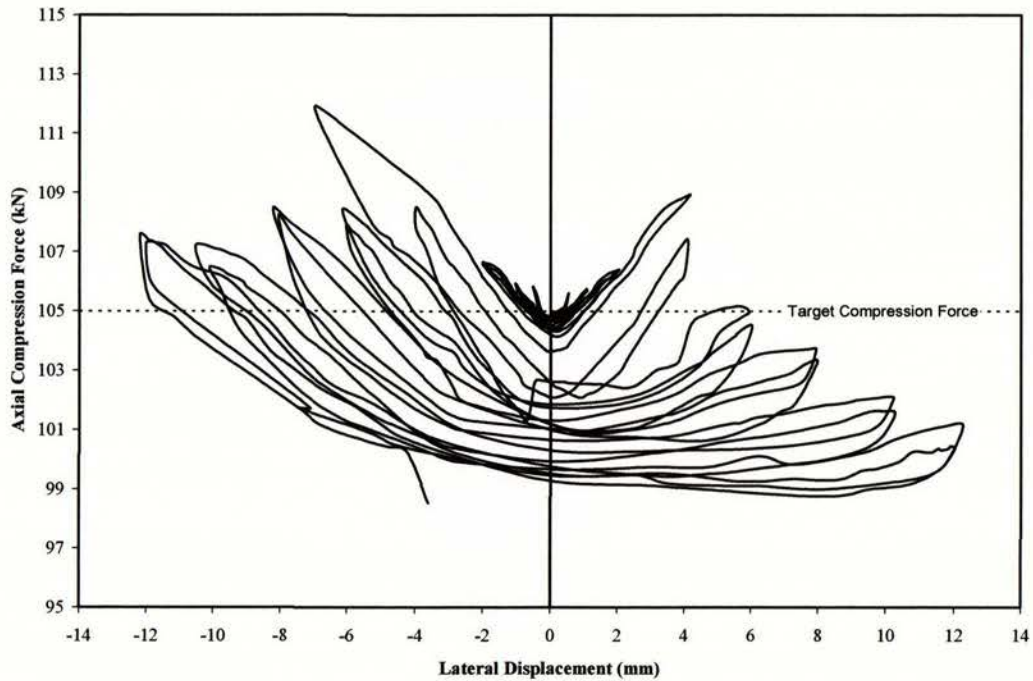


Figure C.2.8 Axial compression force history.

Appendix D- Shear Displacement Component

The objective of decomposition of panel deformation is to calculate and identify the dominant displacement components. The components of deflection are calculated from the test data obtained during testing. This test data was attained from the measuring instrumentation attached to the wall face, and the typical arrangement of the instrumentation is shown in Figure 3.7. This appendix describes calculation of the shear displacement component.

Having measured the relative displacements between points of a panel section on the wall face denoted A, B, C and D, as shown in Figure D.1(a), it is possible to extract the shear displacement component from the deformation in the panel section. The total shear displacement of the wall can be evaluated by summation of shear deformation of each panel section. The method used in this report for the extraction of the shear displacement component is based on Hiraishi (1984) and Brammer (1995).

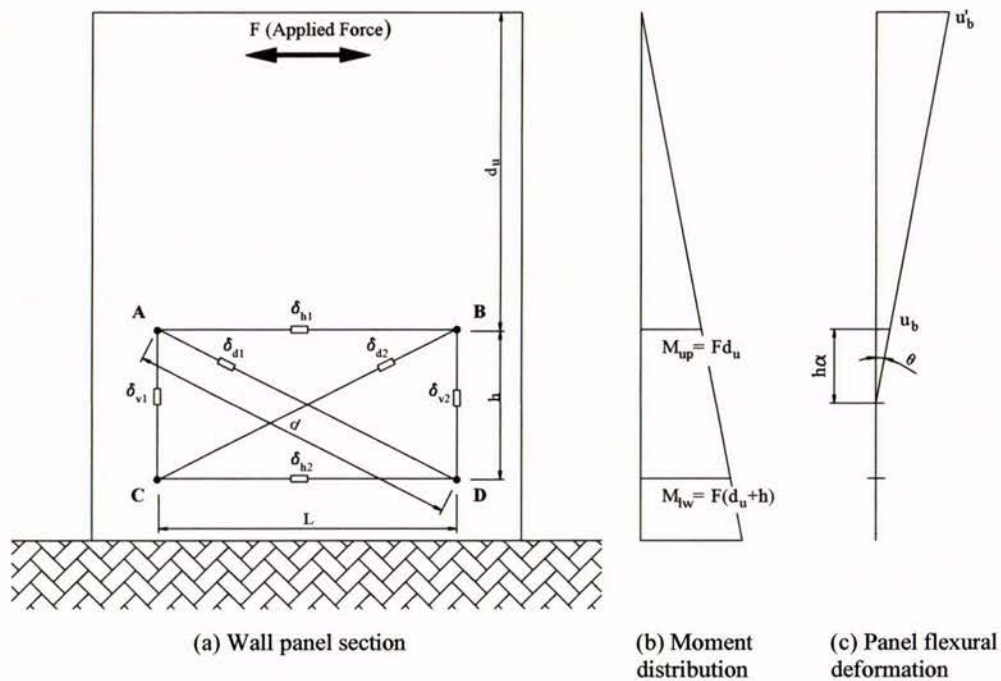


Figure D.1 Wall panel section.

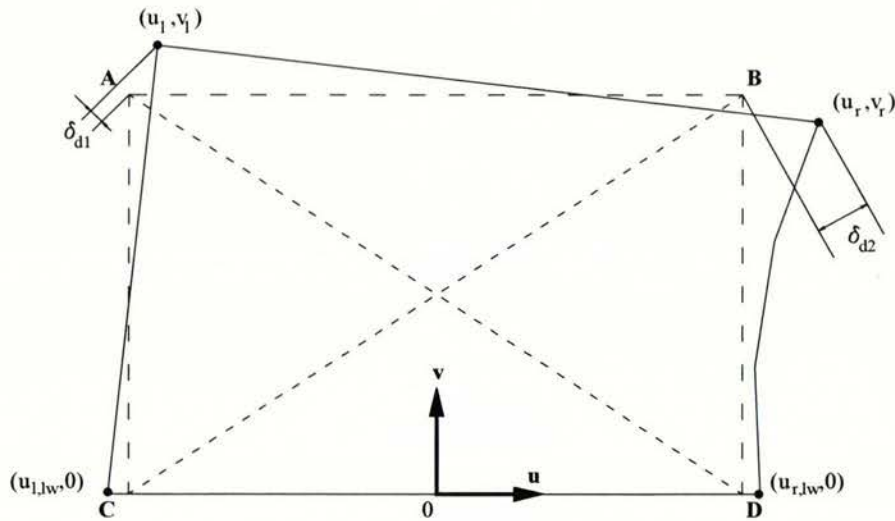
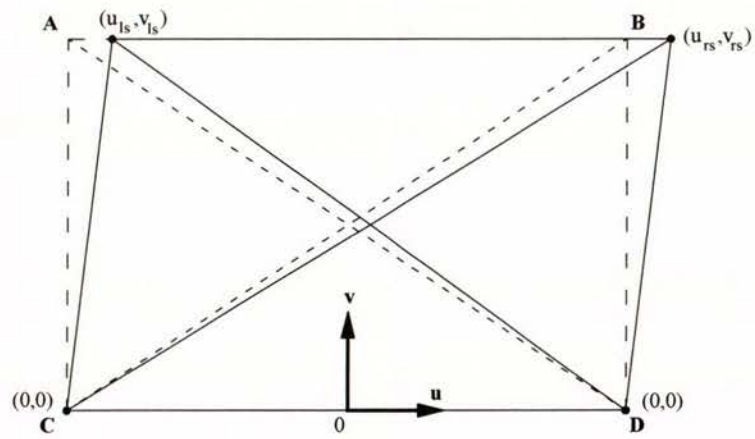


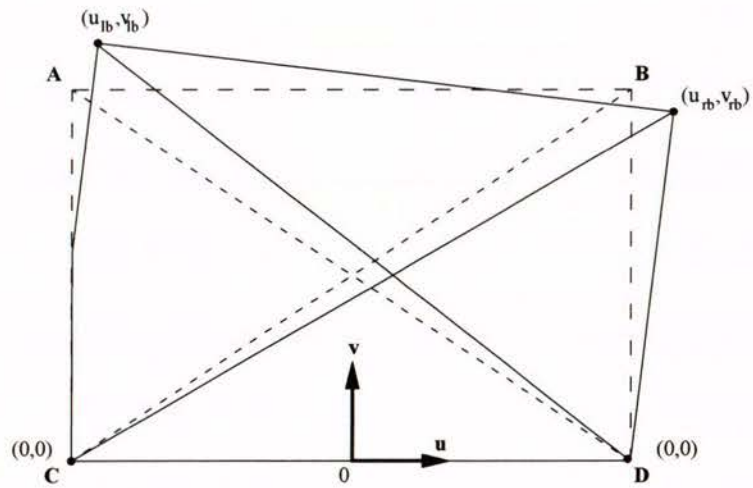
Figure D.2 Nodal displacement of a panel section.

The deformation of a panel section is illustrated in Figure D.2. It is assumed that the two upper points, A and B, may translate horizontally by u_l and u_r , and vertically by the amounts v_l and v_r . The lower points, C and D, are assumed to translate only horizontally by the amount $u_{l,lw}$ and $u_{r,lw}$. The subscripts 'l' and 'r' refer to the left and right hand sides respectively, while the subscript 'lw' refers to the lower points. The sign convention adopted is positive displacements to the right and upwards. As shown in Figure D.1, δ_{d1} and δ_{d2} are the elongation of the respective diagonal, while elongation of the horizontal elements are termed δ_{h1} and δ_{h2} , and elongation of the vertical elements are termed δ_{v1} and δ_{v2} . The dimensions of the panel are defined by the length, L , the height, H , and the diagonal length, d . The term d_u is used to define the position of the panel bracing with respect to the top of the wall, see Figure D.1(a).

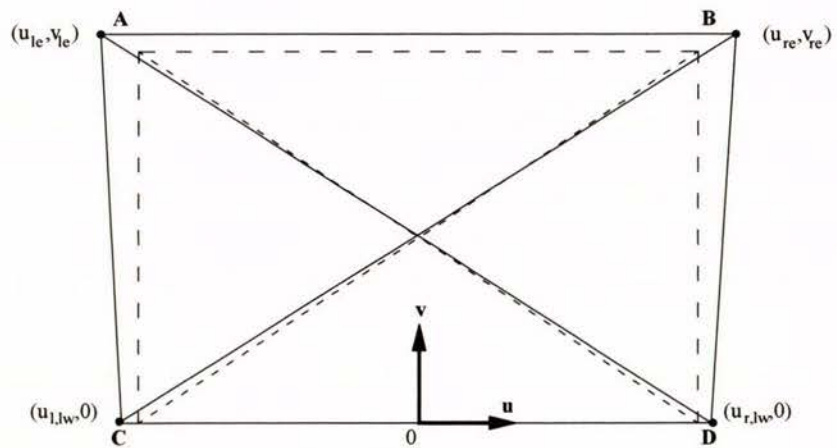
As shown in Figure D.3, the panel section deformation, represented by u_l , u_r , v_l , v_r , $u_{l,lw}$ and $u_{r,lw}$, is assumed to consist of the three components: shear, flexure and elongation. In this figure, the u and v represent the horizontal and vertical deformation components respectively. The subscripts 's', 'b' and 'e' represent the shear, flexural and elongation deformation components respectively.



(a) Shear deformation



(b) Flexural deformation



(c) Extension deformation

Figure D.3 Components of panel deformation.

The primary purpose of the following derivation is to calculate the horizontal displacement at the top of the wall due to shear deformation, U_s , by relating the measured elongation (δ 's) to individual displacement components: u 's and v 's. The following relations are assumed:

1. The left and right horizontal shear deformation components are equal.
2. The left and right horizontal flexural deformation components are equal.
3. The left and right horizontal extension components are equal but of opposite side.
4. The vertical shear deformation components are zero.
5. The upper left and right vertical extension deformation components are equal.

The above assumption can be represented as follow:

$$\begin{aligned}
 \text{a) } & u_{ls} = u_{rs} = u_s \\
 \text{b) } & u_{lb} = u_{rb} = u_b \\
 \text{c) } & u_{re} = -u_{le} = \frac{1}{2} u_e \\
 \text{d) } & u_{re,lw} = -u_{le,lw} = \frac{1}{2} u_{e,lw} \\
 \text{e) } & v_{le} = v_{re} = v_e
 \end{aligned}
 \tag{D-1}$$

The relationships between these displacements and those shown in Figure D.3 are as follows:

$$\begin{aligned}
 \text{a) } & u_l = u_s + u_b - \frac{1}{2} u_e \\
 \text{b) } & u_r = u_s + u_b + \frac{1}{2} u_e \\
 \text{c) } & u_{l,lw} = -\frac{1}{2} u_{e,lw} \\
 \text{d) } & u_{r,lw} = \frac{1}{2} u_{e,lw} \\
 \text{e) } & v_l = v_{lb} + v_e \\
 \text{f) } & v_r = v_{rb} + v_e
 \end{aligned}
 \tag{D-2}$$

The measured relative deformations can be expressed in terms of the global deformations by the following geometric relationships:

$$\begin{aligned}
 \text{a) } & \delta_{d1} = \frac{L}{d} (u_{r,lw} - u_l) + \frac{L}{h} v_l \\
 \text{b) } & \delta_{d2} = \frac{L}{d} (u_r - u_{l,lw}) + \frac{L}{h} v_r
 \end{aligned}
 \tag{D-3}$$

$$\begin{aligned}
 \text{c) } \delta_{h1} &= -u_l + u_r \\
 \text{d) } \delta_{h2} &= -u_{l,lw} + u_{r,lw} \\
 \text{e) } \delta_{v1} &= v_l \\
 \text{f) } \delta_{v2} &= v_r
 \end{aligned}
 \tag{D-3}$$

Substituting Equation D-2 into D-3:

$$\begin{aligned}
 \text{a) } \delta_{d1} &= \frac{L}{d} \left(-u_s - u_b + \frac{1}{2}u_e + \frac{1}{2}u_{e,lw} \right) + \frac{L}{h} (v_{lb} + v_e) \\
 \text{b) } \delta_{d2} &= \frac{L}{d} \left(u_s + u_b + \frac{1}{2}u_e + \frac{1}{2}u_{e,lw} \right) + \frac{L}{h} (v_{rb} + v_e) \\
 \text{c) } \delta_{h1} &= u_e \\
 \text{d) } \delta_{h2} &= u_{e,lw} \\
 \text{e) } \delta_{v1} &= v_{lb} + v_e \\
 \text{f) } \delta_{v2} &= v_{rb} + v_e
 \end{aligned}
 \tag{D-4}$$

From Equation D-4 it seems that the equation is under-determined since the equations are describing the relationship between 6 known measured relative displacements (δ 's) and unknown panel deformation components (u 's and v 's). Inserting Equations D-4(c) and (d) into Equations D-4(e) and (f), and then subtracting D-4(e) from D-4(f) gives:

$$\delta_{d2} - \delta_{d1} = \frac{L}{d} (2u_s + 2u_b) + \frac{L}{h} (\delta_{v2} - \delta_{v1})
 \tag{D-5}$$

Rearranging Equation D-5:

$$u_s = \frac{d}{2L} (\delta_{d2} - \delta_{d1}) + \frac{h}{2L} (\delta_{v1} - \delta_{v2}) - u_b
 \tag{D-6}$$

Equation D-6 can be solved by defining an equation relating the flexural deformation component to the measured relative displacement. This is displayed in Equation D-7:

$$u_b = \theta h \alpha
 \tag{D-7}$$

where:

$$\theta = \frac{\delta_{v1} - \delta_{v2}}{L}$$

Equation D-7 states that the flexural deformation is equal to the rotation at the top of the panel section multiplied by the panel section height and by α . When taking α as $2/3$, the equation captures the exact flexural displacement of an elastic prismatic cantilever with a concentrated horizontal force applied at the top, with θ representing the rotation of the top of the wall. However, for reinforced concrete masonry and reinforced concrete walls, the parameter α is generally higher than $2/3$ since the wall flexural cracking tends to concentrate rotation towards the bottom of the wall, therefore resulting in higher α and higher u_b .

In this study, the flexural deflection u_b for a section of wall was calculated from the measured rotation that occurs within the section under study. This rotation is calculated from the bending moment diagram. The bending moment at the top (M_{up}) and the bottom (M_{lw}) of a panel section are known to vary linearly according to the vertical location as shown in Figure D-1(b).

The moment (M)-curvature (φ) relationship for an elastic section is given by:

$$M = \varphi EI \quad (D-8)$$

where E and I are the modulus of elasticity and inertia moment. As the curvature is a linear function of the moment, the total rotation of the panel section between d_u and d_u+h can be calculated from the average bending moment:

$$\theta = \frac{h(M_{up} + M_{lw})}{2EI} \quad (D-9)$$

The panel flexural deformation, u_b , is evaluated by integration of curvature along the height of the panel section with the following result:

$$u_b = \frac{h^2}{EI} \left(\frac{M_{lw}}{3} + \frac{M_{up}}{6} \right) = \theta h \left(\frac{d_u + \frac{2h}{3}}{2d_u + h} \right) \text{ where } \alpha = \frac{d_u + \frac{2h}{3}}{2d_u + h} \quad (D-10)$$

The α given in Equation D-10 is defined with respect to the top of the investigated panel section.

u_b can be evaluated by incorporating Equation D-7:

$$u_b = \frac{h(\delta_{v1} - \delta_{v2})}{L} \left(\frac{d_u + \frac{2h}{3}}{2d_u + h} \right) \quad (D-11)$$

Subsequently, the shear deformation for the panel section can be evaluated by substituting Equation D-11 into Equation D-6:

$$u_s = \frac{d}{2L} (\delta_{d2} - \delta_{d1}) + \frac{h}{2L} (\delta_{v1} - \delta_{v2}) - \frac{h(\delta_{v1} - \delta_{v2})}{L} \left(\frac{d_u + \frac{2h}{3}}{2d_u + h} \right) \quad (D-12)$$

Rearranging Equation D-12 to give:

$$u_s = \frac{d}{2L} (\delta_{d2} - \delta_{d1}) - \frac{h^2}{6(2d_u + h)} \frac{(\delta_{v1} - \delta_{v2})}{L} \quad (D-13)$$

The total shear displacement, U_s , is given by the sum of the shear deformations from the individual panel sections:

$$U_s = \sum u_s \quad (D-14)$$

In addition, the total flexural displacement can be evaluated as follows. The flexural deformation of the investigated panel section (see Figure D.1(c)) with respect to the top of the wall, u'_b , is evaluated as:

$$u'_b = \theta(\alpha h + d_u) = \frac{(\delta_{v1} - \delta_{v2})}{L} \left(h \frac{d_u + \frac{2h}{3}}{2d_u + h} + d_u \right) \quad (D-15)$$

The total flexural displacement, U_b , is the summation of flexural deformation from individual panel section:

$$U_b = \sum u'_b \quad (D-16)$$

Appendix E- Properties of Available Wall Tests

Fully Grouted Walls

The experimental data sets presented in this section are limited to those of fully grouted concrete and clay brick reinforced masonry walls, which were subjected to reverse cyclic lateral forces and failed in shear. Relevant properties of the tested walls are listed in Table E.1. The data sets selected are (i) tests conducted by Shing et al. (1990), specimen no. 1-10, (ii) tests conducted by Matsumura (1987), specimen no. 11-28, (iii) tests conducted by Okamoto et al. (1987), specimen no. 29-36, (iv) tests conducted by Sveinsson et al. specimen no. 37-57, and (v) tests conducted at the University of Auckland, specimen no. 58-64. Of the 64 specimens listed in Table E.1, nineteen of them were of single-wythe walls constructed with hollow brick units, see shaded rows.

Table E.1 Properties of specimens, fully grouted

Specimen no.	Specimen label	h mm	L mm	t mm	d mm	s _n mm	ρ _n X10 ⁻³	f _{yh} MPa	ρ _{ve} X10 ⁻³	ρ _v X10 ⁻³	f _{yv} MPa	f _m MPa	σ _n MPa	μ _{vmax}
1	1-S	1830	1830	143	1727	406	1.22	385.8	1.48	7.41	496.1	20.67	1.86	4.11
2	2-S	1830	1830	143	1727	406	1.22	385.8	1.48	7.41	496.1	17.91	0	2.82
3	3-S	1830	1830	143	1727	406	1.22	385.8	1.48	7.41	496.1	17.91	0.69	2.50
4	4-S	1830	1830	143	1727	406	1.22	385.8	1.48	7.41	496.1	22.36	0.69	3.20
5	5-S	1830	1830	143	1727	406	1.22	385.8	0.77	3.83	441.3	22.36	1.86	1.0
6	6-S	1830	1830	143	1727	406	2.22	491.6	1.09	5.43	448.2	23.04	1.86	1.40
7	7-S	1830	1830	143	1727	406	1.22	385.8	1.09	5.43	228.2	23.04	1.86	1.68
8	8-S	1830	1830	143	1727	406	2.22	491.6	1.48	7.41	496.1	17.07	1.86	4.13
9	9-S	1830	1830	137	1727	406	1.28	385.8	1.14	5.68	496.1	26.18	1.93	2.31
10	10-S	1830	1830	137	1727	406	1.28	385.8	1.14	5.68	496.1	26.18	0.69	1.67
11	1-M	1800	1590	150	1500	400	1.18	385	4.26	9.43	385	21.8	0.49	---
12	2-M	1800	1190	150	1100	400	1.18	385	4.34	9.46	385	21.8	0.49	---
13	3-M	1800	1190	150	1100	400	1.18	385	4.34	9.46	385	21.8	0.49	---
14	4-M	1800	790	150	700	400	1.18	385	5.41	11.48	385	21.8	0.49	---
15	5-M	1800	1190	190	1095	400	0	385	2.54	5.71	385	22.3	1.96	0.95
16	6-M	1800	1190	190	1095	400	1.67	385	2.54	5.71	385	22.3	1.96	1.14
17	7-M	1800	1190	190	1095	400	3.34	385	2.54	5.71	385	22.3	1.96	3.36
18	8-M	1800	1190	190	1095	400	3.34	385	4.48	9.59	385	22.3	1.96	1.27
19	9-M	1800	1190	190	1095	400	6.68	385	4.48	9.59	385	22.3	1.96	2.28
20	10-M	1800	1190	190	1095	400	3.34	385	4.48	9.59	385	29	1.96	---
21	11-M	1800	1190	190	1095	400	3.34	385	4.48	9.59	385	26.1	1.96	---
22	12-M	1800	1190	190	1095	400	4.00	385	4.48	9.59	385	27.4	1.96	---

Table E.1 Properties of specimens, fully grouted (continued)

Specimen no.	Specimen label	h mm	L mm	t mm	d mm	s _h mm	ρ _h X10 ⁻³	f _{yh} MPa	ρ _{ve} X10 ⁻³	ρ _v X10 ⁻³	f _{yv} MPa	f _m MPa	σ _n MPa	μ _{vmax}
23	13-M	1800	1190	190	1095	400	3.53	385	4.73	10.13	385	26.4	1.96	---
24	14-M	1800	1190	190	1095	400	3.34	385	4.48	9.59	385	31.4	1.96	---
25	15-M	1700	1110	190	1005	378	0	385	2.72	6.12	385	28.6	1.96	1.94
26	16-M	1700	1110	190	1005	378	1.67	385	2.72	6.12	385	28.6	1.96	2.97
27	17-M	1700	1110	190	1005	378	3.34	385	2.72	6.12	385	28.6	1.96	1.83
28	18-M	1700	1110	190	1005	378	6.68	385	2.72	6.12	385	28.6	1.96	2.04
29	1-O	1800	2000	190	1905	400	1.67	354.4	1.49	5.09	378.9	17.9	0	2.32
30	2-O	1800	1200	190	1105	400	1.67	354.4	2.49	6.74	378.9	22.8	1.96	1.12
31	3-O	1800	800	190	705	400	1.67	354.4	3.74	8.79	378.9	17.9	0	7.25
32	4-O	1800	1200	190	1105	400	1.67	354.4	2.49	6.74	378.9	22.8	3.92	---
33	5-O	1800	1200	190	1105	400	1.67	354.4	2.49	6.74	378.9	22.8	5.87	---
34	6-O	1800	2000	190	1905	400	1.67	354.4	1.49	5.09	378.9	26.7	0	2.72
35	7-O	1800	1200	190	1105	400	1.67	354.4	2.49	6.74	378.9	25.2	0	3.37
36	8-O	1800	800	190	705	400	1.67	354.4	3.74	8.79	378.9	21.4	0	3.82
37	1-B	1422	1219	194	1143	284	2.87	406.5	0.85	1.69	465.1	23.1	1.88	5.39
38	2-B	1422	1219	194	1143	284	2.87	406.5	0.85	1.69	465.1	23.1	3.01	5.23
39	3-B	1422	1219	143	1143	284	3.94	437.5	2.22	4.44	390.7	15.8	2.76	4.21
40	4-B	1422	1219	143	1143	284	3.94	437.5	0.74	4.44	410	15.8	2.76	2.20
41	5-B	1422	1219	143	1143	474	1.97	437.5	2.22	4.44	390.7	15.1	2.76	4.90
42	6-B	1422	1219	143	1143	474	1.97	437.5	0.74	4.44	410	15.1	2.76	5.38
43	7-B	1422	1219	143	1143	203	0.75	437.5	2.22	4.44	390.7	15.1	2.76	4.41
44	8-B	1422	1219	143	1143	399	2.72	437.5	2.22	4.44	390.7	15.1	2.76	6.26
45	9-B	1422	1219	143	1143	474	1.97	437.5	2.22	4.44	390.7	15.1	1.74	3.23
46	10-B	1422	1219	143	1143	474	1.97	437.5	2.22	4.44	390.7	15.1	2.76	2.27
47	11-B	1422	1219	143	1143	474	1.95	437.5	2.22	4.44	390.7	20.1	2.76	3.87
48	12-B	1422	1219	143	1143	237	4.87	437.5	2.22	4.44	390.7	20.1	2.76	3.2
49	13-B	1422	1219	143	1143	474	1.97	437.5	2.22	6.74	390.7	20.1	2.76	3.75
50	14-B	1422	1219	143	1143	237	4.87	437.5	1.15	4.59	437.5	20.1	2.76	3.22
51	15-B	1422	1219	143	1143	474	1.97	437.5	0.74	4.44	410	20.1	2.76	4.68
52	16-B	1422	1219	143	1143	237	4.87	437.5	0.74	4.44	410	20.1	2.76	5.18
53	17-B	1422	1219	143	1143	474	1.97	437.5	2.22	1.48	390.7	20.1	2.76	2.21
54	18-B	1422	1219	143	1143	237	4.87	437.5	2.22	4.44	390.7	20.1	2.76	2.68
55	19-B	1422	1219	143	1143	284	2.50	410	2.22	4.44	390.7	20.1	2.76	3.38
56	20-B	1422	1219	143	1143	129	6.25	416.9	2.22	4.44	410	20.1	2.76	3.36
57	21-B	1422	1219	143	1143	203	1.00	437.5	2.22	4.44	390.7	27.6	2.76	2.86
58	1-A	1800	1800	140	1700	400	0.50	325	1.25	6.23	318	17.6	0	2.67
59	2-A	1800	1800	140	1700	1800	0	325	1.25	6.23	318	17.6	0	2.61
60	3-A	1800	1800	140	1700	800	0.62	310	1.25	5.61	6.23	318	17	2.60
61	4-A	1800	1800	140	1700	400	0.50	325	1.25	5.61	6.23	318	18.5	2.73
62	5-A	1800	1800	140	1700	400	0.50	325	1.25	5.61	6.23	318	18.5	2.73
63	6-A	3600	1800	140	1700	400	0.51	325	1.90	9.70	550	24.3	0.25	2.85
64	7-A	1800	3000	140	2900	400	0.51	325	0.75	5.90	318	24.3	0.25	1.33

Partially Grouted Walls

The experimental data sets presented in section are limited to those of partially grouted reinforced masonry walls which were subjected to reverse cyclic lateral forces and failed in shear. Relevant properties of the tested walls are listed in Table E.2. The data sets selected are (i) tests conducted by Matsumura (1987), specimen no. 1-30, (ii) tests conducted by Chen et al. (1978), specimen no. 31-36, and (iii) tests conducted at the University of Auckland, specimen no. 37 and 38. All specimens, except specimens 29, 30, 34, 35 and 36, were constructed of concrete masonry units. The three shaded specimens shown in Table E.2 were constructed of hollow clay brick units.

Table E.2 Properties of specimens, partially grouted

Specimen no.	Specimen Label	h mm	L mm	t mm	D Mm	S _h mm	ρ _h	f _{yh} MPa	ρ _{ve} X10 ⁻³	ρ _v X10 ⁻³	f _{yv} MPa	f _m MPa	σ _o MPa	μ _{vmax}
1	1-MP	1800	1720	150	1655	0	0.71	385.6	3.00	6.83	385.6	16.4	0	---
2	2-MP	1800	1720	150	1655	0	0.71	385.6	3.70	8.23	385.6	27	0	---
3	3-MP	1800	1320	150	1255	0	0.71	385.6	3.90	8.52	385.6	16.4	0	---
4	4-MP	1800	1320	150	1255	0	0.71	385.6	3.57	7.86	385.6	27	0	---
5	5-MP	1800	920	150	855	0	0.71	385.6	5.61	21.40	385.6	16.4	0	---
6	6-MP	1800	920	150	855	0	0.71	385.6	3.67	17.52	385.6	27	0	---
7	7-MP	1800	1320	150	1255	0	0	0	3.91	8.54	385.6	16.4	0	0.65
8	8-MP	1800	1320	150	1255	0	0	0	3.91	8.54	385.6	16.4	0	---
9	9-MP	1800	1320	150	1255	0	0.71	385.6	3.91	8.54	385.6	16.4	0	2.49
10	10-MP	1800	1320	150	1255	0	1.48	385.6	3.91	8.54	385.6	16.4	0	1.76
11	11-MP	1800	1320	150	1255	0	2.22	385.6	3.91	8.54	385.6	16.4	0	1.20
12	12-MP	1800	1320	150	1255	0	0.71	385.6	3.91	8.54	385.6	27	0.69	0.661
13	13-MP	1800	1320	150	1255	0	0.71	385.6	3.91	8.54	385.6	27	1.39	1.61
14	14-MP	1800	1320	150	1255	0	0.71	385.6	3.91	8.54	385.6	27	2.08	1.82
15	15-MP	1800	1320	150	1255	0	0	0	3.77	8.23	385.6	14	0.68	---
16	16-MP	1800	1320	150	1255	0	1.48	385.6	3.77	8.23	385.6	14	0.68	---
17	17-MP	1800	1320	150	1255	0	2.22	385.6	3.77	8.23	385.6	14	0.68	---
18	18-MP	1800	1320	150	1255	0	3.35	385.6	3.77	8.23	385.6	14	0.68	---
19	19-MP	1800	1320	150	1255	0	0	0	3.91	14.98	385.6	27	1.39	0.55
20	20-MP	1800	1320	150	1255	0	0	0	3.91	14.98	385.6	14	1.39	---
21	21-MP	1800	1320	150	1255	0	1.48	385.6	3.91	14.98	385.6	27	1.39	1.27
22	22-MP	1800	1320	150	1255	0	2.22	385.6	3.91	14.98	385.6	27	1.39	2.69
23	23-MP	1800	1970	150	1880	0	1.48	385.6	2.61	6.18	385.6	27	0.69	---
24	24-MP	1800	1970	150	1880	0	1.48	385.6	2.61	6.18	385.6	27	0.69	---
25	25-MP	1800	1770	150	1689	0	1.48	385.6	2.42	5.64	385.6	27	0.68	---
26	26-MP	1800	1370	150	1280	0	1.48	385.6	2.42	5.53	385.6	27	0.67	---
27	27-MP	1800	970	150	880	0	1.48	385.6	2.66	5.81	385.6	27	0.67	---
28	28-MP	1800	970	150	880	0	1.48	385.6	2.66	5.81	385.6	27	0.67	---
29	29-MP	1600	1320	150	1255	400	1.07	385.6	3.84	8.00	385.6	33.6	0	3.05
30	30-MP	1600	1320	150	1255	400	1.07	385.6	3.84	8.00	385.6	31.2	0	1.58

Table E.2 Properties of specimens, partially grouted (continued)

Specimen no.	Specimen Label	h mm	L mm	t mm	d mm	s _h mm	ρ _h	f _{yh} MPa	ρ _{ve} X10 ⁻³	ρ _v X10 ⁻³	f _{yv} MPa	f _m MPa	σ _o MPa	μ _{vmax}
31	1-BP	1422	1219	194	1143	1422	0.73	331	0.85	1.70	488	12.7	0.94	1.63
32	2-BP	1422	1219	194	1143	0	0	0	2.14	4.28	477	13.1	0.92	1.20
33	3-BP	1422	1219	194	1143	711	1.43	331	2.14	4.28	477	13.1	0.98	0.73
34	4-BP	1422	1219	187	1143	1422	0.74	482	0.87	1.74	492	18.8	1.96	0.80
35	5-BP	1422	1219	187	1143	0	0	0	2.20	4.40	477	19.8	1.79	0.70
36	6-BP	1422	1219	187	1143	711	1.48	474	2.20	4.40	477	18.8	1.89	2.12
37	1-AP	1800	1800	140	1700	0	0	0	1.25	6.23	318	18.5	0	1.70
38	2-AP	1800	1800	140	1700	0	0	0	1.25	3.74	318	18.5	0	1.76

Appendix F-Material Properties

During the construction of masonry walls in Series B and C, test cylinders were created to obtain the crushing strengths of the mortar and grout. Samples of reinforcing steel were taken to attain the yield strengths. These data are tabulated in Tables F.1 and F.2 respectively.

Table F.1 Series B and C, mortar and grout strength

Wall no.	Mortar (MPa)		Grout (MPa)		f'_m (MPa)	
	Average		Average		Average	
1 & 2	12.6	12.9	10.4	9.7	16.8	17.6
	13.2		9.3		18.1	
	12.8		9.3		17.9	
3 & 4	11.2	10.9	10.7	10.8	17.2	17.0
	10.7		11.2		16.8	
	10.8		10.5		17.0	
5 & 6	12.6	11.5	12.1	11.0	18.0	18.5
	11.1		10.6		18.7	
	10.8		10.3		18.8	
7 & 8	12.2	12.0	11.1	10.9	18.5	18.8
	12.1		10.9		19.0	
	11.7		10.7		18.9	
9 & 10	12.4	12.3	8.40	9.3	24.7	24.3
	12.6		9.42		23.2	
	11.9		9.93		24.9	

Table F.2 Yield strength of reinforcing steel

	R6 (MPa)	D10 (MPa)	D20 (MPa)
Sample 1	305	318	317
Sample 2	338	325	312
Sample 3	332	317	325
Average	325	320	318

In order to determine the effect of threading on the yield strength of D20 reinforcing bar, two types of bar were subjected to tensile test. Figure F.1 compares the test results of the threaded and unthreaded D20 reinforcing bars. It is clearly illustrated in Figure F.1 that the threading had negligible effect on the yield strength of D20. However, it is also shown here that the threading has significantly reduced the post elastic performance of the reinforcing bars.

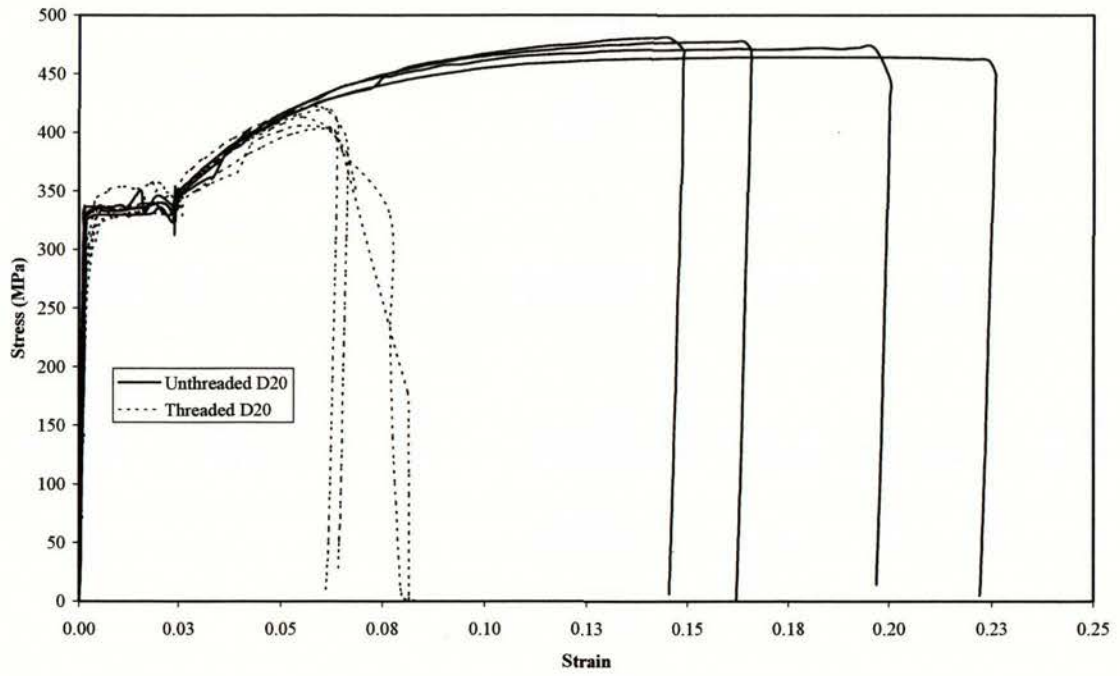


Figure F.1 Stress-strain curve for the threaded and unthreaded D20 reinforcing bars.

Appendix G - Photos



Photo 1 Footing reinforcement cages positioned in boxing.



Photo 2 Position of vertical reinforcing bars.



Photo 3 Masonry wall construction.



Photo 4 Masonry wall grouting.

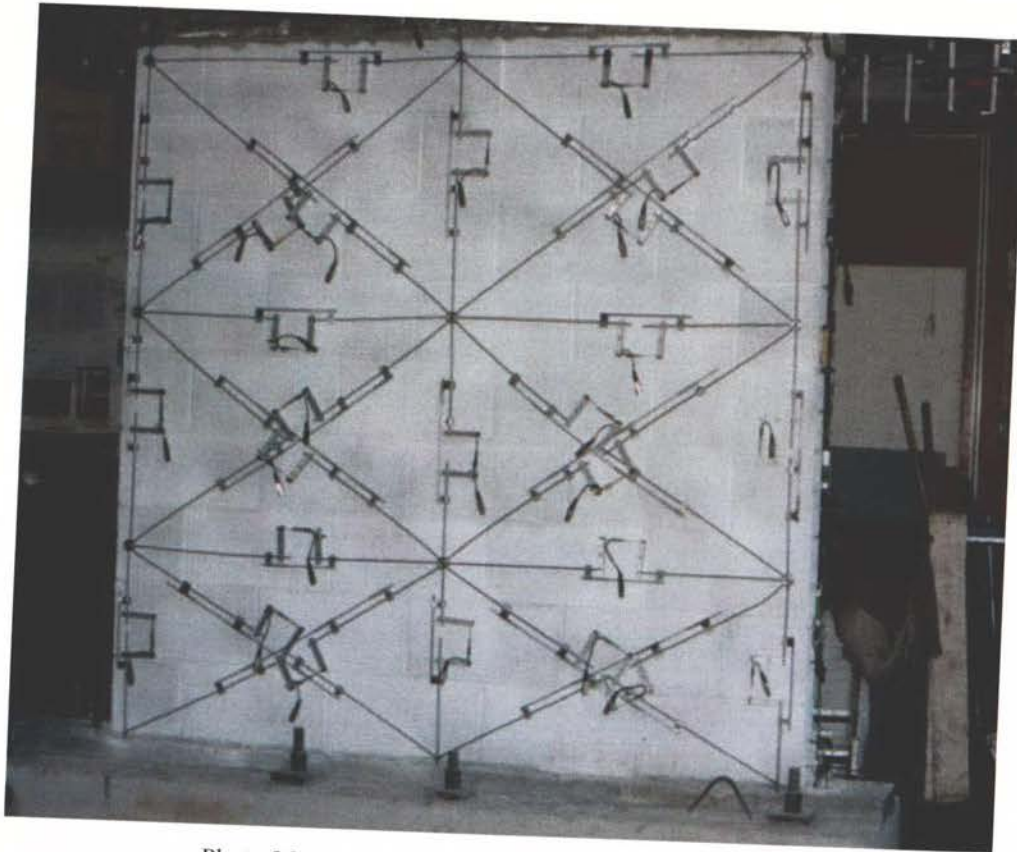


Photo 5 Instrumentation mounted on wall before testing.

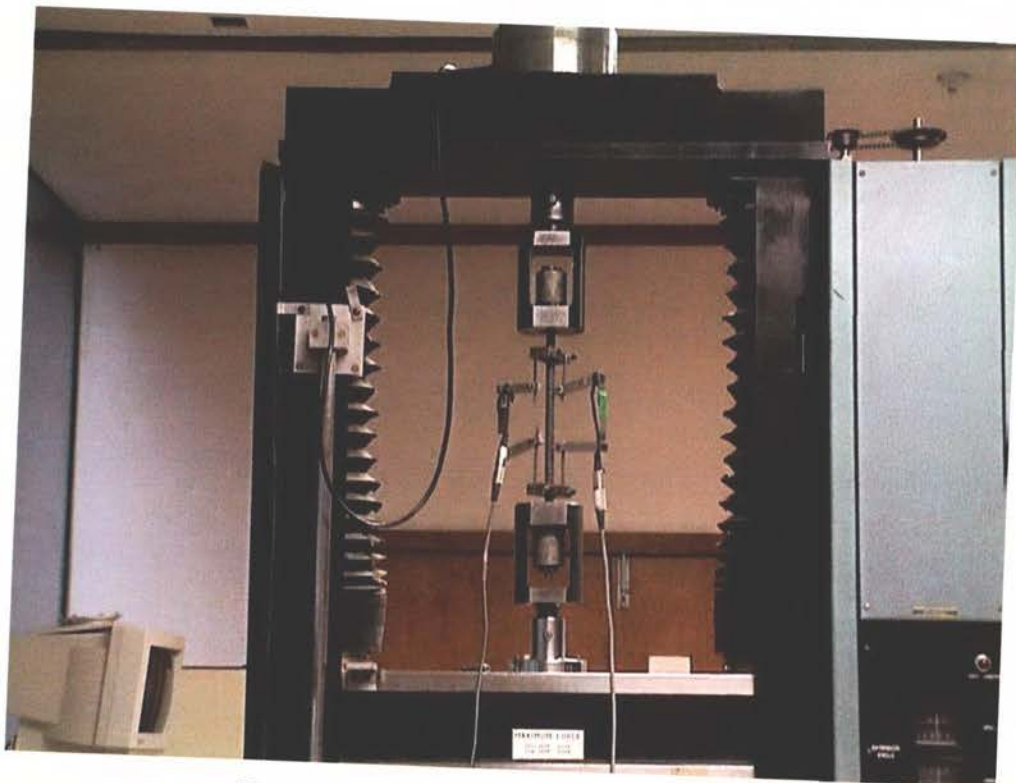


Photo 6 Reinforcing steel subjected to tensile test.



Photo 7 Masonry prisms grouting.

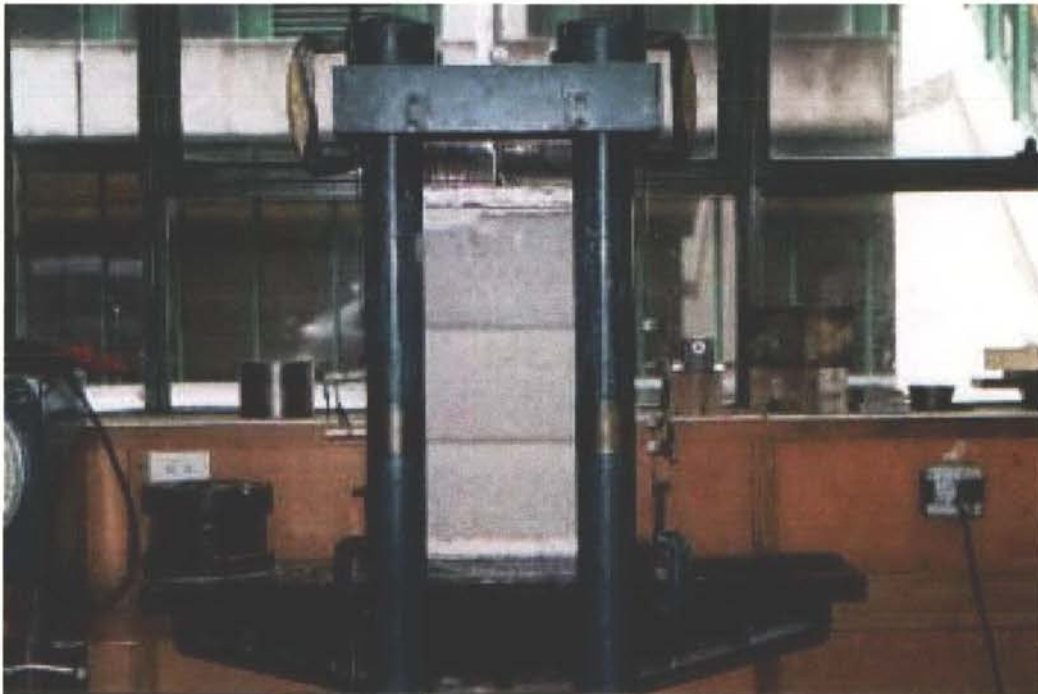


Photo 8 Masonry prism subjected to compression test.

Photos of Wall 1



Photo 9 Diagonal cracking after first cycle of ± 4 mm displacement.

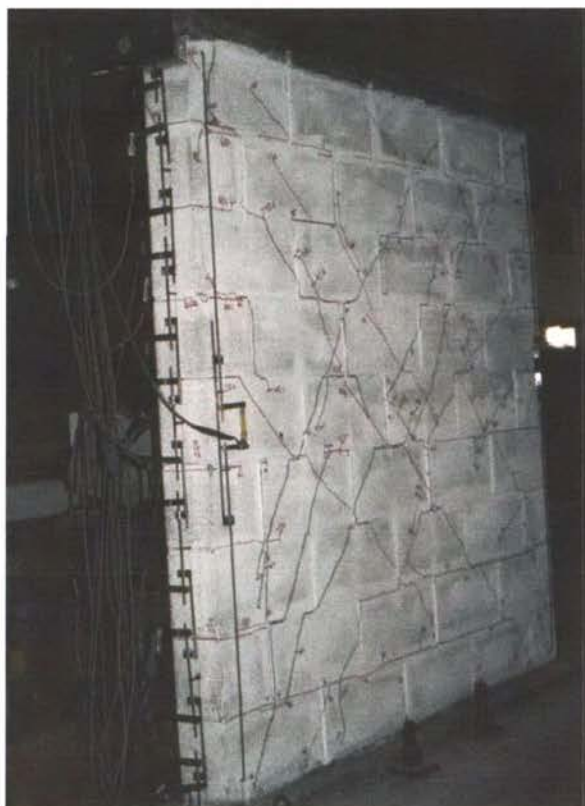


Photo 10 Wall condition after second cycle ± 6 mm displacement.



Photo 11 Compression toe degradation at +10 mm displacement.

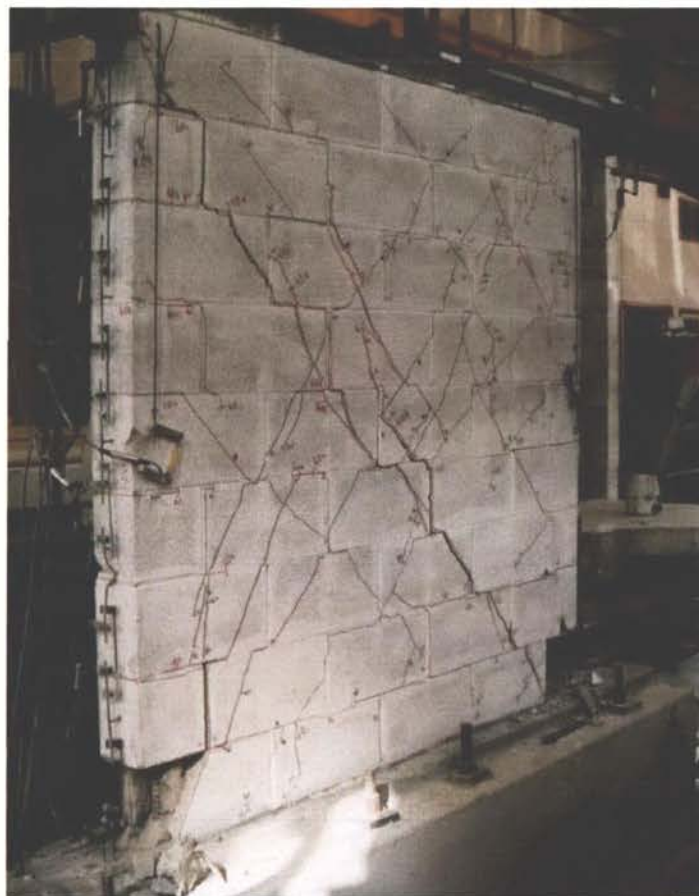


Photo 12 Completed crushing of wall toes at ± 14 mm displacement.

Photos of Wall 2

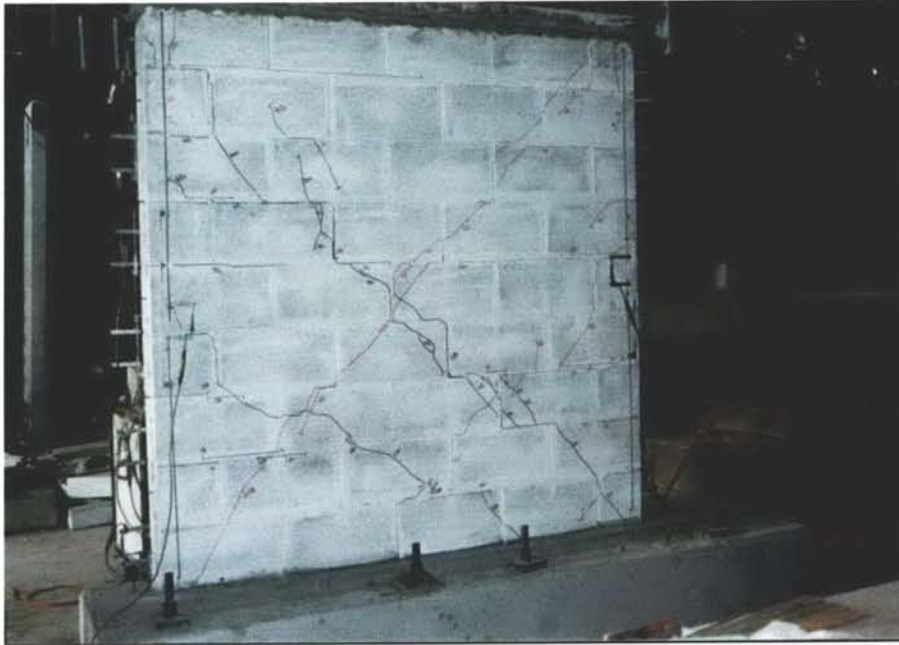


Photo 13 X-shaped diagonal cracking after ± 4 mm displacement.

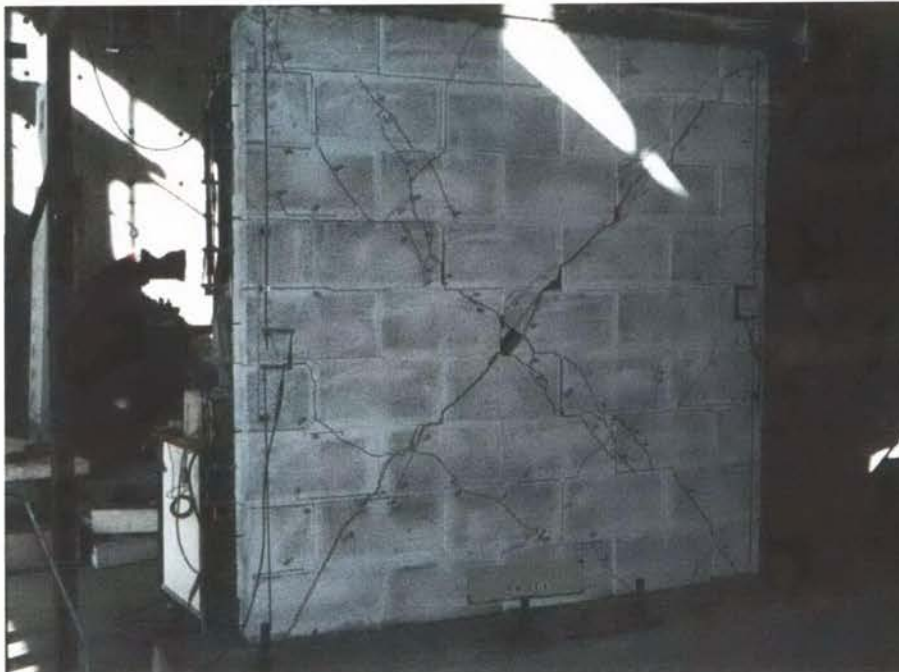


Photo 14 Spalling of face shells at second push cycle of 8 mm displacement.



Photo 15 Crushing of masonry at second cycle of -10 mm displacement.

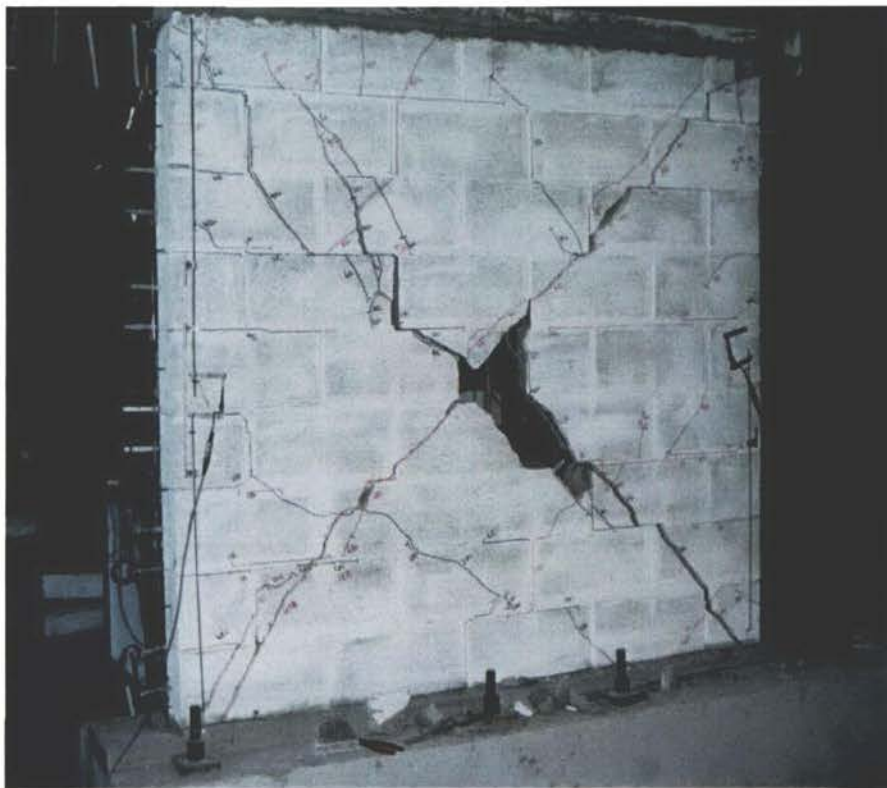


Photo 16 Condition of wall at end of testing.

Photos of Wall 3



Photo 17 Condition of test wall after first cycle to ± 2 mm displacement.



Photo 18 Formation of x-shaped diagonal crack after first cycle to ± 4 mm displacement.

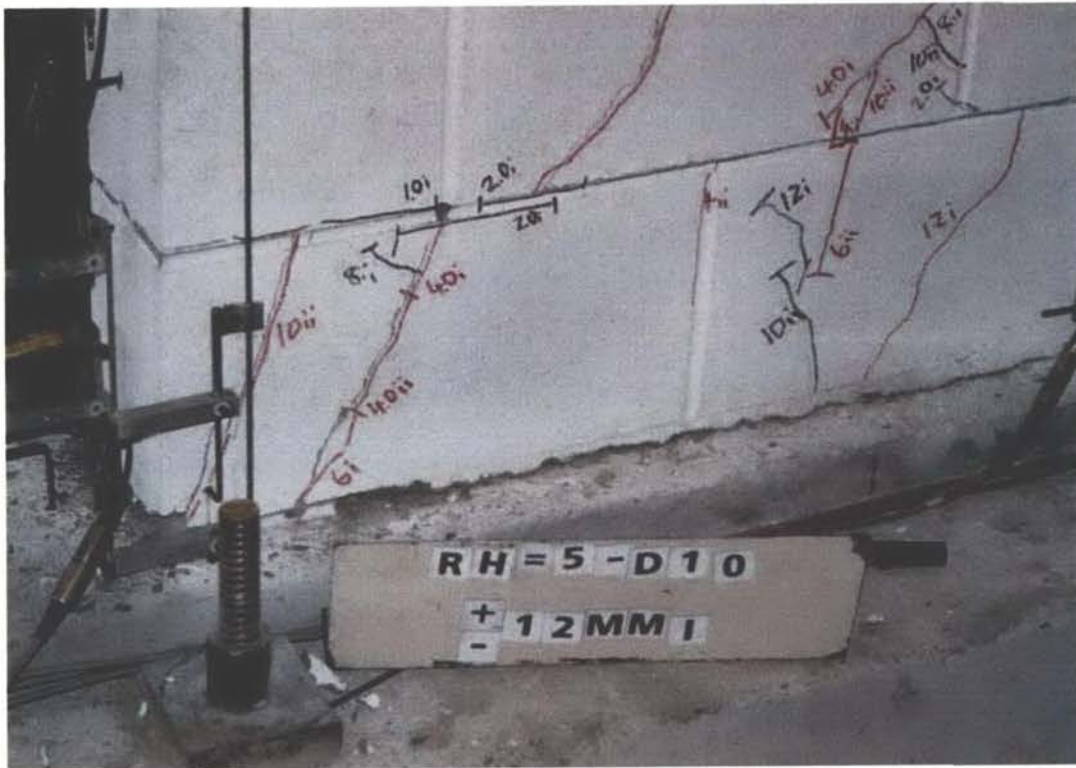


Photo 19 Wall toe condition after first cycle to ± 12 mm displacement.



Photo 20 Wall toe condition after first push cycle to 16 mm displacement.

Photos of Wall 4

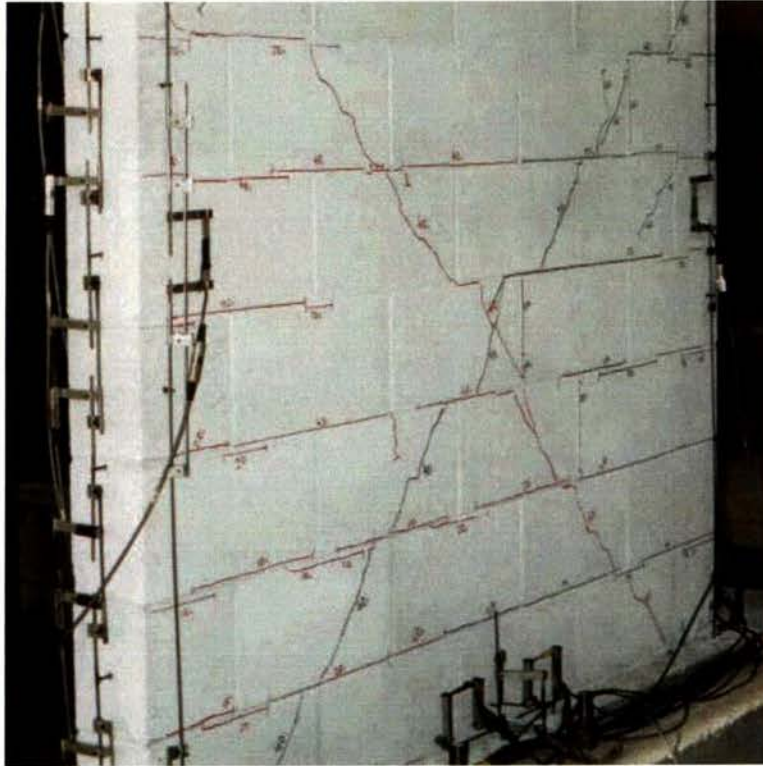


Photo 21 Condition of the test wall after first cycle to ± 4 mm displacement.

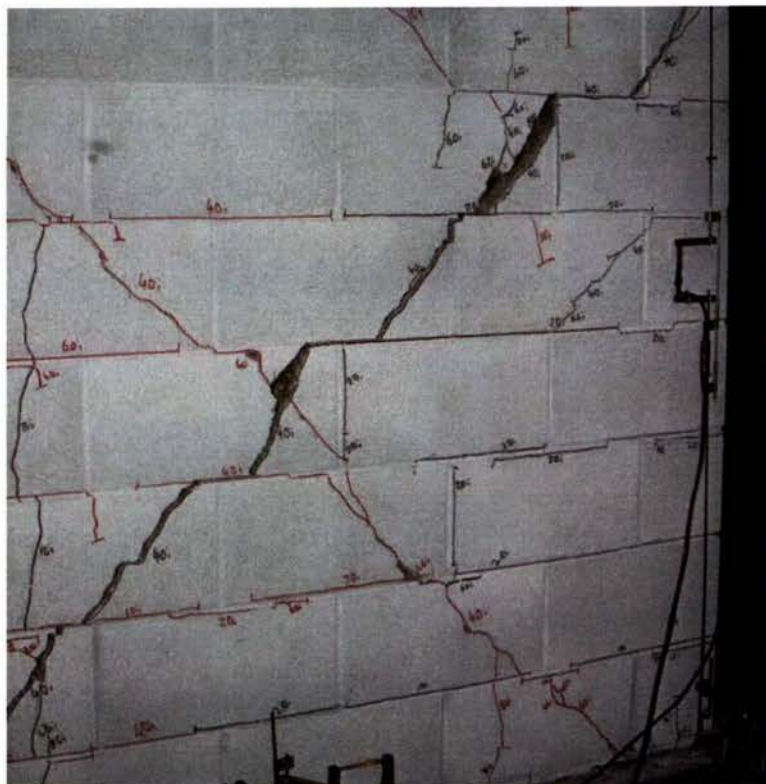


Photo 22 Condition of test wall after second cycle to ± 10 mm displacement.

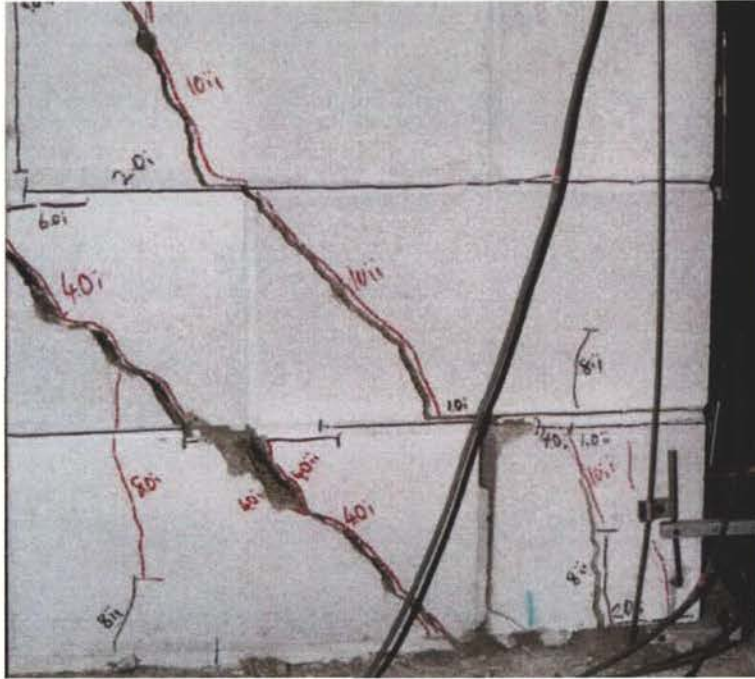


Photo 23 Condition of compression toe after first cycle to 12 mm displacement.

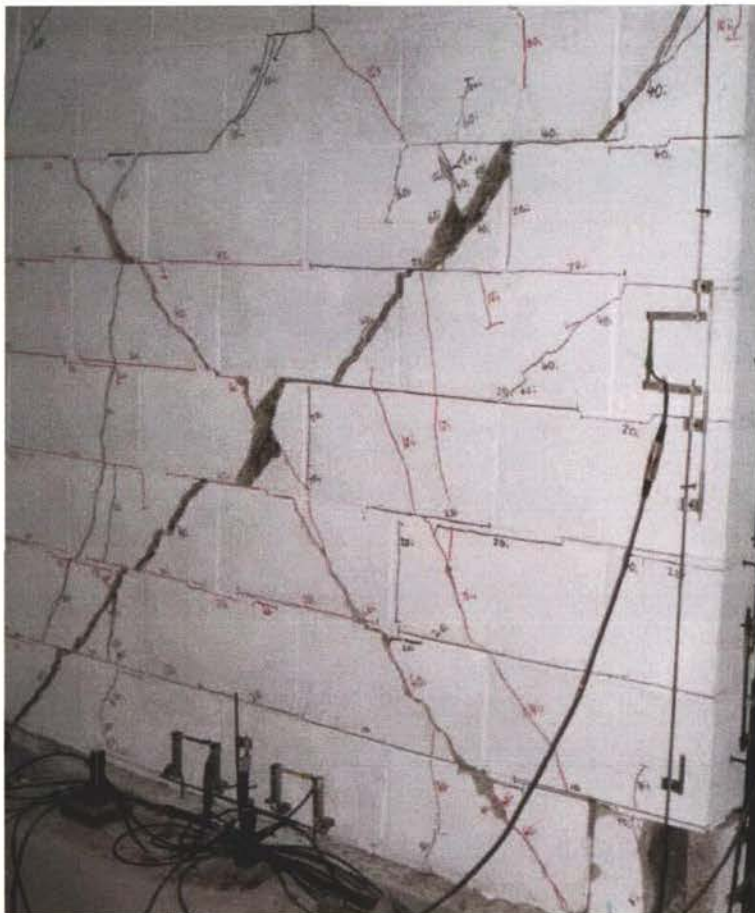


Photo 24 Condition of test wall at end of testing.

Photos of Wall 5

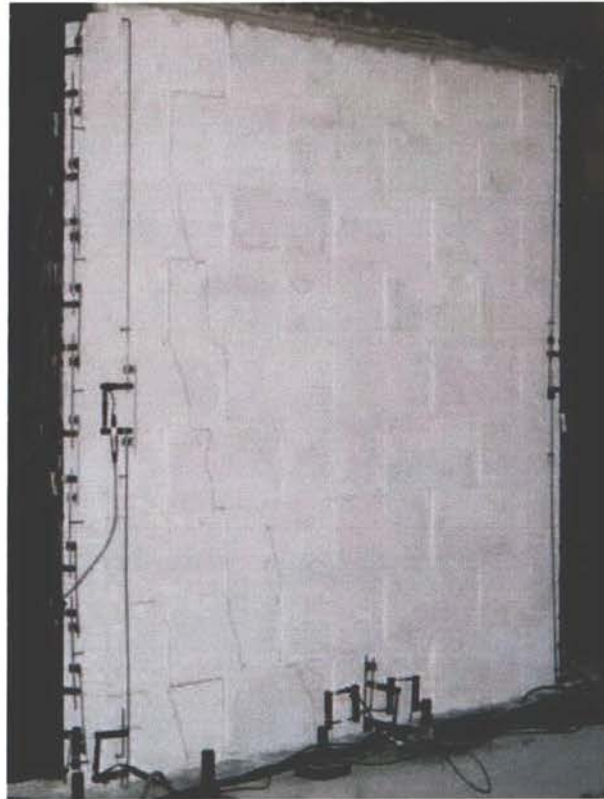


Photo 25 Wall condition before testing.

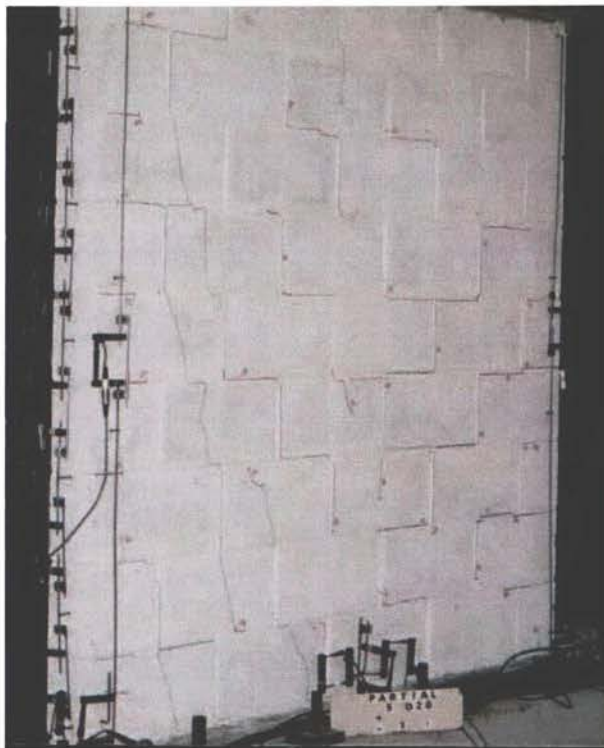


Photo 26 Wall condition after first cycle to ± 1 mm displacement.



Photo 27 Wall condition after second cycle to ± 10 mm displacement.



Photo 28 Wall condition after second cycle to ± 12 mm displacement.

Photos of Wall 6

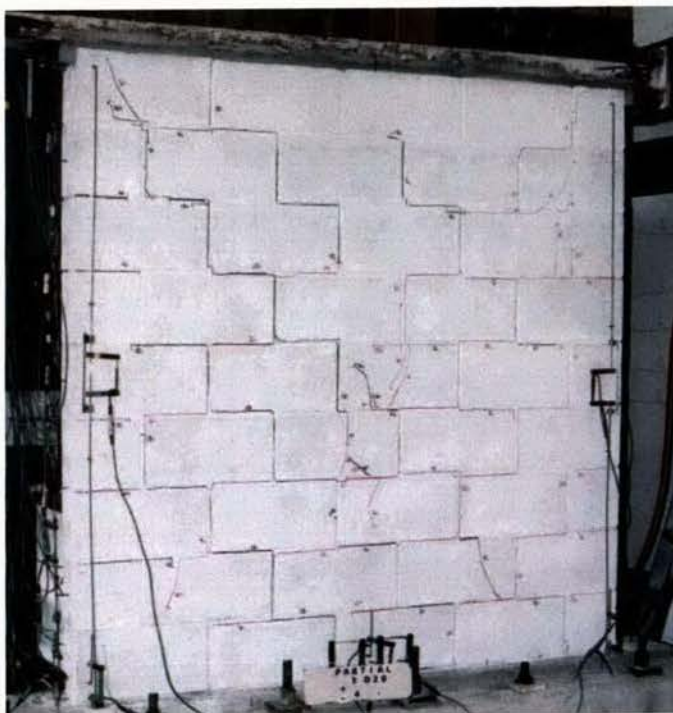


Photo 29 Condition of test wall after first cycle to ± 4 mm displacement.



Photo 30 Condition of test wall after first cycle to ± 16 mm displacement.

Photos of Wall 7

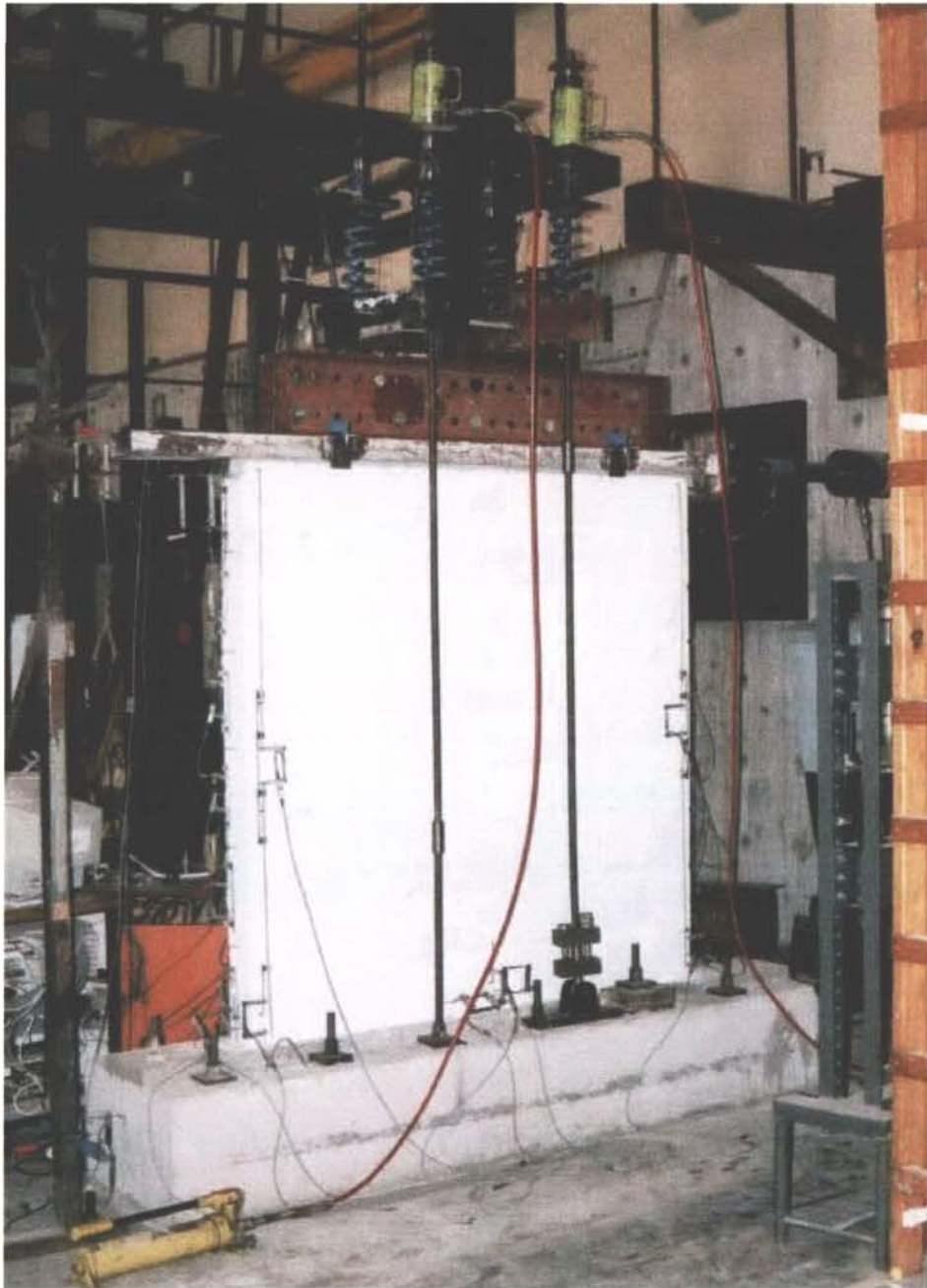


Photo 31 Test set-up for Wall 7.

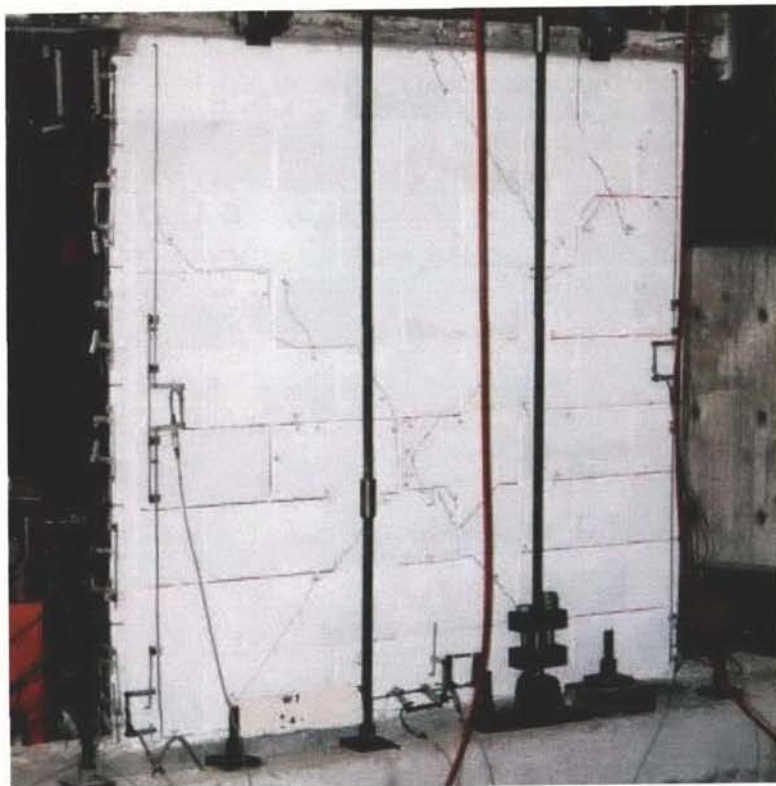


Photo 32 Condition of test wall after first cycle to ± 4 mm displacement.

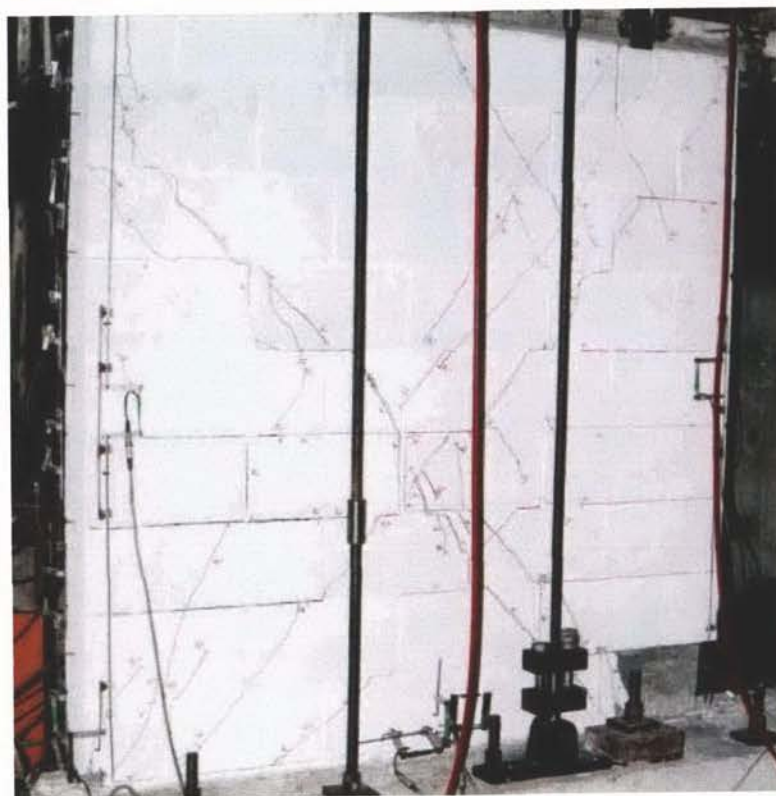


Photo 33 Condition of test wall after second cycle to ± 8 mm displacement.

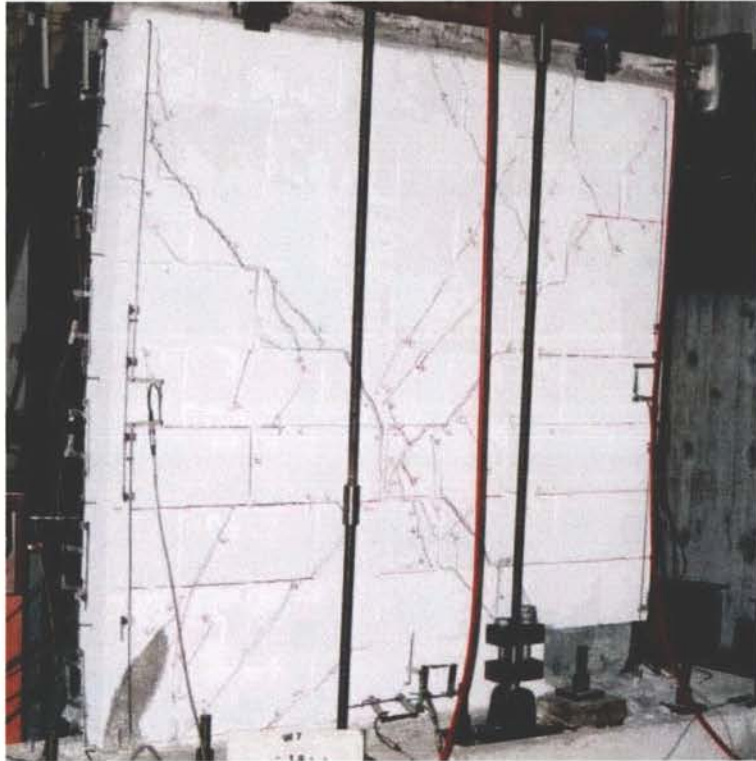


Photo 34 Condition of test wall after second cycle to ± 10 mm displacement.

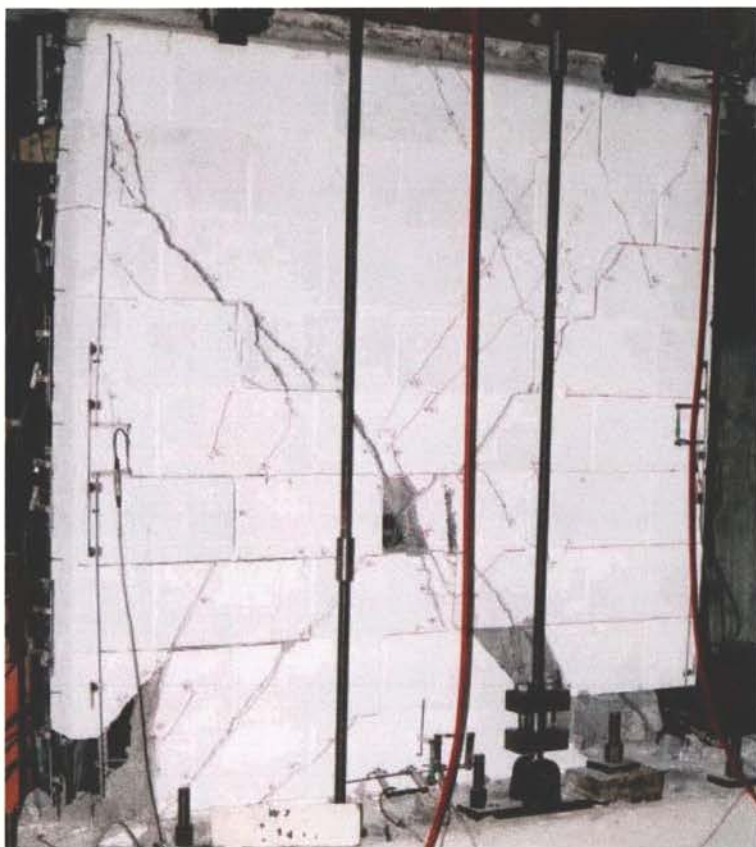


Photo 35 Condition of test wall after second cycle to ± 14 mm displacement.

Photos of Wall 8

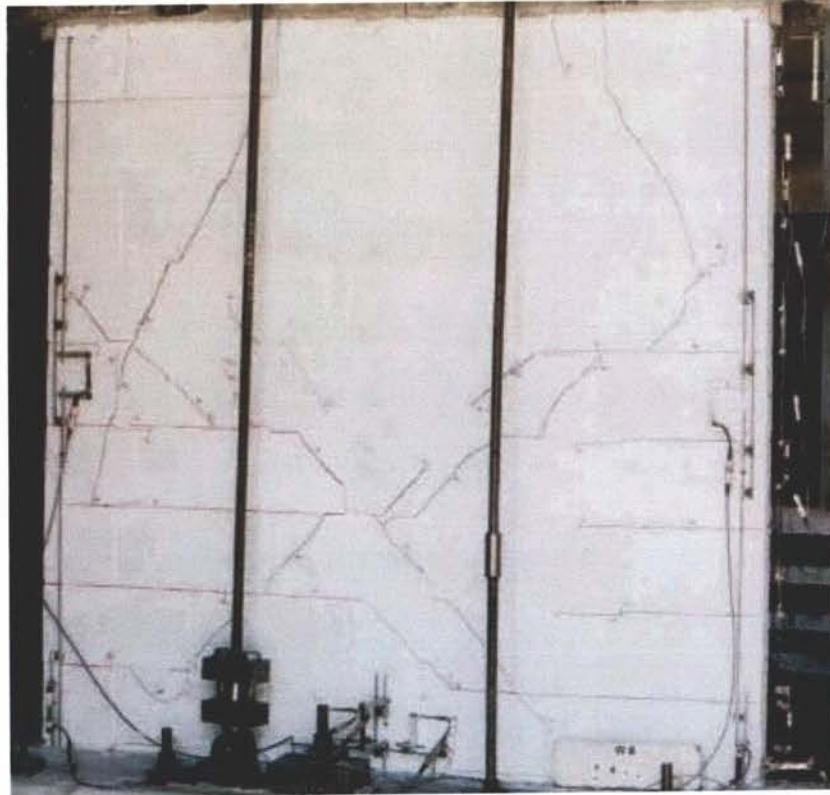


Photo 36 Condition of test wall after first cycle to ± 4 mm displacement.



Photo 37 Condition of test wall after first cycle to -6 mm displacement.



Photo 39 Condition of test wall after first cycle to ± 12 mm displacement.



Photo 38 Test set-up for Wall 9.



Photo 41 Condition of test wall after first cycle to ± 24 mm displacement.

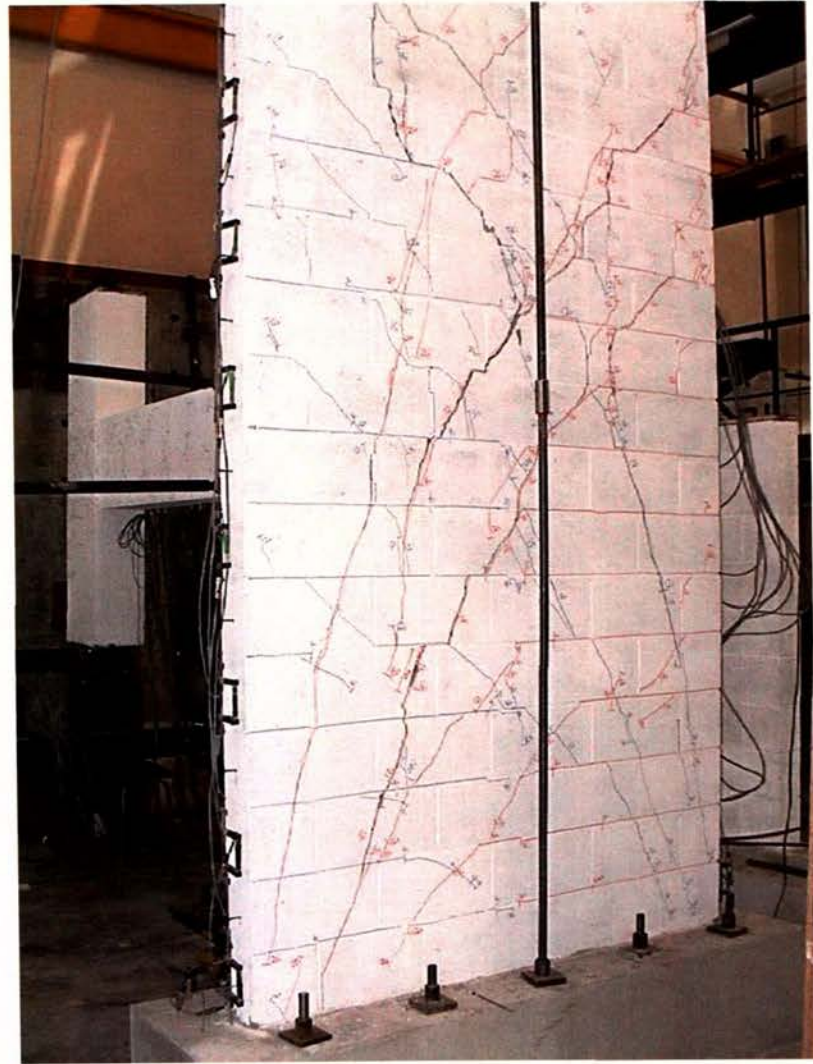


Photo 40 Condition of test wall after first cycle to ± 20 mm displacement.

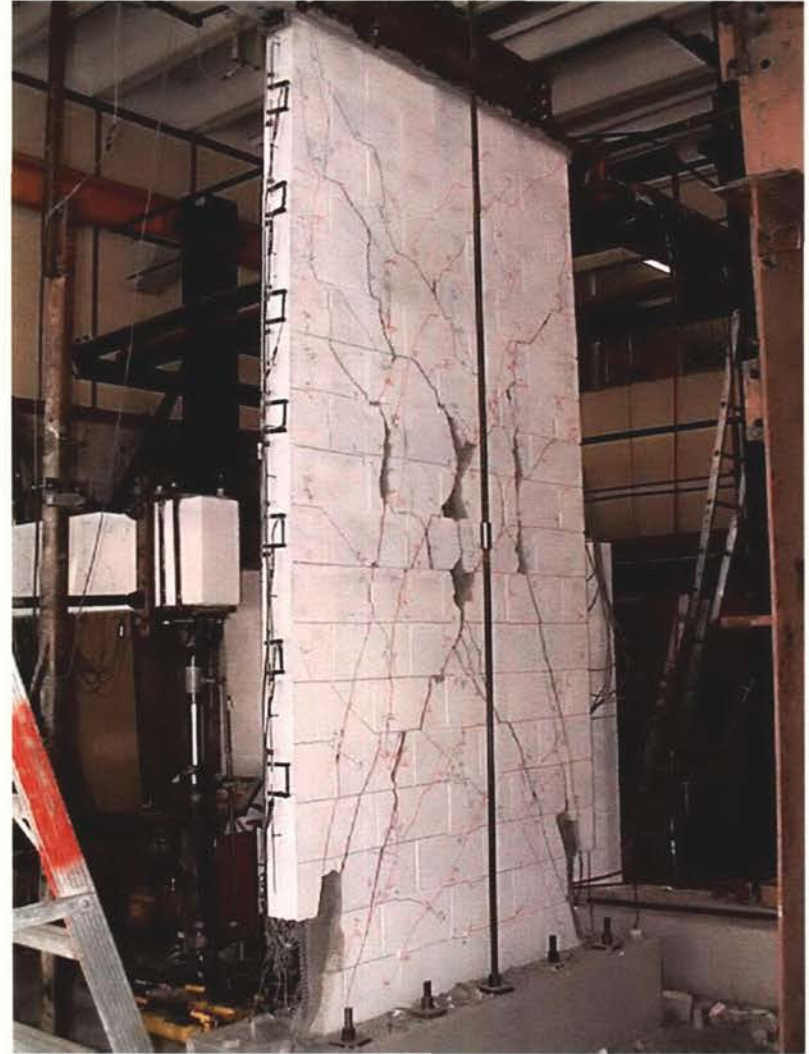


Photo 42 Condition of test wall after first cycle to ± 32 mm displacement.

Photos of Wall 10

Due to technical fault of the camera, significant portion of the photos taken during the testing process were found to be lost after the completion of wall testing. Only a few photos were salvaged but in poor condition. Consequently, the cracking patterns of Wall 10 is shown diagrammatically in Figure G.1. The red lines indicate cracks formed in the pushing direction, while the blue lines represent cracks formed in the pulling directions.

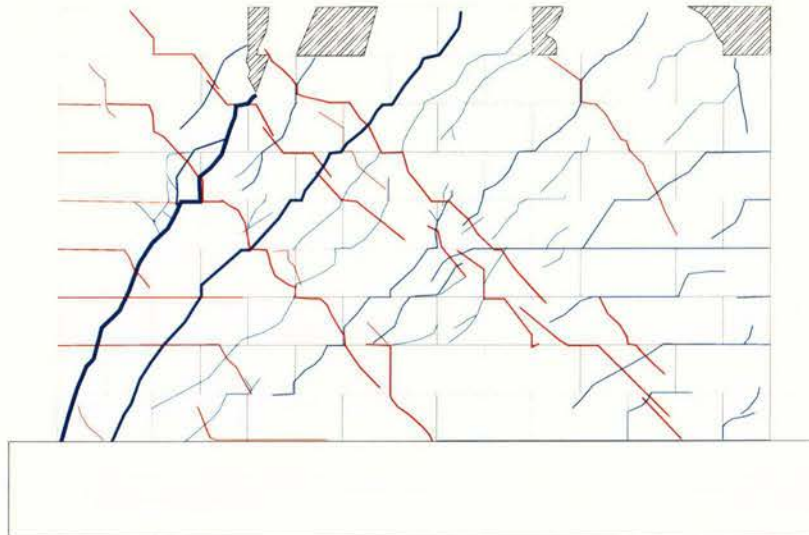


Figure G.1 Wall 10 cracking pattern.

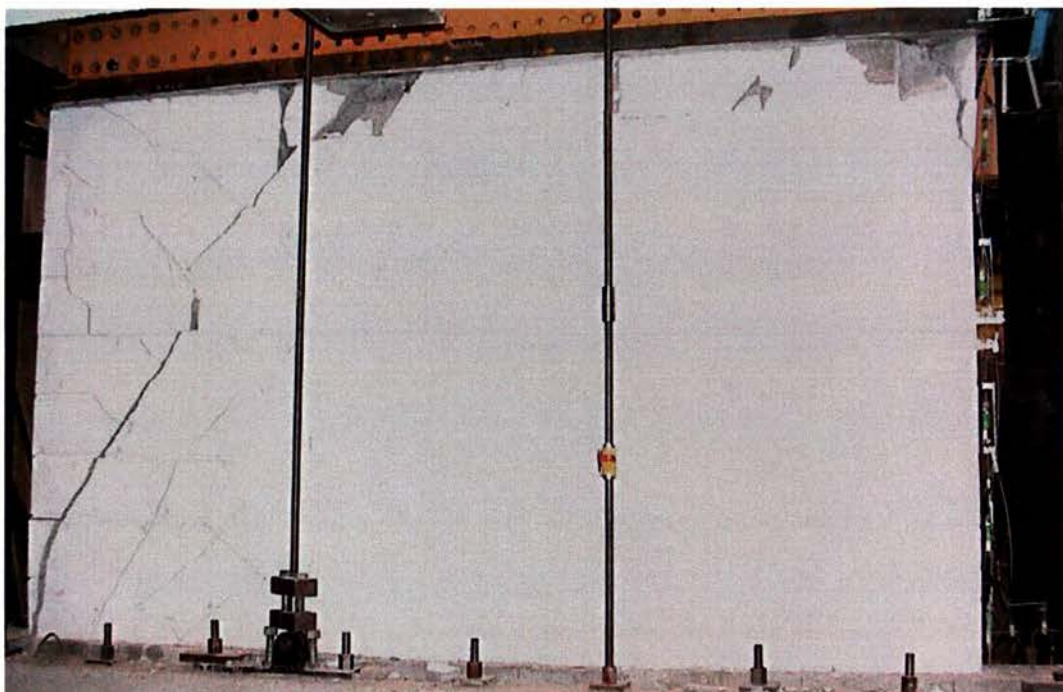


Photo 43 Condition of test wall at end of testing.

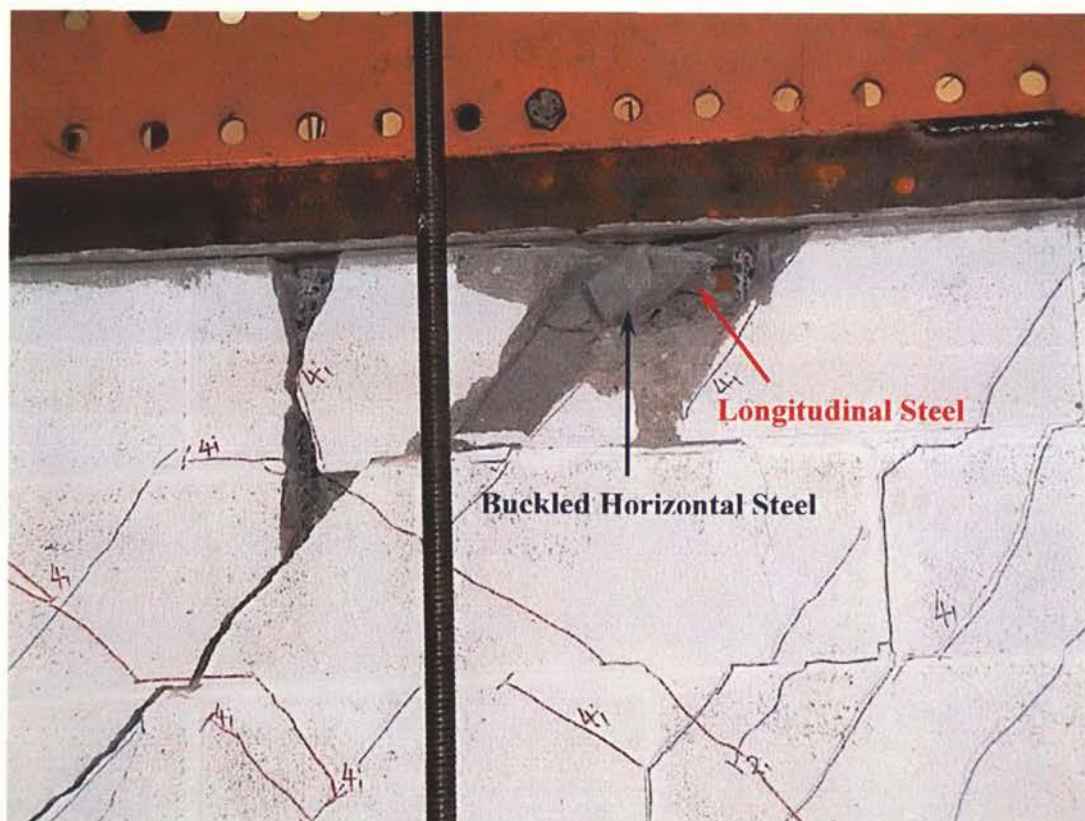


Photo 44 Crushing of masonry at bond beam layer exposing reinforcing steels.